2017

Local meteorology and its effect on electromagnetic wave propagation over the southern coast of the Arabian Gulf

Almehrezi, Ali

Local meteorology and its effect on electromagnetic wave propagation over the southern coast of the Arabian Gulf

by

Ali Saif Ali Saleh Almehrezi

PhD

August 2016

Local meteorology and its effect on electromagnetic wave propagation over the southern coast of the Arabian Gulf

by

Ali Saif Ali Saleh Almehrezi

A thesis submitted to University of Plymouth in partial fulfilment for the degree of

Doctor of Philosophy

School of Marine Science and Engineering,

Faculty of Science and Engineering

August 2016

To all individual to make the world more peaceful

Abstract

Local meteorology and its effect on electromagnetic wave propagation over the southern coast of the Arabian Gulf

Ali Almehrezi

The propagation of electromagnetic (EM) waves of frequencies above 100MHz is affected by the existence and properties of the atmospheric duct, i.e. a horizontal layer in the lower atmosphere in which radio signals propagate more efficiently. Atmospheric ducts can be found in many parts of the world ocean including the Arabian Gulf. Ambient winds blowing from different directions bring air masses of different properties into the area and hence have a significant impact on the formation and strength of the atmospheric duct. However, little information is available on the long-term and intra-annual variability of wind and its effect on the ducting phenomenon in the Arabian Gulf region. This study addresses this gap by characterising the local meteorology, with a special emphasis on its effect on electromagnetic wave propagation.

This study uses a new methodology to measure the persistence of Shamal wind, by considering the number of days associated with the specific wind pattern in addition to commonly used parameters such as the wind speed. In this study, thirty years (1981-2010) of observations and NCEP/NCAR reanalysis data have been analyzed to identify a long-term trend and the intra-annual variability of various wind systems. Results clearly indicate that the Shamal (the northwesterly wind) is the most frequent meteorological feature over the region; therefore it has been investigated in greater detail. The Suhaili (southerly wind) is the second important wind which can occur any time of the year but it is less frequent

than the Shamal. The Al-Nashi (cold and dry northeasterly wind) wind occurs only in December, January and February. The analysis shows that the wind strength and the frequency of Shamal days over the region have decreased over the last thirty years.

Variations in the occurrence of summer and winter Shamal days were studied in relation to global atmospheric phenomena, and relationships have been established, synoptically and statistically between the frequency of Shamal days and large-scale atmospheric fluctuations. These links include atmospheric fluctuations over the Caspian Sea (a correlation coefficient of 0.66) and Siberia (0.69) in summer and Greenland (0.51) and Western Europe (0.65) in winter. The frequency of winter Shamal days during December, January and February are shown to be statistically related (a correlation coefficient of 0.41) to the North Atlantic Oscillation (NAO) and (0.49) the Arctic Oscillation (AO), as they influence the pathway of the westerly depression over the north Atlantic Ocean during the winter season. It is also shown that the decline in the number of Shamal days is linked to a decrease in the number of westerly depressions.

The EM wave propagation has been examined using the Advanced Refraction Effects Prediction System (AREPS) model for different representative air masses. The radiosonde data from Abu Dhabi airport used in AREPS provided evidence of the general influence of each air mass. It was found that atmospheric ducting conditions and characteristics (height, thickness, and type) were variable in the lower part of the atmosphere (surface to 6000m) as a result of changing air masses. The influence of the Shamal conditions develop an elevated duct at approximately 850mb level. The Suhaili increases the thickness of the evaporation duct. In regards to the surface based and elevated duct, Suhaili and Al-Nashi provide standard atmospheric conditions. Land and sea breezes were mostly associated with the surface based duct and sometimes elevated the duct.

Atmospheric ducting could extend the range of electromagnetic wave propagation above the usual range. Good knowledge of atmospheric duct characteristics enables the efficient assessment of the range of EM propagation, which is important for a number of practical applications, for example air traffic control and rescue operations. This could include the selection of the appropriate frequency and altitude of the electromagnetic wave device (e.g. radar and/or communication systems) operating with a frequency above 100MHz to be trapped in the duct to cover long distances.

Contents

List of Figures

Chapter 3

Chapter 4

Chapter 6

List of Tables

List of Symbols

(variations in the symbolism or other symbols are stated in the text to derivation)

$\hat{x}_i$	modelled value
σ	standard deviation
Σ	sum
E	water vapour pressure in millibars
H	altitude in metres above the sea level
μ	mean
M	modified refractivity
N	refractivity of air that contains water vapour
o_i	observed value
ρ_{xy}	correlation coefficient
P	air pressure in millibars
R	mean radius of the earth in kilometres
T	temperature
Z	height above sea level in meters

Acknowledgments

First and above all, I praise God, the almighty for providing me this opportunity and granting me the capability to proceed successfully. Then I would like to thank the UAE government for providing this opportunity and sponsoring me to do this research at the University of Plymouth.

I wish to express my cordial thanks to my first supervisor, Prof Georgy Shapiro for his warm encouragement, thoughtful guidance, continuous support, and critical comments; and who was generous with his time and knowledge and assisted me in each step to complete the thesis. I am thankful to my other supervisors, Dr Sarah Bass, Dr Tim O'Hare and Dr Richard Thain for the trust, the insightful discussion, and valuable advice and especially for their patience and guidance during the writing process.

I am grateful to a number of people, who helped me with various elements of my study, including Dr. Duncan Priestley, Dr. Derek Pilgrim, Dr. Xavier Francis, Mr Alen Collet and Mr Matt Burch. I would like to thank Bahrain, Abu Dhabi, and Sharjah airports for their observational data which were intensively used in this project.

Lastly, and most importantly I wish to thank my mother, wife and other members of my family, I will always be grateful for their constant support and encouragement.

Author's Declaration

At no time during the registration for the degree of Doctor of Philosophy has the author been registered for any other University award without prior agreement of the Graduate Sub-Committee.

Work submitted for this research degree at the Plymouth University has not formed part of any other degree either at Plymouth University or at another establishment.

This study was financed with the aid of a studentship from the UAE Government.

A programme of advanced study was undertaken, which included IMS5101 Research Skills.

Presentation and Conferences Attended:

- European Geosciences Union, Vienna, Austria, 07-12 April 2013. Oral and poster presentation: Seasonal variations of Shamal wind in the Arabian Gulf (A. Almehrezi, G. Shapiro, R. Thain, D. Priestley).
- HTC conference, Abu Dhabi, UAE, February 2013. Oral presentation: General synoptic situation over the Arabian Gulf (A. Almehrezi, D. Priestley).
- European Geosciences Union, Vienna, Austria, 27 April – 02 May 2014. Poster presentation: Seasonal variations of Summer Shamal days in the southern Arabian Gulf (A. Almehrezi, G. Shapiro, R. Thain).

Publications under preparation:

- Almehrezi, A., Shapiro, G., Francis, X.V., Bass, S., O'Hare, T., (end of 2016); Characteristics of the synoptic winds over the southern coast of the Arabian Gulf, Climate dynamics. (to be submitted)
- Almehrezi, A., Shapiro, G., Francis, X.V., Bass, S., O'Hare, T., (end of 2016); Variations in the frequency of the Summer Shamal Days- part1. Climate dynamics. (to be submitted)
- Almehrezi, A., Shapiro, G., Francis, X.V., Bass, S., O'Hare, T., (beginning of 2017); Variations in the frequency of the Winter Shamal Days – part2. Climate dynamics. (to be submitted)
- Almehrezi, A., Shapiro, G., Francis, X.V., Bass, S., O'Hare, T., (beginning of 2017); Impact of the local meteorological conditions on the EM propagations. Meteorological applications (to be submitted)

Word count of main body of thesis: 33934

Signed_____

Sate_____

Chapter 1 – Introduction

1.1 General Introduction

It is important to understand the relationship between different wind patterns and atmospheric refractivity to determine how the wind pattern will effect electromagnetic propagation in the atmosphere. Systems which operate in an electromagnetic wave (such as radar and communication equipment) may not perform as well as would be expected in some regions due to environmental phenomena, particularly atmospheric ducting (Katzin et al., 1960).

Atmospheric ducting is the trapping of EM propagation in the lower layers (surface to 500mb) of the atmosphere in a horizontal layer (Turton et al., 1988). It can occur due to an increase in temperature, a decrease in air moisture with height, or a combination of the two (Katzin et al., 1960). Radar and communication systems operating with a frequency above 100MHz could be affected by such atmospheric ducting (Craig, 2003); frequencies below this figure have wavelengths too large to be trapped in the duct. Higher frequencies are more likely to be trapped.

This phenomenon can either extend or reduce the useful range of the electromagnetic propagation used by radars and communication equipment (Barrios, 2003).

This study explores the influence of local meteorological conditions on electromagnetic wave propagation and ducting over the southern coast of the Arabian Gulf; a region of global economic, strategic and military importance. The influence of the variations of local winds on the ducting and the broader atmospheric dynamics that control them are examined

to provide an enhanced understanding of both the local meteorology and the ducting phenomenon.

Recent research (Atkinson and Zhu, 2005) has identified that ambient winds in the Arabian Gulf have a major impact on the atmospheric duct. The Shamal wind is the primary ambient wind in the region and persists for most of the year over the area, but with varying characteristics (Govinda, Al-Sulaiti and Al-Mulla, 2001). It has been identified that atmospheric duct strength increases on the southern coast of the Arabian Gulf due to the north-westerly Shamal wind (Atkinson and Zhu, 2005). Therefore, gathering detailed knowledge of the Shamal wind will greatly assist in the prediction of variations in the strength of the atmospheric duct and enable a greater understanding of how electromagnetic devices can be adapted to cope with the phenomenon.

1.2 Area of study

The southern part of the Arabian Gulf is situated between 24–26 degrees north and 51.5-56.5 degrees east. It is partly UAE territorial waters and also includes Qatari, Iranian and international waters. UAE territorial waters lie mostly in the Arabian Gulf; the UAE coast line is approximately 300 nautical miles (nm) long. The area is located in the south western part of Asia. This area of study is bordered by the Arabian Gulf and Iran to the north, the UAE land mass to the south, Oman and the Gulf of Oman to the east, and Qatar and Saudi Arabia to the west (Figure 1.1) (UAE Ministry of Energy, 2006).

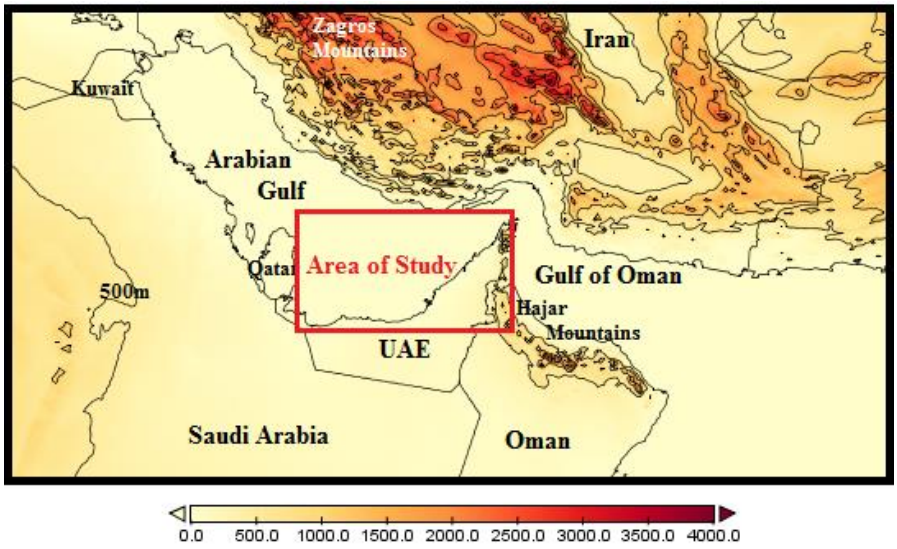

Figure 1.1. Map showing topography of the study area and surrounding countries. (Taken from: http://maps.ngdc.noaa.gov/viewers/wcs-client/).

1.3 Topography

Topography plays an important role in determining the weather and climate of the area (Atkinson and Zhu, 2004). One of the most significant features in the area is the Zagros Mountain range which is situated in south-west Iran, north of the Arabian Gulf, and has an average height above sea level of 3000-4000 metres. The Hajar Mountains are a second important topographic feature running from the Strait of Hormuz in the north, along the eastern edge of the Arabian Peninsula to Sur in the south-east. Their average height is between 1500 and 2500 metres, with a maximum height of 2980 metres at Jebel Akhdar (Ali, 1994). The remaining land mass within the study area is a large sandy desert, with a height of less than 200 metres, and gently sloping toward the Arabian Gulf (Figure.1.1).

The Arabian Gulf extends 530nm from the Shatt Al-Arab delta to the Strait of Hormuz. The maximum width is at Abu Dhabi (150nm), getting narrower eastward (50nm) at the Strait of Hormuz; it is some 130nm within the Shatt Al-Arab delta in the west. The water is relatively shallow, 20-60 metres, although it gets deeper near the Strait of Hormuz (90 metres) (Walters, 1990). The southern part of the Arabian Gulf is full of numerous small islands and scattered oil platforms. There are more than 200 islands in the territorial waters of the Emirate of Abu Dhabi alone (Federation of UAE Chamber of Commerce & Industry, 2010).

1.4 Rationale, aims and objectives

Electromagnetic wave propagation in the Arabian Gulf area is heavily affected by the presence and properties of the atmospheric duct (Atkinson & Zhu, 2006). The Arabian Gulf is an area with one of the highest probabilities of atmospheric ducting around the world (Willis, 2007). Topography, coastal configuration, sea and land breeze circulation, boundary layer characteristics and the ambient wind have effects on the atmospheric duct over the area. However, little or no information is available on seasonal electromagnetic propagation variability over the southern part of the Arabian Gulf. Consequently, this study has been carried out in order to contribute a better understanding of weather conditions in the Arabian Gulf and their effect on radar and communication performance in this region. It is also intended that this study will assist those organizations which operate offshore to select the appropriate radar and communication frequencies to operate their radars according to the weather conditions likely to be experienced in their area of operation. Therefore, the overall aim of this study is:

- To develop an understanding of how the meteorology of the southern Arabian Gulf affects EM wave propagation. This will enable the users of EM wave propagation devices to predict how their instrument will operate.

To meet the study aim the objectives are:

- To introduce the local meteorology of the study area and specify the different air masses that affect the area (Chapter 4) that will enable the identification of the effect of different air masses on the EM propagation.
- To identify the general regional features that characterize the regional meteorology (Chapter 4). This feature once identified will be analysed to find its connection with the global circulation pattern.
- To examine the inter-annual variability of Shamal Days and its correlation with the global circulation pattern (Chapter 5) to be able to predict the seasonal variation over the region.
- To examine EM propagation variability under different meteorological conditions (Chapter 6). This will help the predication of the influence of the different air masses on the EM propagation.

There are many factors affecting electromagnetic propagation, including temperature inversions, humidity, dust and winds. Within this context the Shamal wind is a major influencing phenomenon and must be analysed as it can greatly influence radar and communication performance. Existing literature will provide an important insight into the expected weather conditions over the region. Furthermore, a detailed analysis of the

available meteorological and climate data in the literature can be used to prove or disprove the proposals suggested as to how the Shamal wind affects atmospheric ducting.

1.5 Thesis outline

Following this introduction (**Chapter 1**), the theoretical background to the study is introduced in the literature review in **Chapter 2**. This describes the general picture of the global, synoptic and local meteorology and its effect on electromagnetic wave propagation. Data sources, validation methods and further approaches in methodology are explained in **Chapter 3**. In **Chapter 4** the characteristics of local meteorology are introduced. Air masses affecting the area of study are investigated. Also, a general regional feature that characterizes the region's meteorology is identified. The effect of global circulation systems upon inter-annual variability is explained in **Chapter 5**, which examines the inter-annual variability of Shamal Days and how this correlates with the global circulation pattern. In **Chapter 6** the influence of the different air masses on electromagnetic propagation is assessed. Finally, **Chapter 7** summarises the conclusion of the study and makes recommendations for future research.

Chapter 2 – Literature review

This chapter is designed to build an initial picture about the local meteorology and its effect on electromagnetic wave propagation over the southern coast of the Arabian Gulf. It consists of six sections; 1) The effect of the atmosphere on the propagation of Electromagnetic (EM) waves; 2) key weather influences on the global scale; 3) key weather influences on the synoptic scale; 4) key weather influences on the local scale; 5) climatological analysis; 6) atmospheric duct measurement and prediction tools.

2.1 The effect of the atmosphere on the propagation of Electromagnetic (EM) waves

Most of the long range sensors such as radars, communication equipment, and electronic warfare equipment are operating via electromagnetic waves, propagating electromagnetic waves into the atmosphere and receiving the return echo. This section will describe the key concepts relating to this propagation, namely atmospheric refractivity, the atmospheric duct and formation of the atmospheric duct.

2.1.1 Atmospheric refractivity

Electromagnetic waves are refracted as they move between layers in the atmosphere (Turton, Bennetts and Farmer, 1988). The atmospheric refraction of the electromagnetic waves depends on rate of change of air pressure, temperature and humidity and not simply the absolute values. Normally pressure and temperature decrease with height in the atmosphere and therefore the strength of the refraction of the electromagnetic waves decreases with height. Taking into account the earth's curvature, atmospheric refraction can be calculated by the modified refractivity (M) formula:

$$M = \frac{77.6}{T}\left(p + 4810\frac{e}{T}\right) + \frac{z}{R} \times 10^6 \quad (2.1)$$

where T is the air temperature in Kelvin, p is the air pressure in hPa , e is the water vapour pressure in hPa , z is the height above sea level in meters and R is the mean radius of the earth in kilometres(Bean and Dutton, 1968). Unmodified refractivity, N, which does not take the earth's curvature or height into account and therefore has some limitations, can also be used:

$$N = \frac{77.6}{T}\left(P + 4810\ \frac{e}{T}\right)$$

Atmospheric refraction can be categorized into four types: sub-refraction, normal, super refraction and trapping (ducting) (Figure 2.1).

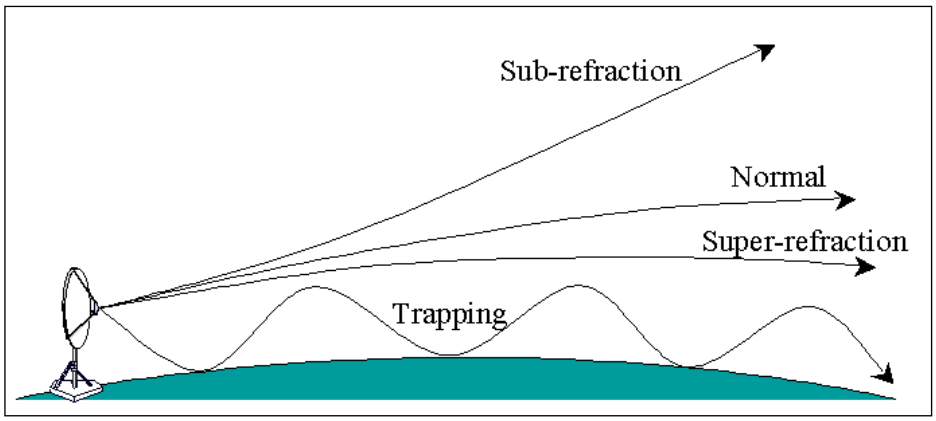

Figure 2.1. Schematic diagram shows the four types of electromagnetic wave paths as a result of variability in atmospheric density; refractivity is measured using modified refractivity, M. . Source (Bruce, 2006, p.4).

Sub refraction occurs when decreases in atmosphere density with height are less than normal. Super refraction occurs when decreases in atmosphere density with height are more

than normal. If the super-refraction bends equal or more than the earth's curvature then trapping occurs and that is called atmospheric duct (Bruce, 2006). To determine which atmospheric refraction category applies one must plot the quantity of modified refractivity (M) against height. A decrease in the quantity of modified refractivity with height forms an atmospheric duct, while an increase in the quantity of modified refractivity with height leads to super-refraction or standard refraction or sub refraction depending on the modified refractivity gradient; further details are shown in figure 2.2(Hydrographic Office, 1994).

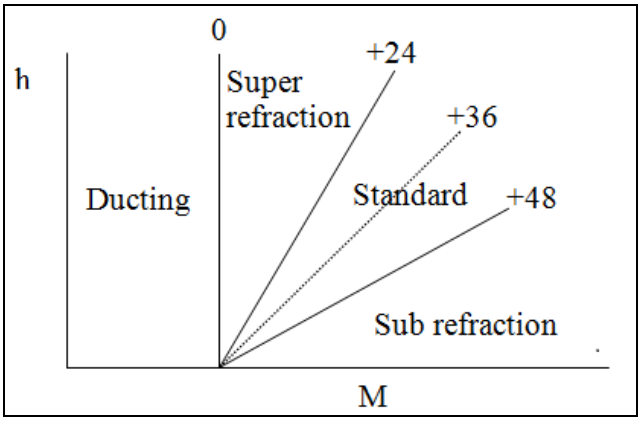

Figure 2.2. Illustrates the quantity of modified refractivity (M) against height (h), gives modified refractivity gradient and associated refraction condition. Source Hydrographic office, 1994.

2.1.2 Atmospheric duct

An atmospheric duct forms when either temperature increases or water vapour decreases sharply with height. It has been noted that water vapour has more influence than temperature (Gao, Brewster, and Xue, 2008). Additionally, as the temperature increases the water vapour influence on the refractivity will increase (Figure 2.3) (Cheong et al., 2005).

Furthermore, during the warm season the atmospheric refractivity is more affected by moisture than temperature (Gao, Brewster, and Xue, 2008).

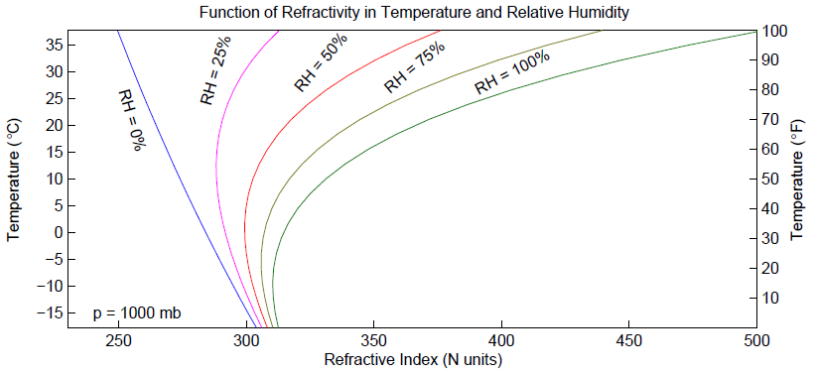

Figure 2.3. As the temperature increases the influence of the relative humidity on refractivity increases. (Cheong et al., 2005).

An atmospheric duct may trap electromagnetic wave propagation into anomalous distances which are significantly greater than usual. This has an operational significance, especially for radar systems, as targets may be detected at ranges where detection is not normally expected, or not detected at ranges where they normally are (when a duct exists, but the target is outside of it); as coverage is increased within the duct, so it is reduced outside of it, creating a shadow zone. (Anderson, 1995)

Trapping of electromagnetic wave propagation depends on the atmospheric duct depth and roughness of the duct layer. If the duct depth is less than the wavelength (a function of frequency, which changes according to the type of wave), then the electromagnetic wave

will not be trapped in the duct. Also, if the roughness of the duct surface is larger than the wavelength, the electromagnetic waves will scatter out of the duct (Willis, 2007).

2.1.3 Formation of the atmospheric duct

There are several processes that lead to the formation of an atmospheric duct including evaporation, temperature inversions, subsidence and advection. An evaporation duct usually occurs over the sea, due to large lapses of humidity occurring just above the sea surface; they reach maximum depths at lower latitude during day-time in the summer months. It extends VHF/UHF propagation to a great distance over the sea causing a significant problem for international frequency coordination (Willis, 2007). A second process leading to duct is formation radiative cooling which takes place on a clear night over land causing a temperature inversion. The third process is subsidence which causes the air that moves down to heat up as it is compressed. The descending air is warmer than the air below, causing an elevated atmospheric duct (Atkinson and Plant, 2001). The final process frequently occurs in the early evening when the warm air mass moves from the land over the cooler moist sea, which causes the advection duct. As such this may extend the height of the evaporation duct (Willis, 2007).

In conclusion, duct can occur for four reasons and is particularly influenced by changes in the moisture content, especially at higher temperature. Therefore, weather is the primary information sources available on the propagation of electromagnetic waves in any part of the world. Within a chosen region, global, synoptic and local scale weather patterns can affect electromagnetic wave propagation patterns. Atmospheric duct could be found by looking into a vertical variation of temperature and dew point. Therefore, any process that

leads to temperature inversion and sharp decreases in water vapour over the study area should be illustrated.

2.2 Atmospheric condition on a global scale

The area of study is located in the Hadley Cell and monsoon region. In this section these circulations will be discussed in detail, along with their influence on electromagnetic wave refractivity focuses in the atmospheric ducting.

2.2.1 The Hadley Cell

The Hadley Cell is an atmospheric circulation pattern which develops in an area between 30N and 30S. It develops due to intensive heating from the sun resulting in air ascending to the top of the troposphere in the equatorial area. Figures 2.4 show the general Hadley Cell circulation.

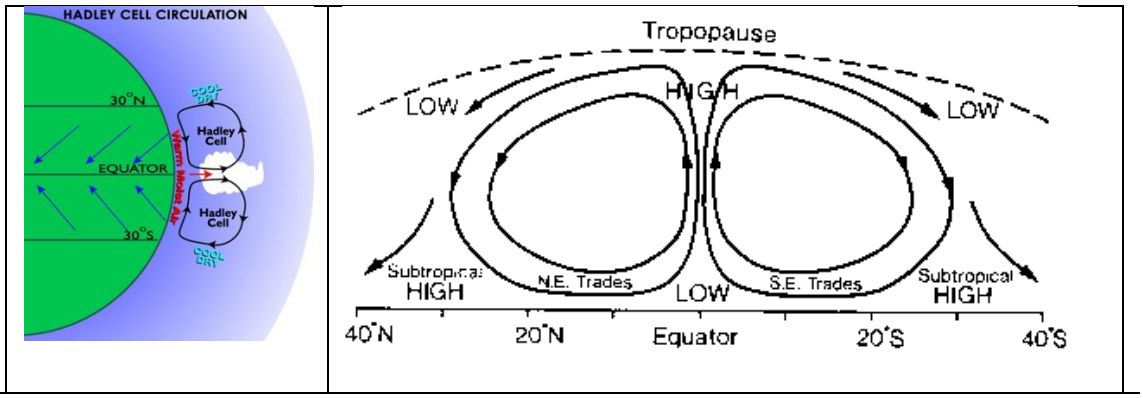

Figure 2.4. Shows atmospheric Hadley Cell circulation. Image source is (http://earth.geology.yale.edu/~avf5/teaching/ResourcesGG523/Lect9.hadley.circ.pdf).

Once at the top of the troposphere, the air moves from the equator to the subtropics north and south; once there some air descends resulting in a semi-permanent subtropical high. This descending air adiabatically warms and dries causing clear skies and a strong temperature inversion (subsidence inversion) over the subtropical regions (Ahrens, 2009, Galvin, 2007a). A subsidence inversion develops between descending air and a boundary layer (well mixed air layer near the surface). A subsidence inversion can be observed by the eye as it results in visible cirrus clouds or a layer of trapped pollution. The height of the subsidence inversion height and width has a diurnal variation.

Additionally, height and width of the subsidence inversion layer will decrease as it moves away from the centre of the anticyclone. Indeed, another subsidence lower and thinner inversion may be developed, if the anticyclone has been interacted on by a weather front. Such a subsidence inversion is localised and will only 'live' for a short period (Craig, 2003). A subtropics subsidence inversion is expected to be between 650-500 millibar (4000-5000m) over the desert (Reid et al., 2008). In the lower part of the troposphere trade wind moves from subtropics north and south toward the equator, subsequently converging there to form a belt that is called the Inter Tropical Convergence Zone (ITCZ). The movement of the ITCZ north and south of the hemisphere, associated with the sun's movement, causes a regional wind system which is called the monsoon (Ahrens, 2009).

2.2.2 Monsoon

Monsoon is an Arabic word meaning season. It is used to refer to the prevailing wind over the Indian Ocean which varies from season to season. This wind is also known as a trade-

wind, and can be used by sail boats to navigate and travel in the monsoon region. The region is shown below in figure 2.5.

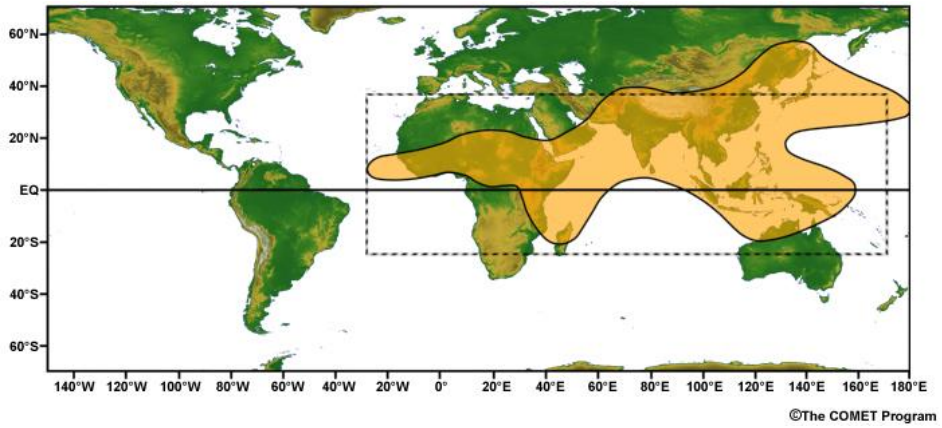

Figure 2.5. Area of monsoon cycle, Image source is (http://www.meted.ucar.edu/tropical/textbook_2nd_edition/navmenu.php).

In winter, the ITCZ moves into the southern hemisphere, allowing the Eurasian landmass to cool down, resulting in the development of extensive high pressure over Siberia; furthermore, a dry cold north-easterly monsoon blows over southern Asia (Figure 2.6 (a)). In summer the ITCZ moves into the northern hemisphere and causes a wet south-westerly monsoon over southern Asia (Figure 2.6 (b)) (Galvin, 2008, Laing &Evans, 2011). At this time, a strong summer monsoon wind causes strong seasonal variation in ducting probability over the Arabian Sea. Wintry offshore north easterly dry monsoon wind comes over a cooler sea causing an advection inversion which increases duct probability over the Arabian Sea during winter. However, in the summer this ducting probability decreases to a minimal level due to the strength of a south westerly monsoon. This results in more mixing of the air, the degree of mixing depending on the strength of the south-westerly monsoon (Engeln & Teixeira, 2004).

There is complex relationship between the strength of the summer south westerly monsoon and the land/sea thermal contrast. The south westerly monsoon creates an upwelling phenomenon as it blows, which brings colder water to the sea surface, therefore increasing thermal contrast between the land and sea, which in turn, adds significant strength to the monsoon wind. In contrast, a weak south westerly monsoon will not significantly affect upwelling or land/sea thermal contrast, therefore little strength is added to a south westerly monsoon (Gao et al, 2005). Additionally, in the spring-time (monsoon transit period) the largest area of ducting probability in the northern hemisphere is found over the Arabian Sea due to hot air coming from the Arabian Desert and passing over the cooler water of the Arabian Sea (Engeln & Teixeira, 2004).

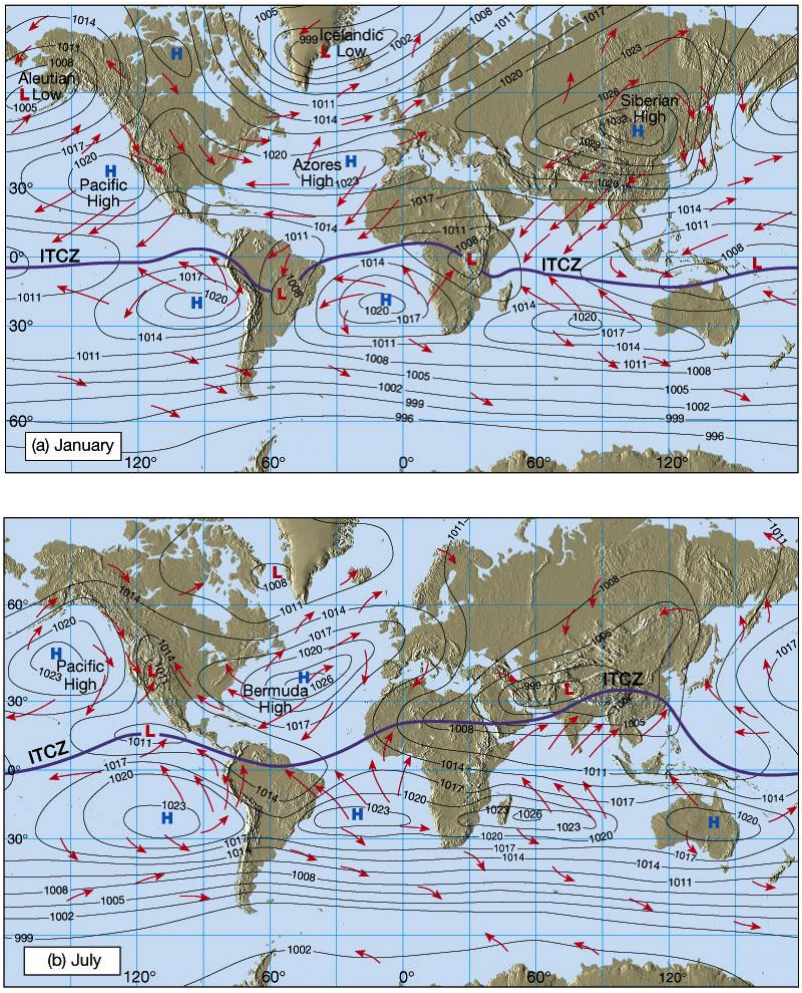

Figure. 2.6. These digrams illustrate the location of the ITCZ and the atmospheric circulation in January and July. Maps taken from (http://www.ux1.eiu.edu/~cfjps/1400/circulation.html).

The Hadley cell subsidence inversion comes at the top of the trade wind cycle and is known as a trade wind inversion. The strength and height of the subsidence inversion changes with variations in longitude and latitude. With changes in latitude this inversion is higher and weaker as it moves westward over the ocean where the Sea Surface Temperature (SST) is hotter than the east side of the ocean. This is diagrammatically shown in figure 2.7. The SST is cooler on the east side of the ocean because of the upwelling phenomena, occurring

due to a strong easterly monsoon wind. Longitudinal trade wind inversion is higher and weaker as it moves toward the ITCZ (figure 2.7).

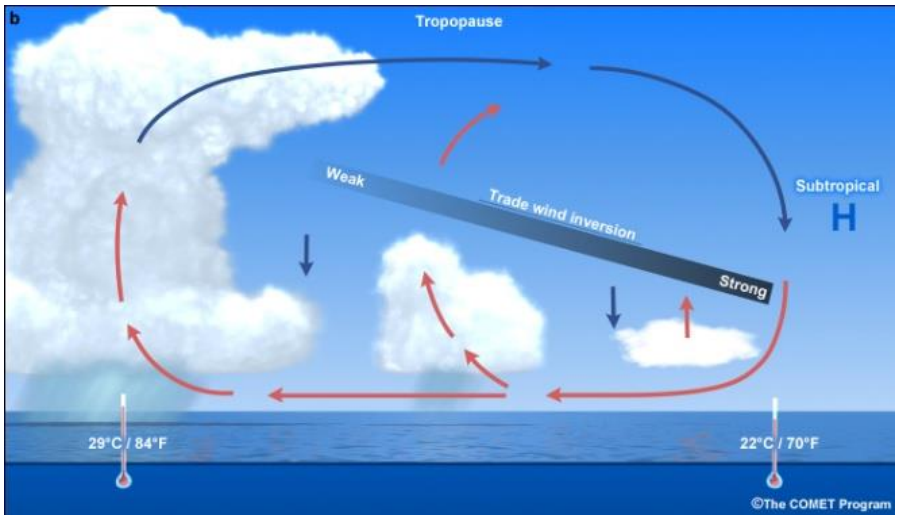

Figure 2.7. Trade wind inversion over ocean in latitudinal scope Image source is (http://www.meted.ucar.edu/tropical/textbook_2nd_edition/navmenu.php?tab=2&page=5.2.0).

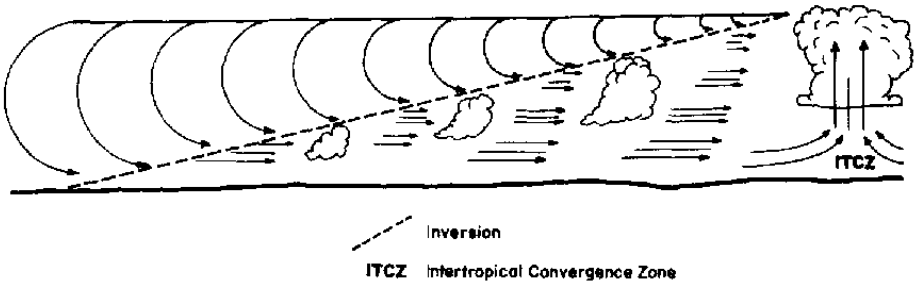

Figure 2.8. Trade wind inversion over ocean in longitudinal scope Image source is (http://www.greenstone.org/greenstone3/nzdl%3Bjsessionid=18AACCE680DA92576BE20C694F31CCFD?a=d&c=ccgi&d=HASHe7f3998ab3a0ef799ea72d.5.1.np&sib=1&p.s=ClassifierBrowse&p.sa=&p.a=b).

Therefore, the elevated duct is stronger on the eastern side of the ocean than the western side, and in the subtropical compared to the tropic regions. For example, during the Second

World War, a strong elevated duct was observed over the Arabian Sea by a radar station in Bombay (over 3000 nautical miles); this displayed the coast of the Arabia on its screen during the north easterly monsoon season (Katzin et al., 1960). This example clearly illustrates how the north easterly offshore wind can extend a radar's capability. The impact of the monsoon cycle is less in the Arabian Gulf due to the region's topography which acts as a barrier preventing any direct effect of the summer and winter monsoon. The Zagros Mountains prevent the very cold, dry, north-easterly monsoon from affecting the area in the winter, and the Hajar Mountains limit the effect of the wet warm south-westerly monsoon to the eastern side of the UAE in the summer (Walters, 1990).

2.3 Atmospheric conditions on a synoptic scale

Literature regarding the study area is largely difficult to identify, it is old and incomplete; most is superficial in detail (Hasanean, 2010). Unfortunately, the study area in terms of both synoptic and local scales has little research available (Villiers, 2010). Whilst Almandoos (2005) described synoptic circulation over the study area, his description was rather limited to describing each system and its related winds and did not try to relate it to other weather conditions or phenomena. In addition, Atkinson and Zhu (2004-2005), do not describe specific systems affecting the study area, but rather discuss only the detail of the Shamal wind and duct phenomenon over the Gulf region.

Unfortunately, with such limited research there has not been any detailed insight into the climatic phenomena in the area of study. The synoptic key weather influences which have been reviewed in this section are as follows: the Siberian High Pressure System, the Indian Monsoon Thermal Low, Mediterranean Depressions, the Red Sea Trough, Rossby Waves

(upper level wave), Subtropical Jet Stream, the subtropical High, easterly Jet Stream, Indirect influences of weather patterns on the area of study, Shamal Wind, South-easterly wind and Al-Nashi wind.

When considering synoptic-scale systems, especially the Shamal, NCEP/NCAR reanalysis is the primary source of wind data. The last thirty years, the focus of the research, is considered to be the most reliable part of this data due to advances in computer science, and from 1979, the incorporation of satellite data (Kistler et al., 2001). Whilst there is some evidence from outside the region to suggest deficiencies within the NCEP/NCAR wind speed data in maritime environments (Goswami and Sengupta, 2003), there is less doubt over wind direction, and NCEP/NCAR data is considered reliable for this type of study, and widely used.

2.3.1 The Siberian High Pressure System (SHPS)

The SHPS is a seasonal thermal system over Asia (Figure 2.6(2)) which forms due to extensive cooling of the land. It is shallow in vertical extent, often confined to approximately below 500mb (Panagiotopoulos et al., 2004), and drives a cold dry north easterly wind over southern Asia. It extends west to Europe, south-west to the Middle East, and eastward, limited only by the Pacific Ocean. It reaches its maximum strength and size in winter when the sea level pressure can reach above 1050 millibars (Panagiotopoulos et al., 2004 used 1031 as a suitable value for a benchmark). The SHPS has an effect as far west as Italy which as a result may subsequently block or reduce the size of any westerly storms reaching the Arabian Gulf.

The SHPS is influenced by the Arctic Oscillation (AO) and El Niño-Southern Oscillation (ENSO) (Wu & Wang, 2002). When both (AO, ENSO) are in a positive phase the strength of the SHPS system is weak and temperatures are higher than normal (Cheung, Zhou, Mok and Wu, 2012). Indeed, the AO affects the strength of the western edge of the SHPS dynamically. The strength of the SHPS depends on the downward motion from the top of the troposphere. When the negative AO's downward motion is stronger, then the SHPS will be stronger than normal. Conversely, when a positive phase of the AOs downward motion is weaker then the SHPS will be weaker than normal (Wang et al., 2001).

The intensity of the SHPS may reflect the severity of the cold air. The maximum intensity of the SHPS occurs during December and January (with a mean maximum SLP of 1051 millibars) and February (with a mean maximum SLP of 1049 millibars). The maximum record of the SHPS SLP was 1082 millibars observed in the month of December. Overall, pressure in excess of 1050 millibars occurred 51% of the time in January, 45% in December and 3 - 4% in October and April. 70% of the SHPS centre was observed in areas bounded by 45 - 55N, 90 - 105E (Wang, 2006).

Since late 1970, surface wind speed has decreased over China due to changes in winter mean temperatures, which have resulted from global warming (IPCC, 2013). In the winter, SHPS is the prominent surface system over the area of study. It appears in November and disappears in April. It retreated to the North for a few days allowing the westerly Mediterranean depression to pass, followed by strong North Westerly cold dry winds (winter Shamal wind) for a few days (Almandoos, 2005). Radar propagation is below average during the passage of a frontal system due to increased moisture aloft and becomes

average in fresh to strong wind (Shamal wind). Radar propagation is above average in anticyclonic conditions (SHPS) and elevated and surface ducts can be formed (Hydrographic Office, 2004).

2.3.2 The Indian Monsoon Thermal Low (IMTL)

Toward the summer season the solar energy and associated ITCZ moves north. As a consequence, the SHPS will fade and a thermal low will build-up over the landmass. This thermal low occurs from June until September (Wang, 2006). In July the ITCZ lies over the southern part of the Arabian Peninsula, Gulf of Oman, the Straits of Hormuz, south Iran and Pakistan (figure 2.9).

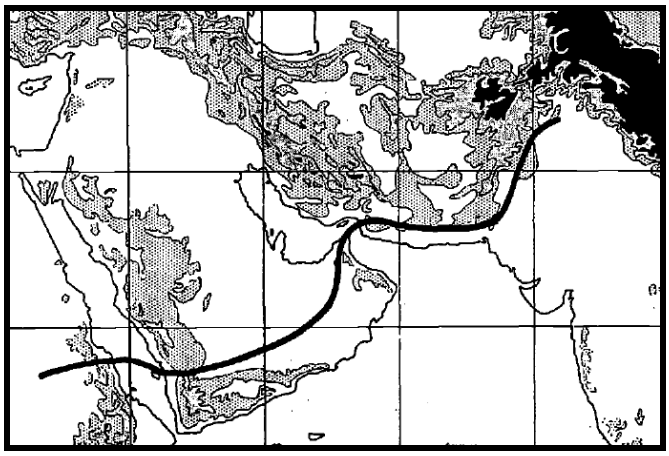

Figure 2.9. The average position of the ITCZ during the summer season. Gray and dark highlights represent mountainous areas. Source (Walters, 1990).

The position of the ITCZ is important in order to identify the weather conditions within an area. The area north of the ITCZ is affected by the monsoon circulation (ex. Arabian Gulf). The IMTL is centred west of Pakistan and extends west-ward over the Arabian Gulf and Arabian Peninsula, causing a north westerly flow (summer Shamal) in the early summer over the study area. As the summer Shamal wind comes off the Kuwait coast the air stream becomes cooler and more stabilized, with moisture to create a Marine Internal Boundary Layer (MIBL). This commences at a few hundred meters deep, but gets more profound as it moves south reaching a maximum depth along the southern coast of the Arabian Gulf (Atkinson and Zhu, 2005). Such a stable layer will trap the moisture within the shallow MIBL. Any increase in moisture and decrease in temperature leads to the formation of a surface atmospheric duct (Garratt, 1990, cited in Brooks, Goroch, and Rogers, 1999, p.1294).

Sometimes the IMTL deepens causing a moderate to fresh north westerly flow over the area which will cause atmospheric mixing that minimises any surface duct. Due both to this circulation and the topography of the area a lee-low develops in the Arabian Gulf (Walters, 1990). A secondary centre of the thermal low develops over the Arabian Peninsula due to high insolation of solar radiation arising during the summer season. This is associated with a southerly hot and dry wind (Almandoos, 2005).

Southerly hot and dry winds coming over the cooler Arabian Gulf water will cause an advection duct. The area south of the ITCZ is affected by the monsoon weather which results in a wet, strong south westerly monsoon wind. As has been discussed previously in paragraph 2.1.2, the strong south westerly monsoon will minimise duct properties. Additionally, under certain conditions when the ITCZ moves northward over the southern

part of the Arabian Gulf it will cause some penetration of the south westerly monsoon (Walters, 1990).

The south westerly monsoon is affected by El Niño and Indian Ocean Dipole ((IOD, "a pattern of internal variability with anomalously low sea surface temperatures off Sumatra and high sea surface temperatures in the western Indian Ocean, with accompanying wind and precipitation anomalies."(Saji et al., 1999)). There is a relationship between the El Niño and the strength of the summer monsoon; the strength of this monsoon is weakened by El Niño and increases in strength during La Nina. The IOD develops in the Indian equatorial region from April and reaches its peak in October (discussed later in detail). Positive IOD will weaken the south westerly monsoon resulting in a warm Arabian Sea. Conversely, a negative IOD will strengthen the south westerly monsoon resulting in a cold Arabian Sea (Saji et al., 1999, Gopal Raj, 2004).

On the other hand UCAR (2010) mentioned in their website that the positive phase of the IOD will enhance the summer monsoon whist the negative phase will weaken the summer monsoon. In the summer there is an extension of the IMTL resulting in a warm moist easterly trough forming over the study area throughout the year (Almandoos, 2005).

2.3.3 Mediterranean Depressions

Mediterranean depressions move from west to east. They are associated with upper troughs and active phases of the subtropical jet-stream as well as the polar front jet-stream; rainfall is produced during their passage (Chakraborty et al., 2006). There are two common storm tracks. One of the storm tracks moves through the Mediterranean just south of Turkey and

curves northward into the Caspian Sea. The other storm track will not curve north but proceeds eastward into the eastern Mediterranean (Jordan, Syria and Iraq) on its way into the Arabian Gulf (ibid). This Mediterranean depression continues to move eastward toward India (NOAA, 2003).

A study by (Kutiel, 1982 cited in El-Kadi, 2001, p.42), suggested that when the storms reach the island of Cyprus they will follow one of three storm tracks: the first one moves directly toward Turkey; the second track proceeds to the east toward northern-eastern Syria causing rain in the northern part of that region; the third track moves south-east of the eastern Mediterranean covering that region, eventually moving eastward into the Arabian Gulf, causing rain in all parts. A further study by Walters (1990) suggests that as the storm reaches the eastern Mediterranean it will then follow one of the three tracks (figure 2.10). The first track runs northeast of Turkey, the second track proceeds eastward over the study area, whilst the third track moves south of Egypt and through the centre of Saudi Arabia and Oman.

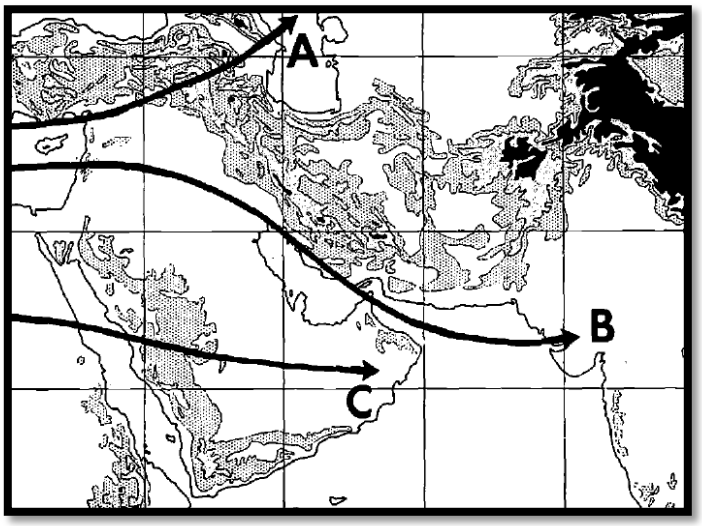

Figure 2.10. Mediterranean Depression tracks suggested by Walters, 1990. Gray and dark highlights are representing mountain areas.

Esfahany, Ahmadi-Givi, and Mohebalhojeh, (2011) mentioned that the Mediterranean Depression track is influenced by North Atlantic Oscillation (NOA) phases. In the negative phase the Mediterranean Depression will affect the northern part of the Mediterranean and then curve northward into the Caspian Sea. Whilst in the positive phase the Mediterranean Depression will affect North Africa and will move eastward into the study area. Figure 2.11 gives a guideline for expected refraction conditions associated with mid latitude frontal systems. Almandoos (2005) and Walters (1990) stated that there is a complex circulation where by the Mediterranean Depression will couple with the Red Sea trough, causing heavy rain over the study area.

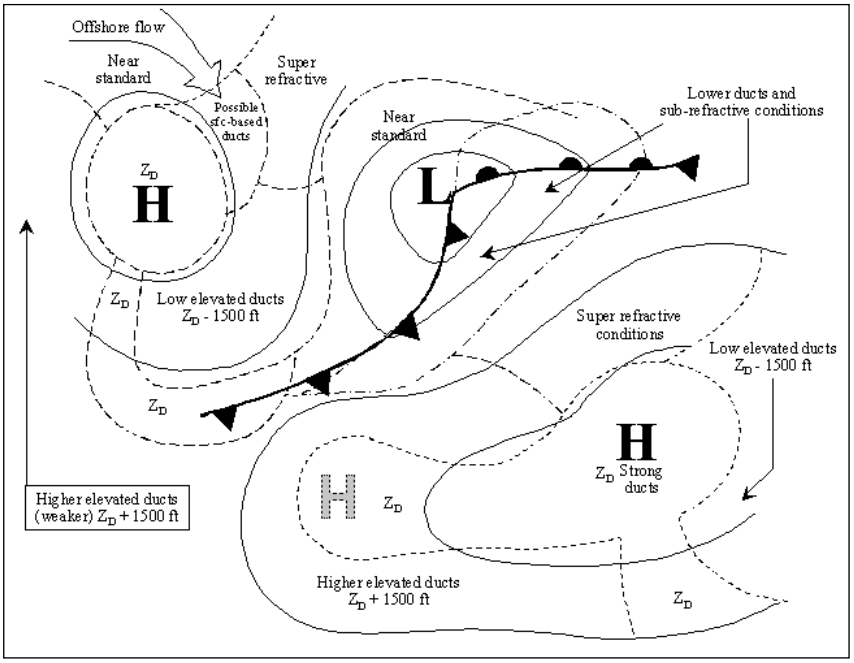

Figure 2.11. Illustrates expected refractivity conditions in different areas of the mid latitude frontal system Source (Bruce, 2006, p.4).

2.3.4 Red Sea Trough (RST)

The Red Sea Trough (RST) is an extension of the Tropical Sudan Monsoon Low over the Red Sea, which is part of a large scale pressure thermal system over Africa. The development, intensity and extension of the RST is dependent upon topographic and thermal force factors over the Red Sea region (Krichak, Alpert, and Krishnamurti, 1997). Sometimes it reaches the area of study causing unstable weather during the transitional period and winter season. It is associated with unstable warm and moist air. The most common occurrence of the RST is in February (Almandoos, 2005).

2.3.5 Rossby Wave (Upper level wave)

The Rossby Wave is a westerly air flow wave aloft in the area between the Polar and Hadley cells. As air moves from west to east it is forced toward the poles as ridges and toward the equator as troughs. The area between the trough and the ridge (along the westerly flow) is a region of divergence and it supports surface cyclonic conditions whilst the area from the ridge to the trough is associated with convergence which supports anticyclonic conditions (figure 2.12). The narrow band of fast wind existing within the Rossby Wave is known as a Jet Stream (Ahrens, 2009, Branstator, 2002, Galvin, 2007b).

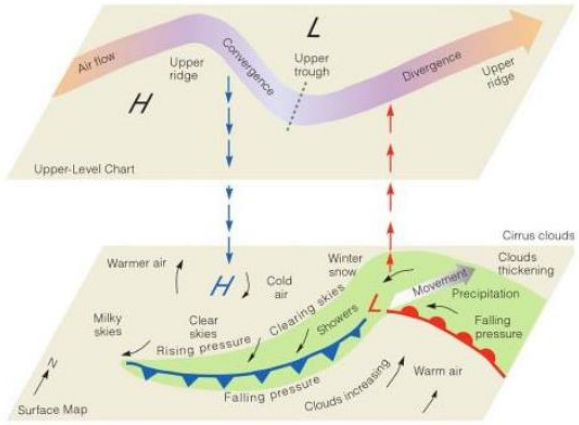

Figure 2.12. Illustrates divergence and convergence directions and associated surface pressure systems. Source Ahrens, 2009

During the winter period the Rossby Wave affects the study area primarily in terms of the subtropical jet stream, westerly trough and westerly ridge. However, during the summer season a westerly Rossby Wave moves northward from the area of study as the sun moves north. This action results in an easterly trough and subtropical high affecting the area of study. The formation of a westerly trough is associated with a subtropical jet stream, which

plays an important role in precipitation during the winter season; it is associated with unstable conditions. The westerly ridge causes north-westerly winds in the upper air system. If this ridge combines with a surface high, then it will develop into a stable atmosphere resulting in mist and fog. Such conditions affect the area during the winter season and the transition period (Almandoos, 2005). These weather conditions enhance formation of strong elevated ducts and surface ducts.

2.3.6 Subtropical Jet Stream

The Subtropical Jet Stream is located above the subtropical region and results from a strong temperature gradient aloft which causes strong westerly wind flows. These conditions will have an effect on temperature and rainfall over the area of study. The formation of a westerly depression over the study area and its interaction with the Polar Jet Stream will result in unstable rainy weather conditions. Additionally, sand-storms over the Middle East occur when the Subtropical Jet Stream pushes up from the south whilst the Polar Jet Stream pushes down from the north. This interaction mostly happens in spring and summer and will result in an occurrence of the Shamal wind (Hasanean, 2010).

The position of the Subtropical Jet Stream is an important tool to forecast weather conditions. Therefore, any unusual shifting of its position should be predicted. Any increase in temperature causes a northward shift of the Subtropical Jet Stream while a decrease in temperature will cause a southward shift of the jet stream. It reaches maximum strength during the winter, and its weakest strength (with a shift northward) in the summer (Hasanean, 2010). On the other hand, there is another study (Yakir, Lev-yadunand Zangvil, 1996) which suggests that the Subtropical Jet Stream shifts southward during El Niño;

known as unusual warming. From a logical and scientific perspective this suggestion is not realistic; however, there may be other factors than temperature which drive the jet stream shift process.

2.3.7 Subtropical High

The Subtropical High is a semi-permanent upper high pressure system which is a part of the Hadley Cell circulation resulting from the subsidence process. The North Atlantic Subtropical High extends from the south-west over the study area. It is the dominant system during the summer season, and reaches its minimum dimensions during the winter period. When it is coupled with a Surface Siberian High, a surface and elevated inversion will be formed and maximised (Almandoos, 2005).

2.3.8 Easterly Jet Stream

The Easterly Jet Stream is an easterly flow aloft occurring only in the summer season from late June until early September over Africa and Southern Asia. The Easterly Jet Stream weakens during the El Niño causing dry conditions and is enhanced during La Niña causing wet conditions (Hasanean, 2010). These conditions affect the eastern part of the study area and are associated with an easterly trough over the Hajar Mountains (Almandoos, 2005).

2.3.9 Indirect influences of weather patterns on the area of study

As has been discussed earlier there are some weather patterns which have an indirect influence on the area of the study. Such influences causing weather variability include El Niño and La Niña, Indian Ocean Dipole (IOD), Arctic Oscillation (AO) and North Atlantic Oscillation (NAO) (figure 2.13).

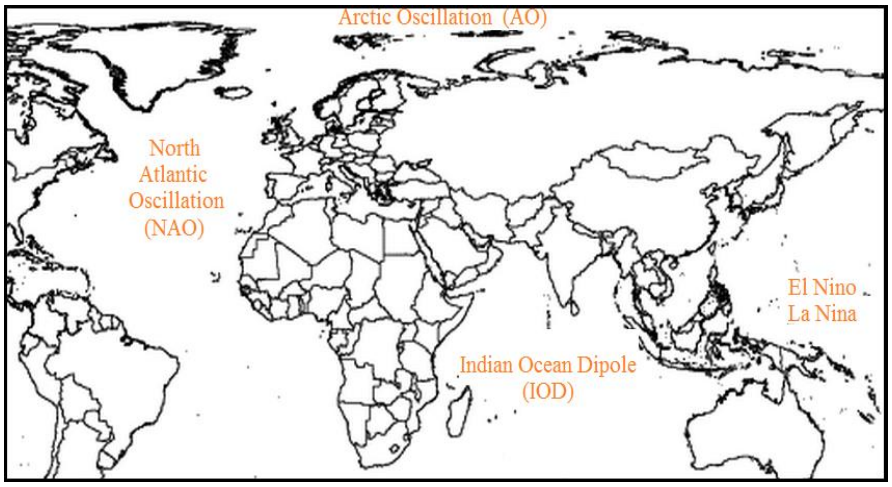

Figure 2.13. Illustrates the location of the weather patterns that have indirect influence on the study area.

2.3.9.1 El Niño and La Niña

The El Niño and La Niña phenomena, which primarily affect the tropical Pacific circulation, are a result of variations in the strength of the trade winds along the western coast of South America. It is the trade wind strength which drives the change in sea surface temperature along the tropical Pacific Ocean. As a result of these trade winds changing strengths there are three ensuing conditions which develop over the tropical Pacific Ocean. Normal conditions occur with light to moderate winds blowing across the tropical Pacific Ocean, which cause upwelling over the western coast of South America. Under these conditions warm water is being pushed west, allowing cold water to come to the surface (Sarachik and Cane, 2010, NOAA, n.d).

The second condition is the La Niña which forms as a result of fresh to strong trade winds in the tropical Pacific Ocean pushing warm sea surface water further to the west. As a result of these circumstances, cumulonimbus clouds (CB) develop in the west of the tropical Pacific Ocean. The third condition is El Niño, which is a weak trade wind (only a breeze) in the tropical Pacific Ocean. Such conditions allow the warm sea surface temperature to extend eastwards along the equator in the Pacific. As a result, cumulonimbus clouds develop along the equator causing a shift in the pacific ocean upper air level atmospheric circulations (Figure 2.14) (Sarachik and Cane, 2010, NOAA, n.d).

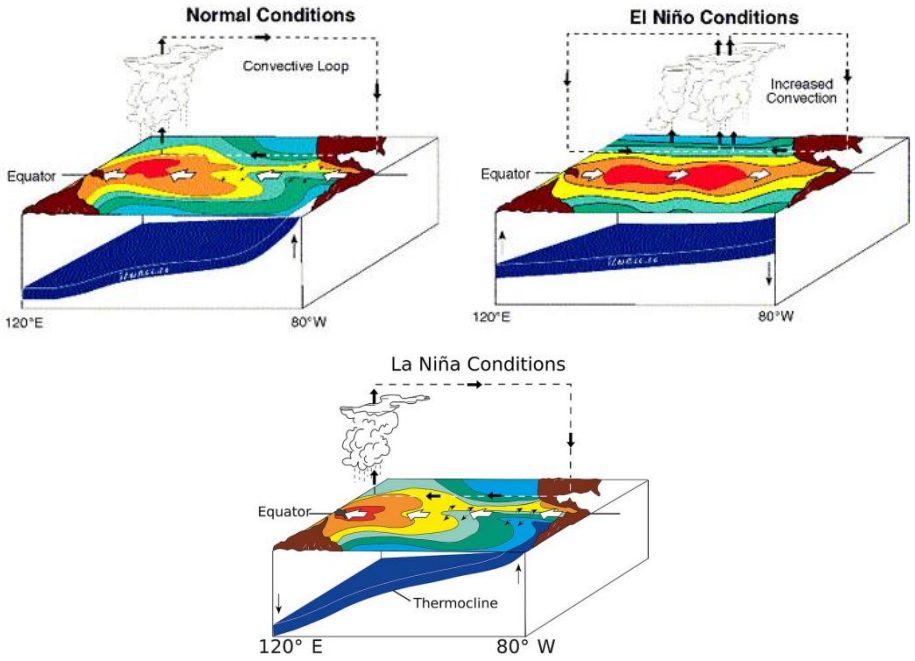

Figure 2.14. (a) illustrates the extension of the warm sea surface temperature and distribution of the CB cloud in El Niño, La Niña and Normal Conditions over the tropical Pacific Ocean. Source is NOAA.

During El Niño, south-west Asia precipitation is above normal in the autumn season (Mariotti et al., 2005) and is below normal during the winter season (Barlow et al., 2002). El Niño weakens the south-westerly monsoon and warms the Arabian Sea. In contrast, La Niña creates a strong gradient pressure over the region causing more precipitation (Nazemosadat et al., 2006). Tropical easterly jet streams are weakened in the El Niño years and enhanced in the La Niña years; this is associated with dry and wet conditions respectively (Hasanean, 2003). A winter-spring La Niña can also have the effect of decreasing rainfall in the Rub' al Khali desert, which has an effect on regional dust activity (Yu et al., 2015).

2.3.9.2 Indian Ocean Dipole (IOD)

The Indian Ocean Dipole is an atmospheric phenomenon observed in the tropical Indian Ocean between the east coast of Africa and west coast of Indonesia. The positive phase of the IOD is similar in principle to the La Niña, when trade winds are stronger than usual, pushing warm surface water towards Africa and causing deeper cooler water to appear along the west coast of Indonesia (UCAR, 2010).

The negative phase of the IOD is similar in principle to El Niño when trade winds are weaker than usual and warm surface water extends along the tropical Indian Ocean. The positive phase will cause drought over the eastern part of the Indian Ocean and heavy rain over the north-western and western parts of the Indian Ocean. Conversely, the reverse of these conditions will occur during the negative phase (Figure 2.15). The cool tropical Indian Ocean also enhances Shamal activity, by producing an anticyclonic circulation over the central Arabian Peninsula in contrast to warmer temperatures in the area enhancing the

summer low, and diminishing the Shamal (Yu et al., 2015). The IOD has an effect on the strength of the summer monsoon as discussed earlier (UCAR, 2010).

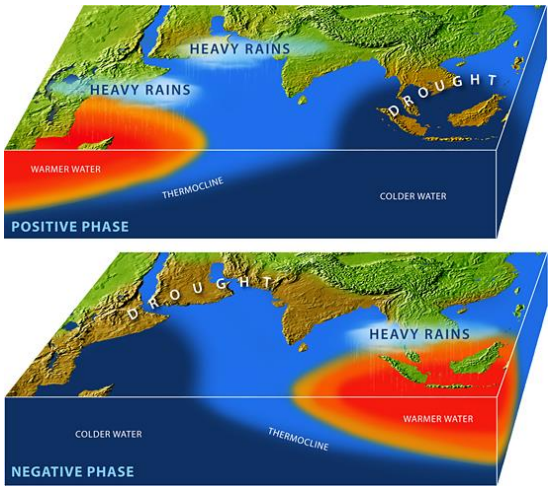

Figure 2.15. This figure illustrates different phases of the Indian Ocean Dipoles and their effect on the Indian Ocean atmosphere (UCAR).

2.3.9.3 Arctic Oscillation (AO)

The Arctic Oscillation occurs when a surface pressure system over the Arctic region is dominant (figure 2.16). If the pressure system over the Arctic region is lower than normal then that is known as a positive phase of AO. The Polar Jet Stream will be stronger, trapping cold air in the Arctic region and causing a warm period over the mid-latitudes. With a negative phase of the AO, when the pressure system over the Arctic region is higher than normal, the Polar Jet Stream will be weaker allowing cold air to penetrate mid-latitude regions. AO patterns can be identified in the troposphere and stratosphere by using zonal wind and geopotential height charts. AO patterns are different from NAO, but both have a

similar influence in their winter Atlantic storm tracks (Hodges, 2000). AO has clear affects in the extension of the western part of the Siberian High as has been discussed earlier.

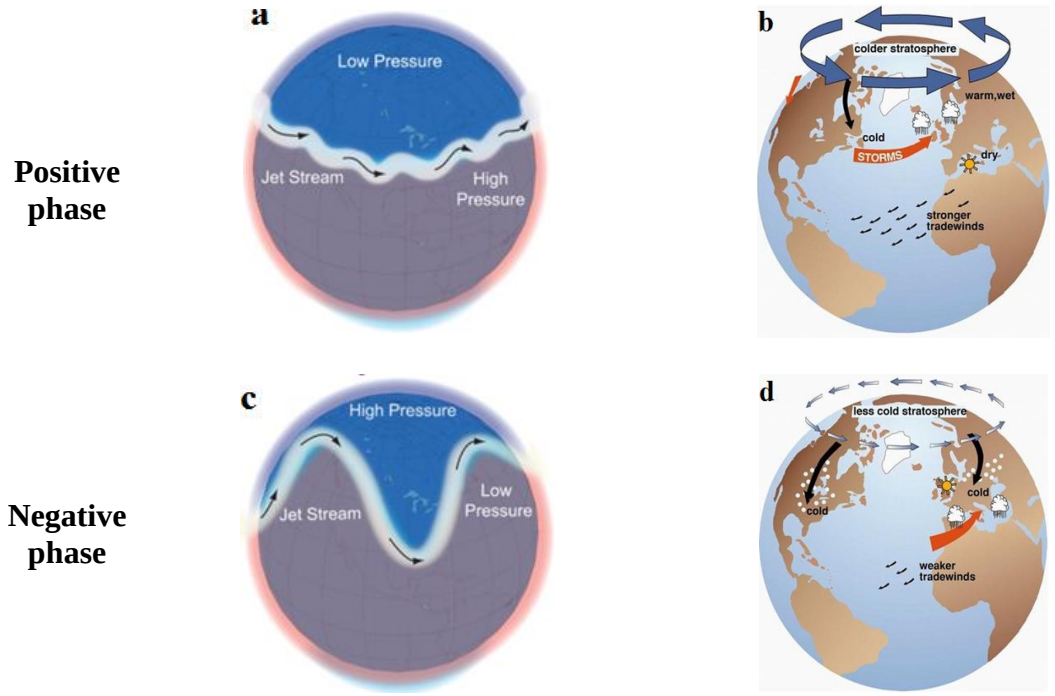

Figure 2.16. Left side (a-c) shows the westerly flow of the jet stream in negative and positive phases of AO (Source NOAA). Right side (b-d) shows weather effect of each phase of AO over the northern hemisphere (source. <http://www.washington.edu/news/archive/id/3261>): viewed in 8 June 2012.

2.3.9.4 The North Atlantic Oscillation (NAO)

The NAO is linked to the surface atmospheric pressure difference between the Icelandic Low and the Azores High occurring during the winter season (Figure 2.17). This NAO controls the strength and tracks of the westerly storms across the North Atlantic Ocean. If there is a strong gradient between the two pressure systems then a westerly depression will move north-west toward North West Europe and is called a positive phase of NAO index. In contrast, if there is a weak gradient between the two pressure systems then the westerly

depression will move eastward toward the Mediterranean and is called a negative phase of NAO index. It is this phase which occasionally impacts on the study area (Hurrell, Kuschnir, and Visbeck, 2001).

NOA has a clear effect on the Mediterranean weather systems. Positive NAO is shown as a colder and drier period over the Mediterranean in the winter season. In contrast, negative NAO is associated with relatively warm and moist air over the Mediterranean Sea, with heavy rainfall over the eastern Mediterranean (Figure 3.16) (Malekifard & Rezazadeh, 2009). Additionally, an increase in flow of the Tigris and the Euphrates Rivers is shown to be associated with negative NAO due to significant precipitation over Turkey, Syria, and Iraq. The opposite patterns are observed in the positive NAO index. Positive NOA causes a reduction of the flow volume in the Middle East (Cullen & Menocal, 2000).

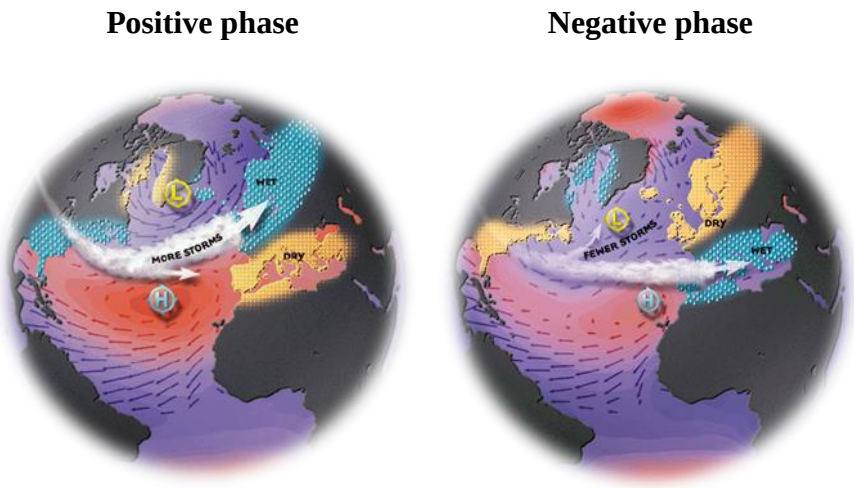

Figure 2.17. This illustrates the tracks of the westerly storm in positive and negative NAO phases. (Source is http://www.aviso.oceanobs.com/en /applications/climate/ nao/what-is-the-nao/ index. html).

2.3.10 Shamal Wind

The most common wind in the Arabian Gulf is a north-westerly wind, which has acquired the local name of Shamal. It is a cool wind that remains for approximately 3-5 days at any one time. Usually the Shamal is associated with dust and sand which can of course severely restrict visibility. In addition, its wind strength is such that it can cause unpleasant weather with rough sea conditions (UKHO, 2013).

A clear relationship exists between the Shamal strength and the northern high latitude glacial periods. The evidence available suggests that during the glacial periods, a strong Shamal type wind transported the northern sediment southward. Conversely, during the interglacial periods the Shamal wind was weak allowing the south-westerly monsoon to function further north causing a higher period of rainfall (Glennie and Singhvi, 2002). The Shamal can be categorized as winter Shamal and summer Shamal.

2.3.10.1 The Winter Shamal.

Shamal winds occur during both winter and summer, due to a synoptically driven system, but with different characteristics. From the synoptic sequence in winter, it can be observed that the Mediterranean depression moves eastward into the Arabian Gulf. As a result of that action, the Siberian High retreats back until the depression moves east of the area. Then the Siberian High extends behind it to build a north-westerly gradient over the Arabian Gulf causing a strong Shamal wind (Govinda, Al-Sulaiti and Al-Mulla, 2001 Al Senafi and Anis, 2015).The effect of this weather condition in EM propagation is discussed in the end of section 2.1.

2.3.10.2 Summer Shamal

The general synoptic situation for the summer season in the area is associated with a low pressure over Iran and high pressure over the Eastern Mediterranean. This combination system plays a prominent role in enhancing North Westerly flow over the Arabian Gulf known as the summer Shamal wind. The topography of the area of study enhances the north-westerly flow, due to the Zagros Mountains in the north of the Arabian Gulf, and Saudi Arabian desert in the south-west (which slopes down toward the Arabian Gulf) causing a gentle funnelling affect (Govinda, Hatwar, Al-Sulaiti and Al-Mulla, 2003, Al Senafi and Anis, 2015).

The strength of this wind is affected by different synoptic situations such as a deepening from the Iranian Low, and ridging from the Mediterranean High. There is also recent evidence that the ENSO system effects the strength of the Iranian Low (inhibited by El Niño and favoured by La Niña), in turn effecting the duration of the Shamal (Yu et al., 2016), as well as effects from sea surface temperatures in the tropical Indian Ocean and Mediterranean Sea (Yu et al., 2015).

The months of May, June and July comprise the main summer Shamal season over the Arabian Gulf. However, June has the highest Shamal frequency, followed by July and then May (Govinda, Hatwar, Al-Sulaiti and Al-Mulla, 2003, Al Senafi and Anis, 2015). Additionally, a lee-low develops west of the Zagros Mountains enhancing Shamal flows over the area. The effect of the summer Shamal radar propagation is discussed in section 2.3.2.

2.3.11 South-easterly wind

The South-easterly winds which occasionally blow over the Arabian Gulf have two names depending on their characteristics and the location of the observer. Firstly, there is the Al-Kaus which is characterised by a warm moist wind arising from its source in the Gulf of Oman or Arabian Gulf as it is moves north-westerly (Habib, 2011). The second name of this wind is Suhaili which persists over the area, and is characterised by a dry warm sandy wind. It usually causes a reduction in visibility due to the spreading of dust and sand. The presence of dust and sand can also have a direct effect on electromagnetic wave propagation, leading to attenuation in high dust densities (Musa, Bashir and Abdalla, 2014), as well as significantly contributing to radar clutter.

In winter, this south-easterly wind persists over the Arabian Gulf whilst a westerly depression approaches. The northern countries of the Arabian Gulf call it 'Al-Kaus' due to its long route over the Arabian Gulf allowing it to pick-up water vapour. On the other hand, the southern countries of the Arabian Gulf call it 'Suhaili' due to its route over the desert (Habib, 2011). The south easterly wind is warmer than the Arabian Gulf therefore it is associated with an advection duct over the sea. Additionally, it is associated with sand which influences radar propagation.

2.3.12 Al-Nashi wind

Al-Nashi is the Arabic name for a cold dry north-easterly wind which is part of the Asian monsoon system. It occurs in winter on the Iranian coast of the Arabian Gulf near the entrance to the Gulf. It is probably an outflow from Asian High weather conditions which

extends over the high ground of Iran. Also, it is possible for this wind to occur as a result of a katabatic wind, and it may cause a notable reduction in temperature (UAE Climate, 1996).

2.4 Atmospheric Conditions on the local scale

There is only limited literature available about the area of study, however, some major points are identified in this section from focusing on land/sea breeze circulation and the boundary layer.

2.4.1 Land and sea breeze circulation (LSBC)

The land and sea breeze circulation is a well-known atmospheric phenomenon over the region especially in the summer season due to the weak synoptic situation (Eager et al., 2008). Strength and direction of the breeze circulation are affected by the temperature gradient between land and sea (which is 10-15^{o}C in summer and 10^{o}C in winter), topography factors (Zagros Mountains lie in the North of Arabian Gulf and Hajar Mountains in the North East of the UAE), katabatic and anabatic winds adding to the breeze strengths, ambient wind (sea breeze can reach more than 250km inland over the southern coast of the Arabian Gulf, due to the north-westerly wind which increases the strength of the sea breeze and decreases the strength of the land breezes) (Atkinson & Zhu 2004).

The onset time of the land breeze varies from last night to early morning (2300 to 0400 local time) while land breeze ends in the late morning (approximately between 1000-1100 local time). In contrast, the onset time of the sea breeze takes place approximately at

midday. The sea breeze ends in late evening at approximately 2200 local time. The duration of the sea breeze is longer than the land breeze, being between 10-13 hours and 7-12 hours respectively. The onset time of the land and sea breeze circulation is very clear in October while less clear in January due to the high energy of the wind at the time (Arritt, 1989). Land and sea breeze circulations and the nature/behaviour of the Marine Boundary Layer (MBL) affects the atmospheric duct's existence, location, duration, dimension, strength and variation (diurnal and seasonal) (Brooks, Goroch, and Rogers, 1999). An earlier onset time of the sea breeze will cause more cooling to the lower part of the boundary layer causing a stronger than usual radiation inversion at night and in the morning that takes more time to burn out during late morning (Villiers, 2010).

2.4.2 Boundary Layer

The boundary layer is the lower part of the atmosphere which is directly influenced by surface conditions. In coastal areas warm dry air moves over cooler water. As a result, the warm air will cool from below to form a stable layer within the boundary layer, which subsequently forms an Internal Boundary Layer (IBL). As the IBL forms over water it is called the Marine Internal Boundary Layer (MIBL). The stable layer will trap the moisture within the shallow MIBL. Increases in moisture and decreases in temperature lead to the formation of a surface atmospheric duct (Garratt, 1990, cited in Brooks et al., 1999, p.1294). The evolution of the advection process may lead to sea fog with a duct near the top of the fog (Atkinson et al., 2001).

Additionally, an environmental duct over the Arabian Gulf is sensitive to any change in the boundary layer. The boundary layer is affected by (1) the meso-scale coastal configuration -

in the northern coast of the Arabian Gulf two marine areas separated by land mass have different amounts of moister air, potential temperature and vertical/horizontal wind speeds causing a variation in the duct top height from one marine area to another. (2) LSBC - boundary layer humidity, temperature and wind speed will be affected by the strength of the LSBC which depends on the land and sea temperature contrast. (3) Topography-steep topography increases the duct top height. (4) Ambient wind - In the southern coast of the Arabian Gulf sea breezes extend the propagation 100km inland in a layer 200m deep; this range and depth increases to 150km and more than 400m deep when the ambient wind blows from the same direction as the sea breeze (Atkinson & Zhu, 2006).

Furthermore, as the north-westerly flow comes off the Kuwait coast the air stream becomes cooler, more stabilized, and moister to create a MIBL. This commences as a few hundred meters deep, but gets deeper as it moves south reaching its maximum along the southern coast of the Arabian Gulf (Atkinson and Zhu, 2004).

The duct types are associated with the structure of the MIBL (Figure 2.18). During the daytime a surface duct occurs over the northern part of the Arabian Gulf due to the shallow MIBL, whist a surface S shape duct occurs over most of the Arabian Gulf waters. An elevated duct occurs over most of the UAE's land, and the far south-eastern water close to the Strait of Hormuz. A complex duct spreads over the Arabian Gulf with a low density, and increases in density around the coast of Qatar. At night, a surface duct occurs over most of the land mass as a result of radiative cooling. In contrast an elevated duct occurs on the eastern part of the UAE land and water areas whilst an S shaped duct occurs in the middle of UAE landmass; extending over most of the Arabian Gulf waters. Complex ducts occur

with a high density in some areas of the eastern and south-west parts of the UAE, whilst low density ducts occur over the Arabian Gulf waters (Atkinson and Zhu, 2005).

The duct top height in day-time exceeds 50m along the northern coast. However, that depth increases the duct top height as the air moves southward 300-400m to the middle of the Gulf and western part of the UAE. This increases to 500-700m in the middle and eastern part of the UAE. At night, the duct top height decreases to 200m and less in the western part of the UAE, but increases to more than 700m in the eastern part; it can reach 1000m over Ras Al Khaimah and Dubai. The duct top height over most of the Arabian Gulf waters was measured at approximately 200m except for the south-eastern part which was 400-600m. The surface duct top height which occurred over the landmass was 50m. Duct strength is directly proportional to duct top height (Atkinson and Zhu, 2005).

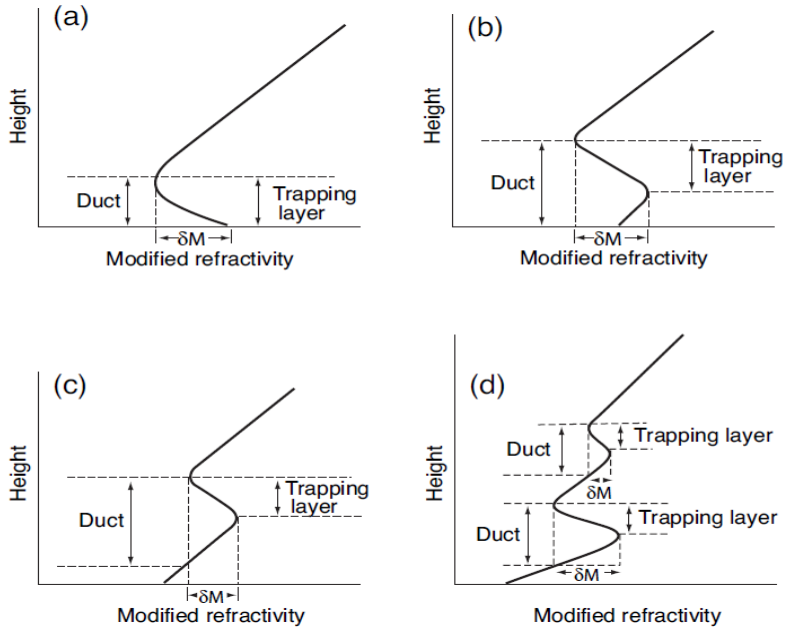

Figure 2.18. Illustrates the atmospheric duct types: where (a) simple surface duct, (b) surface S shape duct, (c) elevated duct, (d) complex duct. (Atkinson and Zhu, 2005).

2.5 Atmospheric duct measurement and prediction tools

Atmospheric refractivity or ducting can be measured by different means. For example, Phased array radar uses phase measurement of the ground clutter to measure and map the atmospheric refractivity (Cheong et al., 2005), satellites have been used by the Naval Postgraduate School (NPS) meteorology department to estimate duct conditions over large regions, the location and strength of elevated ducts, and which duct will reach the surface (Derley, 2006) and radiosondes, which are launched twice a day are used to indicate the duct height and depth by indicating sharp gradients of temperature and water vapour (Kingsley and Quegan, 1999, Willis, 2007). More recently, special software been used to predict the behaviour of electromagnetic wave propagation in the atmosphere. The Advanced Refraction Effects Prediction System (AREPS) is one of the freeware models to predict the electromagnetic wave propagation. AREPS is designed to calculate and present the electromagnetic wave propagation for tactical decision aids such as radar detection probability, ESM vulnerability and HF to VHF communications. The AREPS program is used by many research centres around the world (SPAWAR, 2006). Atkinson & Zhu, 2005 (2006) used AREPS to study the effect of a coastal area in radar propagation.

2.6 Conclusion

There are four objectives to be met in order to meet the study aim (section 1.4). Without doubt, analysis of the limited literature review has provided a good insight into the area of study. Due to its location, area of the study is situated within the Hadley cell subsidence zone and its wind pattern is part of the large monsoon cycle. Subsidence causes inversion at the top of the wind cycle which is one of the main part of the atmospheric duct. The

strength and height of the subsidence inversion changes with the variations of surface temperature (warmer temperature , higher in altitude and weaker inversion, cooler in temperature lower in altitude and stronger inversion), and pressure system (high pressure will lead to strong inversion, low pressure will lead to weak inversion).

In the winter period, the region is affected by the extension of the Siberian High Pressure. It retreats to the North for a few days allowing the Westerly Depression to pass, followed by strong North-westerly winds for a few days. Summer is affected by the Indian Monsoon which acts with the Mediterranean High to enhance North Westerly flow over the Arabian Gulf. Spring and autumn are the transit periods between winter and summer. Additionally, the effect of the global phenomena (NOA, AO, IOD, ENSO) has also been discussed in detail. There are three main winds affecting the area; the north-westerly wind (Shamal); the south-easterly wind (Suahili/Kaus), and the north-easterly wind (Al Nashi). Most of these facts will be discussed further in chapters 4, 5 and 6. The next chapter describes the data and method used in this study.

Chapter 3 – Methodology

This chapter describes data sources, validation methods and further approaches in methodology used in chapters 4, 5 and 6. The aims of this chapter are as follows:

- To present the reanalysis data and observations that have been used for this study.
- To validate the reanalysis data against the observation using statistical measures.
- To outline the procedure of analysis of data in the following chapters including the new methodology.

Section 3.1 describes the data sources, section 3.2 the data validation method and outcome, and section 3.3 describes further methodological approaches. The overall aim of this chapter is to find out to what extent the reanalysis data can be used to describe the meteorological condition of the southern coast of the Arabian Gulf, and then to illustrate methodological approaches for the following chapters.

3.1 Data sources

This study covers approximately thirty years (1981 -2010) of evolution of meteorological characteristics over the area of study. Gridded weather data and available observation data were used over this period in order to analyse the prominent wind patterns and to correlate these with global phenomena. The main sources of data were from the National Centre for Environmental Prediction (NCEP) and the National Centre for Atmospheric Research (NCAR), with measured wind from three locations: Abu Dhabi, Bahrain and Sharjah

airports. NCEP and NCAR data were considered preferable to the (higher-resolution) ECMWF ERA Interim reanalysis data due to the availability and accessibility of open-source software available to analyse the NCEP/NCAR data; by contrast ECMWF data would have required additional training to use the software needed to analyse it. Also, upper air soundings (Radiosonde data) were used to calculate the EM-wave propagation using the Advanced Refractive Effects Prediction System (AREPS) model (SPAWAR, 2006). The following sections will describe the NCEP/NCAR reanalysis data, observed wind data and radiosondes, along with validation of datasets. The electromagnetic (EM) propagation model (AREPS), used to assess electromagnetic propagation, will also be introduced.

3.1.1 NCEP/NCAR reanalysis data.

NCEP and NCAR have cooperated to produce a reanalysis dataset for more than 50 years of global analyses of atmospheric fields. Their aim is to support research and climate monitoring communities with data to enable them to study the past. It contains information from all available climatic data sources (Kistler et al., 2001). The NCEP/NCAR reanalysis uses a state of-the-art global data assimilation system and produces a database that is as complete as possible (Kalnay et al., 1996). The NCEP/NCAR reanalysis datasets are provided by the National Oceanic and Atmospheric Administration's (NOAA) Earth System Research Laboratory's (ESRL) Physical Sciences Division (PSD), http://www.esrl.noaa.gov/psd/).

The NCEP/NCAR reanalysis dataset has been available since 1948 with data assimilation using a wide variety of weather observations from ships, planes, RAdar OBServations (RAOBS), surface and upper air stations, satellites etc. The temporal resolution of the NCEP/NCAR reanalysis datasets includes daily data at 0Z, 6Z, 12Z, and 18Z and daily and monthly mean values. Spatially, it covers the whole globe with 144x73 grid points and a horizontal grid resolution of 2.5^{o}x 2.5^{o}. It covers 17 isobaric levels and 28 sigma levels vertically, and provides most of the key meteorological parameters such as mean sea level pressure, wind, temperature and humidity (Kalnay et al., 1999).

3.1.2 Observed wind data

The present study considered surface meteorological observations obtained from Abu Dhabi (WMO41217, 24^{o}N54^{o}E), Bahrain (WMO41150, 26^{o}N50^{o}E), and Sharjah (WMO41196, 25^{o}N55^{o}E) airports. Bahrain is situated in the middle of the Arabian Gulf where the Shamal winds first enter the study area. Abu Dhabi and Sharjah are situated along the UAE coast, which is at the southern part of the study area. Figure 3.1 describes the locations of the observation points and Table 3.1 shows all the variables and periods of the available data from each of the stations. Statistically, missing data represents 1.9% of the total period for Abu Dhabi, and 3.5% of the total period for Sharjah. Where data is not available from the original local sources, then reanalysis data was used in order to study the synoptic situation and to establish correlations.

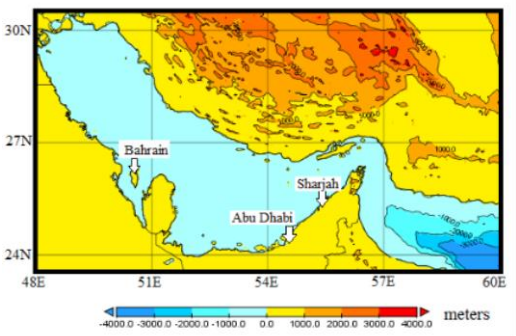

Figure 3.1. Locations of the three observational sites (Bahrain, Abu Dhabi, Sharjah). (Map from http://www.ngdc.noaa.gov/mgg/global/).

Table 3.1. Name of the stations, variables and periods of the data provided.

Stations	Variables	Period
Bahrain	Wind speed (knots) Wind direction (deg) Temperature (Celsius) Mean SLP (hPa)	1981 – 2010
Abu Dhabi	Wind speed (knots) Wind direction (deg)	1982 – 2010
Sharjah	Wind speed (knots) Wind direction (deg) Temperature (Celsius) Relative humidity (%) Pressure (hPa) Visibility (km) Cloud cover/type	1949 – 2010

3.1.3 Radiosondes

The NOAA/ ESRL radiosonde database archive consists of a North America archive which starts in 1946 and an international archive which starts in 1994. Datasets were produced by ESRL Global Systems Division (GSD). In 2007 all available Global Telecommunications

Service (GTS) radiosonde observations were merged with the dataset from the National Climatic Data Centre (NCDC) Integrated Global Radiosonde Archive (IGRA). Updates of the radiosonde database archive are available through the Global Telecommunication Service (Govett, 2014). Upper-air sounding data for most airports in the world are available from http://esrl.noaa.gov/raobs/. The data can be viewed in a number of different ways, for example as raw data or listed in columns headed with upper-air sounding meteorological parameters or plotted on a sounding graph (e.g. skew-T diagram). In this study, raw data from Abu Dhabi airport is used in the EM propagation Model to get a propagation conditions summary.

Skew-T diagrams will be used to illustrate the important changes in the meteorological parameters (temperature, dew point and wind) with height. An example, with an explanation, is included at Figure 3.2.

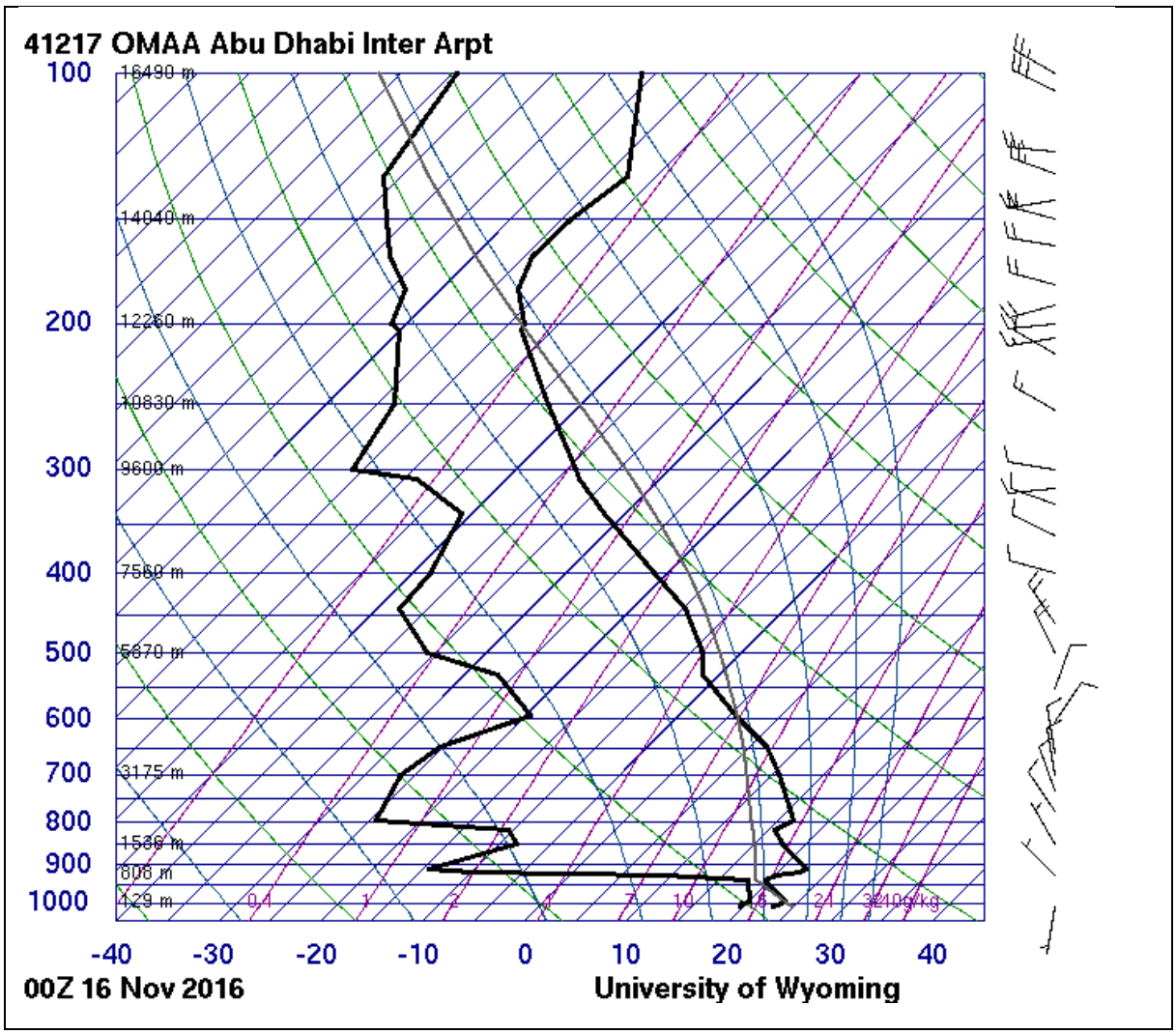

Figure 3.2. In the top-left are the airport/station identification details and running down the left hand side is pressure (mb) and height (in metres). Temperature (C) runs along the bottom, and wind speed and direction are found on the right hand side. The two bold black lines are the air temperature, to the right, and dew point, to the left. Generally, it is used to show differences in temperature and humidity at height; where the lines are close together the air is humid, and where they are far apart, the air is dry. Within the skew-T, the straight, purple lines are the saturated humidity mixing ratio (g/kg) and the straight blue lines at 45 degree angle to the right of the vertical are the isolines, joining points of equal temperature. The curved green lines show the dry adiabatic lapse rate and the curved blue lines show the pseudo-adiabatic moist lapse rate.

3.1.4 Electromagnetic (EM) propagation model (AREPS)

AREPS Version 3.2 is used in this study to examine EM propagation. It is provided by the Space and Naval Warfare System Centre in San Diego (Atmospheric Propagation Branch). The AREPS model calculates and displays EM-wave propagation (height, range, and bearing) to assess the effect of the atmosphere and terrain upon the performance of EM systems working in the range 2 MHz –57 GHz. Radar detection probability, Electronic Support Measures (ESM) vulnerability, and communications assessments are based on EM system parameters such as frequency, peak power, pulse length and rate etc. All calculations depend on atmospheric refractivity data derived from radiosondes (SPAWAR, 2006). AREPS Version 3.2 will be used in this study to assess EM propagation variability under different meteorological conditions.

Input parameters include vertical profiles of pressure (P) in millibars, air temperature (T) in (^{o}C), and dew point (Td) in (^{o}C). The data is acquired from radiosondes (weather balloons) and as such, the resolution is variable depending on local conditions and practices. The AREPS model uses modified refractivity (M) to examine electromagnetic wave propagation in the atmosphere (equation 3.1). M is calculated from the Earth's surface up to the high altitude covers the significant layer of atmospheric refractivity influenced. The effect of modified refractivity on electromagnetic propagation is explained in section 2.1.1.

$$M = N + \frac{z}{R} \times 10^{6} \tag{3.1}$$

Here z Is the altitude in metres above the sea level, R is the earth radius and N is refractivity of air that contains water vapour and given as

$$N = \frac{77.6}{T}\left(p + 4810\frac{e}{T}\right) \tag{3.2}$$

e is the water vapour pressure in millibars and given by

$$e = 6.11\ X\ 10^{\left(\frac{7.5\ X\ T_d}{237.3\ +T_d}\right)} \tag{3.3}$$

More details about the modelling components and the process included can be seen in Patterson (1998). The atmospheric refractivity summary includes the refractivity type, height, and base/top of the refractivity channel (figure 3.3). Furthermore, the AREPS model enables the user to simulate electromagnetic wave energy in selected atmospheric conditions.

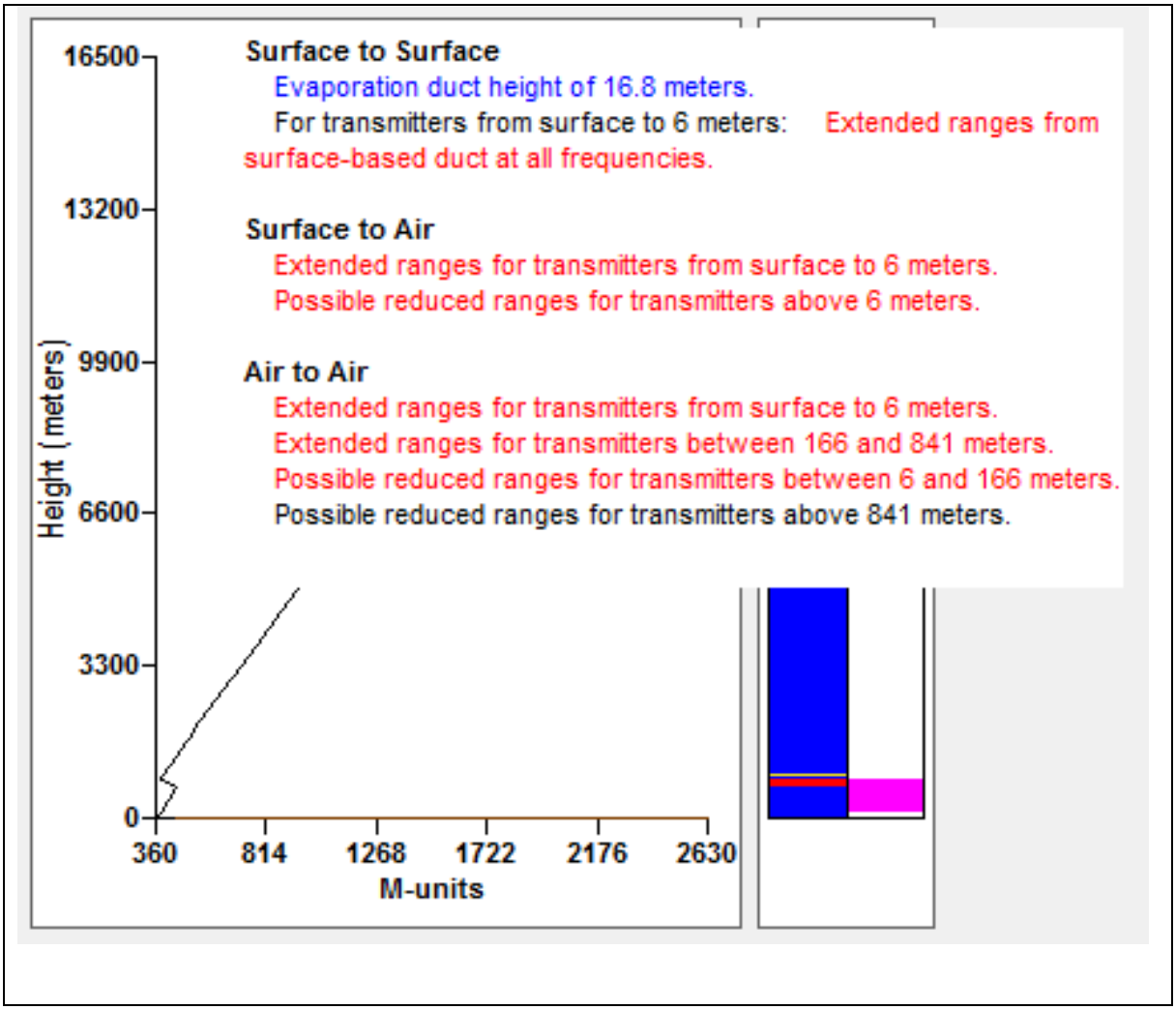

Figure 3.3, illustrates the variation in modified refractivity (M units) with height. This is a screengrab from the AREPS software. The input data was for 16 November 2016 and its graph represented in Figure 3.2. The area affected by ducting is shown in pink, with trapping in red and normal conditions in blue; the text shows effects on various EM equipment.

3.2 Data validation

This section describes the procedure for the preparation of the dataset described in section 3.1 and the methods of analysing the data. This analysis is necessary to determine to what extent the data are reliable enough to be used in the remainder of the study. Finally, the result of validation of the reanalysis data is presented.

3.2.1 Method

NCEP/NCAR reanalysis data are in Network Common Data Form (NetCDF) format. They can be only viewed as a spatial plot of daily, monthly and seasonal averages. (http://www.esrl.noaa.gov/psd/cgi-bin/data/composites/printpage.pl). An additional data process was involved to calculate the daily mean time series of reanalysis data for locations in the study domain (Figure 1.1). NCEP/NCAR wind speed and direction (four readings per day every six hours) were downloaded from the NCEP website and daily average values were calculated. Downloaded NetCDF files must be converted into ASCII format. Therefore, two types of software have been developed specifically for this study to deal with NCEP/NCAR NetCDF files. First, there is a tool which extracts NCEP/NCAR data into a readable format and then the second tool allows extraction of data for the location of interest from the NCEP/NCAR readable format data.

Additionally, Matlab software codes were developed to calculate mean values from the NCEP/NCAR data for the study area. As has been mentioned in the site description (Chapter 1), topography surrounding the area of the study is not the same throughout. For example, data observed in the Zagros Mountains will be different from data observed on Bahrain Island due to the difference in their height from sea level and the sheltered conditions surrounding some of the mountain weather stations. Therefore, NCEP/NCAR data are averaged over the study domain (24-27N, 50-56E), and validated against observations.

3.2.2 Statistical metrics

The reanalysis wind data at the locations of observations and the area averaged wind reanalysis data from NCEP/NCAR were validated against wind observations from the three airports. The validation of wind direction from the reanalysis was carried out using wind rose figures and the wind speed validated using various statistical measures. Statistical calculation for validation include mean average (equation, 3.4), standard deviation (equation, 3.5), correlation coefficient (equation, 3.6), bias (equation, 3.7), and root mean square error (RMSE) (equation, 3.8), as follows:

$$\mu = \frac{\sum x}{N} \tag{3.4}$$

μ is the mean value, $\Sigma$is a total, x is the value, and N is the number of values.

$$\sigma = \sqrt{\frac{\sum(x-\mu)^2}{N}} \tag{3.5}$$

σ is the standard deviation x is the value, μ is the mean value, $\Sigma$is a total, and N is the number of values.

$$\rho_{xy} = \frac{\sigma_{xy}}{\sigma_x \sigma_y} \tag{3.6}$$

The correlation coefficient (ρ_{xy}) is calculated by dividing covariance by the standard deviation of both x and y. Covariance tells how reanalysis and observation are related; positive covariance means that they are positively related while negative covariance are inversely related.

$$BIAS = \frac{\sum_{i=1}^{n}(\hat{x}_i - o_i)^2}{n} \tag{3.7}$$

$\hat{x}_i$ is the modelled value, o_i is the observed value.

$$RMSE = \sqrt{\frac{\sum_{i=1}^{n}(\hat{x}_i - o_i)^2}{n}} \quad (3.8)$$

RMSE tells how reanalysis data will behave and give a more accurate value of the deference between reanalysis and observations; however, the mean BIAS will illustrate swhether the reanalysis data are under or over-estimated relative to the observations.

3.2.3 Validation results

In order to assess the usefulness of the reanalysis data for further analysis, a comparison between NCEP/NCAR reanalysis and the airport wind observations has been carried out. This investigation identifies the differences between reanalysis wind data (speed and direction) and the observations. There are no widely accepted criteria in existence but there is a guideline for model performance established by c. In this, maximum permissible errors are:

- Wind Speed [RMSE $\leq$ 3.9 knots, Mean Bias $\leq \mp$ 1 knots]
- Wind Direction [Gross Error $\leq$30 deg Mean Bias $\leq \mp$ 10 deg]

The gridded wind data from the NCEP/NCAR reanalysis was interpolated (using the tools described in paragraph 3.2.1) for the locations of available observations (Bahrain, Abu Dhabi, Sharjah). Comparison between NCEP/NCAR reanalysis and the available observations at the locations was completed to find out if it was good enough to replace the observations.

3.2.3.1 Wind speed validation

The daily mean wind speed data from the NCEP/NCAR reanalysis at the location of the observations and area averages were compared with observations (1981-2010) at the three locations. Table 3.2 shows that the average as well as standard deviation of daily mean wind speed from the observations is consistently lower than for the gridded daily mean wind speed from NCEP/NCAR for all sites except that the area-averaged value at Bahrain is slightly lower than the observation.

The highest correlation coefficient for wind speed is observed at the Bahrain site (0.75). Furthermore, the correlation coefficient and mean bias values at the location of the observation were better than the area-average for Sharjah and Abu Dhabi. Generally, the NCEP/NCAR reanalysis data overestimates the observed values at all locations (positive bias values) except the area-average value at Bahrain. The NCEP/NCAR reanalysis bias values at the location of the observation were within the Emery and Tai (2001) accepted range for Abu Dhabi and Bahrain. The NCEP/NCAR area average achieved the accepted value only at the Bahrain location.

The high bias values for Sharjah, along with the fact that the local topography (explored in Chapter 4.1) reduces its exposure to the Arabian Gulf wind systems of the study, and therefore its utility, means that this data was rejected as the efforts required to correct this bias were not considered worthwhile.

RMSE values were high, but within the guidelines for model performance established by Emery and Tai (2001), based on their experiences with Texas ozone events. The minimum RMSE values were 2.56 knots for Bahrain and the maximum was 3.4 knots for Sharjah. The RMSEs of area average values were better than the point values for Abu Dhabi and Bahrain.

Generally, the NCEP/NCAR area averaged RMSE was better than NCEP/NCAR at the location of the observation. In contrast the mean BIAS was better at the location of the observation than the area average value. Furthermore, the wind speed validation illustrates that the area average value for Bahrain provided the best correlation, RMSE and mean bias compared to the other two stations. The statistical analysis shows (Table 3.2) that the model result at Bahrain and Abu Dhabi agreed reasonably well with the observation in term of lesser mean BIAS and RMSE. In further analysis Bahrain and Abu Dhabi will be considered as the primary sources of data.

Table 3.2. Illustrates the result of the daily wind speed statistical calculation to validate NCEP data against the observations. Highlighted values are those which fall outside of the acceptable limits (Emery and Tai (2001)). Point values relate to the location of the observation whilst area values relate to the area (24-27N, 50-56E). Wind speeds are recorded to WMO standards and corrected to a standard height of 10m above ground level.

Locations	Parameters	Average in knots	Standard Deviation in knots	Correlation coefficient	Mean Bias≤ ∓ 1 knots	RMSE ≤ 3.9 knots
Sharjah	NCEP (point)	7.6	3.3	0.60	1.58	3.09
	Observation	6.0	1.8			
	NCEP (Area Average)	8.3	2.9	0.53	2.31	3.40
Abu Dhabi	NCEP (point)	7.4	3.6	0.56	0.28	3.02
	Observation	7.2	2.1			

	NCEP (Area Average)	8.3	2.9	0.50	1.14	2.85
Bahrain	NCEP (point)	9.6	4.5	0.75	0.66	3.06
	Observation	8.9	3.8			
	NCEP (Area Average)	8.3	2.9	0.75	-0.60	2.56

3.2.3.2 Wind direction validation

The validation of the wind direction is illustrated in Figure 3.4; wind roses are used rather than a table as they offer a better representation of directional data. It shows the comparison between NCEP/NCAR reanalysis and the observations at the three locations represented as wind roses. Validation was carried out for the total wind direction at any speed and for the wind direction at wind speeds of 11 knots and more, which could represent the synoptic wind.

Consideration of the NCEP/NCAR area average shows that the main wind direction was north westerly. Furthermore, Bahrain achieved the best correlation in the wind direction with the area average among the three stations (visual inspection of Figure 3.4). Abu Dhabi was the second best correlation. The area average was not a good estimation for the Sharjah location due to the complex topography (details are discussed in Chapter 4).

For NCEP/NCAR at the location of the observation, the daily mean observed wind direction at Sharjah was a noticeably lower frequency from the northeast and southwest directions. The frequency of the south-westerly wind direction was overestimated and the northerly wind was underestimated. Additionally, the strong wind comes from the west in

observations and from northwest in the NCEP/NCAR reanalysis. At Abu Dhabi, NCEP/NCAR wind data at the location of the observation was overestimated from the southwest, south and southeast while underestimated from north, northeast and east directions. The stronger wind direction compared well between the NCEP/NCAR reanalysis and observations except for the wind from the north where it showed underestimation. Finally, at Bahrain, the northerly wind is underestimated and the southerly wind overestimated. The stronger wind direction was well captured in the NCEP/NCAR reanalysis but this underestimates the northerly wind. These results confirm that the area average reanalysis data and the reanalysis at Bahrain and Abu Dhabi were closer to the observations.

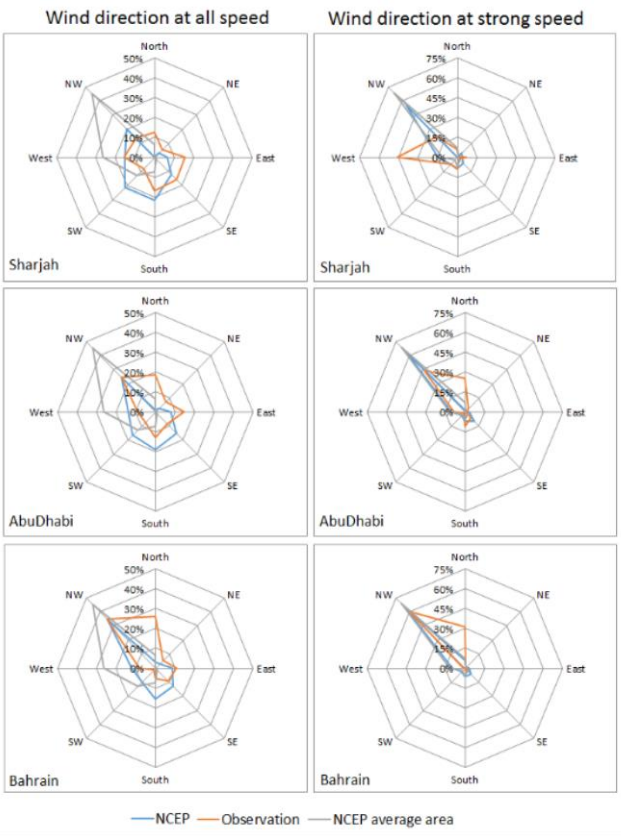

Figure 3.4. Results of the comparison between NCEP/NCAR reanalysis (at point and area average) and the observations at three locations, represented in wind rose figures. The total wind direction is in the left hand column and the synoptic (>11 knots) wind direction in the right hand column.

3.2.3.3 Summary of the validation result

A comparison of reanalysis wind speed data against observations for the three locations indicates that the gridded data were within the allowed error for Bahrain and Abu Dhabi but not for Sharjah. The NCEP/NCAR reanalysis data showed high values of RMSE in comparison to observed wind speeds. Furthermore, a visual inspection of the wind direction confirmed that the NCEP/NCAR reanalysis data were in close agreement with the observations. This could be attributed to misrepresentation of topography (explained in the next chapter) as well as the low resolution of NCEP/NCAR reanalysis data. However, NCEP/NCAR reanalysis data is a vital tool since it covers all the layers of the atmosphere, which is not available from the observations. A regional climate model output is not

available. In this study, NCEP/NCAR data were mainly used to analyse the synoptic situations and represent the relation between different atmospheric systems, despite their failure to perfectly capture conditions at the three specific ground level locations examined.

3.3 Further methodological approaches

The local meteorological analysis, analysis on the Shamal wind and the influence of meteorological conditions on EM propagation are described in the following sections.

3.3.1 Local meteorological analysis

Local statistical analysis was carried out on thirty years (1981-2010) of wind observation data from Bahrain, Abu Dhabi, and Sharjah to find out the dominant wind patterns over the region. Then, the impact of the topography on the local meteorology was studied. Furthermore, the main components behind the dominant wind patterns over the region were recognized using diagrams of the 500mb geopotential height, Sea Level Pressure (SLP) and wind at 250mb from NCEP/NCAR reanalysis data. Lastly, the period of the main components that affect the wind pattern over the region were identified. This enabled the study of the seasonal variation of the main regional meteorological feature (the Shamal wind) over the study area. The results from these investigations are presented in Chapter 4, Sections 1, 2, and 3.

3.3.2 Shamal Analysis

In order to predict future wind patterns, the yearly mean wind strength was reviewed via time series analysis. To provide further information across the entire area, the area averaged wind speed was calculated using NCEP reanalysis. Also, the same process was carried out for the number of Shamal days to identify its correlation with the total wind (Chapter 5, Section 1). Correlation results will indicate significance in the variation of Shamal days. Additionally, the Mann-Kendall trend test (discussed in Chapter 5) was applied to assess the level of significance to all trends in time series data.

3.3.2.1 New methodology

This approach is to introduce a measure of persistence of Shamal wind (and associated weather system) by calculating the number of Shamal days and non-Shamal days. Criteria of a Shamal day is defined as a day when the prevailing wind blows from the north-westerly (270-360 degrees) sector over the Arabian Gulf with a mean wind speed of 11 knots more. Statistical analysis is performed using the number of Shamal days. The study period (thirty years) was separated into years of positive (above average) and negative (below average) numbers of Shamal Days based on the analysis of observational data. To avoid any lack of clarity in the low resolution reanalysis, the years of positive and negative Shamal Days are grouped separately into NCEP/NCAR charts.

Reanalysis data were used to test the significance of the atmospheric pressure fluctuation against Shamal Days variations by applying an ANalysis Of VAriance (ANOVA) test; a statistical hypothesis test and form of linear regression analysis, which incorporates mean squares and F-tests as a measure of whether the means of groups of variables are statistically significant, in this case to examine temporal trends. ANOVA tests limit false

positives and false negatives to a significance level, and are used to establish statistical inference and provide, amongst other figures, a P-value of statistical significance; any figure below 0.05 is considered a significant trend. Time series data for the Shamal Days and associated atmospheric systems were normalized. The results from these investigations are presented in Chapter 5, sections 2 and 3.

3.3.3 EM propagation analyses

The influence of each meteorological condition on EM-wave propagation was examined by uploading associated radiosonde data for each condition into the AREPS model, which predicts radar propagation performance in the assigned environment. Subsequently, the details of available radars were used to simulate EM wave propagation in the assigned environment. The AREPS model gave a summary of the refractivity which could be standard or super/sub refractivity. The height and range of the super or sub EM propagation refractivity was compared between all meteorological conditions. Furthermore, reasons for particular refractivity conditions were explained to build a rule of thumb to facilitate EM propagation. The results from these investigations are presented in Chapter 6.

3.4 Conclusion

NCEP/NCAR reanalysis wind data agreed reasonably well with the observational wind data at Bahrain and Abu Dhabi. Therefore, both observational and reanalysis data can be used for further analyses to find out the wind pattern effecting the study area. Observational data were used mainly for statistical analyses while NCEP/NCAR reanalysis data was used to analyse the synoptic situations and represent the correlation between different atmospheric systems (in Chapter 4 and 5). The methodological approaches were mainly statistical

analyses and the AREPS model (Chapter 6) was used to examine EM propagation in different air masses.

Chapter 4 - Local meteorological characteristics

This chapter has two objectives. The first objective is to introduce the local meteorology of the study area and to specify the different air masses (warm/cold, moist/dry) that affect the area. Identification of the sources of the air masses will be used to examine the EM propagation. The second objective is to identify a general regional feature that characterizes its meteorology; this feature once identified will be analysed to find its connection with the global circulation pattern (Chapter 5). This will enable predictions of seasonal variations over the region. To achieve these objectives this chapter is divided into three sections. The first section describes the topography of the area and its influence on the wind circulation.

The main components behind the dominant wind pattern are described in the second section. The last section covers the various meteorological conditions and their seasonality.

4.1 The topography and wind circulation

The aim of this section is to illustrate the effect of the topography on wind circulation over the region. It is divided into two subsections; the first subsection describes the topography of the area, and the second subsection shows the effect of the topography on wind circulation.

4.1.1 The topography of the area

The study area is located between three mountain chains (Zagros, Hajar and Hijaz mountains). Figure 4.1 shows the topography of the study area. In this regard, the Arabian Gulf has a bowl-like morphology. To the north of the study area, there is a sharp elevation 3000 - 4000 metres (Zagros Mountains). To the east, the Hajar Mountains (1500 - 2500 metres) extend from the Strait of Hormuz along the southern coast of the Gulf of Oman and are separated from the Arabian Gulf by desert. The desert narrows to the north near the Strait of Hormuz and then gradually increases in breadth southwards. In the south and west, the desert gradually increases in height. The western desert extends approximately 500km to the west and ends with the Hijaz Mountains which reach a height of approximately 2000m.

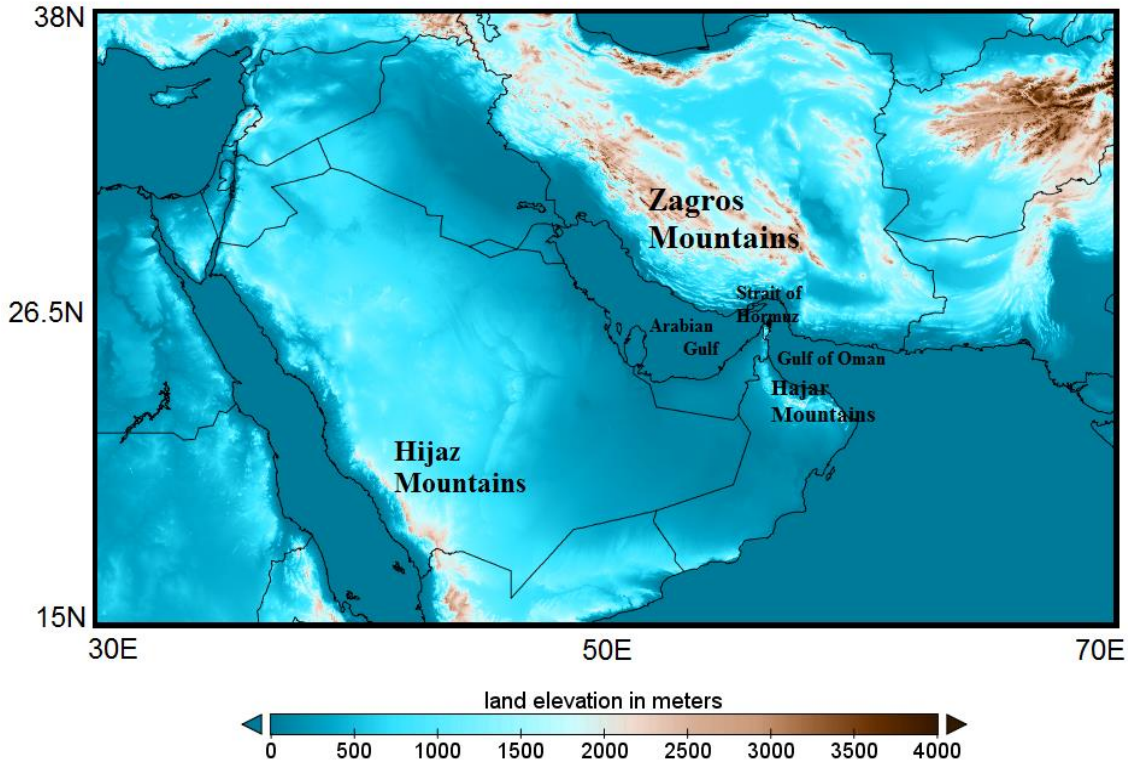

Figure 4.1. Topography of the area of study which shows a bowl-like morphology for Arabian gulf. (Map from http://www.ngdc.noaa. gov/mgg/global/).

4.1.2 The effect of the topography

The effect of topography on the wind pattern is discussed in the following sections: wind direction, wind strength and wind direction at different strengths. This illustrates how the wind pattern is affected by topography.

4.1.2.1 Wind direction

The most important factors arising from the analysis of wind direction data (Figure 4.2) occurring during the period of study for the three stations (Bahrain, Abu Dhabi, and Sharjah) reveal the impact of topography on wind circulation. The effect of topography (*e.g.* mountain ranges and desert) and coastal configuration (*e.g.* its L shape) are clear, especially in Abu Dhabi and Sharjah, with less obvious effects in Bahrain. The occurrence

of the South-easterly wind over Sharjah is more frequent than other sites (Figure 4.2). This could be due to the katabatic effect of the Hajar Mountains. The katabatic effect enhances the south-easterly flow and resists the north-westerly flow over Sharjah. But the katabatic effect has less influence over Abu Dhabi due to the greater distance from the Hajar Mountains. This topography has slight or no effect on Bahrain.

Bahrain is a small island in the middle of the Arabian Gulf, situated in the north west of the study area, where the north-westerly winds first enter the study area (Figure 1.1). Sixty percent of the winds over Bahrain are from a north and north-westerly direction (Figure 4.3). In comparison, Abu Dhabi, situated between two physical masses (land and sea), is affected by north and north-westerly winds 40% of the time; this is due to land and sea breeze circulation and coastal configuration. Sharjah has similar conditions to Abu Dubai, even though its location is further north; north and north-westerly winds over Sharjah were 26% of the total winds affecting the area.

The occurrence of north-easterly and south-westerly winds is less frequent over the three sites. This could be due to the following factors:

- The Zagros Mountains block any north-easterly winds coming from Asia.
- The Abu Dhabi and Sharjah coastal configurations, which extend north-east to south-west, create land and sea breeze circulations which impact mostly from north-westerly and south easterly directions.

- As a result of its location and land and sea configuration (as a relatively small island), there are minimal south-westerly winds occurring over Bahrain (Figure 4.2).

Figure 4.2 also indicates that north-westerly winds clearly occur more often than any other wind direction over Bahrain and Abu Dhabi whilst in Sharjah south-easterly winds occur more often than north-westerly winds.

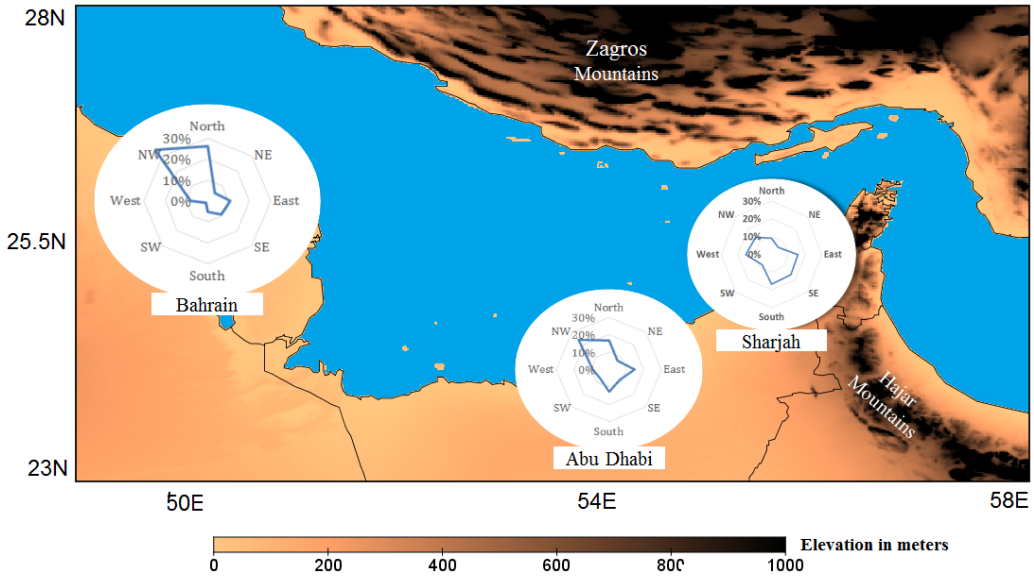

Figure 4.2. Topography and thirty years (1981-2010) wind direction for the three sites (Bahrain, Abu Dhabi, and Sharjah); figure shows how wind directions vary with location due to the topography and coastal configuration.

4.1.2.2 Wind Strength

To simplify the study, the Beaufort scale was used to categorise wind strength into four categories (Table 4.1).

Table 4.1, Beaufort scale wind strength categories.

Wind category	**Wind strength**
Light	6 knots and below
Gentle	7-10 knots
Moderate	11-16 knots
Fresh and strong	17 knots and above

The results of calculating the percentages of occurrence for different wind strengths (light, gentle, moderate, fresh and strong) throughout the period of study are shown in Figure 4.3. It is immediately obvious that Bahrain's wind speeds are stronger than those which occur in Abu Dhabi and Sharjah. Light wind speeds comprised 63% of the total over Sharjah, 50% over Abu Dhabi and 37% over Bahrain. Gentle, moderate, fresh and stronger winds were 63% of the total over Bahrain, 50% over Abu Dhabi, and 37% over Sharjah.

4.1.2.3 Wind direction at different strength

The percentages of occurrence of each wind direction at different wind strengths throughout the period of study are illustrated in Figure 4.3. There are clear differences between the three sites which can be summarized as follows:

- Light wind speeds over Bahrain occur more than 10% of the time in most directions, decreasing in a south and south-westerly direction to 5% and less. Light wind speeds occur over Abu Dhabi with approximately 10% occurrence in each direction. A major light wind direction over Abu Dhabi is easterly with 22% occurrence of the total light winds. Over Sharjah, the main directions of light wind speeds are south-easterly,

easterly and southerly with 23%, 21% and 18% of occurrences respectively; between 5-10% of light winds occur in the remaining directions.

- As winds become stronger (gentle), they move towards the north-west and all other directions are minimized. Furthermore, moderate, fresh and strong winds are for the most part from a 270-360 degree direction (Shamal wind). The second most frequent 'moderate and above' wind strengths are to be seen in the south to the east sector, (Suhaily wind). Such conditions occur some 15% of the time over Abu Dhabi and Sharjah, but in contrast, less than 1% of the time over Bahrain. North-easterly (Al Nashi) winds rarely occurred, with less than 5% 'moderate and above' found over Abu Dhabi, whilst it is negligible over Sharjah and Bahrain due to the Hajar Mountain barrier and Zagros Mountains respectively.

4.1.3 Summary for the topography and wind circulation

It is apparent from the statistical analysis of thirty years (1981-2010) of wind observation data presented in Figure 4.3 that the Shamal wind is the dominant wind pattern over the region. It constitutes 85% of the 'gentle and above' wind strengths, which agrees with the study by Govinda et al. (2001). Furthermore, because of its location, Bahrain is less affected by topography and coastal configuration compared to other stations. Therefore, the Shamal wind is more evident in the wind data over Bahrain.

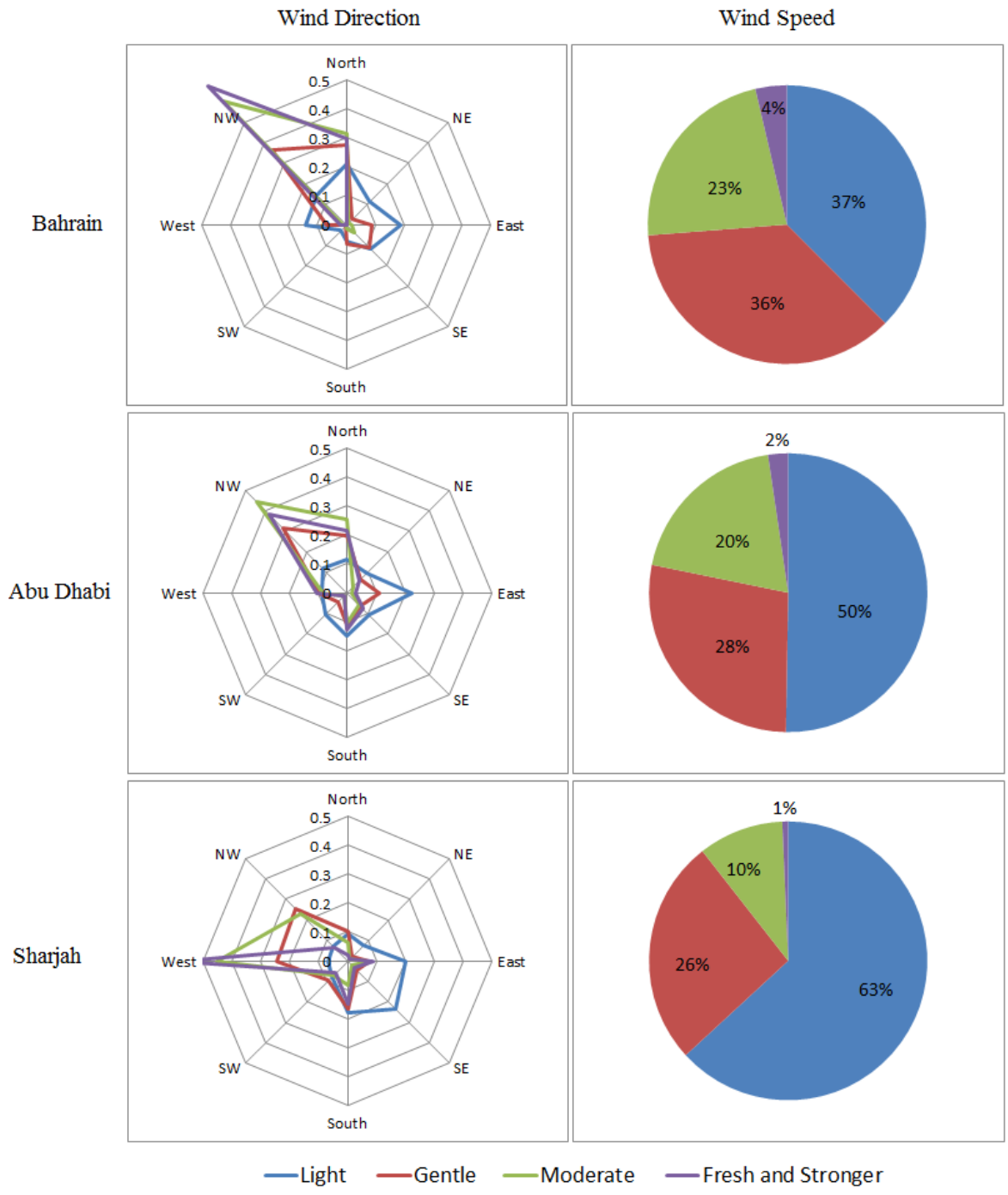

Figure 4.3. A combination of thirty years (1981-2010) observational wind direction and speed for Bahrain, Abu Dhabi and Sharjah. The wind categories (light, gentle, moderate and fresh) were taken from the Beaufort scale.

4.2 The main components responsible for the dominant wind pattern

As described in the previous section, the study area is affected mainly by the Shamal, less so by the Suhaili and rarely by Al Nashi. Local winds such as land/sea breezes and the Hajar Mountains' katabatic winds also affect the study area. The aim of this section is to illustrate the main components behind each wind pattern. Therefore, this section is divided into two subsections which describe the synoptic winds and the local winds respectively.

4.2.1 Synoptic wind.

The approach for this subsection is to calculate the monthly frequency of three synoptic winds by identifying them based on the characteristics presented in section 3.3.1. A case-study wind event is then selected for each of the synoptic and local winds to help identify the main components driving each of the wind patterns over the region.

4.2.1.1 Synoptic wind monthly frequency

Figure 4.4 illustrates the monthly frequency of 'moderate and stronger' Shamal, Suhaili and Al-Nashi days. There were significant differences between the number of occurrences of Shamal days and other winds. Because of their location and topography, the number of Shamal days was calculated from Bahrain observational data as Bahrain best captures the presence of Shamal. The number of Suhaili days was calculated from Abu Dhabi observational data as Abu Dhabi most obviously observes the presence of Suhaili, whilst NCEP/NCAR is the best dataset in which to capture Al-Nashi wind because of a lack of observational data available in the north east of the study area. Shamal and Suhaili winds were observed in all months while Al-Nashi was observed only during December, January

and February. Therefore, Shamal and Suhaili winds were analyzed during the winter and summer meteorological seasons to find out the main components behind them as they persist throughout the year while Al-Nashi were analysed during the winter only.

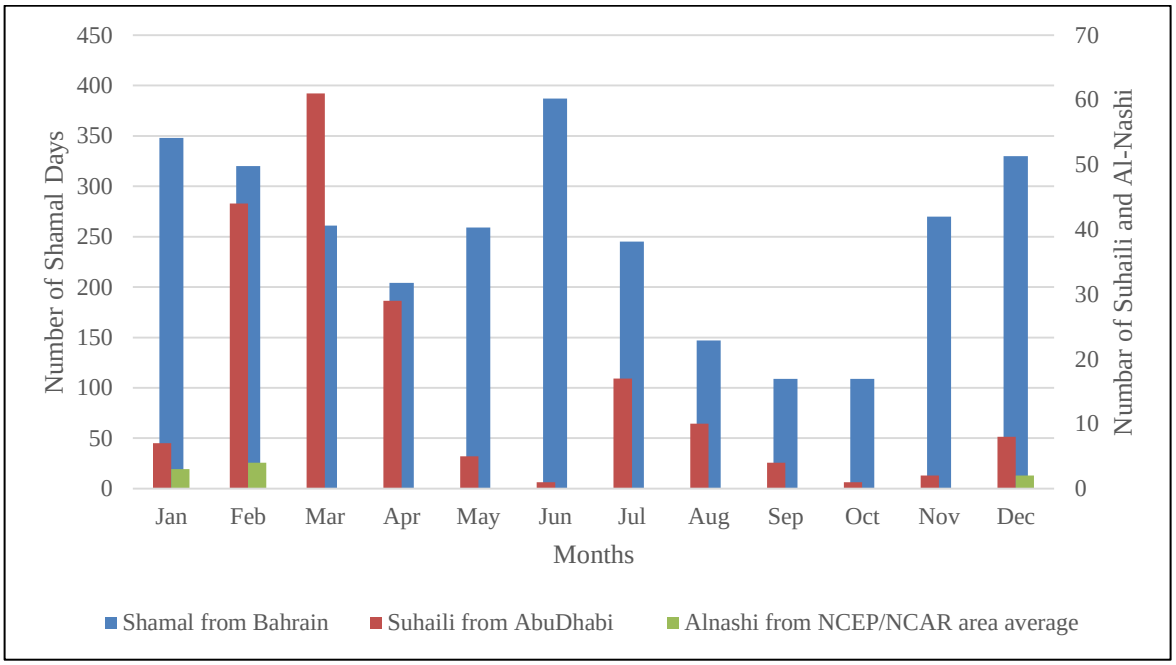

Figure 4.4. Variation in the frequency of moderate and stronger Shamal (left Y axis), Suhaili and Al-Nashi days (right Y axis) throughout the period of the study. Due to the topography effect each synoptic wind was represented from the best site that shows its magnitude.

From the analysis of thirty years of data, five case studies were selected to represent each meteorological condition based on observational wind data. The particular days were selected based the wind appearing in all or most of the sites. These days are as follows:

- Winter Shamal day- 7 February 2010
- Summer Shamal day - 28 June 2005
- Winter Suhaili day - 2 February 1993
- Summer Suhaili day - 28 July 1987
- Al Nashi day - 28 January 2007

These case studies are not definitive examples, but they demonstrate the general characteristics of each of the synoptic winds.

4.2.1.2 Winter Shamal Days (WSD)

Based on observational wind data, a typical winter Shamal day (7 February 2010) was selected (WSD; see Table 4.2), and used to characterise the main features of a Winter Shamal Day. A Shamal day is defined in paragraph (3.3.2), then the winter period is considered to be from November until April as defined in paragraph 4.3.1. Winter Shamal day features are not limited to those apparent on this day but it is verified that the general characteristics of all winter Shamal days are similar.

Table 4.2. Wind data for three sites and NCEP/NCAR area average on the 7th February 2010 which was considered to be a WSD over the area of study (paragraph 4.1.2.3 explains the variation in the recorded wind direction and speed).

Location		Bahrain	Abu Dhabi	Sharjah	NCEP/NCAR area average
Daily Mean Wind	Direction	330	310	263	319
	Speed	20	12	11	18

Figure 4.5 shows the meteorological conditions prevailing on a typical Winter Shamal Day. The NCEP/NCAR sea level pressure map distribution shows a low pressure system set to the east of the study area and high pressure extending over Saudi Arabia in the west (Figure 4.5c), resulting in a strong north-easterly gradient over the study area. The Abu Dhabi radiosonde profile (Figure 4.5d) at1600 local time illustrates how temperature, dew point and wind varied with height; the wind was north-westerly from the surface to 700mb,

becoming westerly and south-westerly at higher levels. The NCEP/NCAR 500mb geopotential height (Figure 4.5b) shows the location and extension of the Rossby Wave and associated trough. A trough extends from the north to the north-west of the study area causing a south-westerly to westerly flow at 500mb. Moreover, the NCEP/NCAR 250mb vector wind (Figure 4.5a) depicts the usual location and strength of the associated jet stream during a Winter Shamal Day.

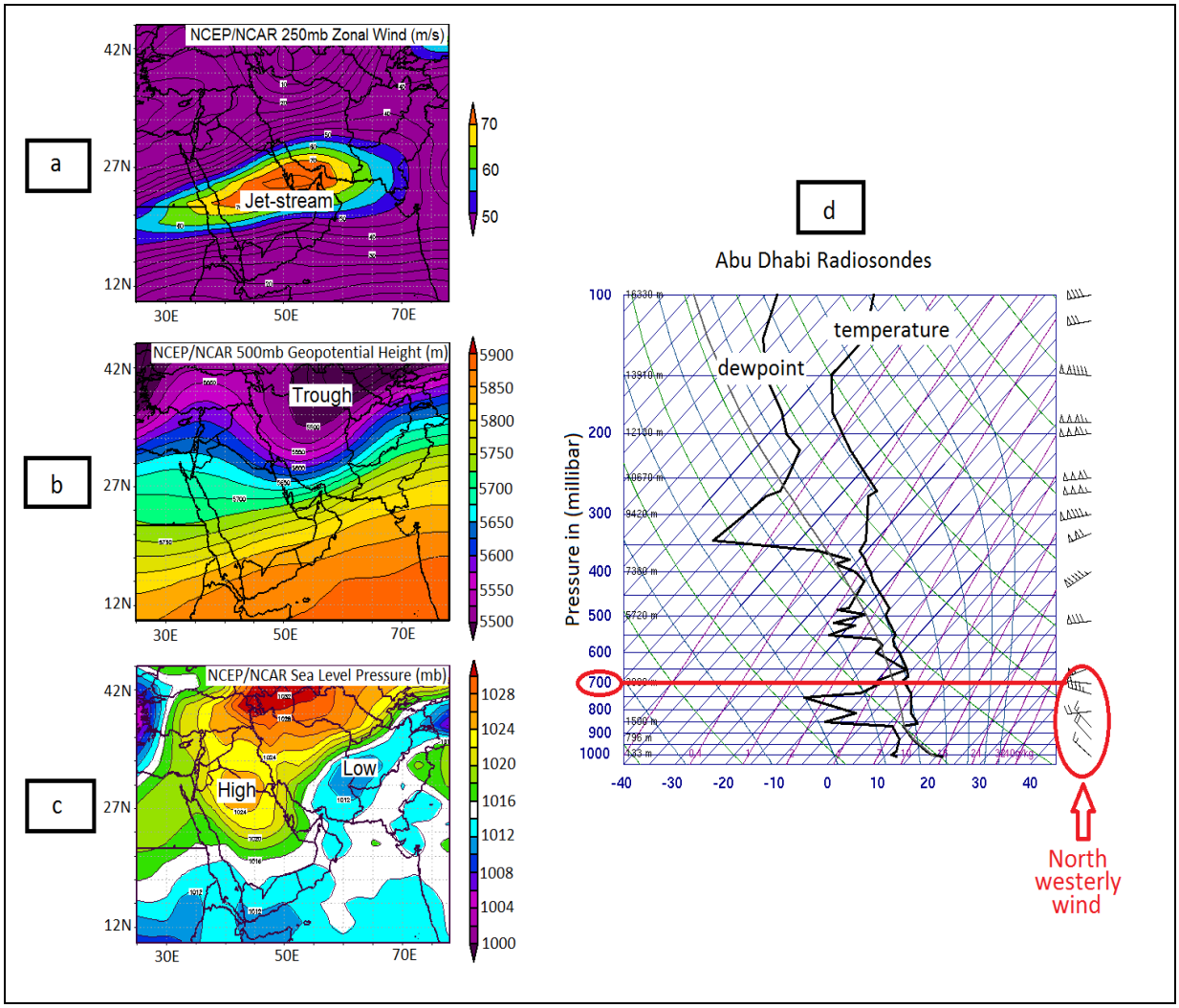

Figure 4.5. The meteorological conditions on a typical Winter Shamal Day over the study area on 7th Feb 2010. (a) NCEP/NCAR 250mb vector wind map shows the active phase of the jet stream over area of the study which drives the low pressure into the area of the study. (b) NCEP/NCAR 500mb geopotential height map shows the location of the associated trough which extends to the area of the study. (c) NCEP/NCAR sea level pressure shows north-westerly gradient over the study area result of the low in the east and high in the west. Finally, (d) Abu Dhabi airport radiosonde data shows the depth of the Shamal up to 700mb then it varies with height to become westerly at higher altitude.

4.2.1.3 Summer Shamal Days (SSDs)

The 28 June 2005 was a typical Summer Shamal Day and it was taken as an example for further discussion (Table 4.3). A Shamal day is defined in paragraph (3.3.2), then the summer period is considered to be from May until October as defined in paragraph 4.3.1.

Table 4.3. Wind data for three sites and NCEP/NCAR area average on the 28 June 2005 which was considered to be a SSD over the area of study.

Location		Bahrain	Abu Dhabi	Sharjah	NCEP/NCAR area average
Daily Mean Wind	Direction	330	302	265	310
	Speed (kts)	13	14	11	18

The NCEP/NCAR sea level pressure map (Figure 4.6c) shows high pressure over the eastern Mediterranean and low pressure over the east of the study area. Furthermore, there was a north-westerly pressure gradient over the study area due to a high pressure ridge from the west and a low pressure trough from the east. The low pressure system was sensitive to the temperature variations caused by the thermal low over the Rajasthan Desert south of Afghanistan. This thermal heating is illustrated in NCEP/NCAR surface air temperature map (Figure 4.6b) and is discussed in detail in Chapter 5 (in SSD variation).

The Abu Dhabi airport radiosonde profile (Figure 4.6d) shows that north-westerly winds were very strong at 900-700mb. Winds veered with height to become south-easterly at

higher altitudes. The veering of the wind indicates the retreat of the thermal low and its replacement by the subtropical high. Additionally, the NCEP/NCAR 500mb geopotential height map (Figure 4.6a) illustrates that the study area was dominated by the subtropical high which extended from west to east across the area and the location and extension of the Rossby wave was further north of the study area. Also, the Abu Dhabi radiosonde (Figure 4.6d) shows a large variation between temperature and dew point in the lower atmosphere as a result of the subsidence of dry air from the subtropical high.

Based on thirty years of analysis, the WSD and SSD data reveals a similarity in the surface patterns such as low pressure in the east, high pressure in the west and a north-westerly pressure gradient over the study area. The main differences between winter and summer Shamal days are in the upper layer at 500mb (Figure 4.5b and Figure 4.6a). Winter Shamal Days are associated with a Rossby wave whilst Summer Shamal Days are associated with a subtropical high. Therefore, it is upper air conditions that distinguish between winter and summer Shamal days.

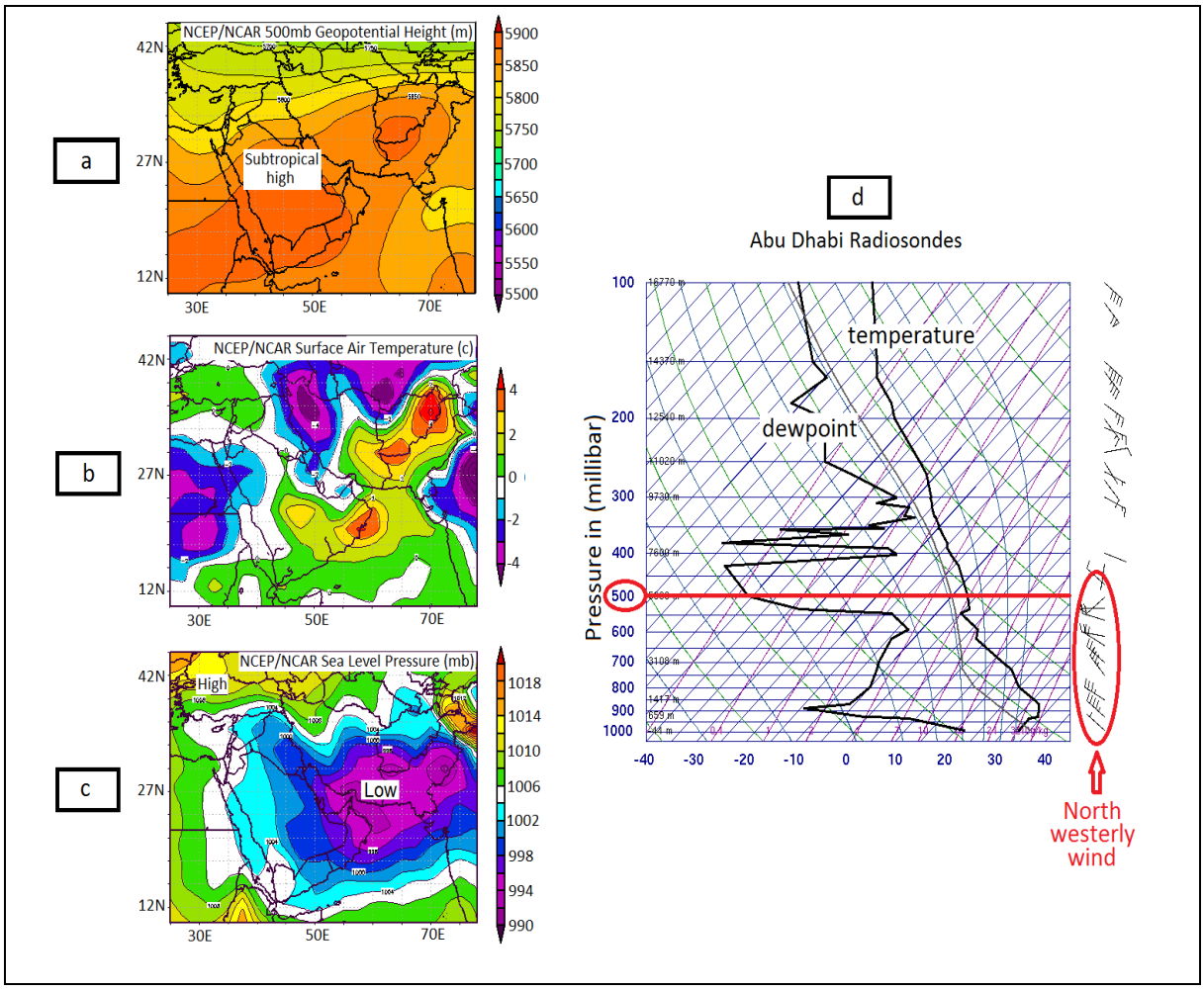

Figure 4.6. The meteorological conditions on a typical Summer Shamal Day over the study area on 28 June 2010. (a) NCEP/NCAR 500mb geopotential height map shows the extension of the subtropical high (which is associated with a typical SSD) over the study area. (b) The NCEP/NCAR air temperature map shows the location of the strongest thermal heating which leads to SSD. (c) NCEP/NCAR sea level pressure shows north-westerly gradient over the study area result of the low in the east and high in the west over Turkey. Finally, (d) Abu Dhabi airport radiosonde data shows the depth of the Shamal up to 500mb then it varies with height to become easterly at higher altitude.

4.2.1.4 Winter Suhaili (southerly to south-easterly) wind

Suhaili winds were observed in winter and summer. They are more frequent than Al-Nashi (north-easterly winds) but less so than Shamals. The 2 February 1993 was a Winter Suhaili day and it was taken as an example for further discussion (Table 4.4).

Table 4.4. Wind data for three sites and NCEP/NCAR area average on the 2 February 1993 which was considered to be a typical Suhaili day over the area of study.

Location		Bahrain	Abu Dhabi	Sharjah	NCEP/NCAR area average
Daily Mean Wind	Direction	135	129	104	147
	Speed(kts)	14	11	9	18

Figure 4.7 The NCEP/NCAR level pressure map (Figure 4.7) shows high pressure over the east and low pressure over the west of the study area. Both systems were causing strong southerly to south-easterly winds over the area (Table 4.4). The Abu Dhabi airport radiosonde profile shows that the altitude of the Suhaili wind was from the surface up to 800mb (lower that for Shamal winds). Temperature and dew point profiles were close, possibly due to unstable weather conditions and cloud development. Moreover, the NCEP/NCAR 500mb geopotential height map reveals an upper air trough over the eastern Mediterranean and the active phase of the Jetstream is shown on the 250mb vector wind map. In summary, the winter Suhaili wind starts as the depression approaches from the study area.

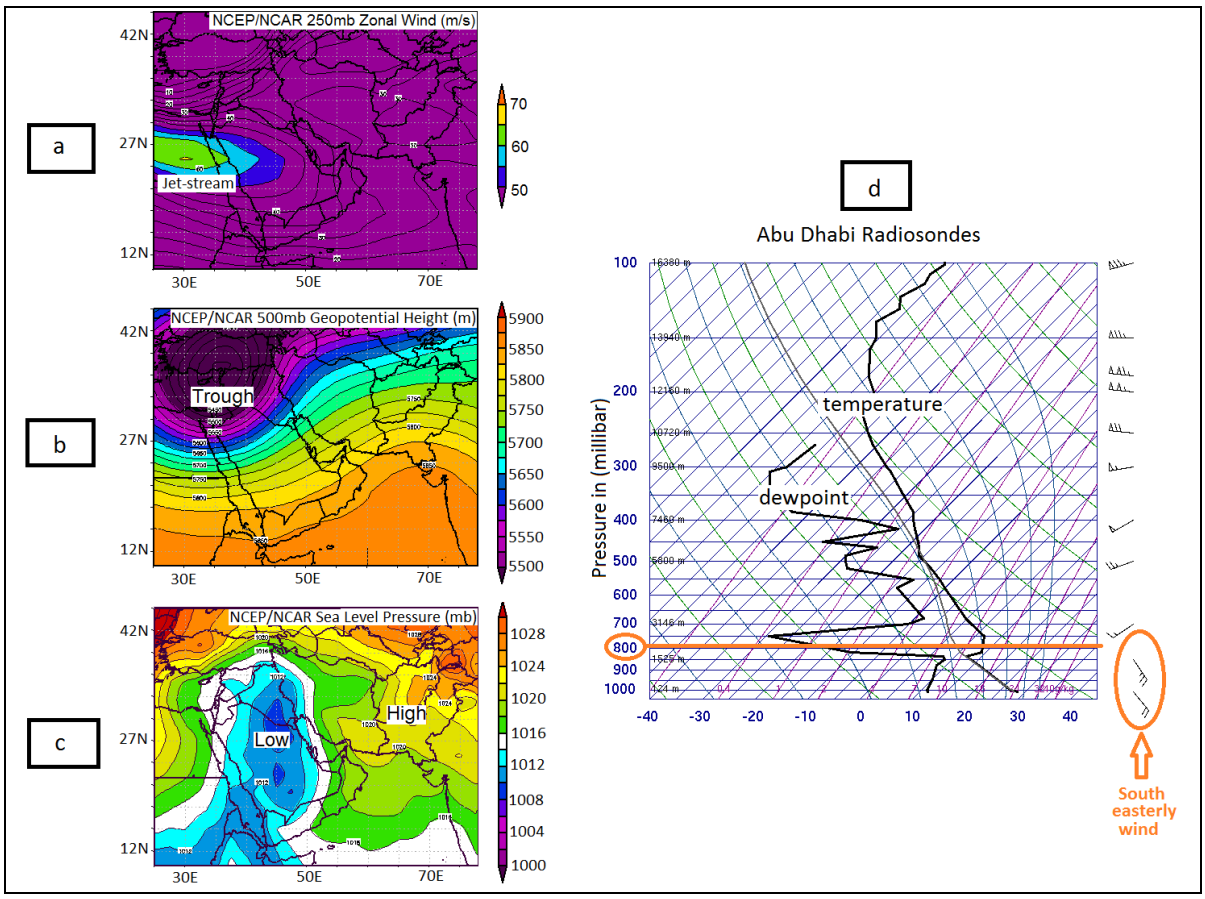

Figure 4.7. The meteorological conditions on a typical Winter Suhaili Day over the study area on 2 February 1993. (a) NCEP/NCAR 250mb vector wind map show the active phase of the jet stream west of the area of the study which drives the low pressure into the area of study. (b) NCEP/NCAR 500mb geopotential height map shows the location of the associated trough which west of the study area. (c) NCEP/NCAR sea level pressure shows south-easterly gradient over the study area result of the low in the west and high in the east. Finally, (d) Abu Dhabi airport radiosonde data shows the depth of the Suhaili up to 800mb, then winds change with height to become westerly at the higher altitudes.

4.2.1.5 Summer Suhaili (southerly to south-easterly) wind

The 28 July 1987 was a typical summer Suhaili day and it was taken as an example for further discussion (Table 4.5).

Table 4.5 Wind data for three sites and NCEP/NCAR area average on the 28 July 1987 which was considered to be a typical Suhaili day over the area of study.

Location		Bahrain	Abu Dhabi	Sharjah	NCEP/NCAR area average
Daily Mean Wind	Direction	135	147	110	151
	Speed (kts)	16	13	8	15

The NCEP/NCAR sea level pressure map (Figure 4.8) shows a thermal low pressure to the west of the study area which was causing strong southerly to south-easterly wind over the area study (Table 4.5). The Abu Dhabi airport radiosonde profile shows the altitude of the Suhaili wind to be from the surface up to 800mb; the wind then backs to easterly, northerly and becomes south-westerly

at higher altitudes (Figure 4.8d). The NCEP/NCAR 500mb geopotential height map shows the associated upper air system, which is a subtropical high.

The Summer Suhaili is a result of a thermal low deepening over the west of the study area (Figure 4.8b-c). The Suhaili Wind in both seasons drives a hot dry sandy air-mass from the Rub Al Khali desert of Saudi Arabia, which can lead to a significant reduction in visibility. During the winter, the Suhaili can enhance instability and precipitation over the study area as the frontal system approaches. Based on the observational data analysis, statistically Suhaili winds occur more frequently in winter than in summer; the highest frequencies are in February and March with less in June, which can be attributed to the presence of Shamal winds in June.

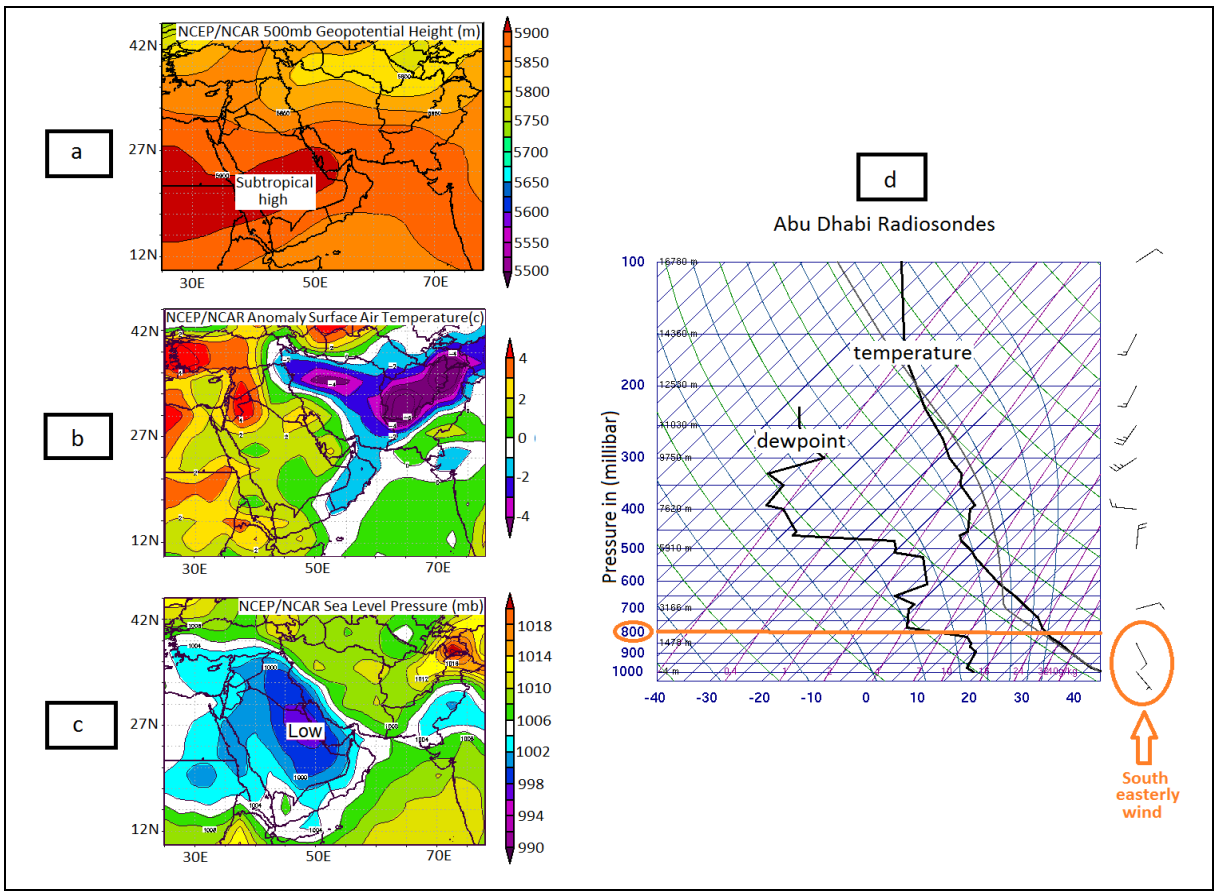

Figure 4.8. The meteorological conditions on a typical Summer Suhaili Day over the study area on 28 July 1987. (a) NCEP/NCAR 500mb geopotential height map shows the extension of the subtropical high over the study area. (b) The NCEP/NCAR air temperature map shows the thermal contrast between east and west of the study area which leads to Suhaili. (c) NCEP/NCAR sea level pressure shows a south-westerly gradient over the study area as a result of the high in the east and low in the west. Finally, (d) Abu Dhabi airport radiosonde data shows the depth of the Suhaili up to 800mb then it varies with height.

4.2.1.6 Al-Nashi (north-easterly) wind

The 25 January 2007 was a typical Al-Nashi day and was taken as an example for further discussion (Table 4.6).

Table 4.6. Wind data for three sites and NCEP/NCAR area average on the 25 January 2007 which was considered to be a typical Al-Nashi day over the area of study.

Location		Bahrain	Abu Dhabi	Sharjah	NCEP/NCAR area average
Daily Mean Wind	Direction	330	50	67	36
	Speed(kts)	7	11	7	11

The Al-Nashi wind is a result of the strong Siberian high over Asia associated with a low over the North West coast of India (figure 4.9c). It is associated with an upper air trough extending over Afghanistan and Pakistan reaching southern Iran (Figure 4.9b). The typical synoptic situation (Figure 4.9) drives fresh to strong north-easterly winds over the Arabian Gulf and occurs only during winter (Figure 4.4). It is observed mostly in December, January and February, and due to its source, it brings a cold dry air mass from the eastern side of the study area. It causes rough seas in the Strait of Hormuz and in the overall area of study. It can cause dusty weather as it passes over the Iranian desert, which significantly affects visibility in the region. The Abu Dhabi airport radiosonde profile shows the altitude of the Al-Nashi wind to be from the surface up to about 800mb; the wind then backs to northerly and becomes westerly at higher altitudes.

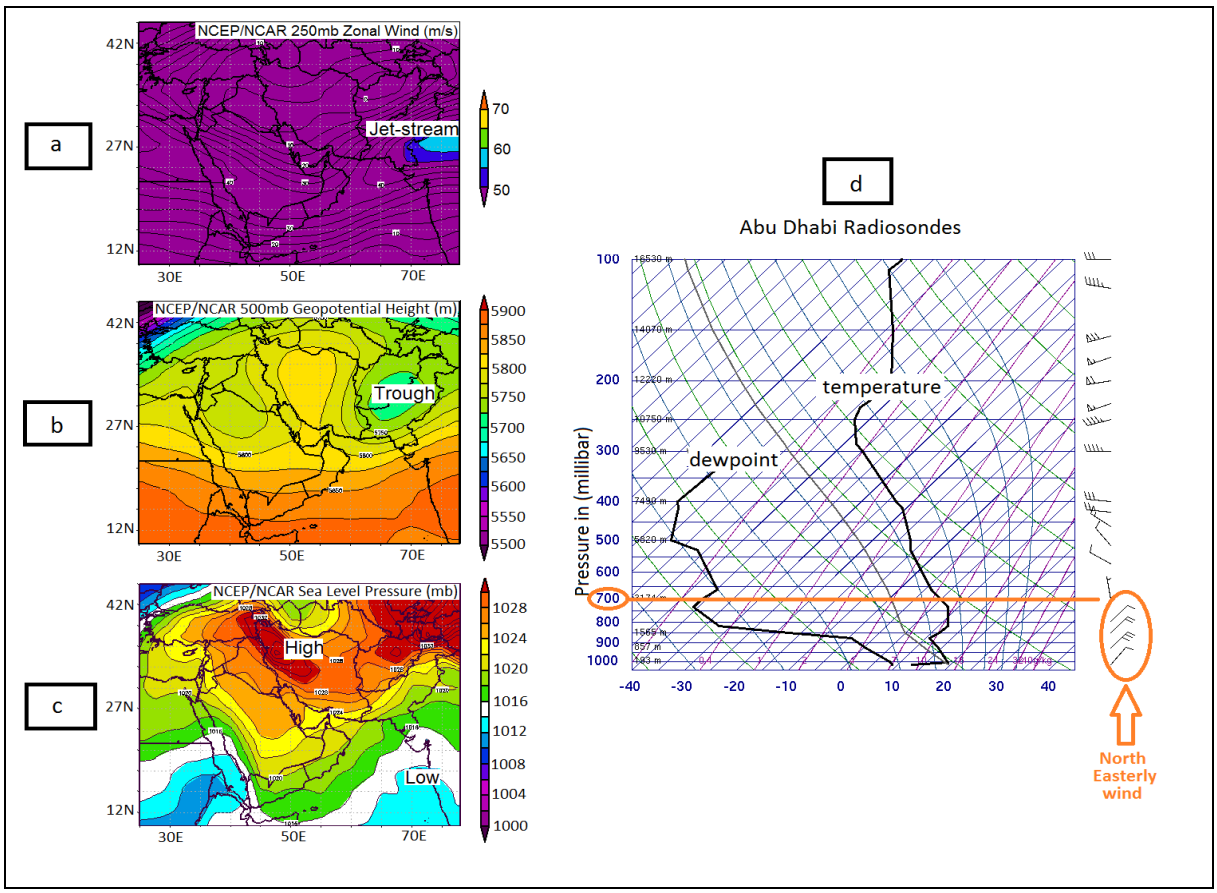

Figure 4.9. The meteorological conditions on a typical Al-Nashi Day over the study area on 25 January 2007. (a) NCEP/NCAR 250mb vector wind map show the active phase of the jet stream east of the area of the study, which associated with an upper air trough. (b) NCEP/NCAR 500mb geopotential height map shows the location of the associated trough which east of the study area extending south west towards the area of the study. (c) NCEP/NCAR sea level pressure shows North-easterly gradient over the study area resulting from the high in the north west of Iran and low over west coast of India. Finally, (d) Abu Dhabi airport radiosonde data shows the depth of the Al-Nashi up to 700mb; which then vary with height to become westerly at higher altitudes.

4.2.2 Local winds

In the absence of synoptic winds, most of the winds over the study area are local such as katabatic and land/sea breezes. Abu Dhabi and Sharjah hourly wind data were used to identify the behaviour of local winds during the period of the study.

4.2.2.1 Katabatic wind

A katabatic wind is the downward flow of cold air from high mountains due to the fall in temperature at night and in the early morning (Met Office, 2015). The area of study is located in the desert zone which is mostly dominated by clear sky. Land cools quickly at night and, in the presence of the high land, katabatic winds often occur from late night to the early morning. As mentioned in the previous chapter, topography plays a major role in the area of study. The strength and duration of the onshore wind over Sharjah is less than at Abu Dhabi, and this could be due to katabatic flow from the Hajar Mountains opposing the onshore wind. The Hajar Mountains are at a greater distance from Abu Dhabi than from Sharjah so the duration of the offshore wind is longer over Sharjah.

4.2.2.2 Land and sea breeze

Due to its location, the area of study is situated within the Hadley cell subsidence region (section 2.6). Therefore, land and sea breezes are the main local winds for most of the year (see Figure 4.3). Strength, direction and the onset time of the breezes vary depending on the strength and direction of the synoptic wind. These are discussed in greater detail in sections 4.3.3 and 4.3.4.

4.2.3 Summary of the main components responsible for the dominant wind pattern

In conclusion, five synoptic winds were studied including the summer and winter Shamal, summer and winter Suhaili, and Al-nashi, which occurs only in winter. Winter synoptic

winds were found to be associated with Rossby waves and upper air troughs while summer synoptic winds were associated with subtropical high and as a result of thermal processes. Katabatic influence is more noticeable in the areas near the highlands due to the arid climate.

4.3 Meteorological conditions and seasonal variations

In order to specify which meteorological systems most affect the area, and their seasonality, characteristics and associated wind circulations, a thorough analysis was undertaken of meteorological conditions using NCEP/NCAR 500mb geopotential height, NCEP/NCAR surface pressure and surface wind observational data, as outlined in sections 4.3.3 and 4.3.4. The first section, 4.3.1, describes the 500mb level where semi-permanent systems shift seasonally north (poleward) and south (equatorward) depending upon changes in solar radiation (Figure 4.10) and facilitates a split into two meteorological seasons: winter and summer. In the second section 4.3.2, the surface meteorological conditions for the specified seasons are described. The third and fourth sections describe the meteorological conditions for winter and summer respectively, based on the period specified from 500mb level analysis.

4.3.1 500 mb meteorological conditions and seasonality

The NCEP/NCAR mean meteorological seasonal reanalysis of the 500mb geopotential height maps (Figure 4.10) illustrate the location of the Rossby waves and subtropical high for each of four meteorological seasons. During the autumn season, the location of peak

solar insolation moves south of the equator and the Rossby waves which drive the upper-air troughs move toward the equator. During the winter the Rossby waves move further south towards the equator. In spring the location of peak solar insolation returns north and the Rossby waves move north towards the North Pole. In the summer, the Rossby waves move north of the study area and are replaced by the subtropical high. Spring and autumn seasons are considered to be transit periods between these two systems over the study area (Almandoos, 2005). In addition, Figure 4.10 clearly shows that the 5850m geo-potential height marks the separation between Rossby waves and the subtropical high.

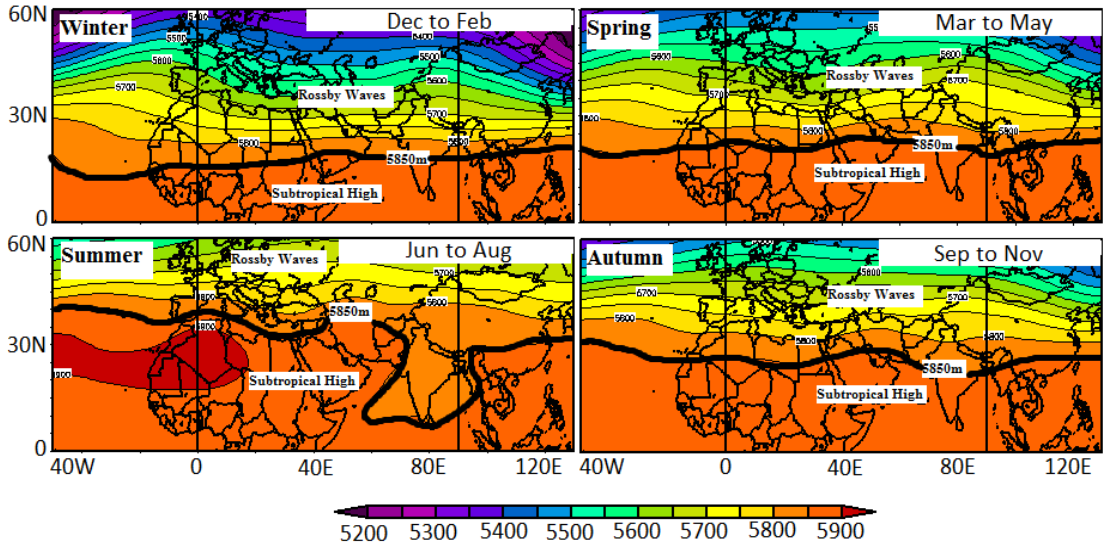

Figure 4.10. NCEP/NCAR means meteorological seasonal reanalysis of the 500mb geopotential height, illustrating location of the Rossby waves and Subtropical High. The position of the 5850m geopotential height is highlighted as the boundary layer between both systems.

5850m was used as the separation height for the study area due to the fact that the 5850m contour is continually (twelve months of the year) in and around the area of study, lying to the south in winter and to the north in summer (figure 4.11). Both 5800m and 5900m were considered during the course of this analysis, but rejected as less suitable due to the more obvious local utility of the 5850m contour. For example, the 5900m is only found within

the area for two months of the year (August and September) whereas Subtropical Highs are relevant for six months. In contrast, the 5800m contour is found for only two months (January and February) whereas Rossby Waves are also considered relevant for six months.

Figure 4.11 shows the spatial variation of the monthly mean of geopotential height at the 500mb level, highlighting the position of the 5850m geopotential height. The figures illustrate that the area is dominated by the subtropical high if the monthly mean position of the 5850m line at the 500mb geopotential height is north of the study area. Similarly, the subtropical high retreats toward the south if the monthly mean position of the 5850m line at the 500mb geopotential height is south of the study area and is replaced by Rossby waves.

The result shows that the 5850m line at the 500mb geopotential height is north of the study area from the beginning of May until the end of October, while south in the remaining period. Therefore, from May until October at 500mb, the area of study is dominated by the subtropical high and from November until April the area of study is dominated by Rossby waves. Therefore, further analysis will be divided into two periods: winter (November until April) and summer (May until October).

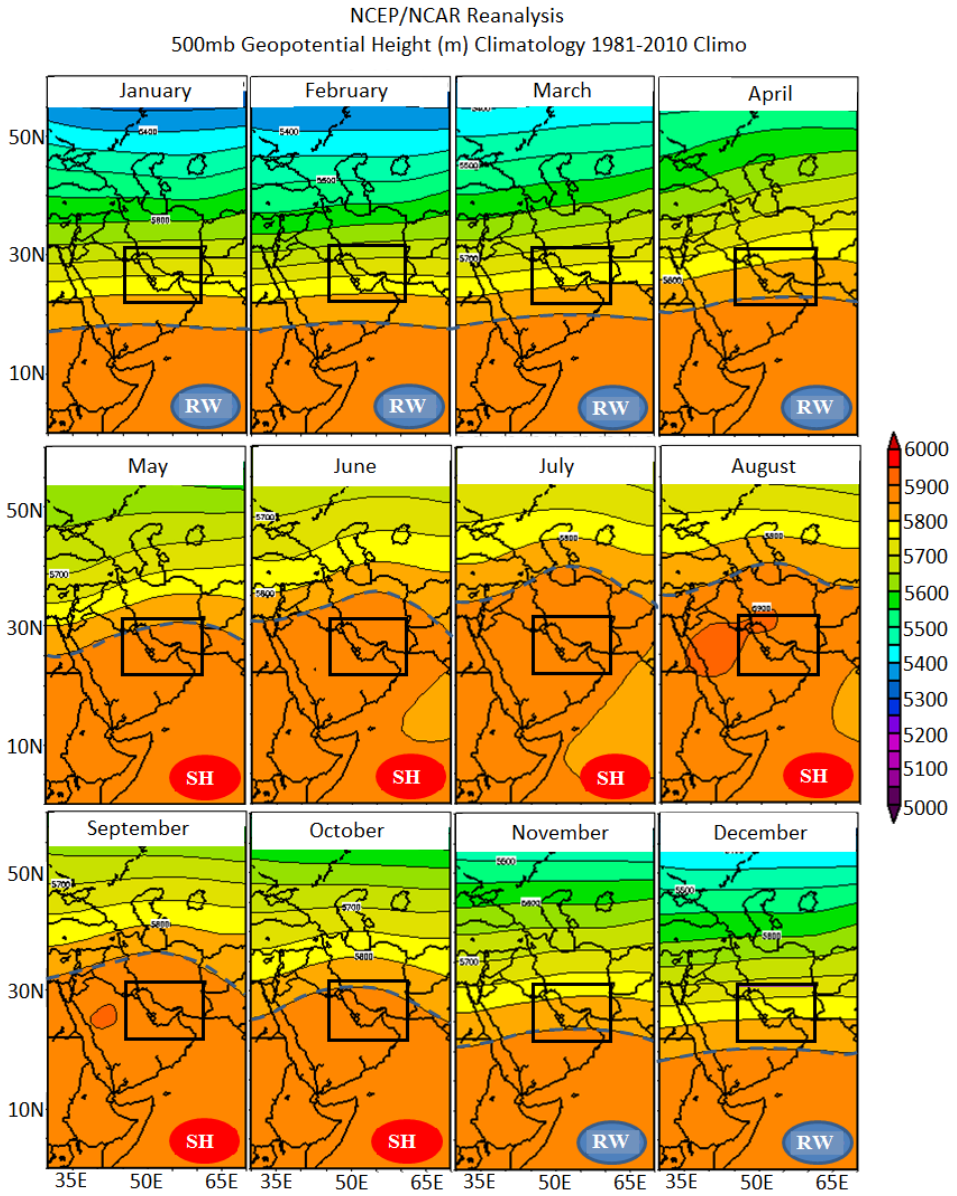

Figure 4.11. The NCEP/NCAR reanalysis showing the monthly mean positions of the 5850m level at 500mb GPH in the NCEP/NCAR composite monthly mean of thirty years (1981-2010) charts. Months when the 5850 level GPH at 500mb is north of the study area, is remarked as SH while others remarked as RW.

4.3.2 Surface level meteorological conditions and seasonality

Figure 4.12 illustrates NCEP/NCAR sea level pressure for both winter and summer. During the winter (Figure 4.12a) the area of study is located between the extensions of two surface atmospheric pressure systems: the Siberian high pressure over central Asia in the east and the Azores high over the Atlantic to the west. In the summer (Figure 4.12b), the Azores high and its extension remains in the same location while the Siberian high pressure retreats to the north and is replaced by the Indian Monsoon Thermal Low (IMTL). The extension of the IMTL affects the area of study from May until the end of October (the summer season).

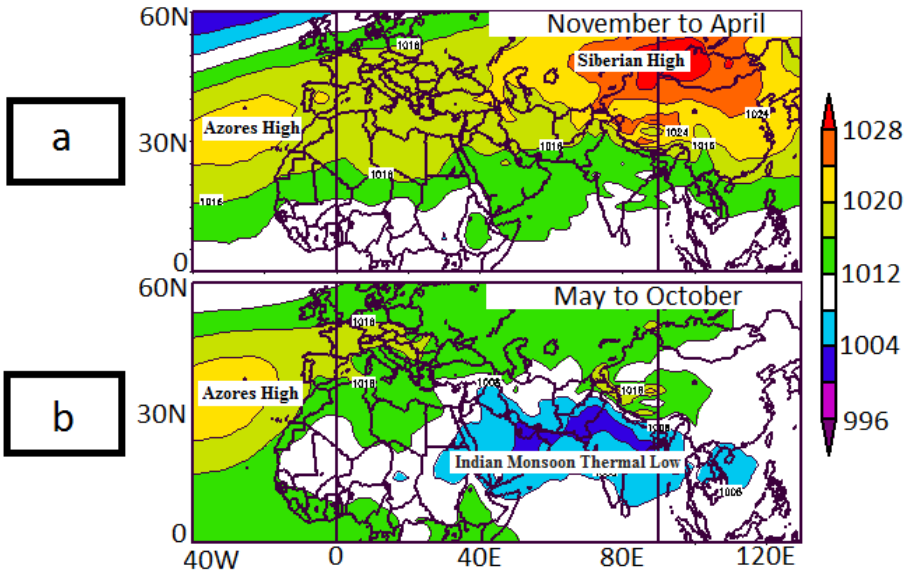

Figure 4.12. NCEP/NCAR reanalysis sea level pressure (mb) climatology (1981-2010) for the two periods (a) November to April map illustrates predominant winter surface pressure systems. (b) May to October map shows predominant summer surface pressure systems.

4.3.3 Winter (November until April) meteorological characteristics

During the winter, the area of study is influenced by an extension of high pressure (Figure 4.12a), which could be a result of land and sea breeze circulations. The analysis of thirty

years of observational and reanalysis data suggests that the main engine for synoptic winds is the passage of westerly depressions. In the following section, the period from 2 to 9 February 2010 was selected as a study case to illustrate the effect of the passage of westerly depressions over the area. The associated wind circulation and its effect on the onset of the sea breeze are also investigated. The influence of these wind patterns on the EM wave propagation will be examined in Chapter 6.

4.3.3.1 Meteorological conditions as the westerly depression approaches

Figure 4.13 shows that on 2 February 2010 an extension of the high pressure retreated for a few days. Two low pressure systems over the eastern Mediterranean and southern Red Sea moved east (Figure 4.13d). The area of study was under a weak pressure system causing a light airflow. In these conditions the sea breeze started at midday (Figure 4.14a). On 3 February 2010 the two lows merged into one depression and continued to move east with the associated upper air trough. At the same time, the Suhaili wind started over the area of study (Figure 4.13b-e). The Suhaili caused a delay in the onset of the sea breeze, reducing its duration by several hours and shifting it to a northerly direction (Figure 4.14b). On the 4 February the surface depression moved further towards the study area and the Suhaili wind strength increased (Figure 4.13f). There was no sea breeze but the influence of the breeze can be observed from the variation of the Suhaili wind throughout the day (Figure 4.14c). The strength of the Suhaili wind increased during the period of the land breeze and decreased during the sea breeze (Figure 4.14c).

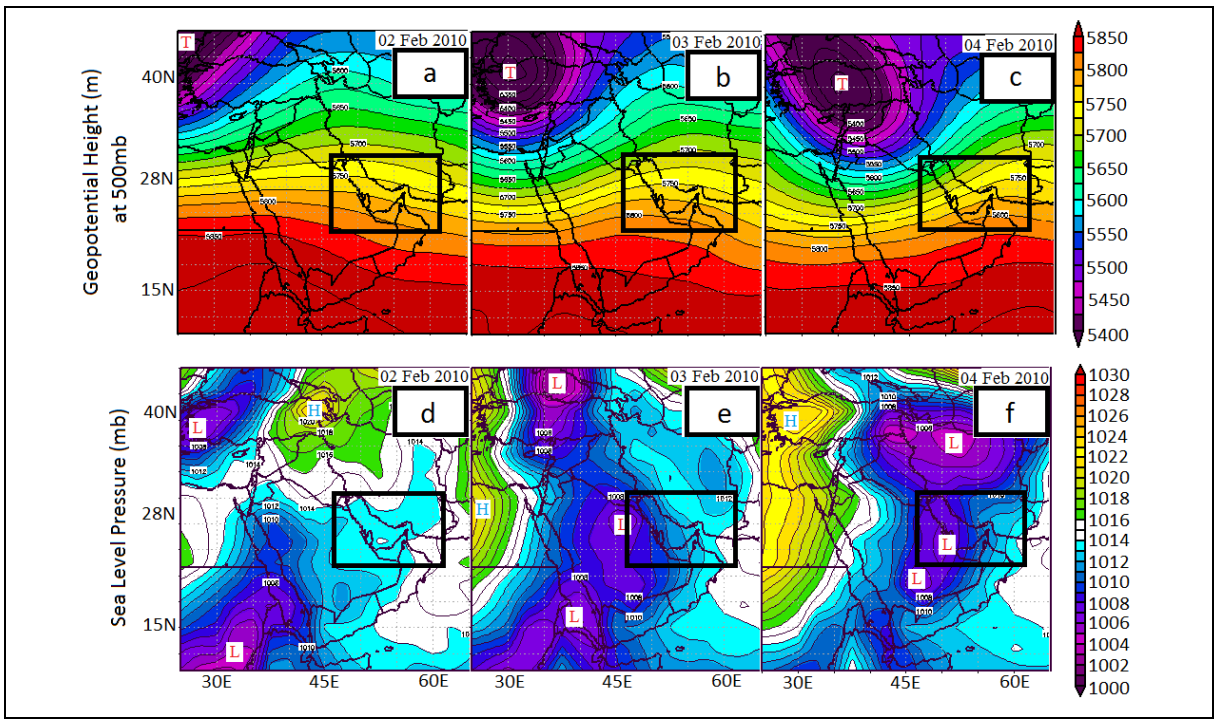

Figure 4.13. The NCEP/NCAR reanalysis sea level pressure (d-e-f maps) and geopotential height at 500mb (a-b-c maps) illustrating the development of meteorological conditions (initiate and persist of the Suhaili wind (Figure 4.14)) over the study area during the approach of westerly depressions.

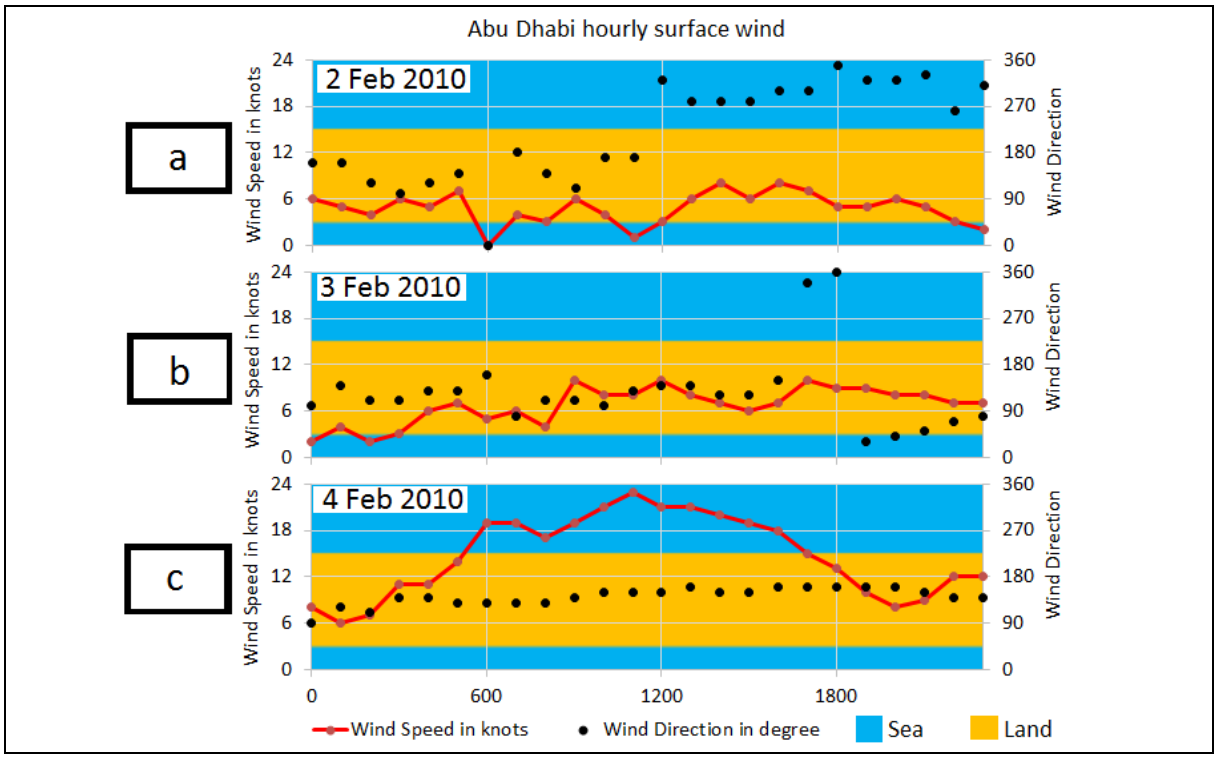

Figure 4.14. Abu Dhabi airport hourly wind direction and speed (a) 2 Feb, (b) 3 Feb, (c) 4 Feb 2010, illustrate the variation in the wind direction and speed as the westerly depression approaches.

4.3.3.2 Meteorological conditions as the westerly depression crossed the area

On 5 and 6 of February 2010 the surface depression associated with the upper air trough crossed the area from west to east (Figure 4.15) causing unstable weather conditions and making the onset time of the sea breeze unpredictable (Figure 4.16). The Suhaili wind veered north-westerly as the depression moved over the area. Furthermore, the depression moved to the east and the high pressure extended behind it causing a build-up of the pressure gradient over the area (Figure 4.15). This caused strong north-westerly winds (Winter Shamal Wind).

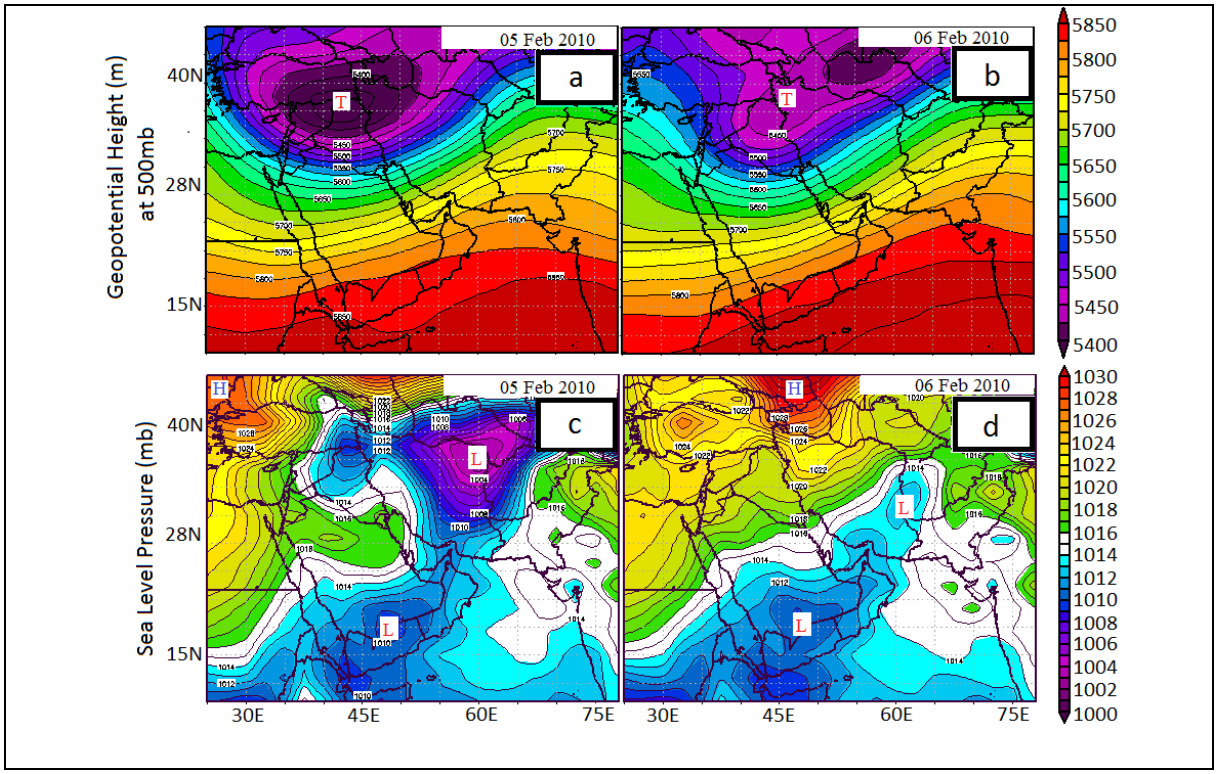

Figure 4.15. (a) The NCEP/NCAR reanalysis sea level pressure (c-d maps) and geopotential height at 500mb (a-b maps) illustrating the development of the meteorological conditions (wind veered from south-easterly to becomes north-westerly (Figure 4.16)) over the area of the study during the passage of the westerly depression.

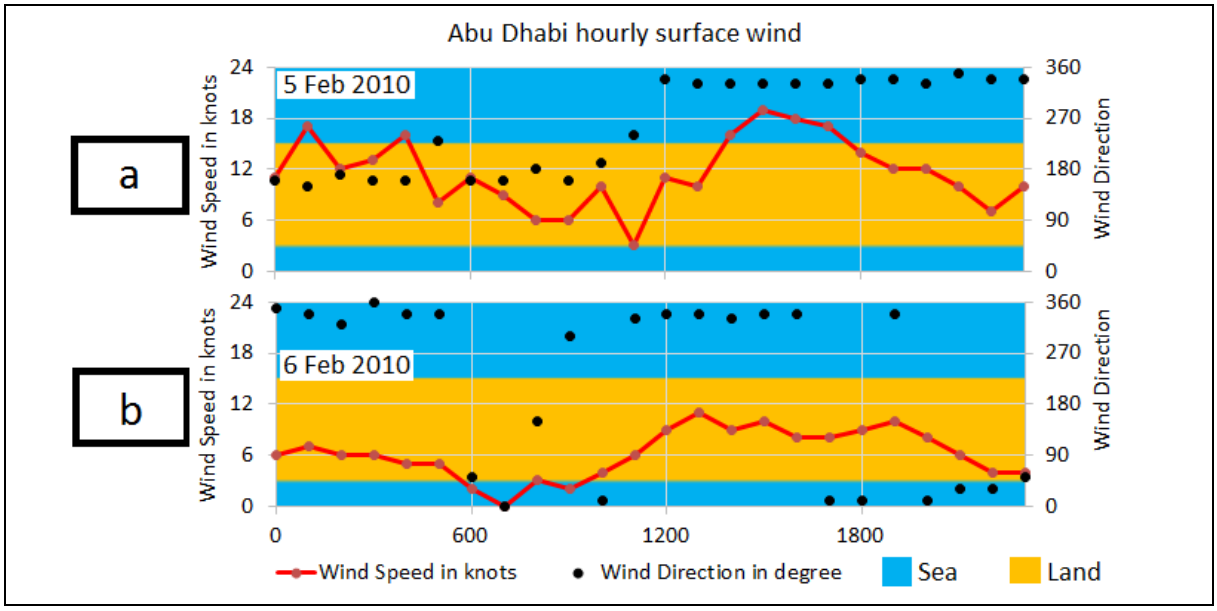

Figure 4.16. Abu Dhabi airport hourly wind direction and speed (a) 5 Feb, (b) 6 Feb 2010, to illustrate the variation in the wind direction and speed as the westerly depression crosses the area.

4.3.3.3 Meteorological condition after the passage of the westerly depression

On 7 February a strong Shamal persisted over the study area (Figure 4.17d and Figure 418a). On 8 February the low continued to move further east and the Shamal became weaker by the end of the day (Figure 4.17e and Figure 418b). No land breeze was observed on either day. On 9 February the westerly depression continued to move further east and was replaced by the high pressure causing easterly to north-easterly winds (Figure 4.17f). There was no extension of the upper air trough over the study area (Figure 4.17c); consequently, the north-easterly wind was not strong. It is seldom the case that the north-easterly wind becomes strong and becomes the Al-Nashi wind. During these conditions, sea breezes predominate and start earlier in the day while land breezes are weak and persist for just a few hours (Figure 4.18c).

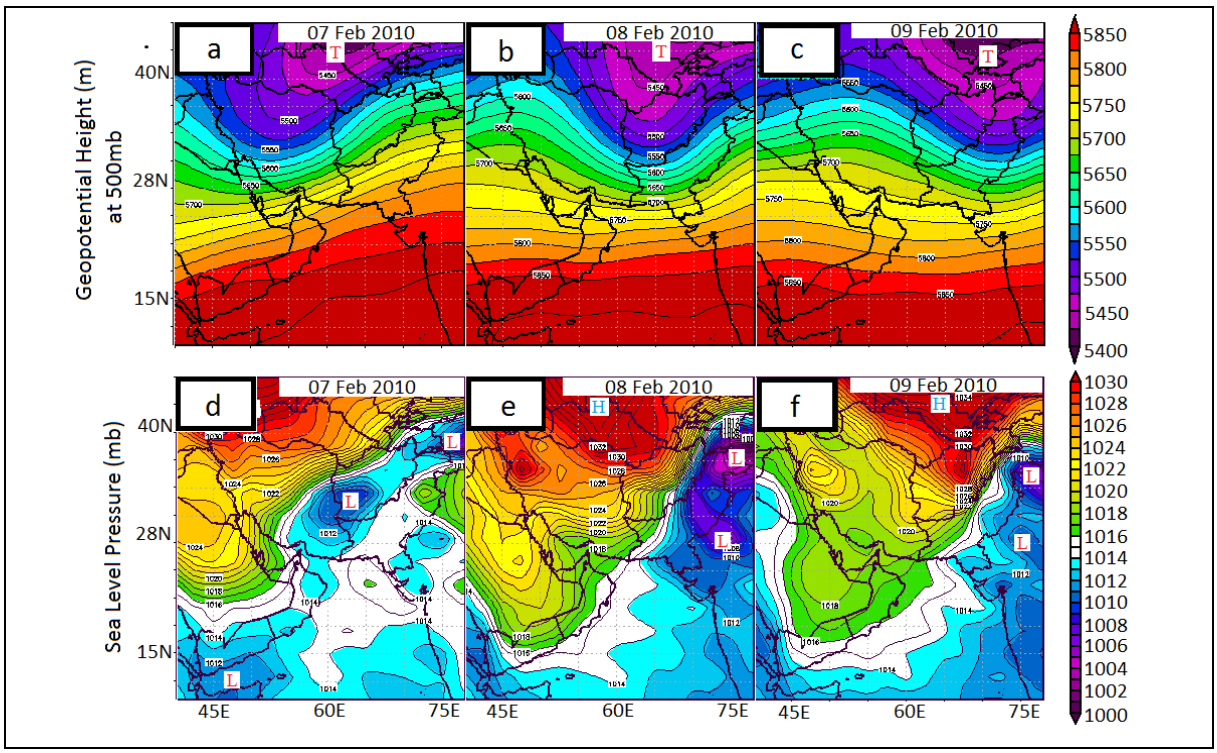

Figure 4.17. The NCEP/NCAR reanalysis sea level pressure (d-e-f maps) and geopotential height at 500mb (a-b-c maps) illustrating the development of the meteorological condition (winter Shamal Days (Figure 4.18)) over the area of study after the passage of westerly depression.

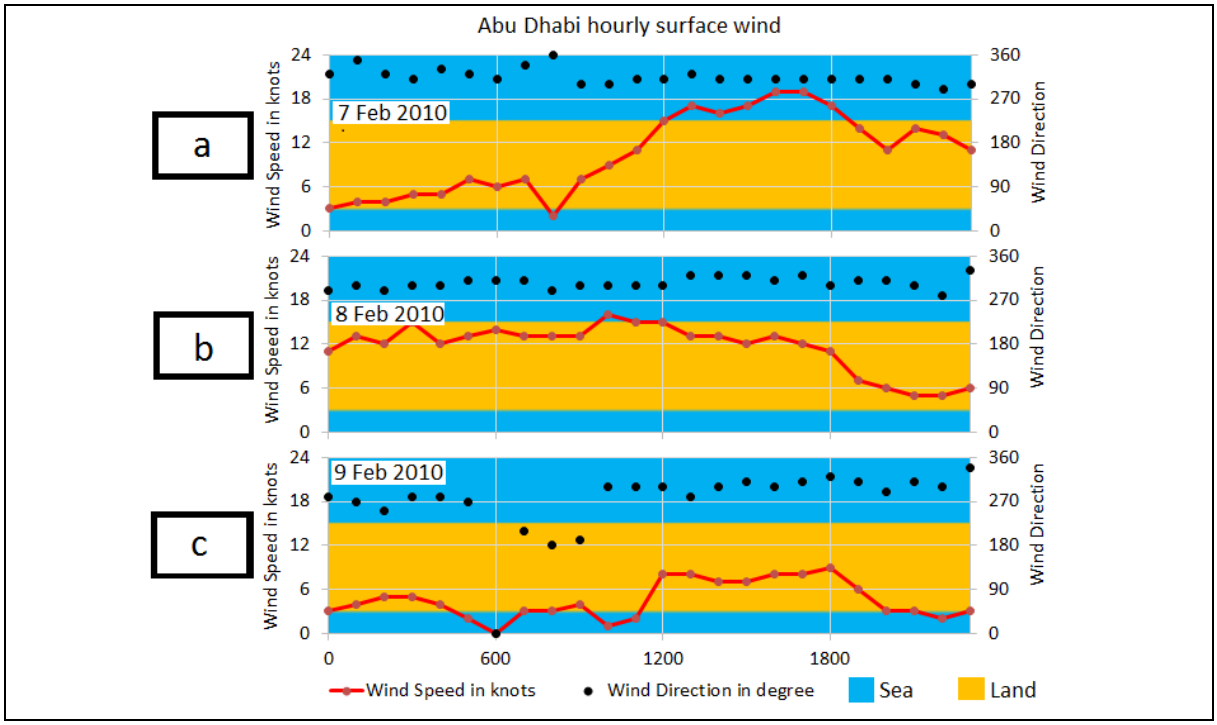

Figure 4.18. Abu Dhabi airport hourly wind direction and speed (a) 7 Feb, (b) 8 Feb, (c) 9 Feb 2010, to illustrate the vitiation in the wind direction and strength after the passage of westerly depression.

4.3.4 Summer (May until November) meteorological characteristics

During the summer the area of study is influenced at the surface by an extension of the Indian Monsoon low extending from the east and the Azores high from the west (Figure 4.12b), while the 500mb level is dominated by the subtropical high (Figure 4.11). The weak extensions of both surface systems (Figure 4.12b) could be attributed to the formation of land and sea breeze circulations. In these conditions the onset of sea breezes is usually observed around midday. Variations in solar radiation are the main engine for the synoptic wind. As described in sections 4.2.1.3 and 4.2.1.5, an extension of the Indian monsoon low and Azores high was a result of solar radiation. Over the area the MSL pressures, which were around 1005mb at the beginning of June, reached their lowest (994mb) in July. MSLP started to increase from the middle of August to reach 1000mb by the end of the month (Figure 4.19).

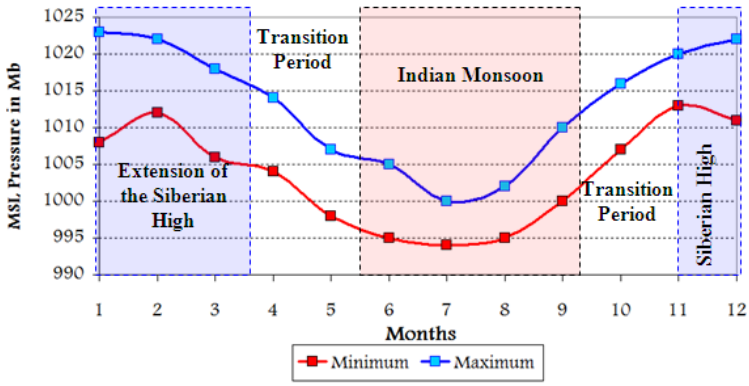

Figure 4.19. Thirty years MSL pressure for each month over the region and details of pressure system based on NCEP/NCAR surface charts.

4.3.5 Summary of the meteorological conditions and seasonality

This section showed that the upper air meteorological conditions divided the period into two seasons. The summer season, from May until October, is dominated by a Subtropical high associated with surface Indian monsoon low and Azores High, which are the characteristics of SSD (section 4.2.1.3). The winter season from November until April is associated with Siberian high and passage of the westerly depression, which is the characteristics of WSD (section 4.2.1.2).

4.4 Conclusion

This chapter shows that winter and summer Shamal, winter and summer Suahili, and Al-Nashi affect the area of study, but the Shamal wind is the main synoptic wind over the region, as demonstrated in section 4.1.2. As described in section 4.2.1.3, the Summer Shamal Days are associated with a subtropical high at 500mb, a surface westerly extension of deep IMTL in the east and an easterly extension of the Azores High in the west. The Azores High is a semi-permanent system, while the IMTL starts to develop by the end of April/beginning of May and disappears during October.

In contrast, Winter Shamal Days are associated with an upper air trough driven within the Rossby waves at 500mb. The upper air trough is associated with the passage of the surface westerly depression. The Winter Shamal persists after the passage of a westerly depression and the extension of the Siberian high pressure. The Siberian high pressure replaces the Indian Monsoon Thermal Low from November until April. As the Shamal is the main wind

pattern influence the area of the study, a good understanding of Shamal behaviour and its connection with the global circulation will enable its prediction and an understanding of its influence on local meteorology (Chapter 5). The synoptic and local wind pattern along with the propagation of electromagnetic waves is investigated in Chapter 6.

Chapter 5 – Effect of global circulation systems upon inter-annual variability

The previous chapter identified the Shamal as the main meteorological feature affecting the area of study. The variability of the Shamal wind and the connection between Shamal and the global circulation are studied in this chapter. Chapter 6 investigates the effect of the different air masses, including Shamal, on atmospheric refractivity.

The objective of this chapter is to examine the inter-annual variability of Shamal Days and its connection with the global circulation pattern. This will help to improve seasonal forecasts for the frequency of Shamal days in relation to the global circulation pattern.

The chapter structure includes a brief description of the variability of total wind strength over the area of the study and the variation in the frequency of summer and winter Shamal days is discussed in section 5.1. This is followed by an investigation of the connection between the occurrence of Shamal days and associated global circulation patterns, which is discussed in sections 5.2 (summer) and 5.3 (winter). Finally, the conclusion of the chapter with a summary of its findings is given in section 5.4.

5.1 Inter-annual variability

The aim of this section is to illustrate the inter-annual variabilities of wind strength over the period of the study and how it is affected by the frequency of Shamal days. This section is

divided into two subsections; the first subsection describes total wind inter-annual variability and the second subsection covers the inter-annual variability of Shamal winds.

5.1.1 Total winds

The inter-annual variations of annual average wind speeds at Bahrain, Abu Dhabi, and Sharjah stations, as well as area averaged wind speed from NCEP/NCAR during the period of study are shown in Figure 5.1. The following sections will describe the trend's behaviour and its significance from the Mann-Kendall test.

5.1.1.1 Behaviour of the wind speed trends

All four trend lines indicate an apparent decline in wind strength over time. Figure 5.1 shows that the strongest wind strength occurs in Bahrain, and the weakest wind strength occurs at Sharjah. This difference between stations could potentially be due to variations in regional topography and coastal configuration (section 4.1.2). The weaker annual wind strength at Sharjah could be attributed to the presence of south-easterly winds enhancing the katabatic effects, which oppose the stronger Shamal wind. However, Bahrain is an island (Figure 1.1) along the route of the strong Shamal wind and this leads to more substantial yearly mean wind strength than at any of the other stations (Figure 4.2). NCEP/NCAR and Bahrain have similar trends in wind strength over time (Figure 5.1). However, there are noticeable variations in wind strength from NCEP/NCAR data which was calculated as an average across the entire area (highlighted in red box of Figure 1.1(24-27N, 50-56E)). The trends in wind speed at Abu Dhabi and Sharjah are similar, and Abu Dhabi shows stronger wind strengths than Sharjah.

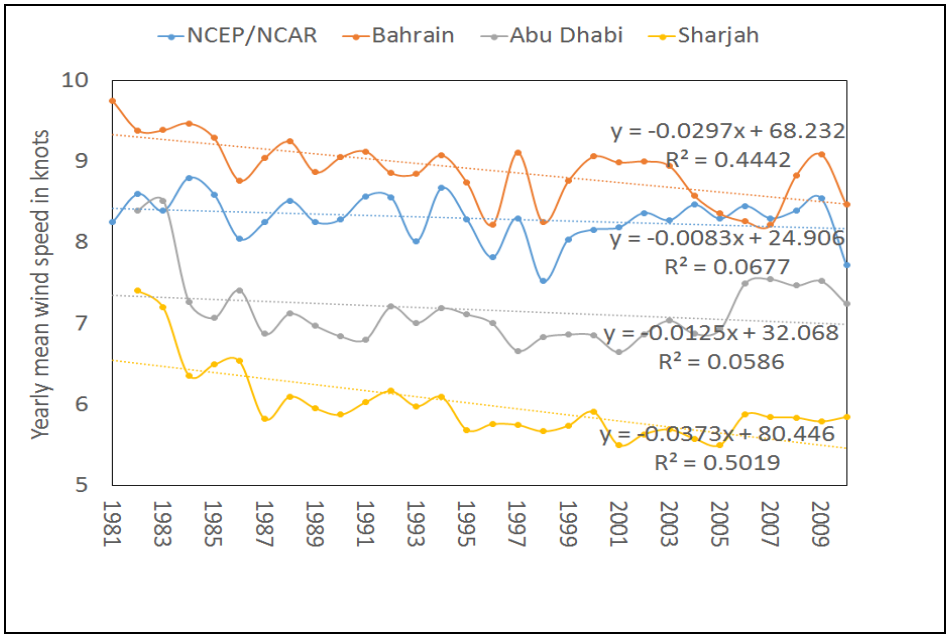

Figure 5.1. Calculated yearly mean wind speed (in knots) trend lines from observational data for three stations (Bahrain, Abu Dhabi, Sharjah) and the area averaged from NCEP/NCAR over time. Summary of trend lines significance in table 5.1.

5.1.1.2 Mann-Kendall test for wind speed trends

The significance of the downward trend in annual mean wind speeds was examined by using the Mann-Kendall test. Table 5.1 shows the results of the Mann-Kendall test. The results indicate that the annual averaged wind speed at Bahrain and Sharjah has shown a trend in the series (statistically significant), while there is no trend in the series (not statistically significant) at Abu Dhabi and NCEP/NCAR (the whole area). As mentioned in section 4.1.2, Bahrain is less influenced by topography and coastal configuration, therefore Bahrain's wind speed downward trend line is selected to represent the study area.

Table 5.1. Results of the Mann-Kendall test for downward trend in yearly mean wind speed data for the four sites. The P value indicates its statistical significance.

Source of data	P Value	Significance level α (alpha)	**Test interpretation:** H_o: There is no trend in the series H_a: There is a trend in the series
Bahrain	0.0001	0.05	p-value < alpha, reject Ho and accept Ha
Abu Dhabi	0.396	0.05	p-value > alpha, accept Ho and reject Ha
Sharjah	0.0001	0.05	p-value < alpha, reject Ho and accept Ha
NCEP/NCAR	0.502	0.05	p-value > alpha, accept Ho and reject Ha

5.1.2 Shamal winds

The Shamal wind is the primary wind over the study domain and any variations in the strength of the Shamal wind could influence average wind strength over the region. The wind speed is stronger at Bahrain compared to any other station in this study and represents the Shamal wind over the study area. Consequently, wind data from Bahrain are used in this study to analyse variations in the Shamal wind strength. Figure 5.2 shows that the occurrence of the Shamal wind (270-360 degree at any speed) has decreased throughout the period of study, which could be interpreted as the reason for overall decreases in wind strength.

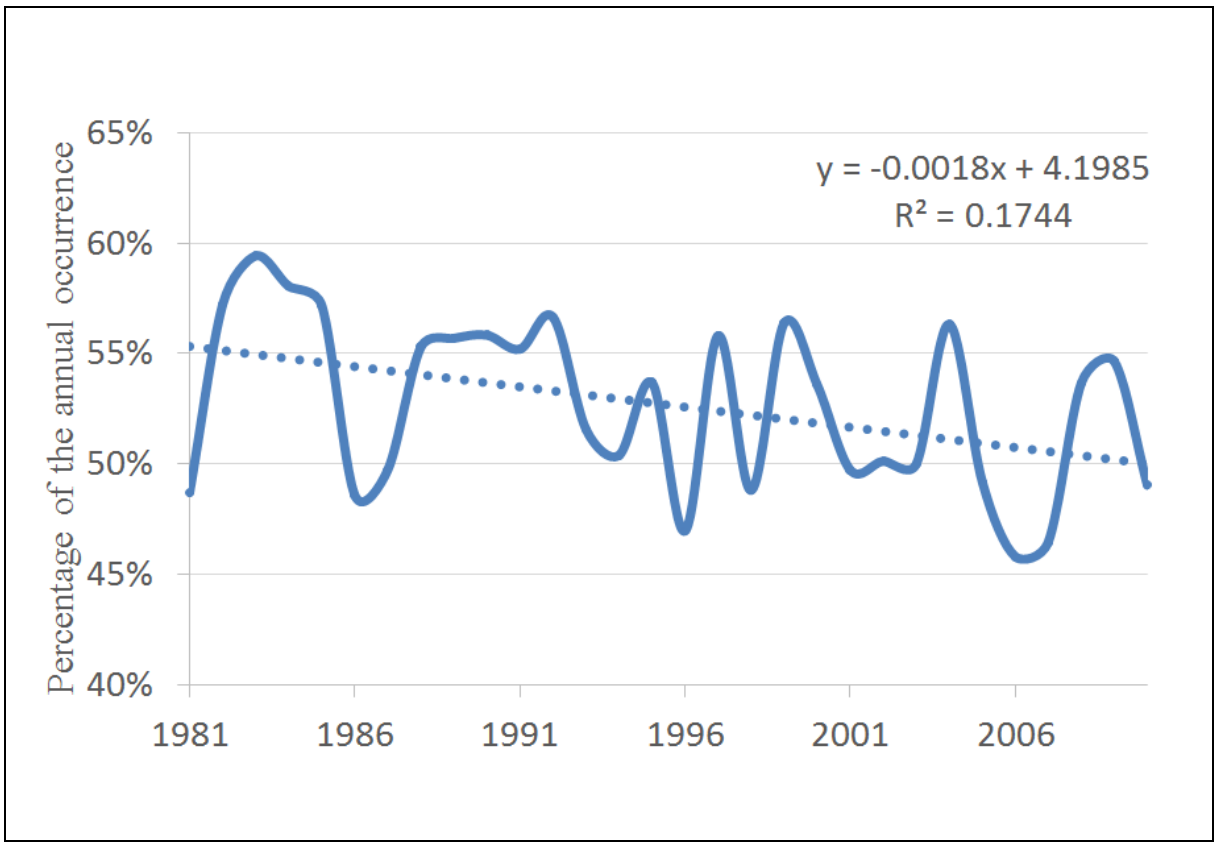

Figure 5.2 trend line of the occurrence of annual Shamal wind throughout the period of the study (1981-2010). The trend is statistically significant.

Furthermore, Shamal days (strong Shamal wind) which were introduced in paragraph 3.3.2 are used to analyse variations in the Shamal wind strength. Monthly frequencies, the Mann-Kendall test, and statistics of Shamal seasonal variation are described in the sections below.

5.1.2.1 Monthly frequency of Shamal days

Figure 5.3 shows the frequency of monthly mean Shamal days from Bahrain observations during the period of study (1981-2010). The figure shows that the highest frequency of Shamal days was in June and the lowest frequencies were in September and October. Standard deviation minima are in September and October and maximum in August. This chapter discusses summer and winter Shamal days separately; the monthly mean variation

in the frequency of the Shamal days is divided into two seasons (Figure 5.3). During Winter Shamal Days (WSDs) the frequency of Shamal days increased from November reaching a maximum in January and then decreasing gradually until April. During Summer Shamal Days (SSDs) the frequency of Shamal days increased from May reaching a maximum in June, then fell and reached the minimum in October (Figure 5.3).

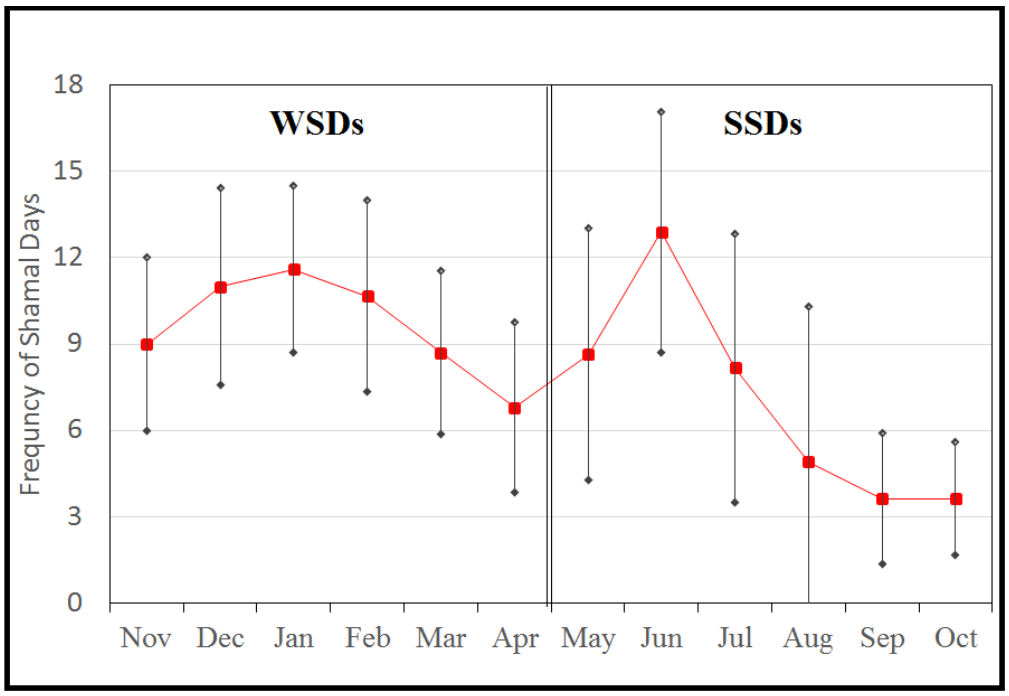

Figure 5.3. Monthly mean and ±1 standard deviation plots for the frequency of Shamal days calculated from Bahrain observational data for the period of study (1981-2010). Winter Shamal Days are indicated by WSDs and Summer Shamal Days are indicated by SSDs.

Statistical analysis results are presented in Table 5.2. They indicate that the total frequency of monthly Shamal days occurring during the period of the study (1981-2010) were as follows:

- Winter Shamal days occurred on 37% of January days across the period, which represents around 20% of the total WSDs. Additionally, WSDs occurred on 32% of the entire winter period (November to April).

- Summer Shamal days occurred on 387 days (43%) across the June months which represent around 31% of the SSDs. The SSDs occurred on 23% of the entire summer period (May-October).

Table 5.2 is a consolidated summary of Bahrain observational data. The complete dataset shows that the highest frequency of Shamal days was 21 days (70% of the month); this occurred during June 1983 and August 1986. However, no Shamal days occurred in July (1989, 1996), August (1985, 1986, 1998, 2001, 2006, 2010), September 1986, and October (1993, 2004). The analysis shows that the minimum frequencies of Shamal days occurred in 1996 (72 days) and 2007 (76 days). However, the maximum frequency of Shamal days occurred in 1983, 1984, and 2001(117 days).

Table 5.2. Statistics of the frequency of Shamal Days for each month of the study period (1981-2010), showing number and percentage. Years of maximum and minimum values are not in the table but are mentioned in the text. Moreover, the table shows the result of Mann-kendall tests of each monthly trend. The maximum figure (green) and minimum figure (red) are highlighted.

Seasons	Months	Total in percentage	Max	Mean	Min	STDEV	Mann-Kendall test	
							P-value	S-value
Winter	Nov	30 %	17	9	5	3.03	0.364	49
	Dec	35 %	18	11	5	3.42	0.205	-68
	Jan	37 %	17	12	6	2.90	0.475	-39
	Feb	36 %	19	11	5	3.33	0.233	-64
	Mar	28 %	14	9	2	2.83	0.066	-98
	Apr	23 %	13	7	2	2.94	0.955	4
Summer	May	28 %	18	9	2	4.37	0.462	-40
	Jun	43 %	21	13	6	4.19	0.004	-154
	Jul	26 %	17	8	0	4.68	0.168	74
	Aug	16 %	21	5	0	5.38	0.405	-45
	Sep	12 %	10	4	0	2.28	0.101	87
	Oct	12 %	8	4	0	1.96	0.761	-17

5.1.2.2 Mann-Kendall test

Table 5.2 shows that S values for June and March are negative which indicates a negative trend in the frequency of Shamal days over time. However, in July and September the S values are positive indicating a temporal increase in the number of Shamal Days. There were no statistically significant trends in any of the months except June when there was a significant decline in the frequency of Shamal days over the period of study. The P value for the June Mann-Kendall test (carried out for 30 values) was only 0.004 (Table 5.2).

Figure 5.4 shows trend line analyses that indicate a clear decline in the annual number of Bahrain Shamal days over time. The results of the Mann-Kendall test (also for 30 values) showed a trend in the series which is statistically significant with a P value =0.034.

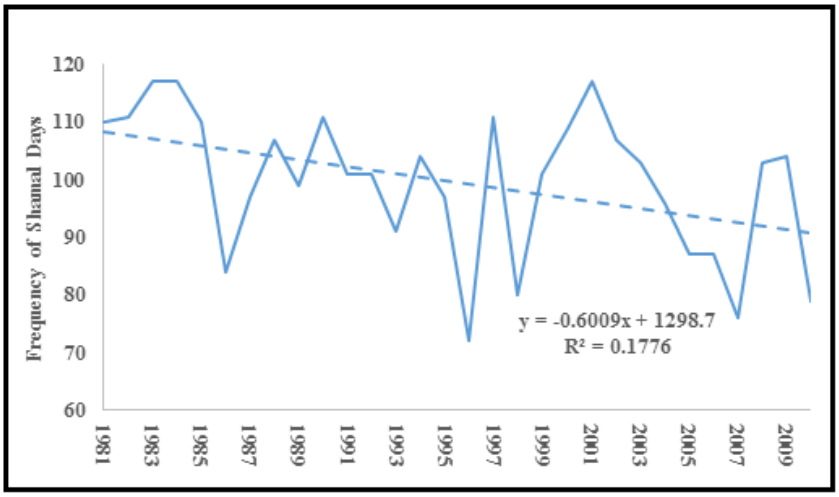

Figure 5.4. Annual variation of frequency of Bahrain Shamal days over time.

5.1.2.3 Trends and statistics of winter and summer Shamal seasons

As shown in Figure 5.5, seasonal variation also reveals a clear reduction in winter Shamal days over time. The winter trend line is statistically significant (P value = 0.025) while the summer temporal trend line is not (P value = 0.475). The frequency of winter Shamal days is more than the frequency of summer Shamal days. The maximum number of Winter Shamal Days recorded was 75 days in 1982, with a minimum of 40 recorded in 2005, while the maximum number of Summer Shamal Days was 56 days in 1983, with a minimum of 21 days recorded in 1996.

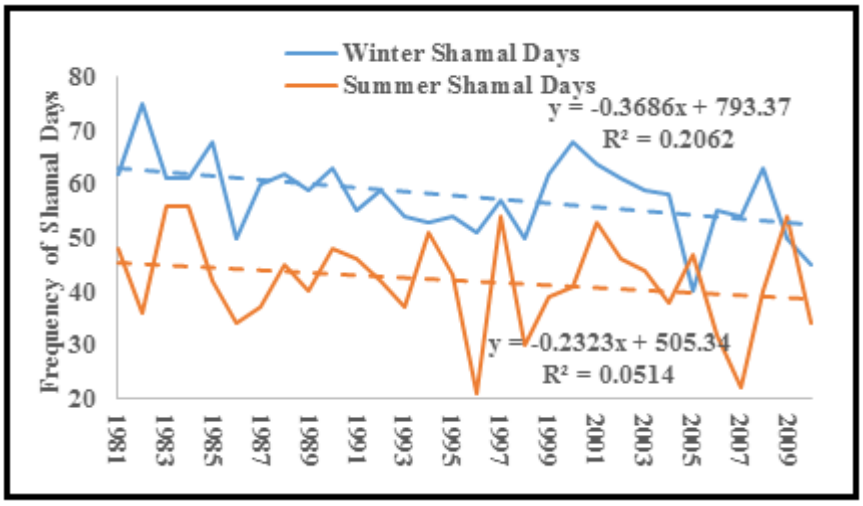

Figure 5.5. Seasonal variation in the frequency of Shamal days and associated trend line over thirty years. The winter trend line is statistically significant (P value = 0.025) while the summer temporal trend line is not (P value = 0.475).

5.1.3 Summary of the inter-annual variability.

Bahrain site trends data was used to represent the wind strength and the frequency of Shamal days in the area of the study. The statistical analysis reveals there was a decline in wind strength over the period of the study (1981-2010) (Figure 5.1), this could be a result of the decline in the frequency of Shamal days (Figure 5.4); the Shamal being the strongest wind. Furthermore, during the period of study there was a significant reduction in winter Shamal days. The month of June shows the highest frequency in the number of Shamal days, although it also shows there was a significant decline in the frequency of Shamal days. The following sections describe a detailed analysis of the both winter and summer Shamal days and how there are connected with global wind patterns. Global circulation patterns will then be used to offer an explanation for the observed trends in wind strength, Shamal days and Winter Shamal Days.

5.2 Summer Shamal Days (SSDs) and connection with global circulations

The aim of this section is to investigate the connection between SSDs and the general global circulation pattern. This investigation, of direct and indirect effects of large-scale atmospheric circulation on the inter annual variability of SSDs, was carried out for the period of May to October. Thirty years of reanalysis data for SSDs were divided into Positive (above average in the frequency) SSDs (PSSDs) and Negative (below average in the frequency) SSDs (NSSDs) years and examined against large-scale circulation systems (Figure 5.6).

In order to understand the dynamic processes associated with PSSD and NSSD years, the analysis was focused on the following variables: pressure, geopotential height at 500mb, air temperature and wind at available atmospheric levels. This section is divided into three subsections the first subsection describes how the frequency of SSDs correlates with global phenomena in whole summer seasons (May- October). The second subsection investigates the correlation during periods of high frequency of SSDs. The correlation between low frequency of SSDs and global circulation is investigated in subsection 5.2.3.

5.2.1 Six-month period (May-October)

This subsection describes the global atmospheric circulation pattern associated with frequency of SSDs for six month periods. Then it illustrates results of ANOVA F tests for significance and correlation between the frequency of SSDs data and the atmospheric

circulation pattern data (30 values for each variable). Finally, the interpretation of the dynamic connection between the Shamal and the global circulation is explored.

5.2.1.1 Global atmospheric circulation pattern associated with frequency of SSDs

Figure 5.6b shows that the PSSD years are associated with below-average atmospheric pressure over the Caspian Sea extending towards the southern coast of Iran and Pakistan. The above-average atmospheric pressure pattern can be observed over Siberia; and from the North Sea extending west to Iceland and south-east to Egypt, the Red Sea and the Arabian Peninsula and west over Sudan. The sea level pressure anomaly during NSSDs is a complete reversal of that during PSSDs (Figure5.5d). Furthermore, the 500mb geopotential height anomaly suggests that the atmospheric fluctuations penetrate to the 500mb level over three separate areas - the Caspian Sea, Siberia and the North Sea (Figure 5.6a-c).

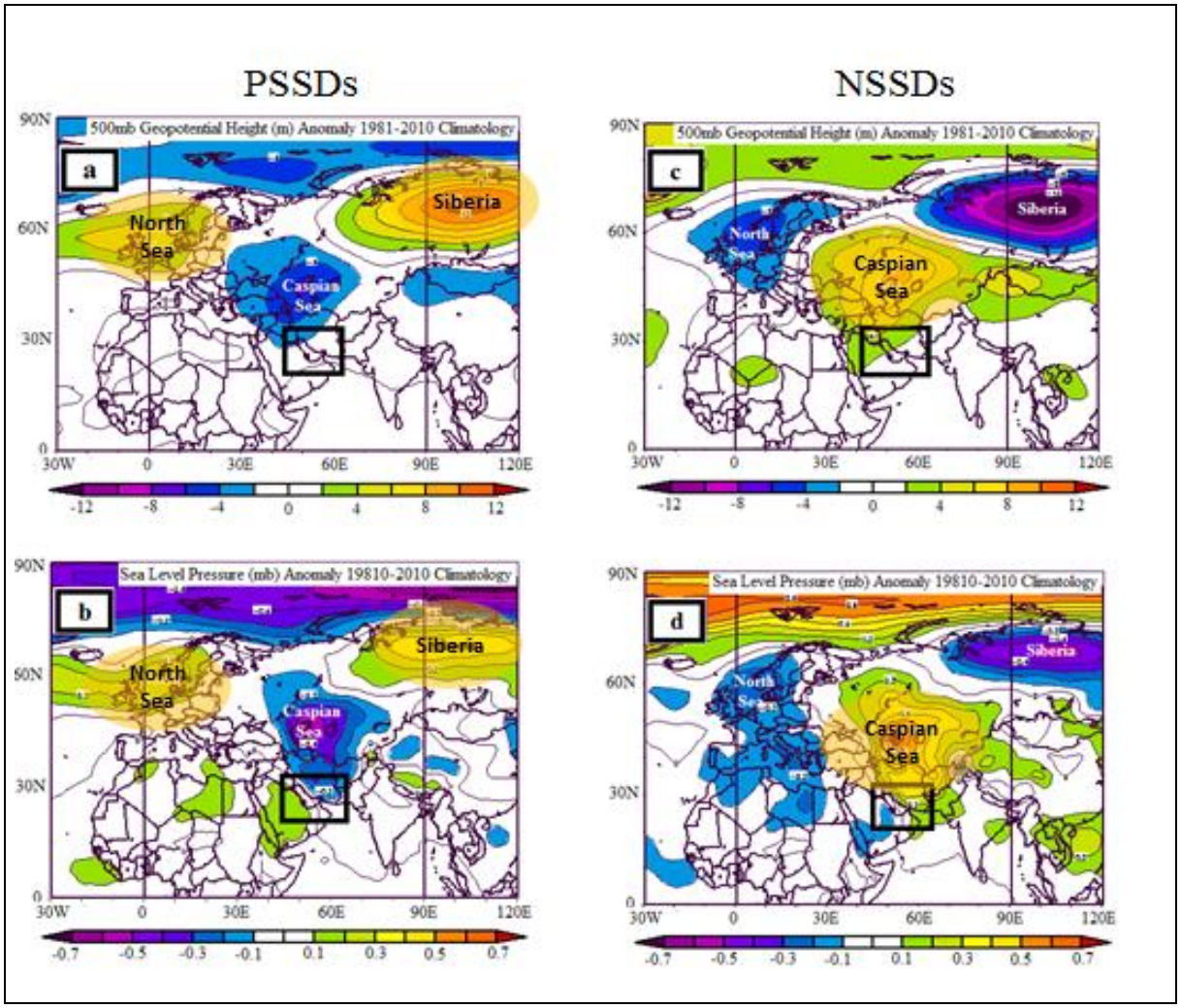

Figure 5.6. In the left hand charts (a and b) the PSSD years are grouped in one NCEP/NCAR reanalysis 500mb geopotential height anomaly chart (a) and SLP chart (with isobaric line intervals (0.1)) in the bottom left (b). The charts on the right (c and d) indicate NSSD years grouped in one NCEP/NCAR reanalysis 500mb geopotential height anomaly chart (c) and SLP chart (with isobaric line intervals (0.1)) in the bottom right (d).

5.2.1.2 ANOVA-F test

To identify the significance of the atmospheric air pressure fluctuation at these three locations on the inter-annual variability of the frequency of the SSDs, an ANOVA-F test (mentioned in paragraph 3.3.2) was carried out between the frequency of SSDs data and the summer (May – October) 500mb geopotential height fluctuation data at three locations (Siberia 65-75N,90-110E; Caspian Sea 40-50N,45-55E; North Sea 50-60N,0-10E) for the

period of the study. The results show that the link between SSD frequency and the atmospheric fluctuation over Siberia and the Caspian Sea is statistically significant (P-value = 0.000025, 0.0055), with a correlation coefficient of 0.69 and 0.50 respectively (Figure 5.7). However, the correlation between SSD frequency and the atmospheric air pressure fluctuation over the North Sea is not statistically significant (P-value = 0.25), with a correlation coefficient of only 0.21 between the two systems.

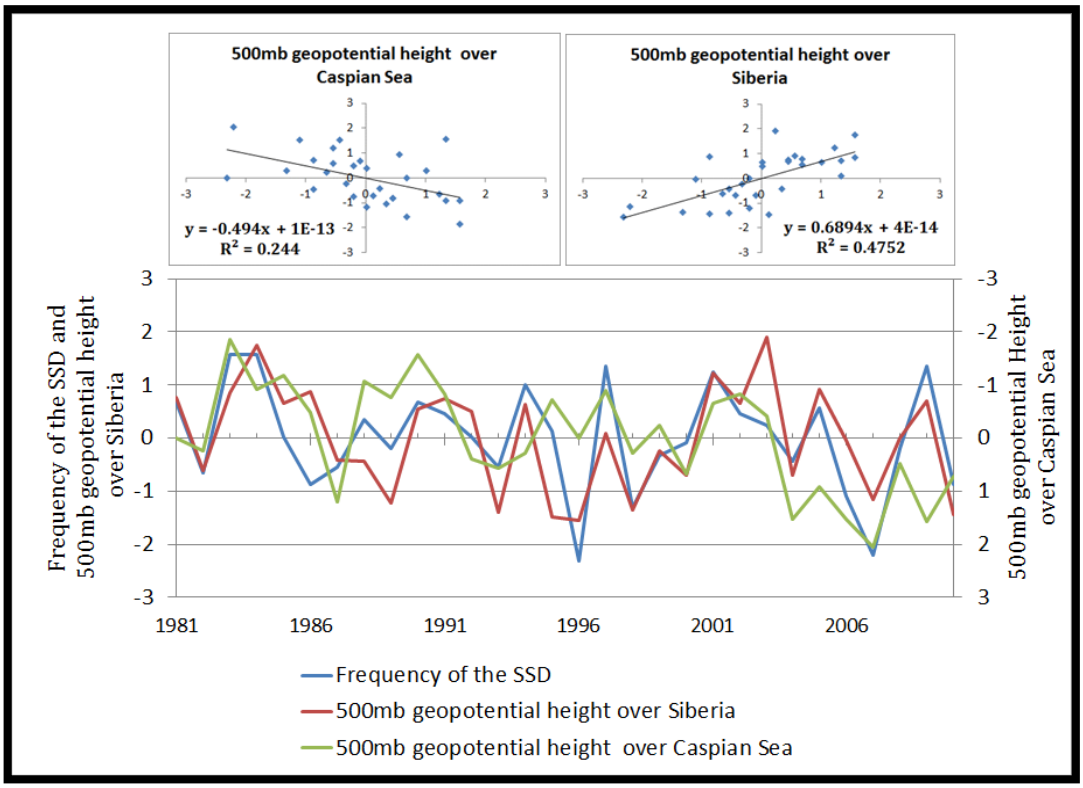

Figure 5.7. Correlation between frequency of the SSDs variation and 500mb geopotential fluctuation over Siberia and the Caspian Sea, showing SD variations from normalised (mean) values (SSDs=42days , Siberia=5484m, Caspian=5739m). This relationship is represented in the top scatter chart for both locations and in the bottom line chart which uses the frequency of the SSDs as a baseline against atmospheric fluctuation over the two locations.

5.2.1.3 Interconnection between SSDs and global circulation pattern

To interpret the connection between the frequency of SSDs variation and atmospheric air pressure fluctuations over both Siberia and the Caspian Sea, an analysis was carried out of

the prevailing synoptic situations. This was a wider study area than Yu et al. (2015) who concentrated on more local situations over Saudi Arabia, though connected these to summer ENSO and Mediterranean SSTs. Figure 5.8 shows the vertical cross-section of meridional wind anomalies averaged over 25°N to 35°N and the spatial distribution of wind anomalies during PSSDs and NSSDs.

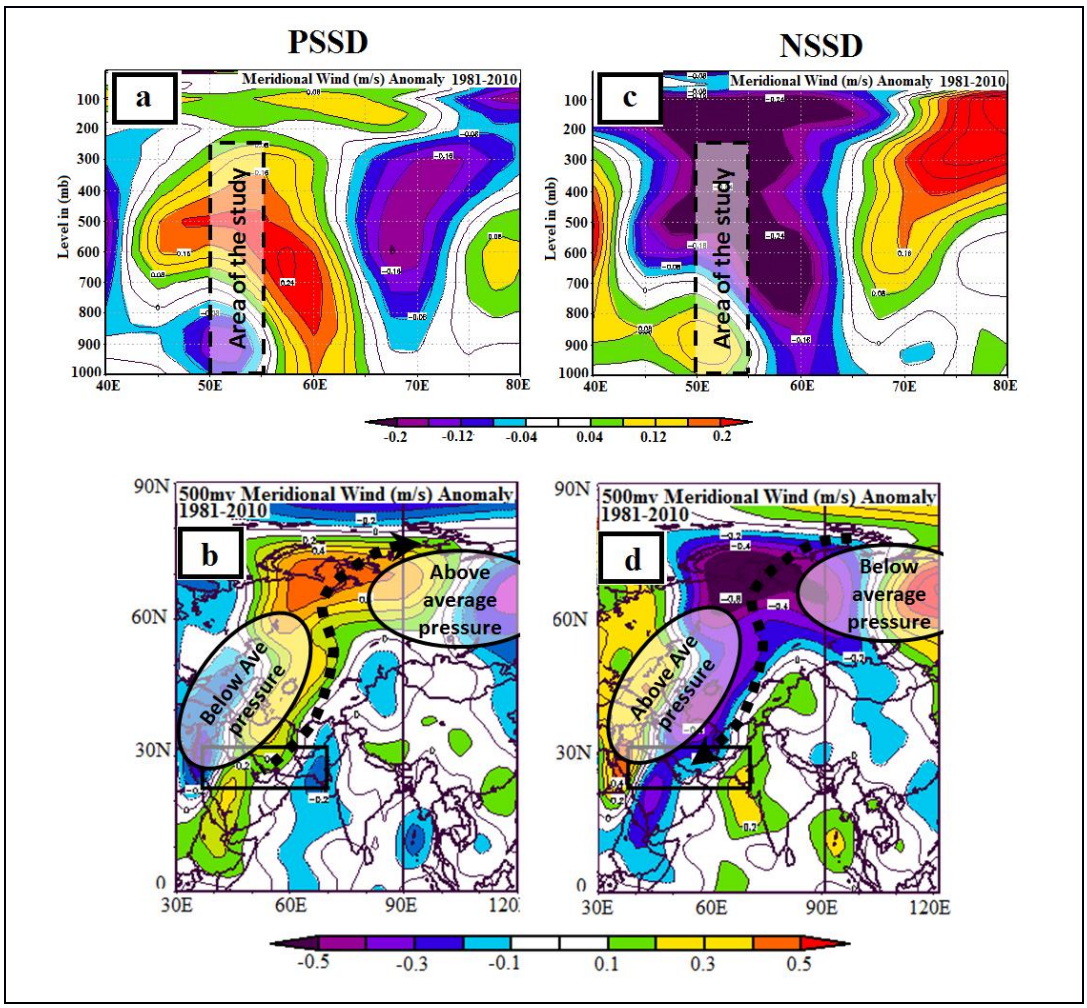

Figure 5.8. NCEP/NCAR meridional wind anomaly (ms^{-1}) horizontal (in the bottom charts (b and d)) and vertical cross section average 25°N to 35°N, 40°E to 80°E (in the top charts (a and c)). PSSDs are illustrated in the left hand charts; (a) positive meridional wind east of the study area. Figure shows negative meridional wind over the study area extends till 700mb. (b) 500mb meridional wind comes from south to the north across the study area. NSSDs in the right-hand charts (c and d) reverse picture of PSSDs.

During PSSDs, a warm southerly flow moves from the southern part of the area of study towards Siberia (as indicated by the dashed arrow in Figure 5.8b). Additionally, the vertical cross-section illustrates a warm southerly flow occurring from the surface to the 100mb level (Figure 5.8a). There is penetration of the northerly wind from the surface to 700mb which indicates the presence of a Shamal wind over the study area (figure 5.8a). The warm southerly flow over the eastern part of the area warms its passage, which could enhance the thermal low further west over the Zagros Mountains. Simultaneously, the above-average pressure in the eastern part of the Arabian Peninsula may increase due to the cooler Shamal wind and enhance the strength of the Shamal. The result suggests that the southerly flows are driven by atmospheric pressure systems over both the Caspian Sea and Siberia (Figure 5.8b).

In contrast, for NSSDs, Figure 5.8d suggests that a cooler northerly wind moves air south, anticlockwise around the below-average atmospheric pressure over Siberia, merging with a clockwise wind around the above-average atmospheric pressure over the Caspian Sea, penetrating into the area of study. Figure 5.8c shows that there is a cooler northerly flow over the eastern part of the study area from the surface to the 100mb level. The northerly flow is penetrated by warm southerly wind from the surface to the 700mb level (Figure 5.8c). This could weaken (below average) atmospheric pressure over the eastern Arabian Peninsula. The cooler northerly flow to the east could limit the development and westerly extension of the thermal low (IMTL) over the Zagros Mountains. Both weak below-average atmospheric pressure over the eastern Arabian Peninsula and above-average atmospheric pressure over the Zagros Mountains may lead to below average SSDs.

Figure 5.9 shows variations in frequency of the SSDs with the atmospheric pressure difference between the IMTL and the Eastern Mediterranean High Pressure (EMHP) in the west. In June, the largest pressure difference between the IMTL and the EMHP coincides with the highest frequency of SSDs. Also, the smallest pressure differences in September and October coincide with the lowest frequency of SSDs. During periods of high frequency of SSDs, the difference between the EMHP and the IMTL pressures becomes greater, with a maximum difference of 8mb in June. At the same time, the EMHP weakens by approximately 6mb during May-June. This suggests that the main reason for the high frequency of SSDs is the presence of a strong IMTL (lower values of pressure). Furthermore, during the low frequency SSDs the IMTL weakens by an average of 7mb, with the EMHP getting stronger by 12mb. This suggest that the main reason for the low frequency of SSDs is the presence of weak IMTL (Figure 5.9)

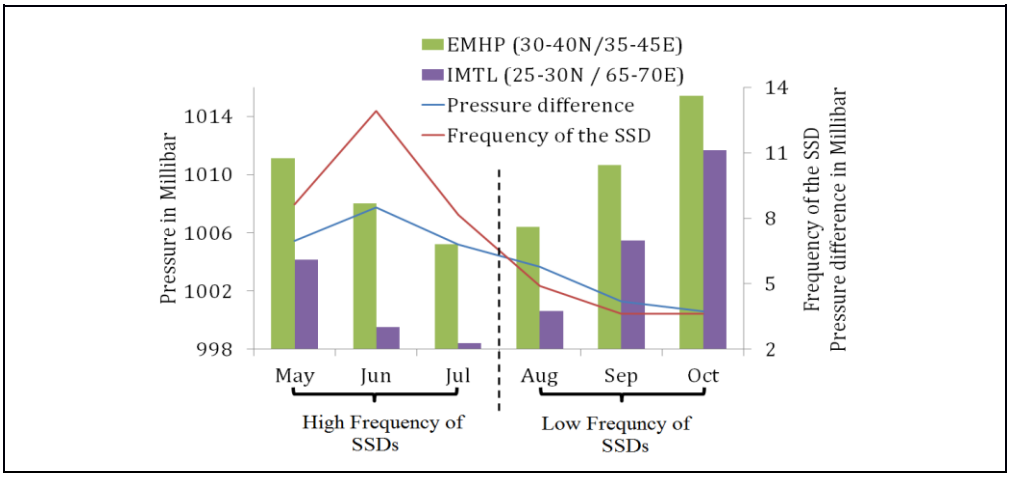

Figure 5.9. Monthly mean atmospheric pressure variation of the EMHP and IMTL. This is represented in column bars while the pressure difference between them and frequency of the SSDs is represented by a line chart; the periods have been divided into HFSS and LFSSDs.

5.2.2 High frequency of SSDs (May – July)

During this period the IMTL becomes stronger (Figure 5.9) and consequently that could be the reason for high frequency of SSDs. Therefore, any direct influence on the IMTL may have an indirect influence on the frequency of SSDs. Moreover, to investigate the connection between the global atmospheric circulation and the frequency of SSDs through the IMTL, this subsection is divided into three sections: surface conditions, 500mb conditions and significance of the global atmospheric circulation connection.

5.2.2.1 Surface conditions

The synoptic situation during high frequency PSSDs over the study area and adjacent regions from the NCEP/NCAR reanalysis is shown in Figure 5.10. The SLP (Figure 5.10b) is below average (~1mb) over the north-eastern edge of the Caspian Sea, which extends south over Iran and the southern part of Afghanistan and Pakistan, finally reaching the north of India. However, the above-average pressure region can be seen only over Northern Europe, extending from Siberia to Scandinavia, with small patches over the middle of the Red Sea, and west of the Arabian Gulf and northern Afghanistan.

The below-average pressure over the Caspian Sea is the nearest system that has a direct effect on the area of study. It causes warmer south and southwesterly winds to move over the eastern part of the study area (Iran, southern Afghanistan and West Pakistan) in Figure 5.10c. This may cause an increase in the average air temperature (positive anomaly) over the adjacent area between Iran, Afghanistan and Pakistan (Figure 5.10a). This in turn could

contribute to an above-average westerly extension of the IMTL which leads to a period of PSSDs.

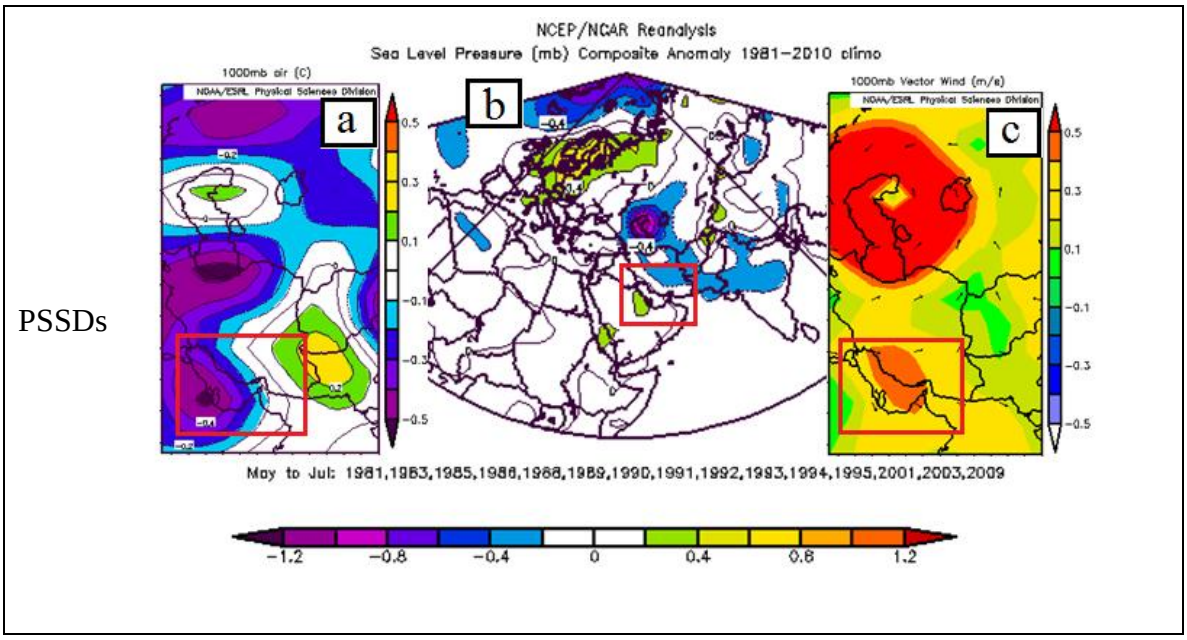

Figure 5.10. NCEP/NCAR reanalysis charts (SLP anomaly (b) in the middle, with the associated wind vector anomaly (c) in the right-hand chart and the associated air temperature anomaly (a) associated with PSSDs in the left-hand chart). There is a red square around the area of study.

Figure 5.11 shows the synoptic situation over the study area and adjacent regions from the NCEP/NCAR reanalysis during high frequency NSSDs, which is exactly the opposite of that which was described for the PSSDs. The above-average pressure over the Caspian Sea has an indirect effect over the area of study, causing cooler northerly winds to move over Iran and adjacent areas (Figure 5.11c). This may cool the land (negative air temperature) over the adjacent area between Iran, Afghanistan and Pakistan (Figure 5.11a). This contributes to a below average westerly extension of IMTL which will lead to a period of NSSDs.

NSSDs

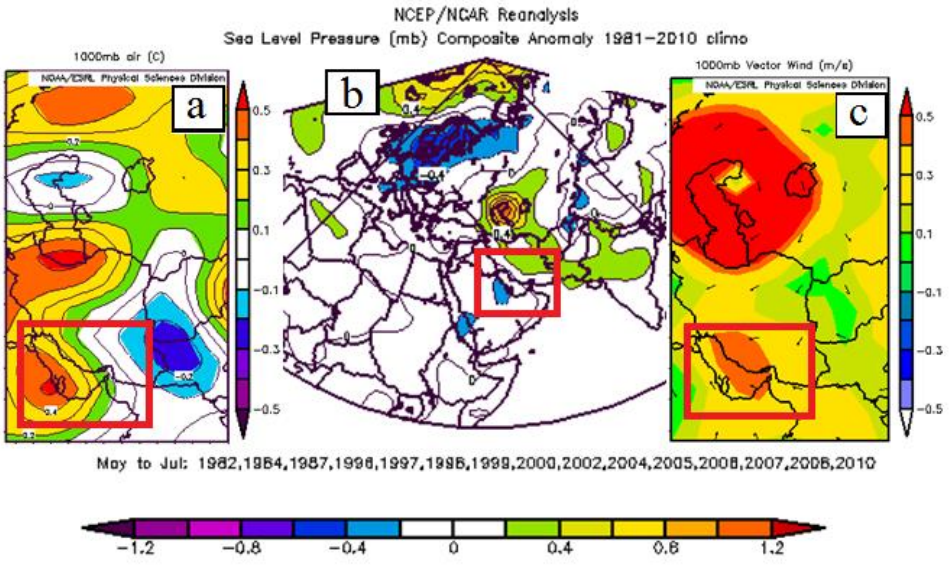

Figure 5.11. NCEP/NCAR reanalysis charts (SLP anomaly (b) in the middle, with associated wind victor anomaly (c) in the right-hand chart and the associated air temperature anomaly (a) in the left-hand chart) associated with NSSDs. There is a red square around the area of study.

5.2.2.2 The 500mb atmospheric condition

Figure 5.12 shows the variations in the 500mb geopotential height anomaly during high frequency SSDs over the north of the Caspian Sea, Scandinavia and the Arctic. It indicates the strength and depth of the Shamal wind. It has been observed that these atmospheric systems go through all layers from the surface to the 500mb level. Additionally, there is a clear visual contrast in the synoptic situations between PSSDs and NSSDs, as is shown graphically in Figure 5.12.

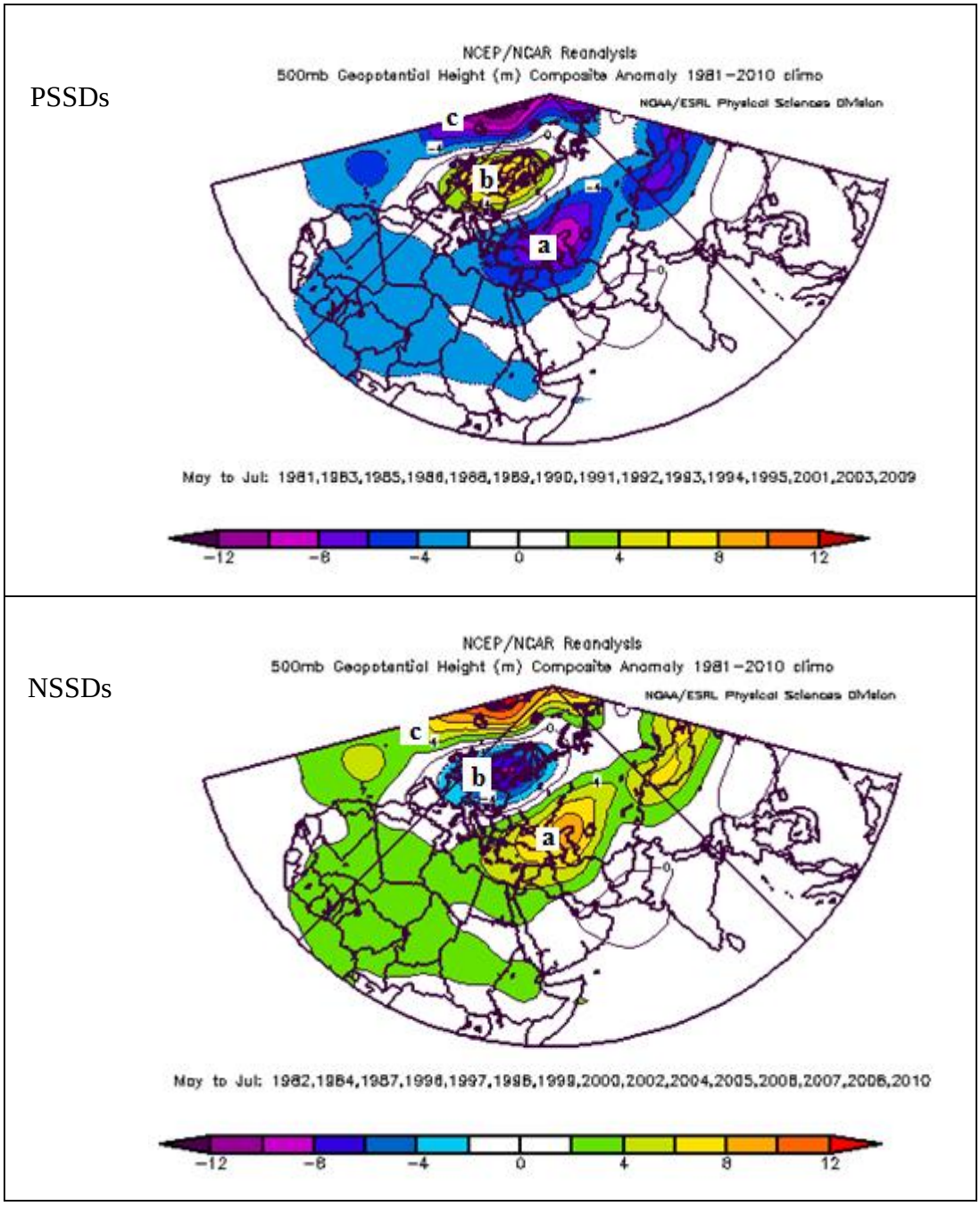

Figure 5.13. The distribution of atmospheric pressure fluctuations at 500mb GPh associated with PSSDs (in the top chart) and NSSDs (in the bottom chart) during high frequency of SSDs. (a) is the atmospheric fluctuation over Caspian Sea, which is statistically significant (paragraph 5.2.2.3), (b) is the atmospheric fluctuation over Scandinavia, (c) is the atmospheric fluctuation over Arctic.

Figures 5.9 – 5.11 suggest that during high frequency SSDs the atmospheric fluctuation over the Caspian Sea which extends to the 500mb (Figure 5.12) affects the westerly extension of the IMTL and this could be attributed to increases in the number of SSDs.

5.2.2.3 Significance of the global atmospheric circulation connection

The ANOVA-F test for Bahrain observational frequency of SSDs and NCEP/NCAR reanalysis data at 500mb geopotential height over the Caspian Sea indicates that during high frequency SSDs the atmospheric fluctuation over the Caspian Sea is statistically significant with P-value = 0.000079, with a correlation coefficient of 0.657 for SSD variations between both systems. Furthermore, a correlation coefficient of 0.74 for meridional wind fluctuation at 500mb over the south east of the Caspian Sea (36-39N, 52-57E) and the frequency of Shamal wind have been calculated. This result shows (Figure 5.13) that meridional wind fluctuation in the south east of the Caspian Sea has the strongest relationship with inter-annual variability of the SSDs. Additionally, another atmospheric fluctuation over North West Europe (Figure 5.12) is statistically significant with P-value = 0.02 and a correlation coefficient of 0.4, which may have an indirect effect on the variability of SSDs as it reacts with the Caspian Sea pressure system.

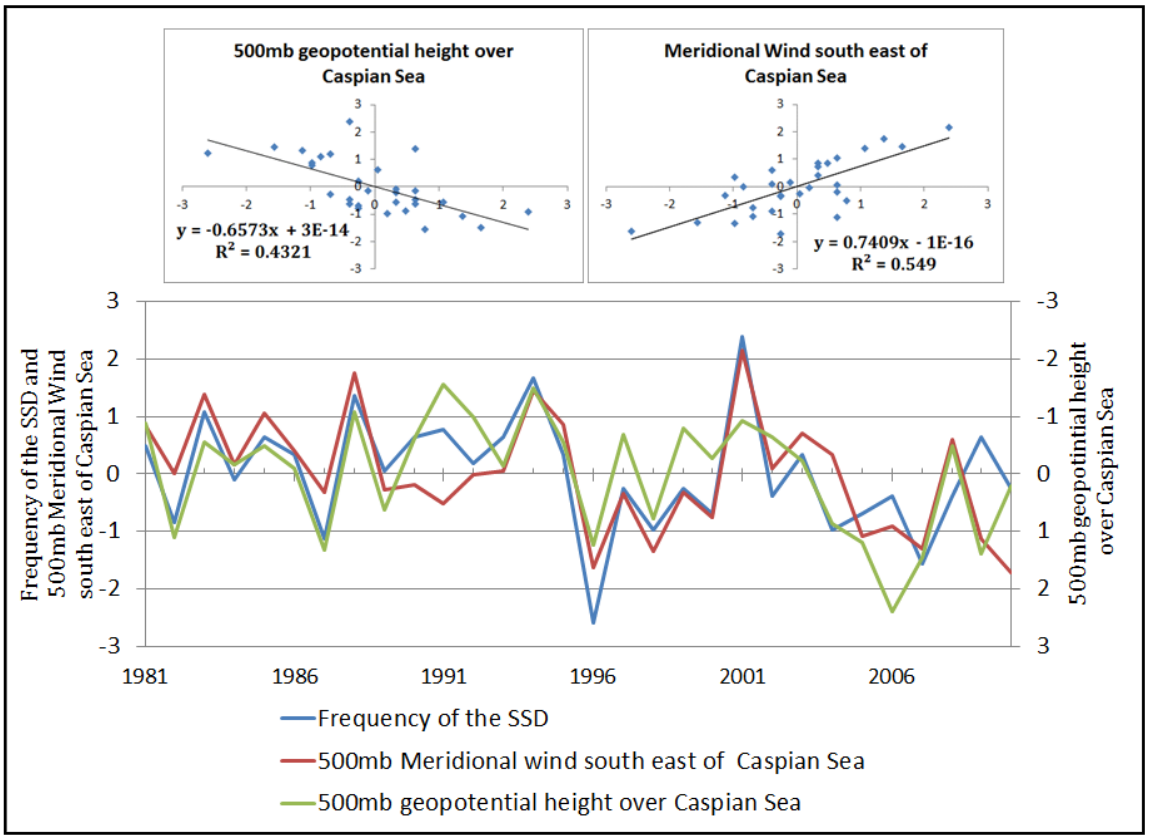

Figure 5.13. The correlation, during the high frequency SSDs, between the frequency of SSDs variation and the 500mb geopotential height over the Caspian Sea and 500mb Meridional wind south east of the south east Caspian Sea. Showing SD variations from normalised (mean) values (SSDs=30days , Siberia=2m/s, Caspian=5766m). This link is stronger in Meridional wind; the relationship represented is illustrated in the top scatter charts, whilst the bottom line-chart uses the frequency of the SSDs as the baseline against the atmospheric fluctuation and Meridional Wind.

5.2.3 Low frequency of SSDs (August - October)

During August to October, the IMTL gets weaker (Figure 5.9) and consequently it decreases the frequency of SSDs. The other important atmospheric fluctuation associated with SSDs is over Siberia; this has less effect on high frequency SSDs (section 5.2.2), but it has a strong effect on low frequency SSDs, as will be discussed in the next two sections.

5.2.3.1 PSSD during low frequency of SSDs

Figure 5.14 illustrates the synoptic situations and vertical cross-section of PSSDs from NCEP/NCAR reanalysis. Figure 5.14b suggests that during PSSDs the strong Siberian high pressure system is associated with a low pressure system over the Zagros Mountains. During PSSDs, a strong above-average sea level pressure anomaly appears over Siberia (Figure 5.14b-c) and the cold air from Siberia extends southward and subsides over the eastern Mediterranean (Figure 5.14b). This causes a below-average temperature anomaly over the eastern Mediterranean (Figure 5.14a). Consequently, the high pressure system extends further south-west over the Arabian Peninsula causing a strong high pressure region (Figure 5.14b). At the same time, there is a below average pressure anomaly over Iran, central Asia (Kazakhstan, NE China, and Mongolia) and the North Atlantic Ocean.

Figure 5.14d indicates that east of the study area there is a strong thermal low associated with a positive meridional wind (Figure 5.14e) and a positive geopotential height from 700mb to 150mb (Figure 5.14f). The positive meridional wind over Iran may enhance the thermal low. The positive geopotential anomaly could indicate a clear sky and favourable weather conditions for the development of below average pressure (thermal low) over the Zagros Mountains. That drives an above average Shamal wind over the study area.

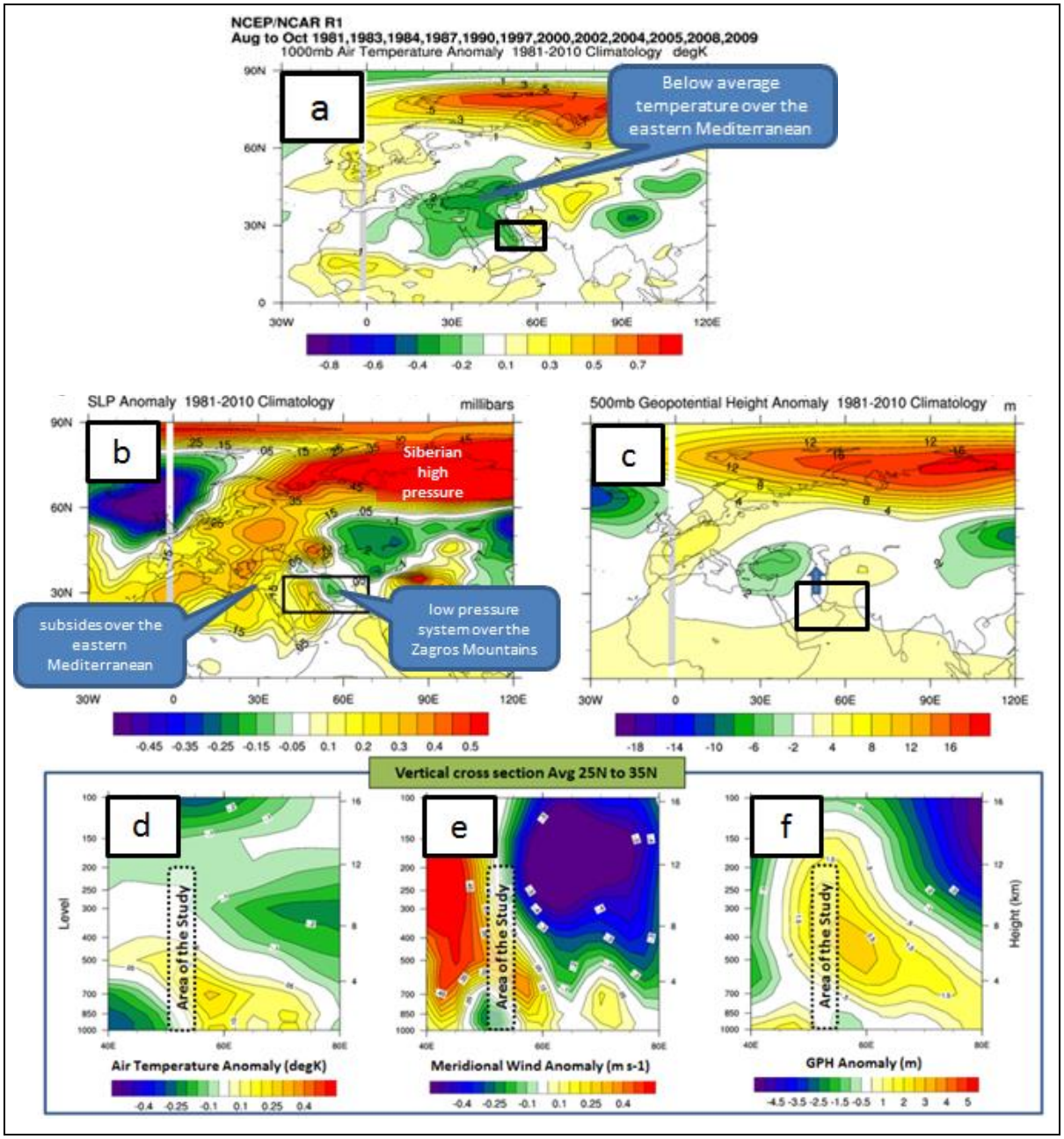

Figure 5.14. The PSSD synoptic situation anomalies, showing the physical process associated with PSSDs. (a) Is the temperature at 1000mb to show thermal effects over the eastern Mediterranean. (b) SLP anomaly illustrates the extension of the Siberian high over east Mediterranean and other associated systems. (c) 500mb geopotential height associated with PSSD. (d-e-f) The vertical cross section average at Lat 25^{o}N to 35^{o}N Long 40^{o}E to 80^{o}E represents geopotential height, meridional wind and air temperature respectively.

5.2.3.2 NSSD during low frequency of SSDs

Figure 5.15 shows a reverse picture which represents the NSSDs where a pressure system has below-average temperature and atmospheric pressure over Siberia (Figure 5.15a-b-c). In this case, below-average pressure (Figure 5.15b) extends south-west and extends west of the study area. In the east, the pressure is above average over the Zagros Mountains (suggesting a weak extension of the IMTL), which could be due to the below-average subsidence in the upper layer between 700mb and 150mb (Figure 5.15f) and cooler air from the north (Figure 5.15e). Both cooler air from the north and below-average subsidence could cause below-average temperatures which result in above-average pressure over the Zagros Mountains.

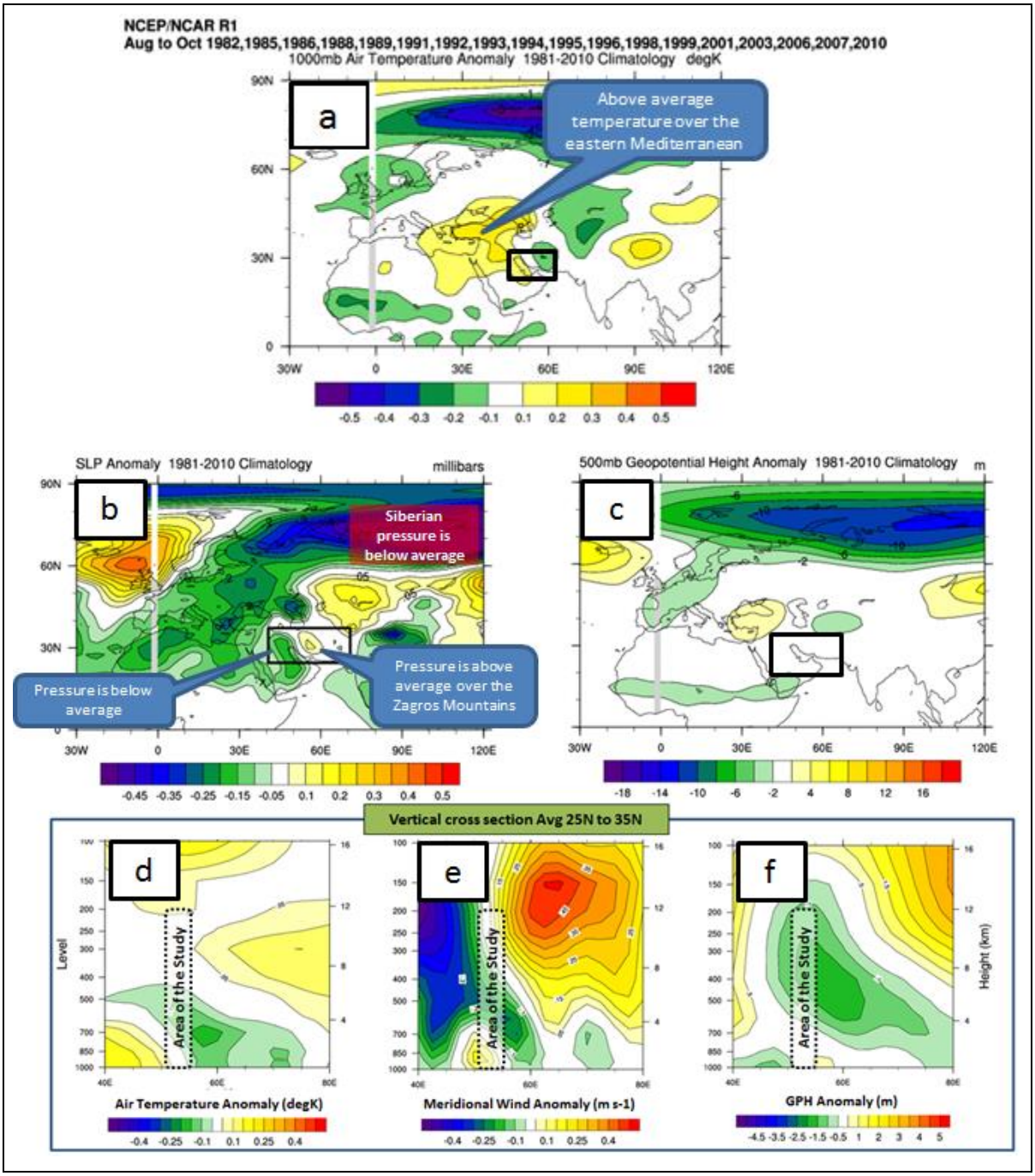

Figure 5.15. The NSSDs synoptic situation anomalies, showing the physical process associated with PSSDs. (a) is the temperature at 1000mb to show thermal effects over eastern Mediterranean. (b) SLP anomaly illustrates below average extension of the Siberian high over east Mediterranean and other associated systems. (c) 500mb geopotential height associated with NSSDs. (d-e-f) The vertical cross section average at Lat 25oN to 35oN Long 40oE to 80oE represents geopotential height, meridional wind and air temperature respectively.

5.2.4 Summary of SSDs and its connection with global circulations

During SSDs, there were two atmospheric fluctuations (over the Caspian Sea and over Siberia) which are potentially linked with the frequency of the SSDs. During periods of high frequency of SSDs, above average pressure occurs over the Caspian Sea which may limit the westerly extension of the thermal low by the cooler northerly wind, resulting in below-average frequency of SSDs. On the other hand, below-average pressure over the Caspian Sea may enhance the westerly extension of the thermal low over the Zagros Mountains caused by warm southerly winds. During low frequency of SSDs, above-average pressure over Siberia feeds cold air into the easterly Mediterranean High, which concurrently is associated with an above-average meridional wind (Figure 5.14b-e). This subsequently extends to the surface over the Zagros Mountains, enhancing a deepening of the thermal low over this topographic feature, which consequently causes above average frequency of SSDs.

Table 5.3. illustrate the Summary of the SSDs and its connection with global circulations in table forms

Phenomena	time of the years	Moderator	Effect	result
High frequency of SSDs	May – July	Caspian Sea High pressure	limit westerly extension of the IMTL	Below average frequency of SSDs
		Caspian Sea Low pressure	enhance the westerly extension of the IMTL	above average frequency of SSDs
Low frequency of SSDs	August - October	Siberian High pressure	Enhance easterly extension of the EMHP	above average frequency of SSDs
		Siberian Low pressure	Limited easterly extension of the EMHP	Below average frequency of SSDs

5.3 Winter Shamal Days (WSDs) and its connection with global circulations

The aim of this section is to investigate the connection between WSDs and the global circulation pattern. Figure 5.16 is the result of combining winter months SLP. It highlighted four large pressure systems which influence the area of study (Siberian high from the east, Azores high, Iceland low and Sudan low in the west). The frequency of WSDs was investigated for a six-month period, November – April. Later, the influence of high frequency of WSDs (December, January and February) on global atmospheric circulations is examined.

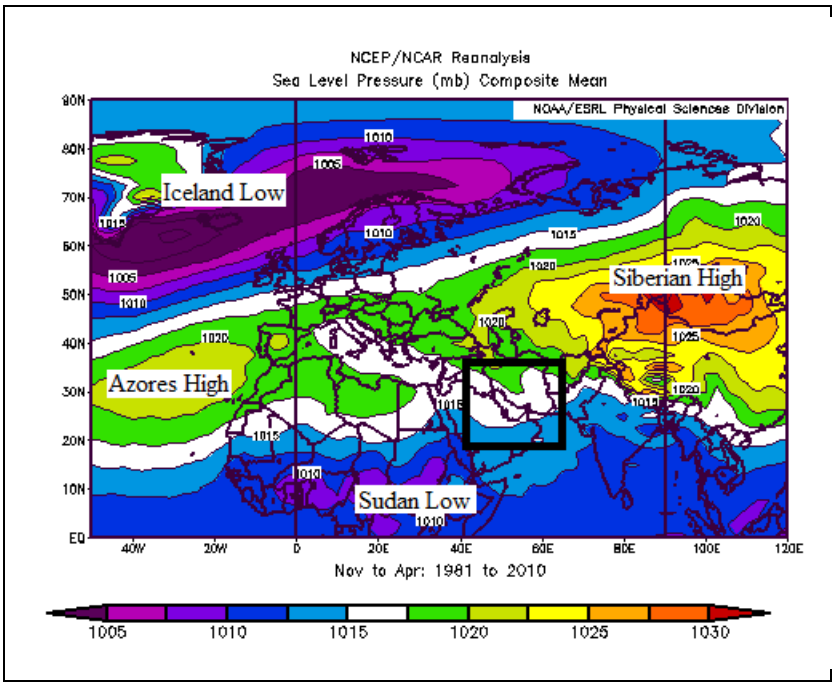

Figure 5.16. NCEP/NCAR reanalysis charts thirty years (1981 - 2010) mean sea level pressure for the Winter months (Nov-Apr), highlighting the main atmospheric pressure systems in the region.

5.3.1 Six-month period (November - April)

This subsection is divided into three sections; the first one explores the global atmospheric circulations pattern associated with each WSD phase. Then, the interpretation of the connection between frequency of WSD and global circulation is illustrated in section two. The third section covers the discussion on the hypothesis of the connection between the frequency of WSDs and NAO/AO.

5.3.1.1 Associated global atmospheric circulations

Thirty years of the frequency of WSD data were divided into Positive (above average) WSDs (PWSD) years and Negative (below average) WSDs (NWSD) years, in order to capture the main features of each period. These data were used to identify the important atmospheric features associated with PWSDs as well as NWSDs. The analysis of PWSD years and NWSD years was carried out by using NCEP/NCAR SLP; 1000, 700, 500 mb geopotential height; and 250 mb level wind vector (m/s).

The results (Figure 5.17a) reveal that during PWSDs, at 500mb geopotential height there were negative belts extending from North America deepening over Greenland (-15) and reaching the Arctic. Furthermore, there was one negative spill over Africa and three positive spills over Atlantic, Europe and Siberia. The NWSDs meteorological conditions (Figure 5.17b) were the reverse of the PWSDs. For the mean of the six-month period, the only atmospheric fluctuations at 500mb level geopotential heights over Greenland were linked to frequency of WSDs variations. The link between WSD occurrence and the

atmospheric fluctuation over Greenland was statistically significant with P-value = 0.01 and a correlation coefficient of 0.43.

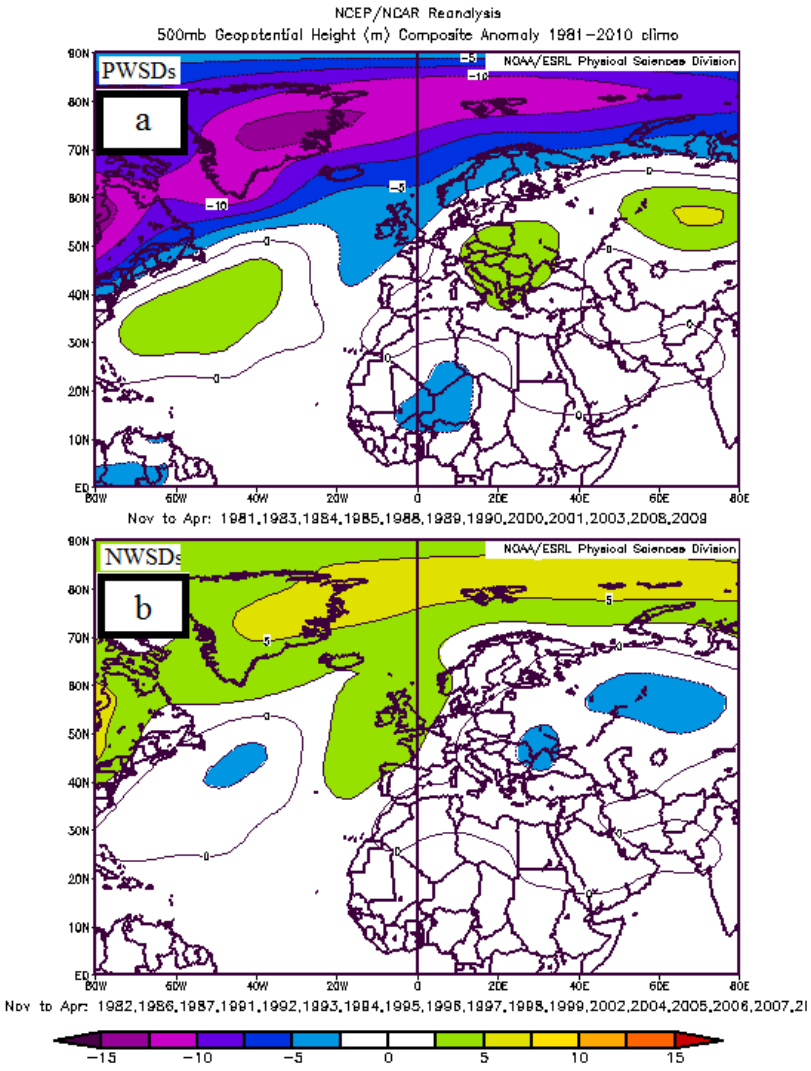

Figure 5.17. NCEP/NCAR reanalysis at 500mb geopotential height for PWSDs and NWSDs, highlighting atmospheric systems that linked with each of them. Atmospheric fluctuation over Greenland was statistically significant to the variation in the frequency of WSDs, while others were not.

5.3.1.2 Connection between frequency of WSDs and Greenland atmospheric fluctuation

The significant correlation between the frequency of WSDs variation and atmospheric fluctuation over Greenland could be interpreted as indicating that the westerly cyclone is the main engine initiating wintery synoptic wind over the region. As an example, the period from 26 January until 2 February 2008 is used to describe the route of the westerly cyclone that affects the area of the study. The sequence of 500mb geopotential heights (Figure 5.18) suggests that the westerly cyclone which affects the area of the study originates in northern Europe.

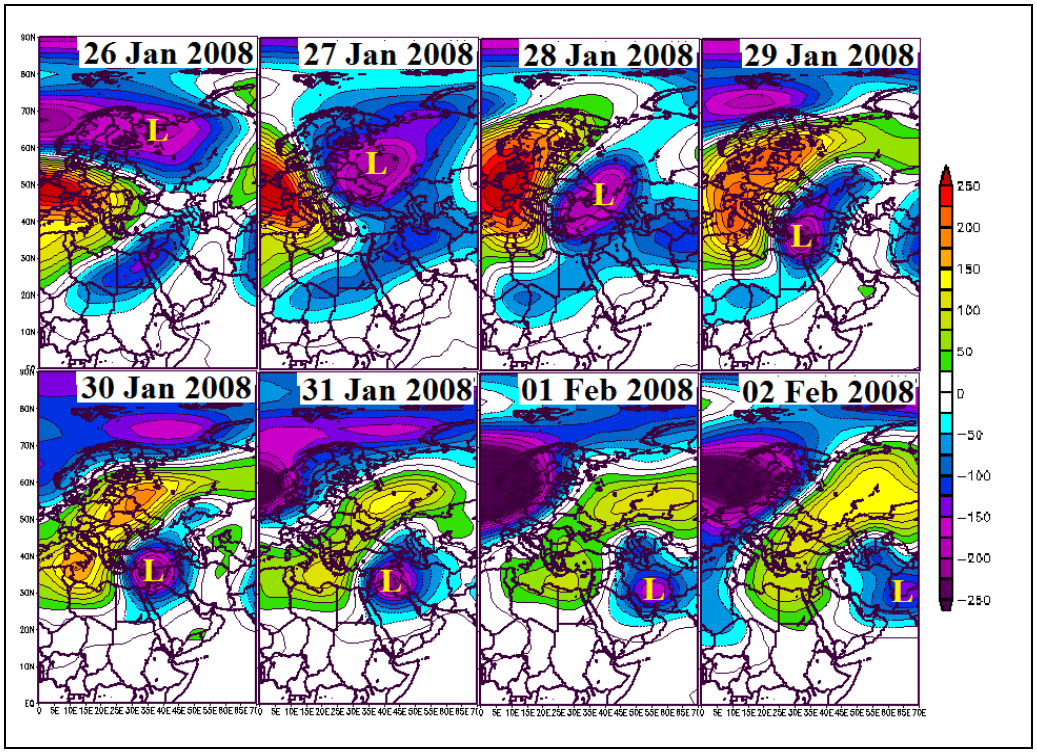

5.18. The track of westerly depression (L) from 26 January until 2 February 2008 is illustrated by NCEP/NCAR 500mb geopotential height from 26 January 2008 to 2 February 2008. The westerly depression (L) moves from north of Europe through east of the Mediterranean region passing over the area of the study. Later it moves further east of the study area allowing High to extend behind it to build the north westerly pressure gradient (Shamal wind) over the area of the study.

Additionally, the upper air pattern at 250mb level (Figure 5.19) which drives north Atlantic depressions into northern Europe and then into the area of study, is affected by pressure fluctuations over Greenland. This could be the main reason for the relationship between the frequency of variation in the WSDs and atmospheric fluctuations over Greenland.

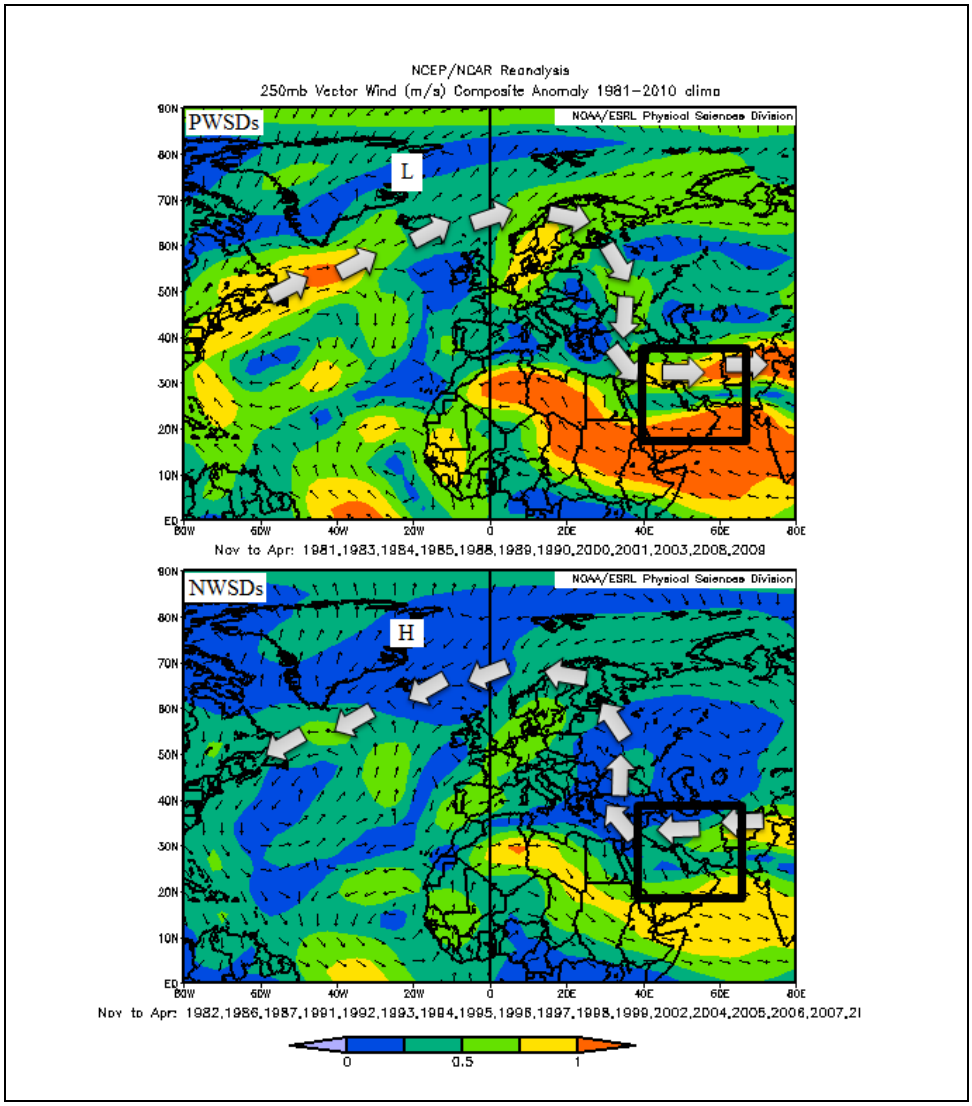

Figure 5.19. NCEP/NCAR 250mb vector wind (m/s) illustrating the upper air flow pattern associated with PWSDs and NWSDs which suggests that the low over eastern Greenland drives North Atlantic storms to northern Europe - and some of these affect the area of the study, while high pressure over eastern Greenland reduces the frequency of North Atlantic storms affecting northern Europe which as a result will reduce the frequency of the storms crossing the area of the study.

5.3.1.3 NAO and AO connection

The North Atlantic Oscillation (NAO) controls the strength and tracks of westerly storms across the North Atlantic Ocean, as explained in section 2.3.9.4. A positive NAO index drives westerly depressions toward North-West Europe (Hurrell, et al., 2001). NAO patterns are different from Arctic Oscillation (AO), see more in section 2.3.9.3, but both have a similar influence in their winter Atlantic storm tracks (Hodges, 2000). Therefore, investigating the correlation between both systems (AO and NAO) with WSDs is vital, because if there is any correlation it will facilitate the future prediction of variation in WSDs.

NCEP/NCAR data for the AO index and NAO index from November until April based on 30 years (1981-2010) were examined against the frequency of WSDs data by using an ANOVA-F test. AO patterns can be identified in the troposphere and stratosphere by using zonal wind and geopotential height charts (Hodges, 2000). The results (Table 5.4) indicate that there is no statistically significant correlation between both atmospheric phenomena (AO and NAO) and frequency of WSDs for a six-month period. However, there is a statistically significant correlation for high frequency (December, January, February) of WSDs which is described in section 5.3.2.3.

Table 5.4. Results of statistical examination (ANOVA-F test) for Bahrain observational WSDs and NCEP/NCAR data which represent AO and NAO from November until April.

Regression Statistics	AO	NAO
P-value	0.214	0.314
R Square	0.054	0.036
correlation coefficient	0.23	0.19

5.3.2 High frequency of WSDs (December- February)

The connection between the high frequency of WSDs and the global circulations pattern is investigated in three sections, which includes associated global systems, analysis of the correlation with the atmospheric fluctuation over Greenland and west of Europe, and the connection with NAO and AO.

5.3.2.1 Associated global systems

Further analyses were carried out for December, January and February due to the increased frequency of WSDs. Figure 5.20 shows the meteorological conditions at 500mb geopotential height for PWSDs and NWSDs. The figure suggests that there are two atmospheric fluctuations associated with variation in Shamal Days over Greenland and Western Europe. During PWSDs (Figure 5.20a) there was positive (+25m) atmospheric fluctuation over Western Europe while there was negative (-33m) atmospheric fluctuations over the eastern coast of Greenland. The negative atmospheric fluctuations extends around the positive atmospheric fluctuation in the eastern Mediterranean and indicate the route of westerly depressions that affect the area of study. The NWSDs meteorological conditions were the reverse of those of the PWSDs (Figure 5.20b).

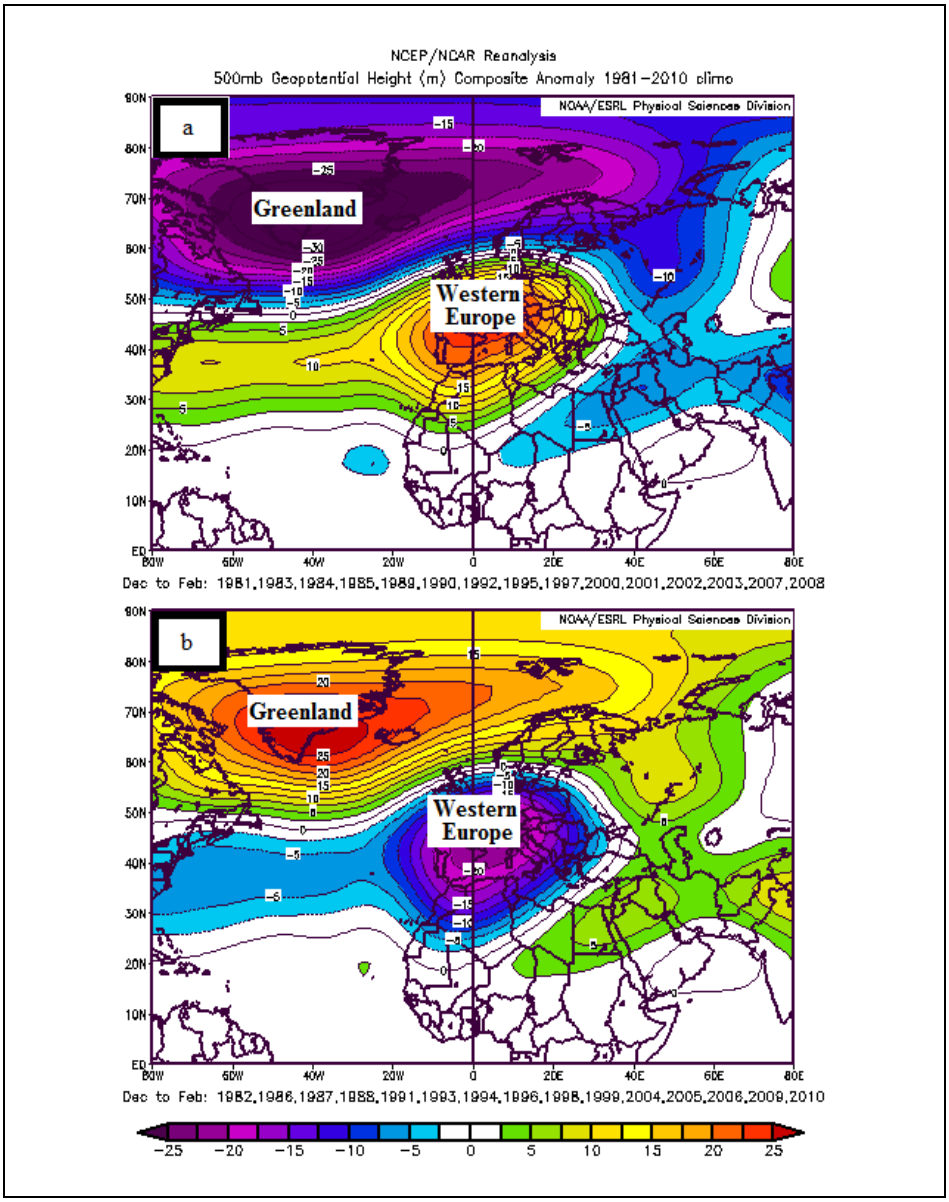

Figure 5.20. NCEP/NCAR reanalysis at 500mb geopotential height for (a) PWSDs and (b) NWSDs, highlighting atmospheric systems that linked with each of them. Atmospheric fluctuations over Greenland and Western Europe are statistically significant.

The ANOVA-F test was carried out for Bahrain observational frequency of the WSDs against NCEP/NCAR reanalysis at 500mb level geopotential height for Western Europe

and the eastern coast of Greenland. The result (in Table 5.5) indicates that the atmospheric fluctuations over both locations were statistically significant for the frequency of WSDs.

Table 5.5. Results of statistical examination (ANOVA-F test) for Bahrain observational WSDs and NCEP/NCAR data which represent AO and NAO from December until February.

Regression Statistics	Atmospheric fluctuation over	
	Western Europe	Eastern Greenland
P-value	0.001	0.004
R Square	0.32	0.26
correlation coefficient	0.56	0.51

5.3.2.2 Analysis of the correlation with the atmospheric fluctuation over Greenland and Western Europe

The results suggest that air pressure / geo-potential height fluctuations over Western Europe have the strongest relation with the inter-annual variability of the frequency of the WSDs. This can be explained as follows: both systems drive westerly depressions into northern Europe while the atmospheric fluctuations over western Europe have a significant influence upon the westerly depression route to the eastern Mediterranean, and hence to the study area (Figure 5.21).

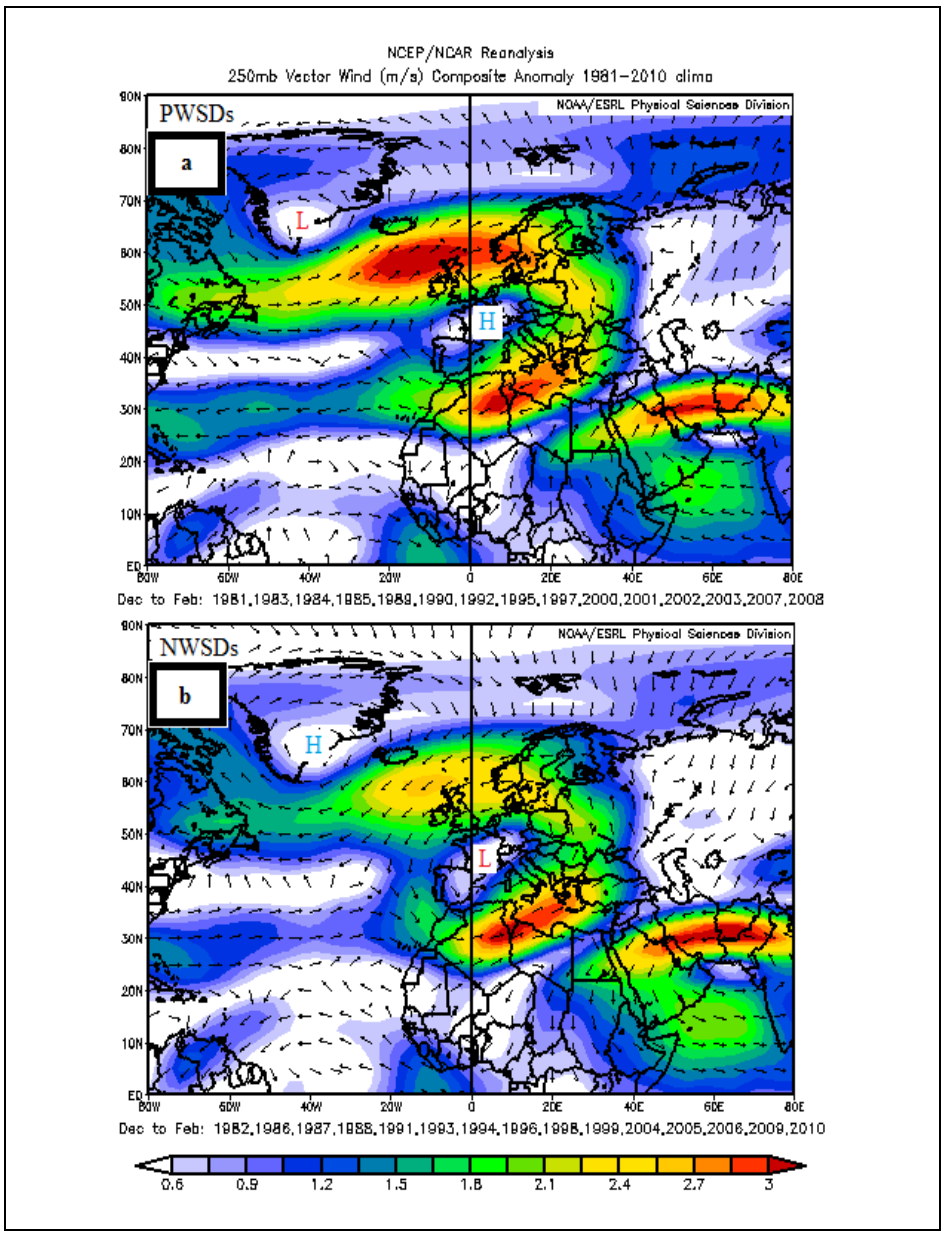

Figure 5.21. NCEP/NCAR reanalysis at 250mb wind vector (m/s) for (a) PWSDs and (b) NWSDs, showing the influence of the atmospheric fluctuations over western Europe in the wind circulation which drives westerly depressions into the eastern Mediterranean.

5.3.2.3 NAO and AO influence

Negative and positive phases of the frequency of the WSDs, NCEP/NCAR NOA index, NCEP/NCAR AO index were compared. The NCEP/NCAR reanalysis at 500mb geopotential height and SLP for positive (above average) and negative (below average)

phases of the frequency of the WSDs, NAO index and AO index are shown in figures 5.22 and 5.23 respectively. The value of these indices has been cited from < http://www.cpc.ncep.noaa.gov/products/precip/CWlink/daily_ao_index/teleconnections.shtml >. The results show that the three phenomena have similar surface and upper air meteorological conditions for positive and negative phases as shown in Figures 5.22 and 5.23.

During the positive phase at 500mb geopotential height (Figure 5.22), there was a negative pressure system over Greenland extending over northern Europe whilst there was a positive pressure system over Western Europe. At the surface (Figure 5,23), it was apparent that the highlighted atmospheric fluctuation was the Iceland low in the northwest of Europe and the Azores high in Western Europe. This meteorological condition was the favourable atmospheric condition for westerly depressions to move from the North Atlantic Ocean toward the area of study, causing frequent WSDs.

Furthermore, figures 5.22 and 5.23 show the negative phase of the three phenomena (WSDs, AO, and NAO) which is the reverse of the positive phase. The negative phase represented unfavourable meteorological conditions for westerly depressions to move towards the area of study, which, as a result, caused infrequent WSDs. Additionally, the ANOVA-F test was carried out for the frequency of WSDs against NCEP/NCAR AO index and NAO index. Results indicate that the correlations between WSD frequency and AO/NAO fluctuations were statistically significant (see Table 5.6)

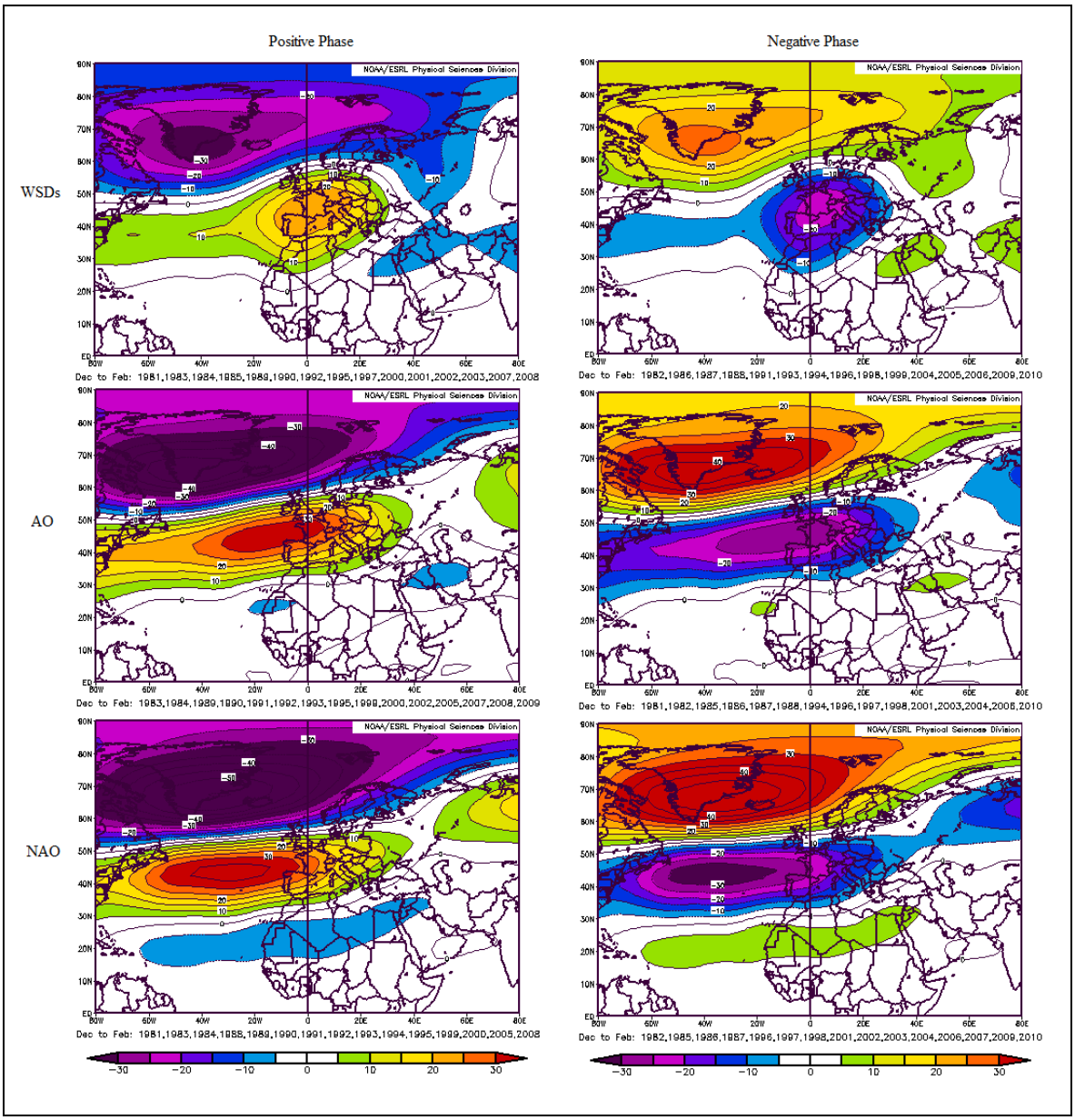

Figure 5.22, NCEP/NCAR reanalysis 500mb geopotential height anomalies for positive and negative phases of the three phenomena (WSDs, AO, NAO), highlighting atmospheric systems that are linked with each of them. Atmospheric fluctuation of the 500mb geopotential height over Greenland and the west of Europe were statistically significant to the frequency of WSDs (Table 5.4), furthermore AO index and NAO index were statistically significant to the frequency of WSDs (Table 5.5).

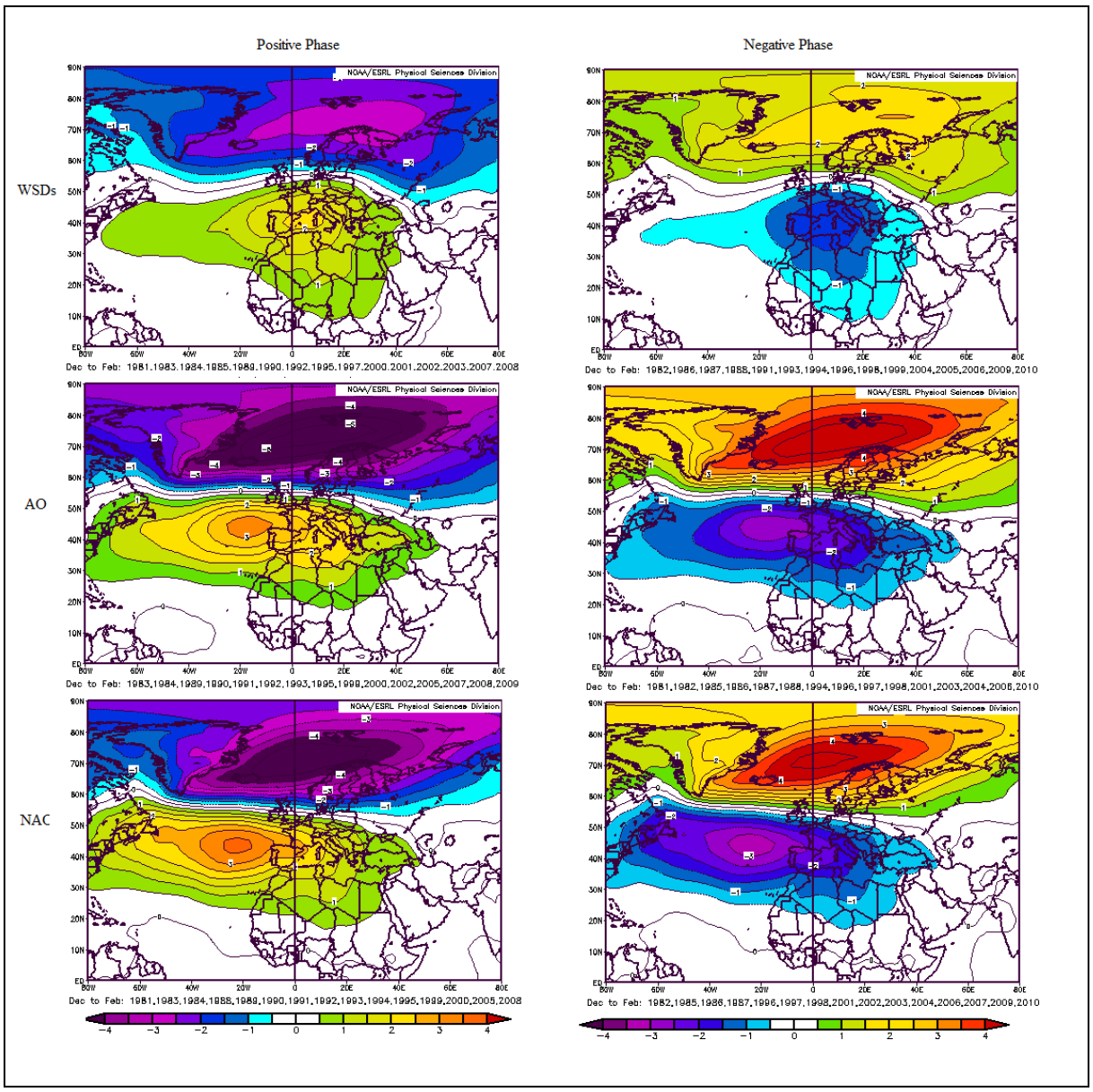

Figure 5.23. NCEP/NCAR reanalysis sea level pressure anomalies for positive and negative phases of the three phenomena (WSDs, AO, NAO), highlighting atmospheric systems that are linked with each of them. Atmospheric fluctuation of the 500mb geopotential height over Greenland and the west of Europe were statistically significant to the frequency of WSDs (Table 5.4), furthermore AO index and NAO index were statistically significant to the frequency of WSDs (Table 5.5).

Table 5.6. Result of statistical analysis (ANOVA-F test) of Bahrain observational WSDs and NCEP/NCAR AO and NAO data for December, January and February.

Regression Statistics	AO	NAO
P-value	0.006	0.02
R Square	0.24	0.16
correlation coefficient	0.49	0.41

The result shows that the AO has the strongest relationship with the inter annual variability of WSDs. This can be interpreted as both pressure systems (AO/NAO) having a similar influence in their westerly depressions tracks, but the AO seems to have more influence on the westerly depression tracks into the area of the study. This is likely to be due to the AO's role in blocking westerly depressions or forcing them to track into the area of study. On the other hand, NAO development does not guarantee that the depression will affect the study area.

Additionally, the AO dynamically affects the strength of the western edge of the Siberian High. The strength of this Siberian High depends on downward motion from the top of the troposphere (Wang, et al., 2001). When the negative phase of the AO's downward motion is stronger, then the Siberian High will be stronger than normal, which in turn will block or reduce the size of the westerly depressions approaching the area. Conversely, for a positive phase of the AO, when the downward motion is weaker, the Siberian High will be weaker than normal and the number of westerly depressions will approach normal or be greater, thereby increasing the number of Shamal days.

5.3.3 Summary of WSDs and its connection with global circulations

The main catalyst for WSDs is the passage of westerly depressions over the area. These depressions originate over the North Atlantic Ocean. Therefore, the occurance of WSDs is affected by atmospheric fluctuations over Greenland and Western Europe. However, the main reason for the reduction in WSDs could be the result of a reduction in the number of westerly depressions crossing the area. Moreover, there is a study (Lionello and Giorgi, 2007) suggesting that the number of westerly depressions crossing the Middle East is decreasing due to climate change.

Table 5.7. Summary of the occurrence of WSDs and the connection with global circulations.

Phenomena	time of the years	Moderator	Effect	result
WSDs	November-April	Low pressure over Greenland	Increases the frequency of the westerly depression into northern Europe which may proceed into area of the study	above average frequency of WSDs
		High pressure over Greenland	Decreases the frequency of the westerly depression into northern Europe	below average frequency of WSDs
High frequency of WSDs	December – February	Low pressure over Greenland associated with High pressure over western Europe (+NAO, +AO)	Increases the frequency of the westerly depression into area of the study	above average frequency of WSDs
		High pressure over Greenland associated with low pressure over western Europe (-NAO, -AO)	Decreases the frequency of the westerly depression into area of the study	below average frequency of WSDs

5.4 Conclusion

The statistical analysis described in this chapter reveals there was a decline in wind strength over the period of the study (1981-2010), which could be a result of the decline in the frequency of Shamal days. During the period of study there was significant reduction in Winter Shamal days. Global atmospheric fluctuations have been used to explain these observed trends.

During SSDs, there were two atmospheric fluctuations (over the Caspian Sea and Siberia) which interconnect with variability in the SSDs. During the high frequency SSD (May-July), above-average pressure occurs over the Caspian Sea which limits the westerly extension of the thermal low by the cooler northerly wind, resulting in below average SSDs. On the other hand, below-average pressure over the Caspian Sea enhances the westerly extension of the thermal low over the Zagros Mountains caused by a warm southerly winds. The occurrence of SSDs is linked to pressure variations in the Caspian Sea region. During low frequency SSDs, above-average pressure over Siberia feeds cold air into the easterly Mediterranean High, which concurrently is associated with an above average meridional wind at 500mb level west of the Caspian Sea. This subsequently extends to the surface over the Zagros Mountains, enhancing a deepening of the thermal low; this topographic feature consequently causes above average SSDs.

During WSDs, there were two atmospheric fluctuations (over the east of Greenland and west Europe) which interconnect with the WSDs variability. For the six-month winter period, only atmospheric fluctuations over Greenland were significant to the WSDs

variation. In contrast, during the period of increased frequency of WSDs (December, January, and February), atmospheric fluctuations over the west of Europe became more significant to the frequency of the WSDs variation. Both systems have no direct effect in the WSD's variation, but they affect the frequency of westerly depressions that cross the area, which may be considered as the ignition of WSDs. Therefore, the main reason for the reduction in the frequency of the WSDs is the reduction in the number of westerly depressions crossing the area. This is strongly linked to both the NAO and the AO.

Chapter 6 – Influence of the local meteorological condition on EM propagation

The aim of this chapter is to examine electromagnetic wave (EM) propagation in each key meteorological condition in the study area, including winter and summer land and sea breeze circulation, winter and summer Shamal, winter and summer Suhaili, and Al Nashi (a winter feature). EM propagation is influenced by atmospheric refractivity, which depends on noticeable variations in temperature and relative humidity with height and time (Grabner, Kvicera, 2011). There are four types of atmospheric refractivity which include sub refraction, normal, super refraction and ducting (details are given in chapter 2 – section 2.1). This chapter will focus on atmospheric ducting as it has a significant effect on EM waves.

Ducts are divided into four types: the evaporation duct (Figure 6.1c, developed over the sea as a result of change in humidity and temperature), the surface duct (Figure 6.1a, developed on the surface due to night time cooling for example), the surface-based duct (Figure 6.1b, gives the same results as a surface duct, but the trapping layer is not on the surface) and the elevated duct (Figure 6.1d the trapping layer at specific height and it has normal EM propagation beneath it) (Chou Y, and Kiang J, 2014), illustrated in figure 6.1. The surface duct and surface-based duct have different structures for the trapping layer (red in figure 6.1), but they have the same trapping conditions (pink in the figure) (details in section 2.1.3). Therefore, in this study both the surface duct and surface-based duct are considered to be surface-based ducts.

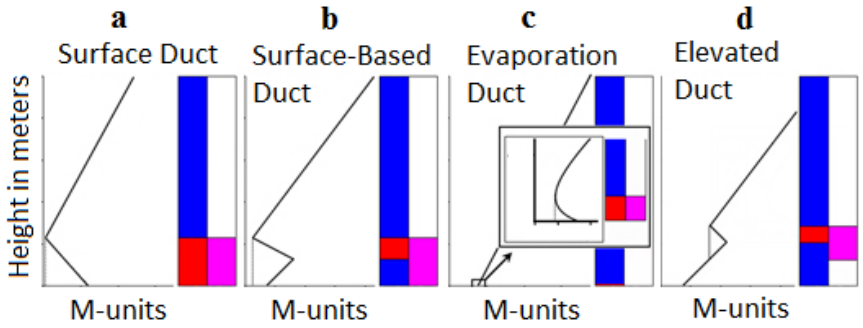

Figure 6.1. Type of duct represented in refractivity profile where blue is normal refractivity, red is trapping, and pink represents the duct channel (US Navy/NMOPDD Atlantic).

In this chapter, a summary of the propagation conditions was calculated using the AREPS model (described in section 3.1.4) for each air mass, using input data from radiosondes at Abu Dhabi airport (the continuously available source of radiosonde data in the study region). Abu Dhabi airport radiosonde data starts at 27 meters above sea level, and data is gathered twice a day at 0400 and 1600 local time. Therefore, the first few metres of the radiosondes represent only Abu Dhabi air. It is different from the air above the sea due to the elevation difference and large diurnal variations in temperature over land compared to sea.

It was found that most of the time, light wind was observed over the area of study, which can be considered as land and sea breeze circulation (Figure 4.3). In this chapter, land and sea breezes are categorised into two air masses based on case studies from winter and summer seasons. Furthermore, five synoptic winds were observed and each one of them

considered as an individual air mass for this study. The air masses were examined by using radiosonde data in the AREPS model. Then, the AREPS model provided a propagation condition summary for each scenario and predicted radar propagation performance in the assigned environment. The AREPS model runs were performed for an EM frequency of 400MHz as this is the frequency of the simulated Airborne Early Warning (AEW) radar, and the default setting for the trial version of software used. Because of its application in AEW radar, it is a useful frequency to discuss. Different frequencies would behave in a different manner and be trapped in different sized ducts – higher frequencies are trapped within a larger number of ducts. This chapter is divided into three subsections that describe temporal variations in different ducts, duct conditions in winter and summer air masses. All the statistical analysis is based on the data during 2006-2010. In section 2 (winter) and 3 (summer) case studies of different air masses are used to illustrate and discuss the associated duct conditions.

6.1 Temporal variations in different ducts

The aim of this section is to introduce a general picture of the duct phenomena over the study area. The reason behind the formation of different types of duct is illustrated in the following sections (6.2 and 6.3). Five years (2006-2010) of Abu Dhabi radiosonde data is used to describe duct variation over the area of the study. Ducting conditions were examined twice daily (0400 and 1600) for every day, giving a total of approximately 3600 runs to provide data for analysis. This section is divided into three sub sections: evaporation duct, surface-based duct, and elevated duct. Some of the facts coming from the analysis of this section relating to the various wind will be discussed in section 6.2 and 6.3.

6.1.1 Evaporation duct

Data from Abu Dhabi radiosondes was fed into the AREPS model to calculate the behaviour of the evaporation duct over Abu Dhabi. In addition, wind speed data from Abu Dhabi airport and sea surface temperature (^{o}C) (http://www7320.nrlssc.navy.mil/global_ncom/glb8_3b/html /Links/sst_list_pgulf.html) were provided to the model as additional information. This enabled the prediction of the structure of the evaporation duct starting from sea surface rather than just 27 meters.

Five years (2006-2010) of Abu Dhabi daily radiosonde data illustrated that the evaporation duct is a permanent phenomenon over the southern coast of the Arabian Gulf, at an average height above the sea surface of 24 meters. The morning average height (0400 local time) was 19 meters, while the afternoon average height (1600 local time) was 30 meters. The minimum height was in winter while the maximum heights were in summer. In January and December, the average height of the evaporation duct was 10 meters in the morning and 20 meters in the afternoon. In contrast, in July the average height of evaporation duct was 27 meters in the morning and 38 meters in the afternoon. Figure 6.2 illustrates the monthly variation of the evaporation duct.

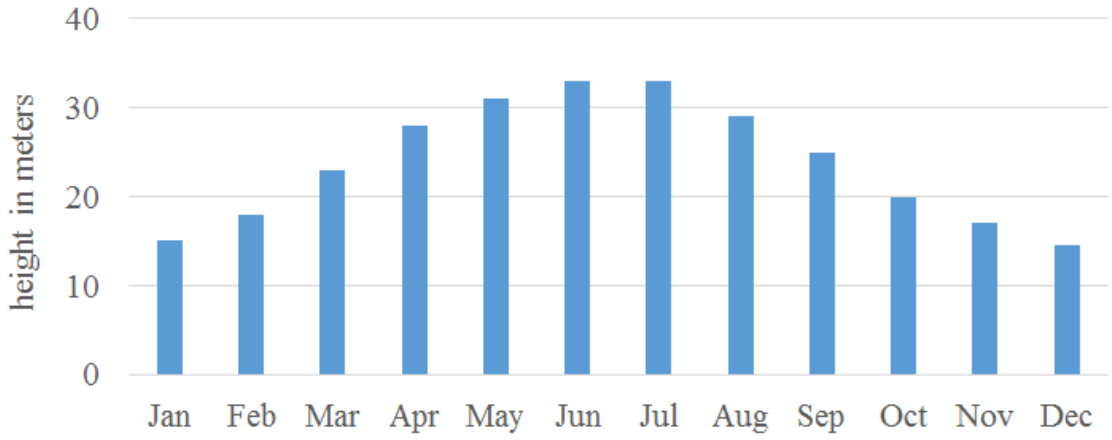

6.2. Five years (2006-20010) monthly mean variation of evaporation duct height calculated from Abu Dhabi radiosonde data.

Also, it has been observed that the height of the evaporation duct increases with an increase in wind strength, air/sea surface temperature and decrease in humidity. This could be due to the dry warm air over cooler a sea giving a strong inversion and sharp decrease in the dew point. In contrast, high relative humidity, light wind, cooler air and cooler sea decrease the height of the evaporation duct. Furthermore, it has been observed during the analysis that the Suhaili and Shamal increase the height of the evaporation duct. However, the Suhaili has more effect on the evaporation duct due to its dryness rather than the Shamal, which comes via a long sea route. The evaporation duct reaches its minimum height during the night as radiation cooling overland increases the humidity of land breezes, and reduces the humidity contrast between the two air masses. By contrast, humid sea breezes during the day increase the evaporation duct height by increasing the contrast (details in section 6.2 and 6.3).

6.1.2 Surface-based duct

Results show that a surface-based duct occurred 75% of the time during the period of study, with an average height of 117 meters. It occurred on 89% of mornings (0400 local time) with an average height of 175 meters, and on 61% of afternoons (at 1600 local time) with an average height of 59 meters. The minimum height was in winter months while the maximum heights were in summer months (Figure 6.3). In January, the average height of the surface-based duct was 68 meters in the morning and 6 meters afternoon. In contrast, in July the average height of the surface based duct was 303 meters in the morning and 166 meters in the afternoon. Furthermore, it was observed that the surface-based duct is significant and thicker during land and sea breezes, and minimized with moderate and stronger Shamal. It disappears with during the Suhaili and a Strong Al-Nashi (details in section 6.2 and 6.3).

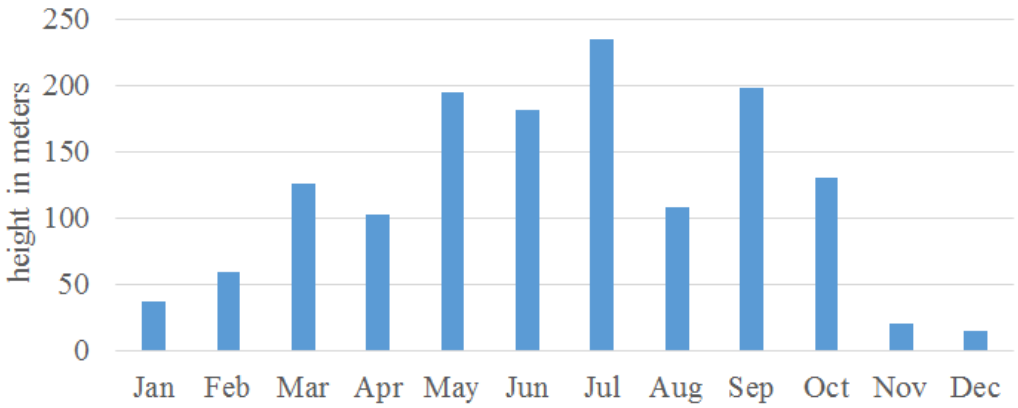

6.3, Five years (2006-20010) monthly mean variation of the surface based duct height calculated from Abu Dhabi radiosonde data.

6.1.3 Elevated duct

Table 6.1. shows that an elevated duct occurred 54% of the time during the period of study with an average thickness of 260 meters. It mostly occurred in a layer approximately between 1000-2000 meters. It was rarely (9% of the time) associated with an additional elevated duct at higher altitude (approximately between 3000-4000 meters). Figure 6.4 illustrates that the elevated duct during the summer months moves to a higher altitude, while in winter months it moves downward. Furthermore, the elevated duct more frequently occurs during January, October, November and December. Its occurrence decreases in the remaining months and reaches the minimum occurrence during May. Usually it is associated with westerly to north westerly flow (e.g. Shamal) and is rarely associated with southerly to south-easterly flow (e.g. Suhaili) and if so, occurs as a thin layer. An elevated duct was observed on around 81% of Shamal days and 52% of winds under 11knots. The elevated duct was rarely observed (7%) during the Suhaili.

Table 6.1. Five years (2006-20010) mean of the morning and afternoon elevated duct occurrence, altitude and thickness calculated from Abu Dhabi radiosonde data.

	first layer				Second layer			
	occurred	from	to	thickness	occurred	from	to	thickness
Morning	51%	1519	1780	261	10%	2958	3115	175
Afternoon	56%	1144	1404	259	7%	3756	3916	160
Average	54%	1331	1592	260	9%	3357	3515	167

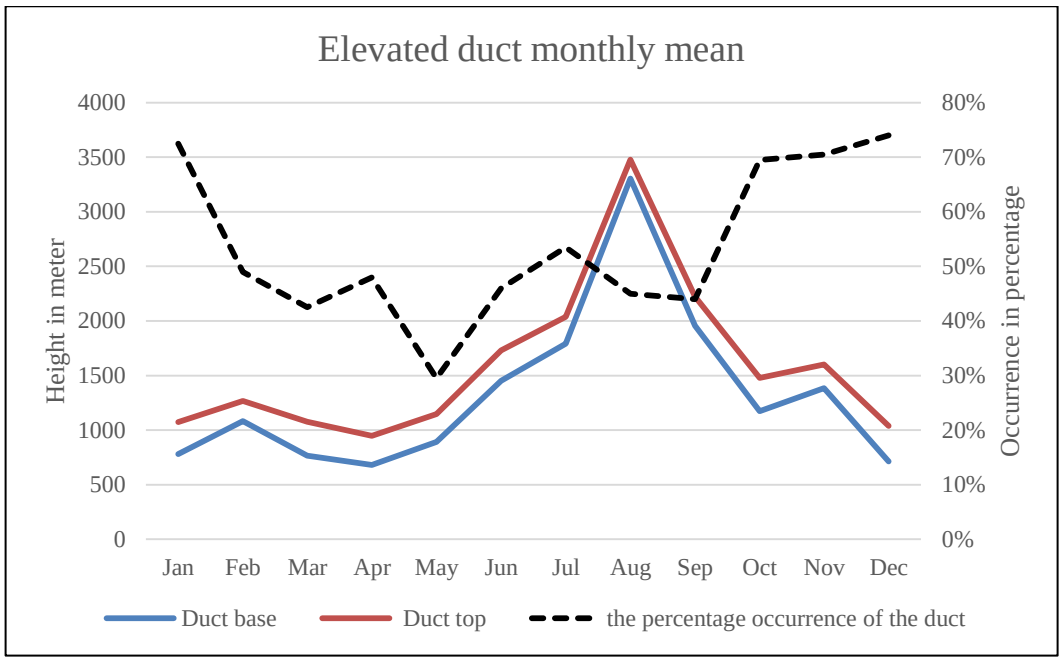

Figure 6.4. Five years (2006-2010) monthly average of the elevated duct altitude and duct its thickness. The dotted black line is representing the monthly average occurrence in the percentage. Figure calculated from Abu Dhabi radiosonde data.

In Figure 6.5 the occurrence of the elevated duct shows some correlation with the frequency of the Shamal days. This relationship is further explored in paragraphs 6.2.3.1.3 and 6.2.3.2.3.

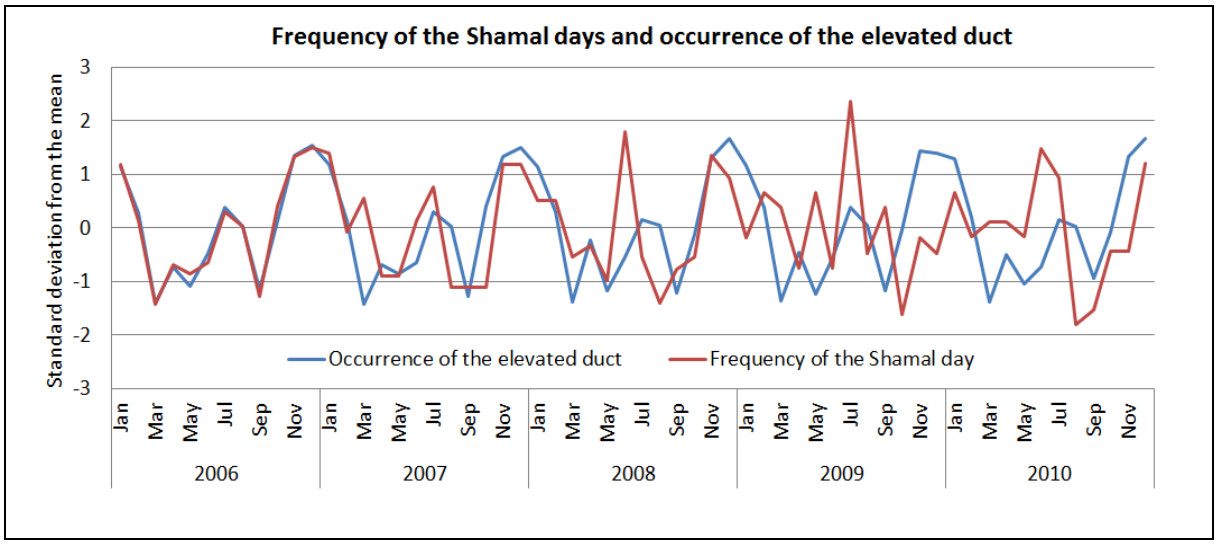

Figure 6.5. Five years (2006-2010) monthly averages for Shamal frequency and elevated duct occurrence.

6.1.4 Summary of temporal variations in different ducts

Furthermore, Figure 6.6a,c shows that evaporation and elevated ducts are seasonal phenomena whilst the surface based duct (Figure 6.6b) has some seasonality; most notably the September peak is due to the predominate land/sea breeze circulation.

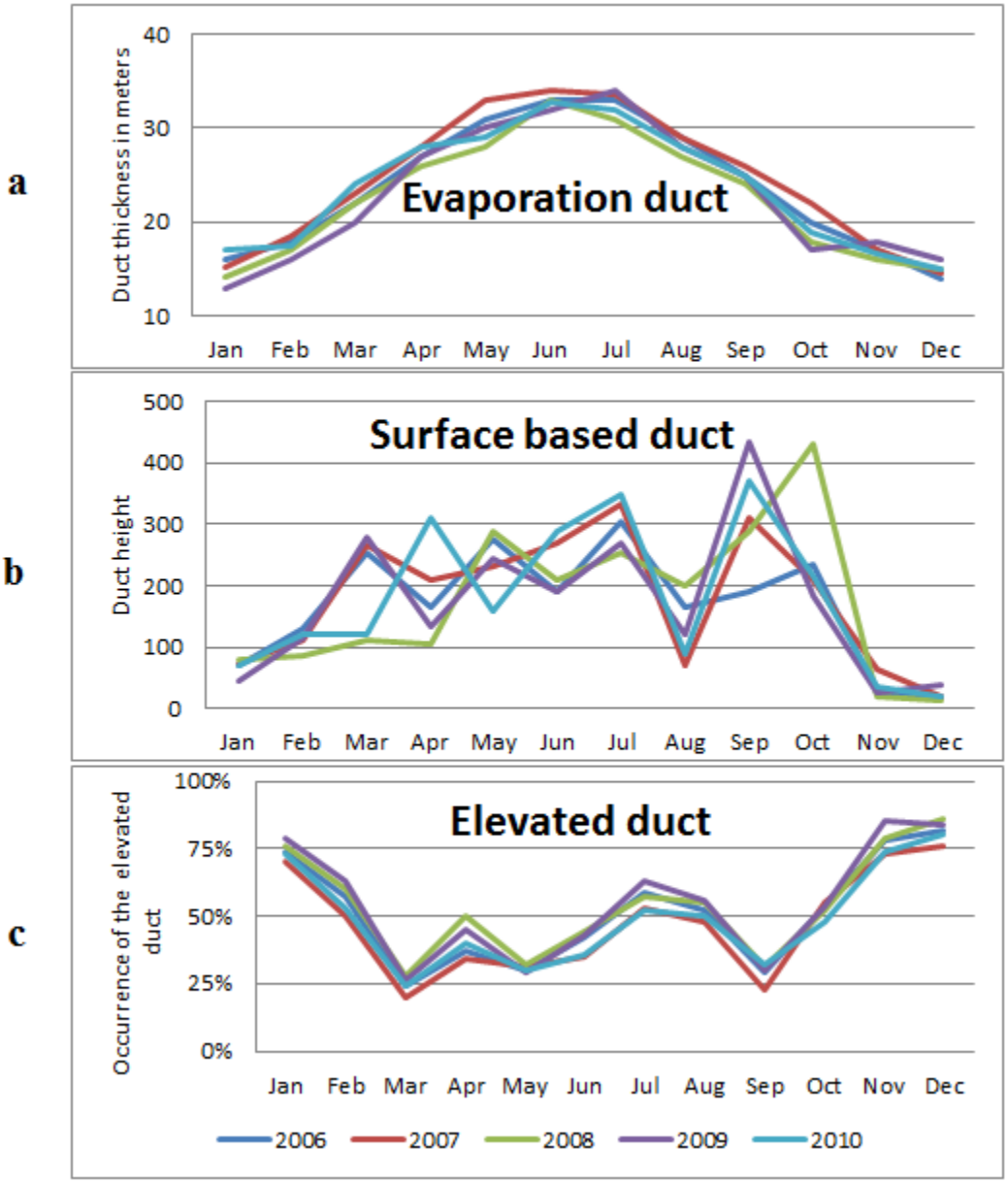

Figure 6.6. Five years (2006-2010) monthly average of duct thickness, heights, and occurrences, calculated from Abu Dhabi radiosonde data.

In conclusion, the atmospheric duct is a feature over the study area and it exists permanently in the study area. The evaporation duct occurred 100% of the time with an average height of 24 meters. Its height increased with strong and dry wind (e.g.Suhaili) and it minimised with light and humid wind (e.g. light sea breeze). The surface-based duct occurred 75% of the time with an average height of 117 meters. It reaches its maximum during the night in the presence of light and humid winds. While its height decreases or disappears during the day in the presence of strong winds and dry air masses (e.g. strong Suhaili). The elevated duct occurred 54% of the time with an average thickness of 260 meters. Usually it is associated with offshore wind (e.g. Shamal or Sea breezes). In the next two sections, different case studies on atmospheric duct conditions related to the different air masses are discussed.

6.2 Duct conditions in winter air masses

The aim of this section is to describe the effect of the winter meteorological air masses upon the EM propagation (duct conditions). Three winter air masses were observed: Shamal, Suhaili and Al Nashi. In the absence of these air masses land and sea breezes may take place. Therefore, this section is divided into three sub sections: wintery land and sea breeze circulation, Al Nashi, and Winter Suhaili and Shamal. In these subsections, the synoptic situation from NCEP/NCAR reanalysis and radiosonde data at Abu Dhabi will be analysed in detail, focusing on the atmospheric duct layers. Also the atmospheric duct will be examined for different air masses.

6.2.1 Land and sea breeze circulation in winter

Figure 6.7 shows the meteorological conditions on 31 January 2010 which is the ideal synoptic situation for stable weather conditions. It was dominated by land and sea breeze circulation in the absence of strong ambient wind (Figure 6.7c). The area of study was influenced by an extension of the Siberian high pressure associated with an upper air ridge at 500mb (Figure 6.7a – b). This meteorological condition may cause the land to cool at night. As a result of this, relative humidity increases to 90-95% from the surface to the 365 m level (Table 6.2). Above this, moderate north-westerly winds and sharp decreases in water vapour appear up to 700 m. A sharp decrease in water vapour is associated with a temperature inversion (Table 6.2 and Figure 6.7d).

Table 6.2. Abu Dhabi radiosondes data on 31 January 2010 at 0400 local time, from the surface up to 850mb illustrating two different layers caused by night cooling.

pressure (millibar)	Height (meters)	Temperature (c)	Dew point (c)	Relative humidity (%)	Wind direction (degree)	Wind speed (Knots)	Remarks
1015	27	15	13.5	91	210	4	Moist air
1014	36	14.8	13.6	93	199	4	
1007	96	17.6	16.9	96	125	3	
1000	157	17.4	16.2	93	50	2	
976	365	15.8	14.8	94	6	6	
964	470	18.4	1.4	32	344	8	Inversion layer
951	587	20.5	-9.5	12	320	10	
944	651	21.6	-15.4	7	303	10	
943	660	21.5	-15	7	300	10	
925	826	20.2	-7.8	14	320	9	
850	1547	15.2	-9.8	17	285	11	

Sea breezes started at midday (1200) local time and ended by midnight with an average speed of 6 knots (Figure 6.7c). By 1600 local time, the layer of temperature inversion and

associated decreases in water vapour had uplifted and had become shallower and weaker (Figure 6.7e).

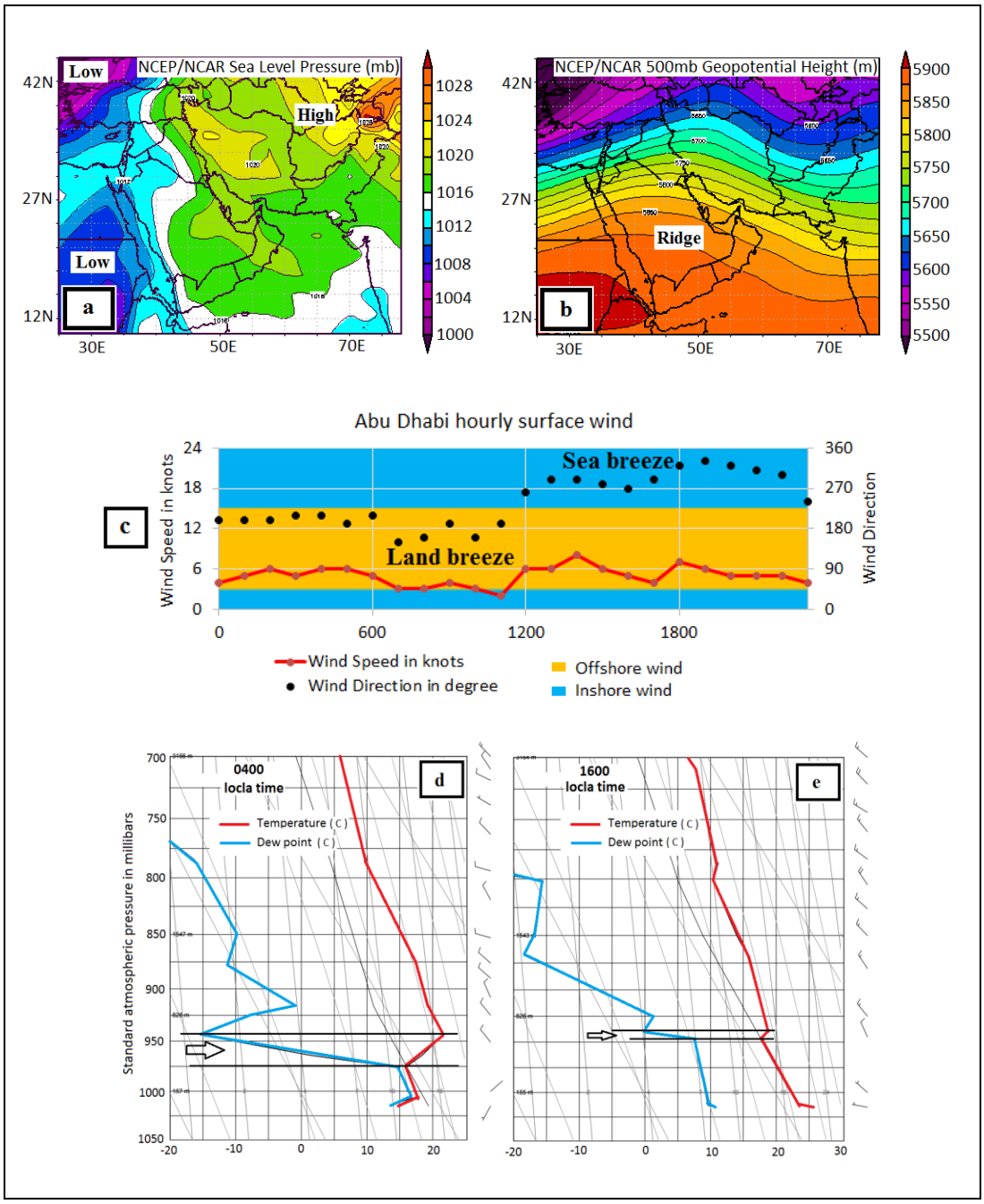

Figure 6.7. Meteorological conditions on 31 January 2010 illustrated by (a) NCEP/NCAR sea level pressure (top left), (b) 500mb geopotential height (top right), (c) Abu Dhabi hourly surface wind chart (centre) and (d – e) Abu Dhabi radiosondes (bottom). These charts represent an example of winter land and sea breeze meteorological conditions. Also, the black arrows in the radiosondes point to the temperature inversion and sharp decrease in water moisture.

The AREPS model provides atmospheric refractivity summary for each model run in the assigned environment. At 0400 there was an evaporation duct at a height of 7 meters, and an elevated duct between 40 and 624 meters. At 1600, the evaporation duct height increased to 19 meters due to solar heating during the day. Also, the base of the elevated duct lifted to 504 meters and its top was at 667 meters. The thickness of the elevated duct at 0400 was 584 meters, decreasing to 163 meters at 1600 local time.

Propagation performance of AEW radar from the aircraft at a height of 150m (within the atmospheric duct) has been simulated with each atmospheric refractivity condition. The result is that EM wave propagation at 0400 is trapped at a lower level (surface to 500 meters), which extends the range of detection to more than 150 nautical miles (Figure 6.8a). At 1600, EM wave propagation of AEW was similar to the standard propagation (Figure 6.8b). There was no unusual EM wave propagation due to the weakness of the elevated duct which could not trap the AEW propagation. This means that an aircraft flying within 500m of the ground could be detected by radar at distance of 150nm compared with 35nm in normal conditions.

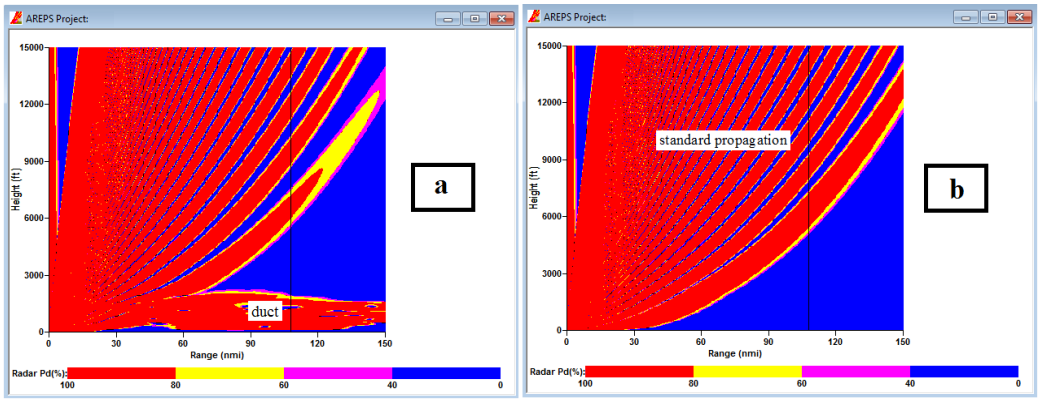

Figure 6.6. AEW Radar propagation performance for each of the propagation conditions, (a) at 0400 local time there was a strong surface-based duct at the surface. (b) At 1600 local time there was a standard atmospheric condition.

6.2.2 Al Nashi air masses

The Al Nashi is a north-easterly wintery wind which rarely occurs; it was discussed in section 4.2.1.6. Figure 6.9 shows the meteorological conditions on 25 January 2007, which was an ideal example of the synoptic situation of Al Nashi air masses; these were dominated by a north-easterly wind (Figure 6.9c). A strong Siberian high building over north-west Iran and a low pressure system north-east of the Arabian Sea caused a north-easterly gradient over southern Iran (Figure 6.9a). It was associated with an upper air trough extending from the north-east at 500mb (Figure 6.9b). This meteorological condition drives cold dry north-easterly wind over the study area (Figure 6.9d) with average surface speeds of 11 knots over Abu Dhabi (Figure 6.9c).

Abu Dhabi radiosondes (Figure 6.9d) show wind strength increased, with height reaching more than 20 knots above 200 meters and caused a well-mixed layer from the surface to 850mb. A surface temperature inversion developed in a layer between the surface and 100 meters. Furthermore, the Al Nashi wind crossed Bandar-Abbas before entering the area of the study. However, it has been observed that the wind strength at Bandar-Abbas was less than that at Abu Dhabi. That could be due to the topographic effect. The radiosondes at Bandar-Abbas (Figure 6.9e) showed similar behaviour to Abu Dhabi radiosondes, which are considered dry profiles.

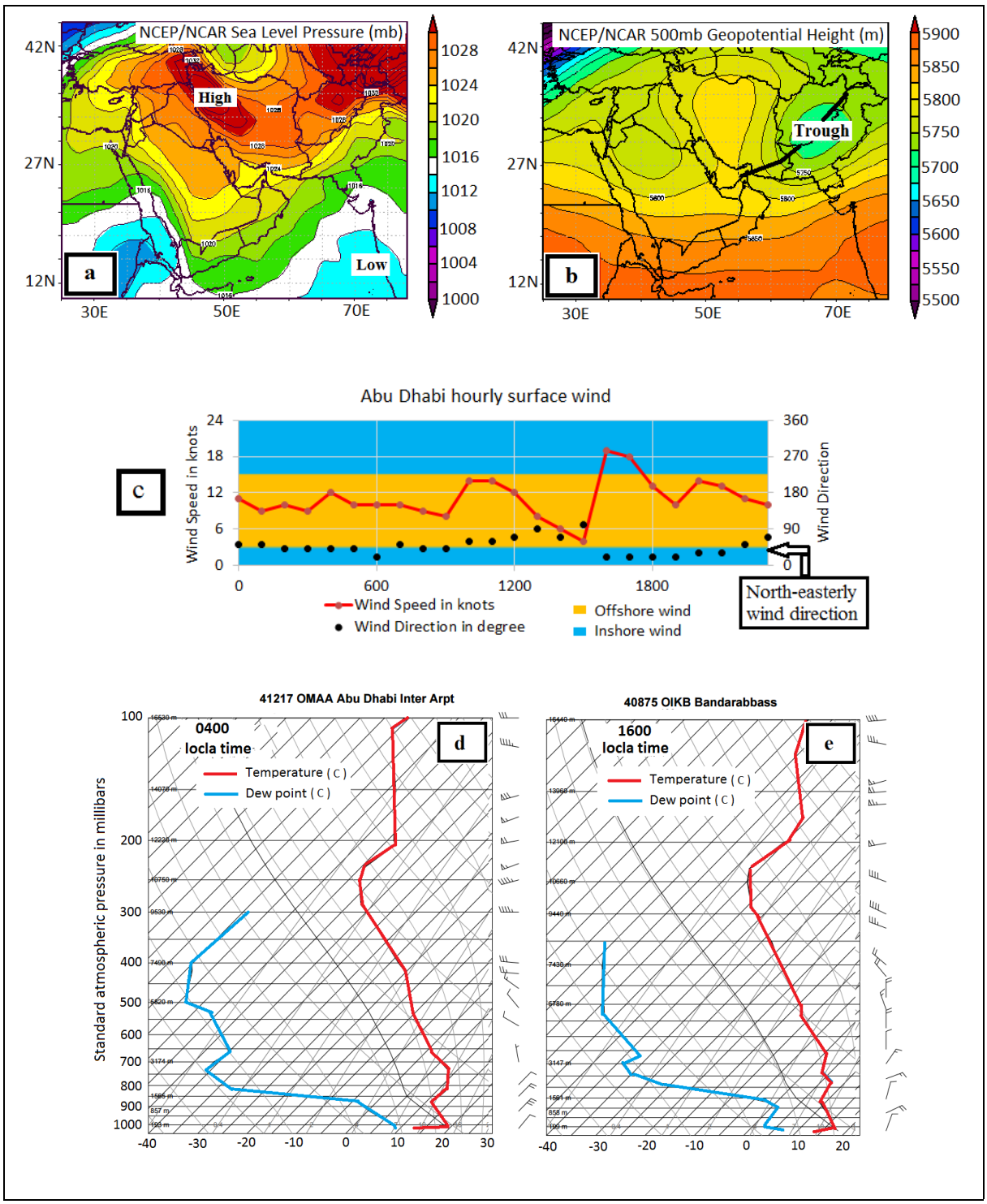

Figure 6.9. Meteorological conditions on 25 January 2007 illustrated by (a) NCEP/NCAR sea level pressure (top left), (b) 500mb geopotential height (top right), (c) Abu Dhabi hourly surface wind chart (centre) and (d) Abu Dhabi and (e) Bandar-Abbas (27N,57E) radiosondes (bottom). These charts represent Al Nashi meteorological conditions.

The atmospheric refractivity condition summary for each model runs in the assigned environment. At 0400 over Abu Dhabi, there was only an evaporation duct with a height of 13 meters. At 0400 over Bandar-Abbas there was an evaporation duct with a height of 16 meters and there was also a surface-based duct with a height of 72 metres.

Propagation performance of AEW radar from the aircraft at a height of 45m (to be with in the duct over Bandar Abbas) has been simulated with each propagation condition (Figure 6.10). There are no significant trapping conditions for AEW radar existing over Abu Dhabi and Bandar-Abbas. Therefore, it suggests that Al Nashi meteorological conditions provide standard atmospheric refraction due to their meteorological characteristics.

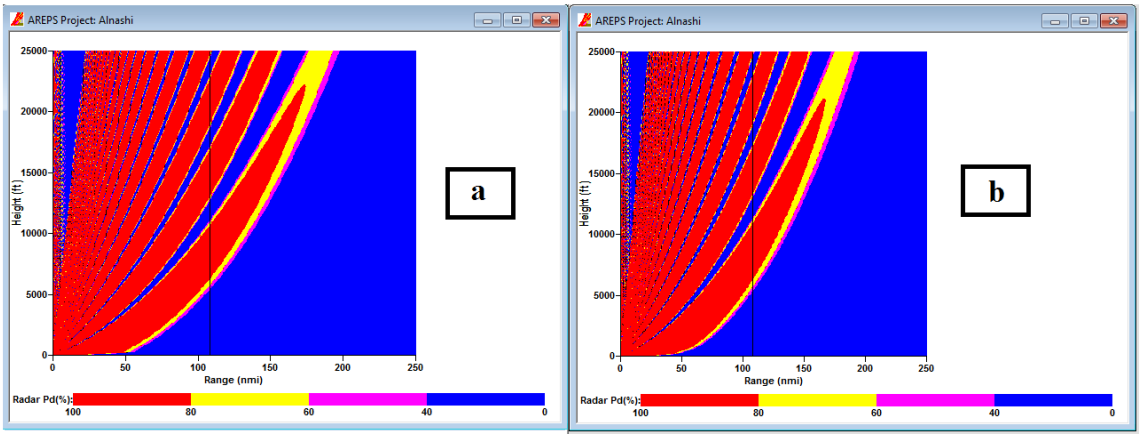

Figure 6.10. AREPS model simulating AEW radar propagation conditions from the aircraft at a height of 45m over (a) Abu Dhabi and (b) Bandar-Abbas at 0400 local time.

6.2.3 Winter Suhaili and Shamal air masses

In this subsection both Suhaili and Shamal air masses, which are associated with the passage of the frontal system over the study area, are discussed. The period from 2 to 9

February 2010 was selected as a case study to illustrate the effects of the winter Suhaili and Shamal on atmospheric refraction. This subsection is divided into two sections: the development of the meteorological conditions and the atmospheric refraction.

6.2.3.1 The development of meteorological conditions

The meteorological conditions associated with the wintery Suhaili and Shamal were discussed in section 4.4.1. The aim of this section is to show how the radiosonde parameters vary as the meteorological conditions develop. The variation in temperature and humidity with height is an important factor in EM propagation (Grabner, Kvicera, 2011). This section is divided into three subsections which include the development of the winter Suhaili wind, the passage of the frontal system, and the winter Shamal.

6.2.3.1.1 Winter Suhaili

The winter Suhaili wind develops as a westerly depression approaches the area of the study. The period from 2-4 February 2010 is used to illustrate its development in the Abu Dhabi radiosondes (Figure 6.11). On 2 February land and sea breezes were the predominant systems over the area of study (section 4.3.3.1). This was associated with a surface temperature inversion and a sharp dew point gradient at 0400 (Figure 6.11a), which could be due to the night cooling. At 1600 (Figure 6.11b), both the temperature inversion and dew point gradient had disappeared; this may be due to surface heating and a weak sea breeze.

On 3 February, the Suhaili wind started and predominated for most of the period with an average speed of 7 knots (Figure 4.14b). That the sea breeze persisted for only two hours could be due to the presence of strong Suhaili wind. The 0400 Abu Dhabi radiosonde (Figure 6.11c) revealed a surface inversion with a sharp decrease in dew point. Also there was an elevated thin layer of inversion and sharp decrease in dew point at a height of 3150 meters. At 1600, there was no temperature inversion (Figure 6.11d).

On the 4 February, the Suhaili wind was the predominant wind for the whole day with an average wind speed of 15 knots (Figure 4.14c), which inhibited sea breeze development. There was no dew point gradient near to the surface observed in the Abu Dhabi radiosondes at 0400 or 1600. Furthermore, Abu Dhabi radiosondes showed an elevated thin layer of temperature inversion and sharp decrease in dew point at a height of 5000 metres.

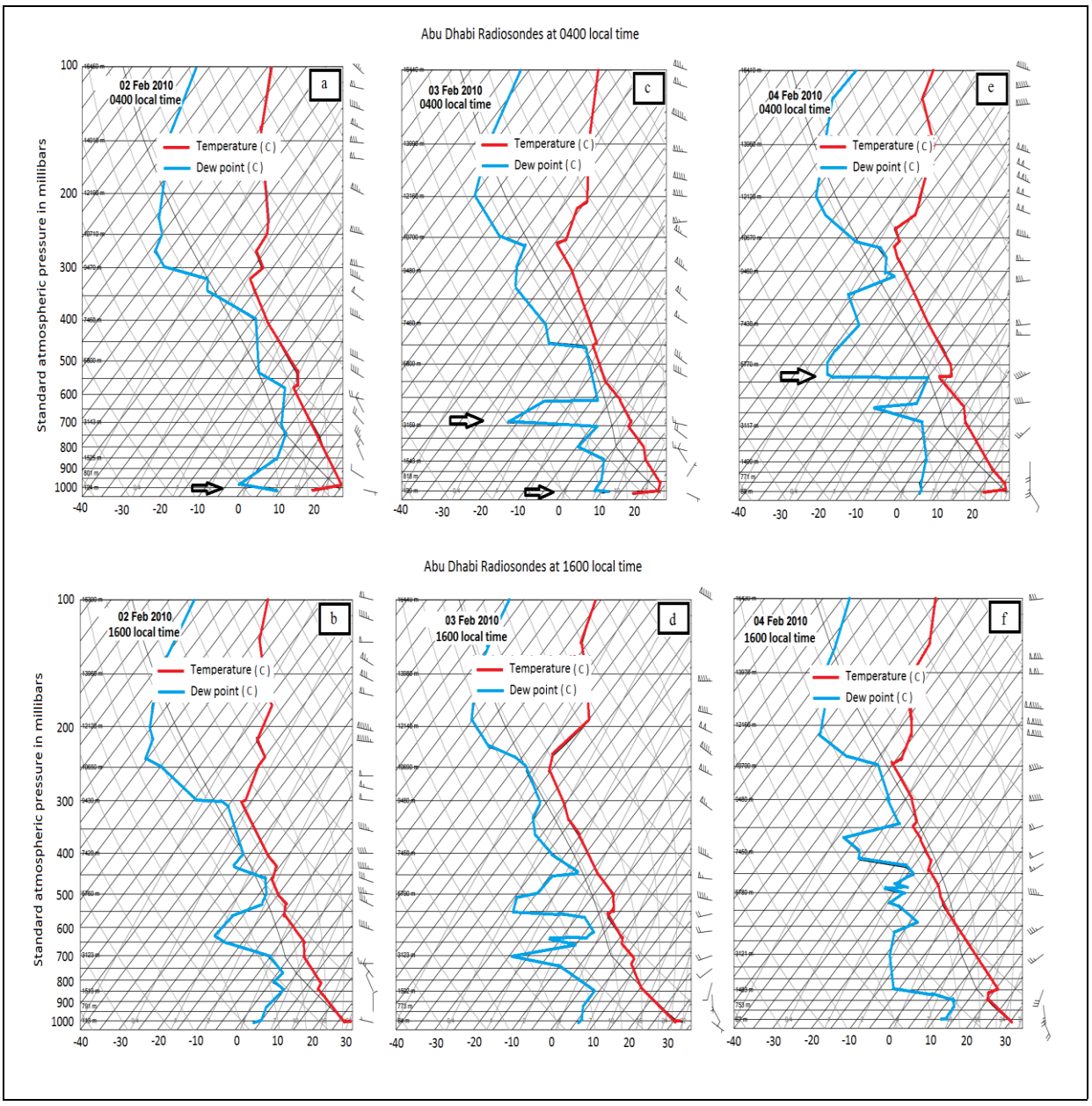

Figure 6.11. Abu Dhabi morning (0400 local time) and afternoon (1600 local time) radiosonde conditions on 2, 3, and 4 February 2010. It illustrates variations in the lower part (surface to 700mb) from land and sea breezes circulations into Suhaili air masses. The arrow indicates areas of expected atmospheric ducting.

6.2.3.1.2 Passage of the frontal system

Figure 6.12 shows Abu Dhabi radiosonde development on 5 and 6 February as the depression crossed the area of study from west to east (Figure 4.15). This caused unstable

weather conditions and small differences between temperature and dew point with height, as observed in the Abu Dhabi radiosondes. Furthermore, there are no potential layers of the atmospheric duct (temperature inversion associated with sharp decreases of dew point) in figure 5.12.

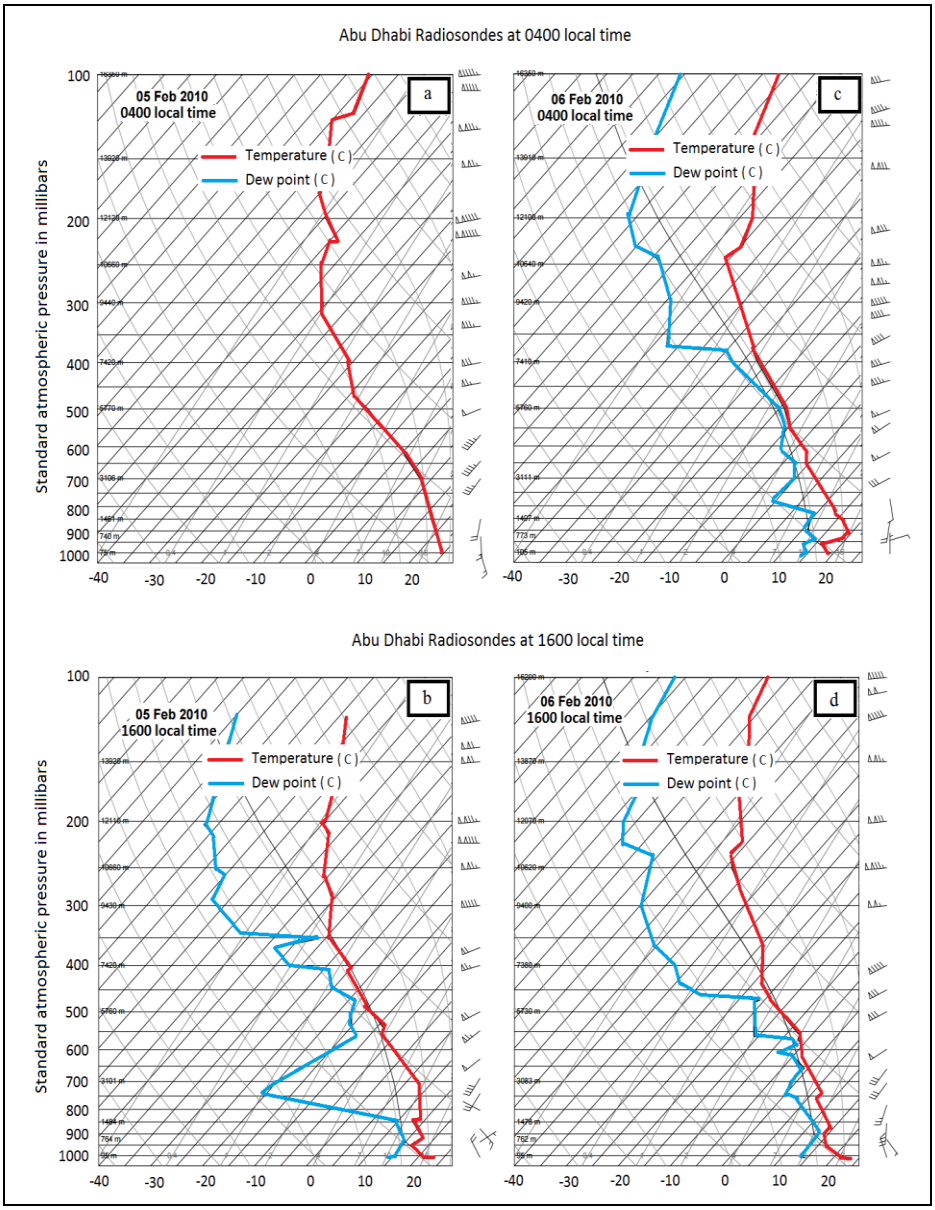

Figure 6.12. Abu Dhabi morning (0400 local time) and afternoon (1600 local time) radiosonde conditions on 5 and 6 February 2010. They illustrate how temperature, dew point and wind vary with height on the passage of the frontal system. There is dew point data missing at 0400 on 5 February 2010.

6.2.3.1.3 Winter Shamal

Figure 6.13 shows development of the radiosondes on the 7, 8 and 9 February 2010, after the passage of the westerly depression. The 7 February is considered a Shamal day with an average speed of 11knots over Abu Dhabi (Figure 4.18a). The 8 February was the second Shamal day with an average speed of 12knots (Figure 4.18b).

On the 9 February, a weak Shamal flow of 5 knots caused an early onset of the sea breeze and land breeze observed between 0600 and 1000 local time (Figure 4.18c). The strong Shamal caused a well-mixed surface layer from the surface to 1000 m, as is clear on the 8 February 2010 (Figure 6.13c-d). Directly above that layer there is a sharp decrease in dew point associated with a weak inversion. This could be due to the subsidence which warms adiabatically to form a subsidence inversion.

So the potential layer of atmospheric duct in Abu Dhabi radiosondes for each air masses were discussed, in the next sections AREPS model will be used to calculate each atmospheric duct and how is influence the AEW radar propagations.

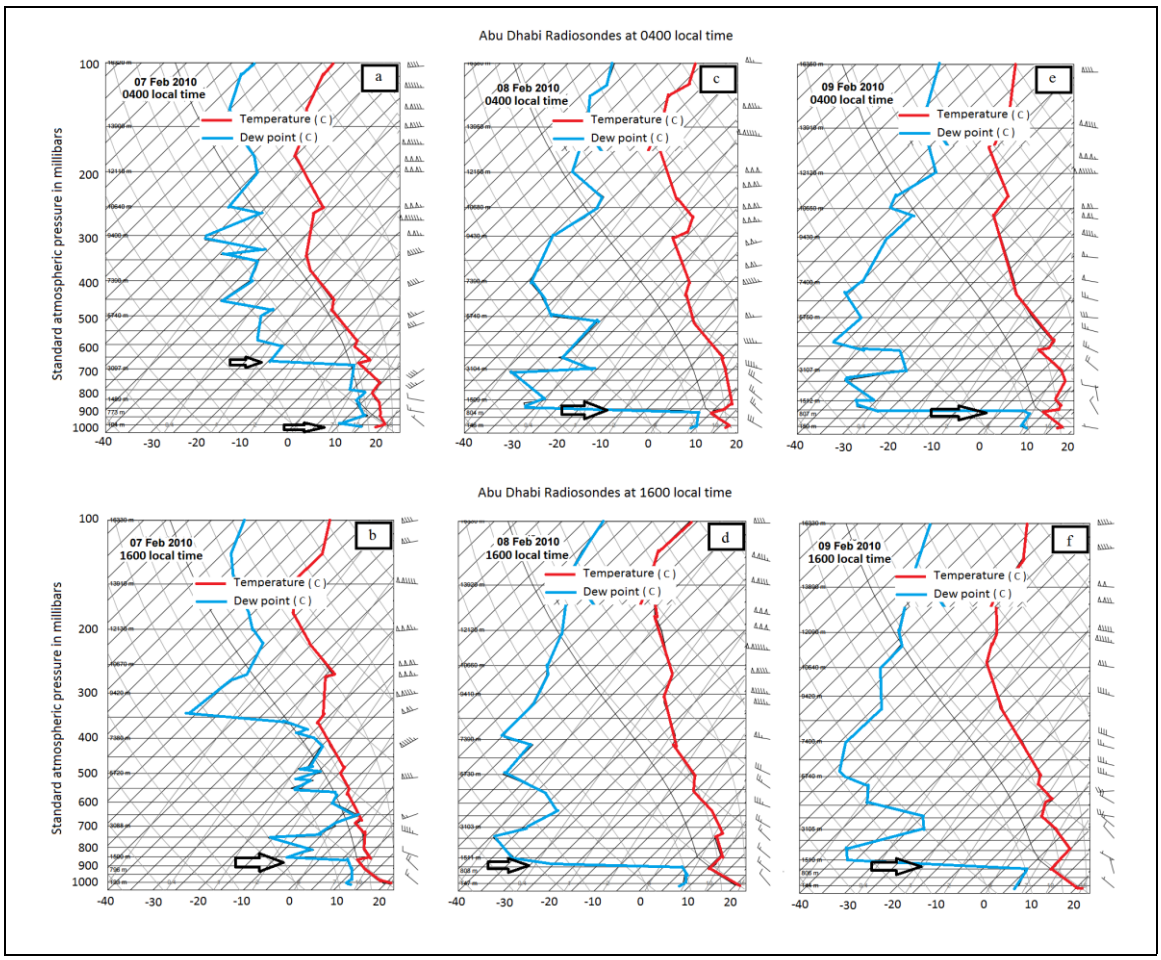

Figure 6.13. Abu Dhabi morning (0400 local time) and afternoon (1600 local time) radiosonde conditions on 7, 8, and 9 February 2010. They illustrate how temperature, dew point and wind vary with height after the passage of the frontal system and establishment of a Shamal wind.

6.2.3.2 Atmospheric refractivity

This section is divided into three subsections: Winter Suhaili, passage of the frontal system and Winter Shamal. Table 6.3 shows the summary of propagation conditions from 2-9 February 2010. The evaporation duct reduced during the morning hours and increased in the afternoon due to surface heating. It reached its maximum (40 meters) in the afternoon during the strong Suhaili wind. In contrast, the passage of the frontal system could be the reason for the decrease of the evaporation duct height. During the Shamal, the evaporation duct height decreased in comparison to the Suhaili. Significant surface-based ducts were

found during land and sea breeze circulations and disappeared with the influence of the synoptic wind. Elevated ducts were found with gentle Suhaili and Shamal winds while they disappeared during land and sea breeze circulations.

Table 6.3. Atmospheric ducting summary for the period of study and associated wind systems. The highlighted cells indicate that ducting was significant to AEW radar propagation. All heights in meters.

Date	Meteorological conditions	At 0400 local time			At 1600 local time		
		Evaporation Duct	Surface based duct	Elevated duct	Evaporation Duct	Surface based duct	Elevated Duct
2	Breezes	12	169	-	22	-	-
3	Gentle Suhaili 7 knots	15	4	18-143 3079-3133	31	-	-
4	Strong Suhaili 15 knots	38	6	5156-5235	40	-	-
5	Passage of depression	20	-	-	25	-	-
6		10	-	-	15	-	-
7	Moderate Shamal 11 knots	14	108	3299-3469	21	6	1197-1395
8	Moderate Shamal 12 knots	17	4	633-979	24	4	863-1005
9	light Shamal 5 knots	12	6	657-989	20	6	1028-1050

6.2.3.2.1 Winter Suhaili

On the 2 February 2010, there was a significant surface-based duct during the morning which could be attributed to night cooling. The thickness of the evaporation duct increased in the afternoon due to daytime solar heating. This atmospheric condition is typically associated with land and sea breezes, as is clear from section 6.2.1. On the 3 February

2010, a gentle dry Suhaili (average wind speed 7 knots) may have dried the lower part of the atmosphere, which could have weakened the sharp decreases in dew point.

Furthermore, a morning Suhaili brought cooler air which may have enhanced the development of the inversion. This could produce a significant near-surface elevated duct. The afternoon brought warmer air, which may have weakened or destroyed any development of the inversion. On the 4 February 2010, which was a strong Suhaili day (average wind speed 15knots), the evaporation duct height reached its maximum. There was no sharp decrease in dew point due to the dryness of the air mass. Therefore, there was no significant ducting during the day.

Figure 6.14 shows the propagation of AEW radar from the aircraft at a height of 50m (within the duct channel), which has been simulated with each atmospheric refractivity condition. The result is that the surface coverage of EM wave propagation at 0400 (Figure 6.14a-c-e) varied due to the significant variation in the atmospheric layers, which in sequence affected atmospheric refractivity. At 1600 local time (Figure 6.14b-d-f), the atmospheric conditions did not have a significant effect on the AEW radar propagation. The surface-based duct (Figure 6.14 a-c) caused an extension of the radar surface coverage which enabled radar of long range surface coverage, in contrast to standard atmospheric conditions (Figure 6.14b-d-e-f).

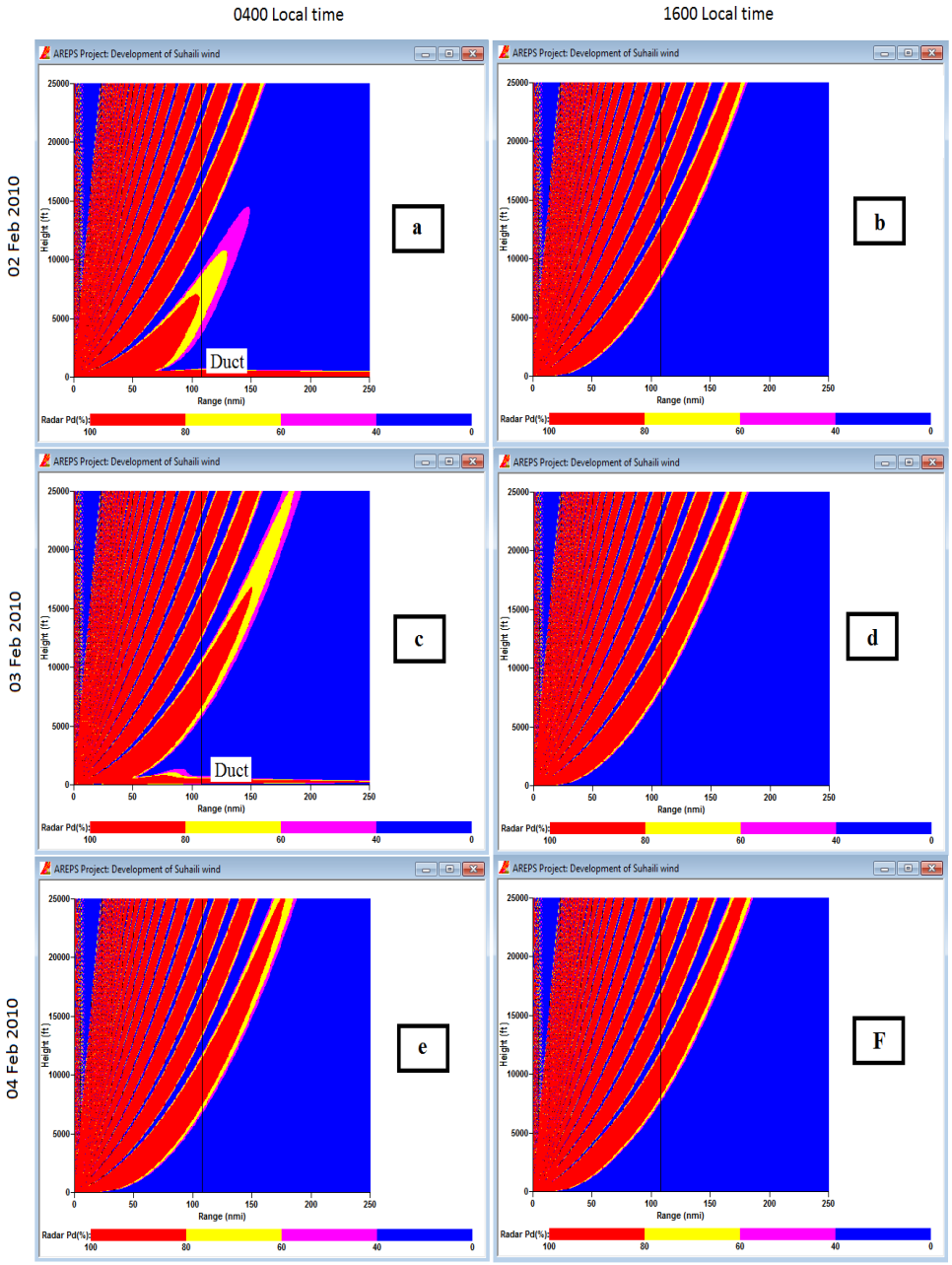

Figure 6.14. AREPS propagation coverage (in red) results for AEW radar propagation at each atmospheric condition at 0400 and 1600 local time during 2, 3, and 4 February 2010. In the morning at 0400 there was a clear difference in the surface coverage during the three days while in the afternoon it was nearly the same.

6.2.3.2.2 Passage of the frontal system

On the 5 and 6 February 2010, there were unstable weather conditions (Figure 6.12) which caused the temperature and dew point to be close to each other, from the surface into higher altitudes. This atmospheric condition led to standard atmospheric refractivity and reduced the height of the evaporation duct. Simulating the propagation of the AEW radar (Figure 6.15) shows normal propagation conditions.

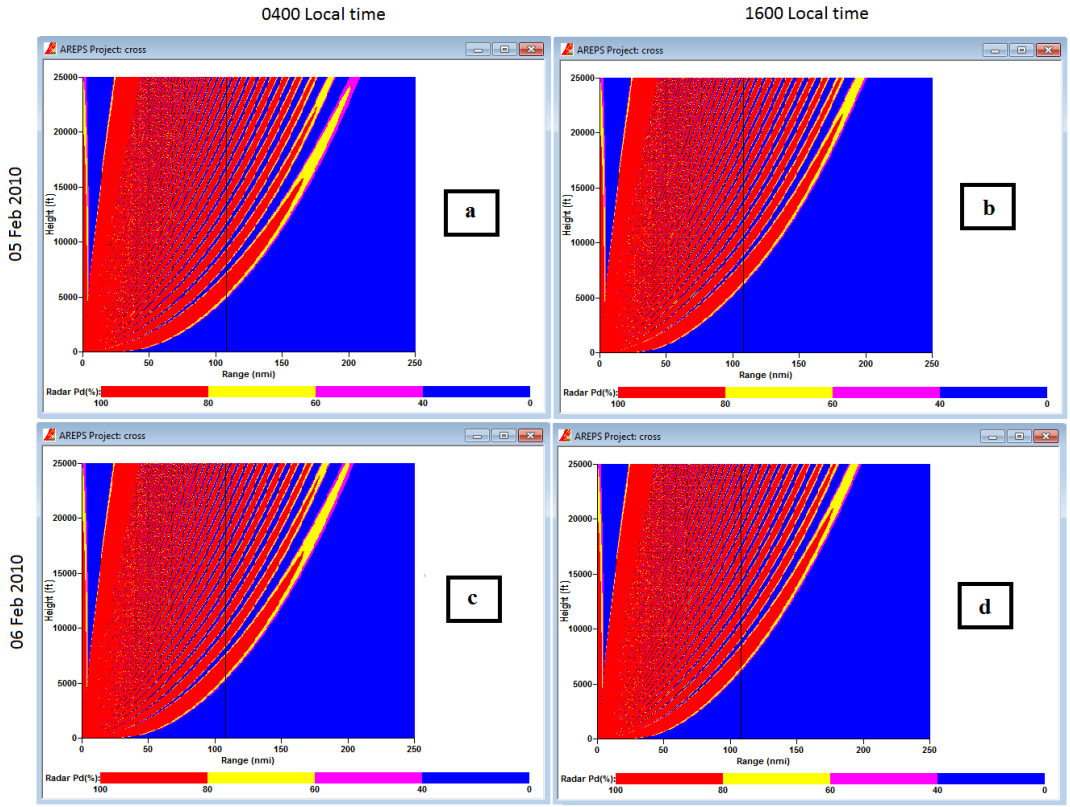

Figure 6.15. AREPS propagation coverage results for AEW radar propagation at each atmospheric condition at 0400 and 1600 local time during 5 and 6 February 2010. The EM wave propagation of the AEW radar was nearly the same during the morning and afternoon on both days.

6.2.3.2.3 Winter Shamal

On the 7 and 8 February 2010 (Figure 6.16 a-b-c-d), a significant elevated duct developed. This could be due to the strong moist cooler north-westerly wind (Shamal) which started over the study area. It also extended to a maximum at a higher altitude. This may have caused well mixed air aloft, where the temperature and dew point were noticeably different, while in the lower part of the atmosphere, less mixed air may have lead the temperature and dew point to be closer than at higher altitude. This could have caused sharp decreases in the dew point, associated with an inversion (figure 6.10c-d on 8 February 2010). On the 9 February at 0400 local time (Figure 6.16e) the elevated duct remained at the same height as seen in the case of the Shamal day, and later (Figure 6.16f) it weakened. The simulation of the AEW radar propagation within the elevated duct layer is illustrated in figure 6.16. The elevated duct enables radar in the aircraft to detect long rang target at duct layer.

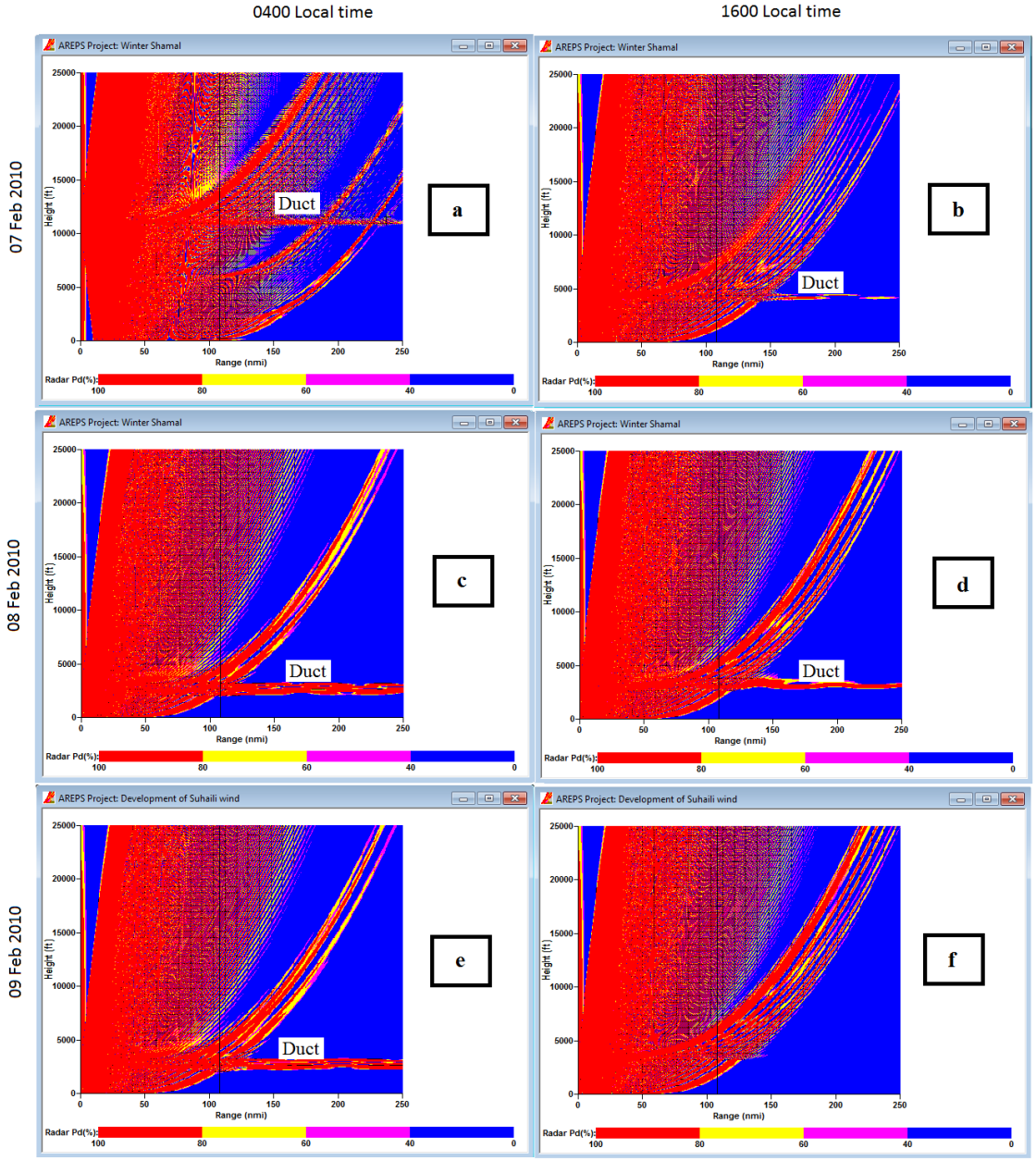

Figure 6.16. AREPS propagation coverage results for AEW radar propagation at each atmospheric condition at 0400 and 1600 local time during 7, 8, and 9 February 2010. Some of the EM wave propagation of the AEW radar was trapped within the elevated duct which started at a higher altitude and then moved down.

6.2.4 Summary of the duct conditions in winter air masses

Wintery Shamal conditions are associated with an elevated duct while Al Nashi and Suhaili destroy duct channels over the land due to their dry conditions. Furthermore, the Suhaili weakens any duct conditions (temperature inversion and sharp decrease of dew point) over the land (surface based duct) but strengthens any over the sea (e.g. evaporation duct). Usually these air masses (Al Nashi and Suhaili) are associated with standard atmospheric refractivity. Also, strong Shamal (daily average 15 knots) and the passage of a frontal system destroy any duct and produce standard atmospheric refractivity. Land and sea breezes are usually associated with a surface-based duct. Winter air masses and associated major ducts are summarised in table 6.4.

Table 6.4. illustrating major ducts which can be expected during winter season (November - April)

Air-masses	Expected duct
LSBC	Evaporation duct (10-20 meter), usually surface based duct ≈ 150-200 meter, sometimes elevated duct in layer between 1000-2000 meter.
Suhaili	Evaporation duct (30-40 meter)
Shamal	Evaporation duct (15-25 meter), elevated duct (≈ 250-300 meter) in the level of 1000-3000metres
Al Nashi	Evaporation duct (10-20 meter)

6.3 Duct conditions in summer air masses

The aim of this section is to describe the effect of the summer meteorological air masses on the EM propagation. There were two summer air masses observed: Shamal and Suhaili. In the absence of these air masses land and sea breezes could develop. Therefore, this section is divided into three sub sections: summer land and sea breeze circulation, summer Suhaili and summer Shamal.

6.3.1 Land and sea breeze circulation in summer

Figure 6.14 shows the meteorological conditions on 4 July 2004 which is the ideal synoptic situation of stable weather conditions. It was dominated by land and sea breeze circulation in the absence of strong ambient winds (Figure 6.17c). Figure 6.17a suggests that the area of study was under the influence of a thermal low which was part of the extension of the Indian Monsoon Low. It was associated with an upper air Subtropical High at 500 mb level (Figure 6.17b). This meteorological condition could cause the land to cool at night producing a temperature inversion and a sharp decrease in water vapour in the lower part of the atmosphere as has been highlighted in Table 6.5.

Table 6.5. Abu Dhabi radiosonde data on 4 July 2004 at 0400, from the surface up to 850mb, illustrating two different layers caused by night cooling.

Pressure (millibar)	Height (meters)	Temperature (°C)	Dew point (°C)	Relative humidity (%)	Wind direction (degree)	Wind speed (Knots)	Remarks
995	27	30	27.8	88	170	5	Moist air
994	36	28.8	26	85	171	5	
967	281	27.4	25.8	91	209	5	
946	476	30.2	10.2	29	239	6	Inversion layer
930	628	33.2	6.2	19	260	7	
925	676	34	3	14	260	9	
911	814	34.8	0.8	12	237	10	
868	1249	32.2	-0.9	12	165	13	
850	1436	30.6	-2.4	12	165	11	

Sea breezes set in at 1200 local time and ended at midnight with average speeds of 6 knots (figure 6.17c). A comparison between Abu Dhabi radiosondes at 0400 (Figure 6.17d) and 1600 (Figure 6.17e) from surface to 1000 meters showed that the temperature inversion

became shallower at 1600, while there were minor changes in the amount of water vapour between both profiles (table 6.5). This may be due to the strength of the sea breezes which feed cooler moist air into the land.

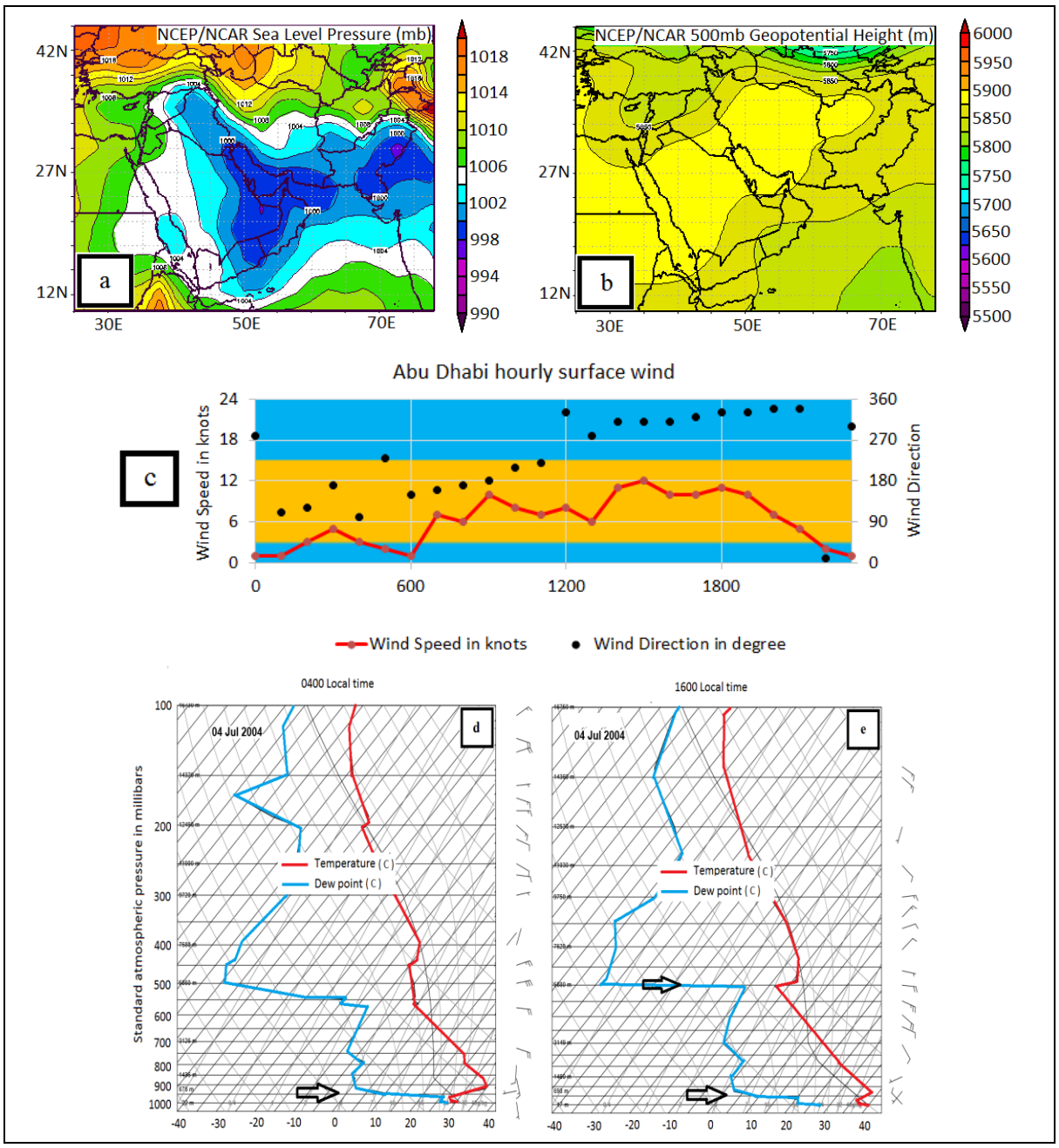

Figure 6.17. Meteorological conditions on 4 July 2004 illustrated by (a) NCEP/NCAR sea level pressure (top left), (b) 500mb geopotential height (top right), (c) Abu Dhabi hourly surface wind chart (centre) and (d – e) Abu Dhabi radiosondes (bottom). These charts represent summer land and sea breeze meteorological conditions. Black arrows point to a layer which is categorised by a temperature inversion and associated sharp decreases in dew point.

Table 6.6. Abu Dhabi radiosonde data on 4 july 2004 at 1600 from the surface up to 460mb, illustrating different layers developing during the day.

Pressure (millibar)	Height (meters)	Temperature (^oC)	Dew point (^oC)	Relative humidity (%)	Wind direction (degree)	Wind speed (Knots)	Remarks
996	27	39.8	26.8	48	310	12	Moist layer
969	277	35.8	20.8	42	278	9	
940	552	38.2	6.2	14	243	6	Inversion
850	1460	30.6	-1.4	13	250	6	
508	5757	-7.7	-15.7	53	98	19	Moist layer
503	5833	-8.5	-17.5	48	96	19	
501	5864	-7.7	-29.7	15	95	18	inversion
485	6120	-4.3	-53.3	1	97	13	
460	6534	-5.9	-54.5	1	100	4	

The propagation condition summary for each model run and the predicted radar propagation performance in the assigned environment are as follows:

- At 0400 there was an evaporation duct height of 13 meters and a surface-based duct between the surface and 454 meters.
- At 1600, the evaporation duct height increased to 30 meters due to solar heating during the day. Also the surface-based duct thickness increased to 533 meters. Furthermore, there was a thin weak elevated duct at a height of between 5795 and 5839 meters that may be due to subsidence of cold air.

Propagation of AEW radar from the aircraft at a height of 91m (within the duct channel) has been simulated with each propagation condition. As a result, EM propagation at 0400 (Figure 6.16a) and 1600 (Figure 6.16b) local time was trapped at lower levels (surface to

approximately 500 meters) which extends the range of detection to more than 150nm. The elevated duct was very shallow and weak, and could not trap any EM propagation.

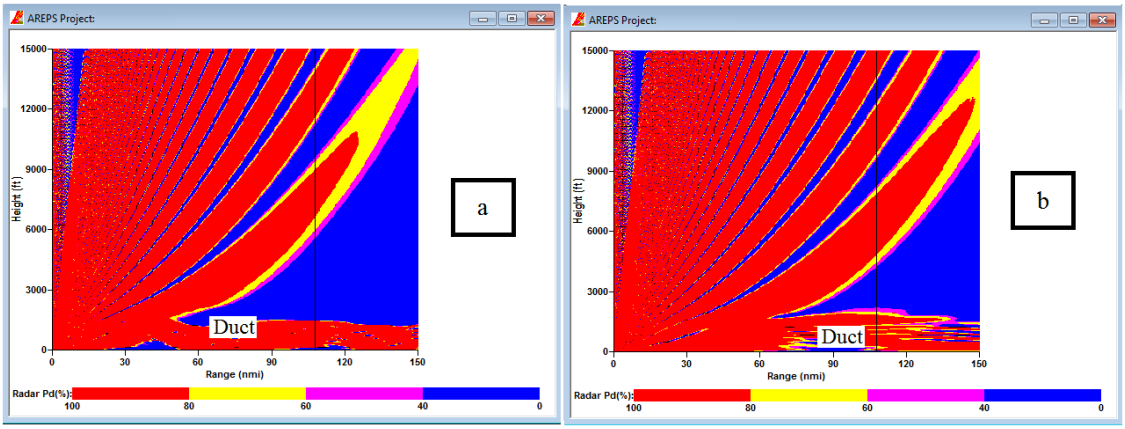

Figure 6.18. AREPS propagation coverage result for AEW radar propagation at each atmospheric condition at 0400 (a) and 1600 (b) local time during 4 July 2004. The EM propagation of the AEW radar was nearly the same during the morning and afternoon.

6.3.2 Summer Suhaili air masses

The Suhaili is a dry south to south-easterly wind characterised by dust and sand as it moves over the desert before crossing the southern coast of the Arabian Gulf. It is the second most important wind in the region and occurs during winter and summer (section 4.2.1.1). Figure 6.16 shows the meteorological conditions of 14 July 2010 which was the ideal example of the synoptic situation of Summer Suhaili air masses; it was dominated by south-easterly winds (Figure 6.19c). A thermal low developed north of the Gulf (Figure 6.19a). It was associated with subtropical air at 500mb (Figure 6.19b). This meteorological condition drove dry south easterly wind over the study area with average surface speeds of 11knots over Abu Dhabi (Figure 6.19c). The Suhaili wind was stronger before midday and decreased during a sea breeze. Sea breezes persisted for only 2 hours between 1700 and

1900. The Suhaili wind during the night and morning may drive cold air causing a surface temperature inversion as its coming from the land. During the daytime, it could bring warm air that breaks the temperature inversion, as is obvious from Abu Dhabi radiosondes (Figure 6.19d-e). Furthermore, in the morning, wind strength increased with height reaching more than 20 knots in a layer between 100-300 meters, possibly due to the combination with the land breeze; this strength decreased in the afternoon to less than 10 knots which may be due to the sea breeze.

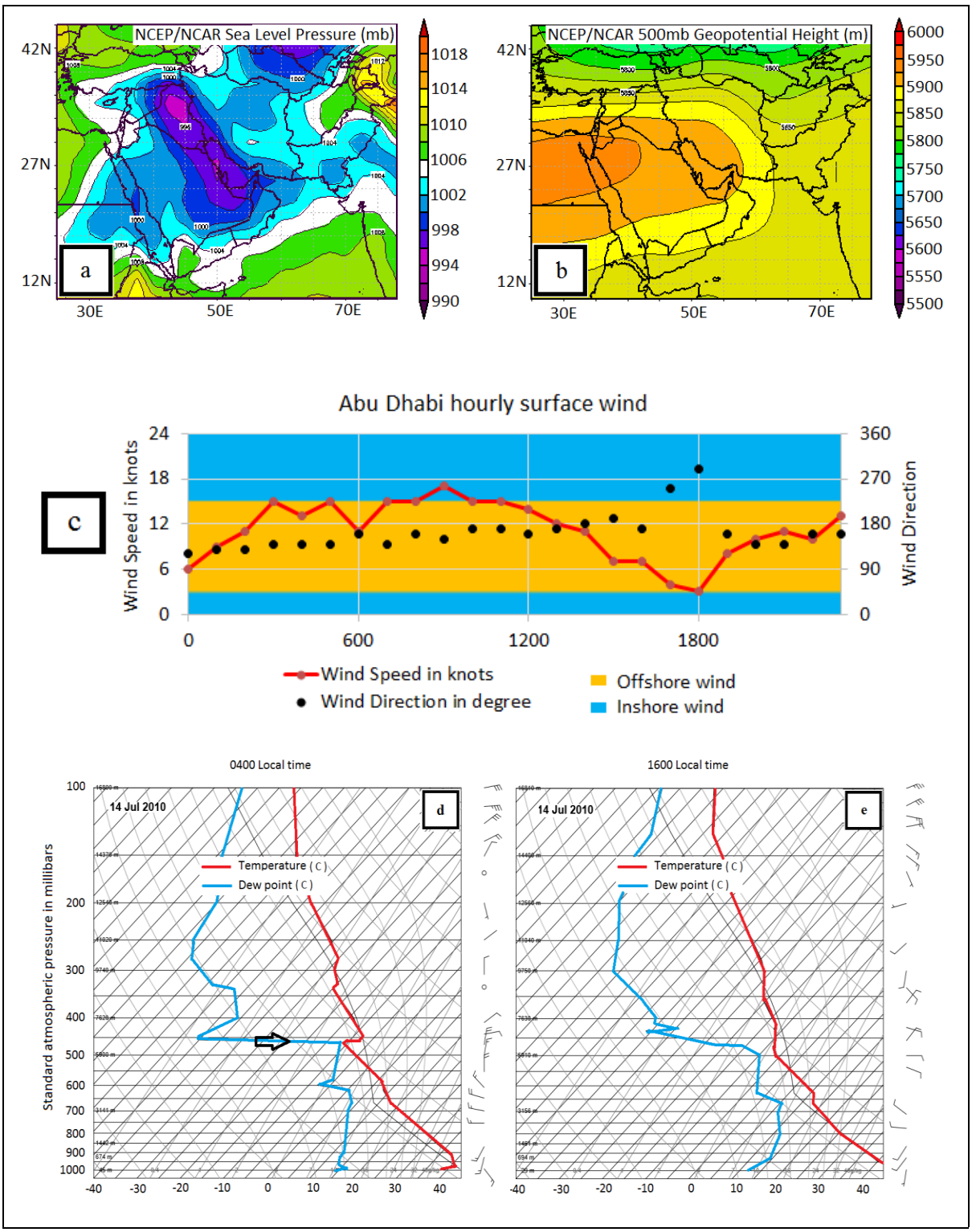

Figure 6.19. Meteorological conditions on 14 July 2010 illustrated by (a) NCEP/NCAR sea level pressure (top left), (b) 500mb geopotential height (top right), (c) Abu Dhabi hourly surface wind chart (centre) and Abu Dhabi radiosondes (bottom) at 0400 and 1600. These charts represent summer Suhaili meteorological conditions.

The propagation conditions summary for each model run and the predicted radar propagation performance in the assigned environment is as follows:

- At 0400 there was an evaporation duct height of 38 meters and a surface based duct from the surface to 4 m. Furthermore, there are two shallow elevated ducts: one from 33 to 70 m, the second one is from 6428 to 6523 m.
- At 1600, the evaporation duct height had increased to 40 meters due to solar heating during the day.

Propagation of AEW radar from the aircraft has been simulated at different heights, in the morning at a height of 6470m within the elevated duct channel (Figure 6.20a), while in the afternoon at 20m within the evaporated duct (Figure 6.20b). Result shows there is no abnormal propagation, because both ducts were a very shallow and weak feature that could not trap EM propagation of AEW radar. This might be significant for systems that operate in higher frequency.

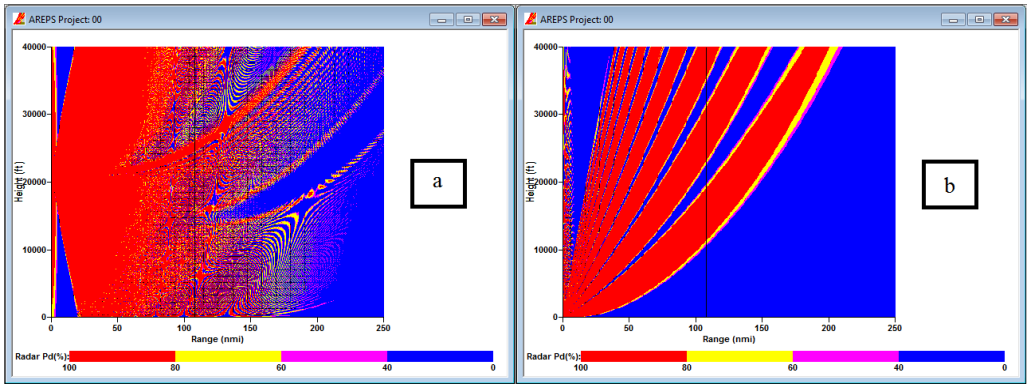

Figure 6.20, Simulation of AEW radar during summer Suhaili day. (a) 0400 local time AEW radar simulated at 6470m (21351feet) and (b) 1600 local time AEW radar simulated at 20m (66feet). Both simulations shows slandered atmospheric refractivity.

6.3.3 Summer Shamal air masses

Figure 6.21 shows Abu Dhabi airport hourly winds on the 28 and 29 June 2005, which was a summer Shamal wind. Figure 6.222 shows Abu Dhabi radiosondes for the same days at 0400 and 1600 local time. There was a strong north-westerly jet (Figure 6.21) at 1000 meters enhancing the surface north-westerly wind. On 28 June 2005 (Figure 6.21) the surface wind increased from 0800 local time reaching a maximum wind speed of 24 knots at 1600. This then remained strong at 12 to 18knots until 1800 local time on 29 June 2005. In the four radiosondes there were noticeable decreases in dew point with height at different gradients. There was a temperature inversion in the three radiosondes, except at 1600 on 28 June (Figure 6.22b) due to the strong wind.

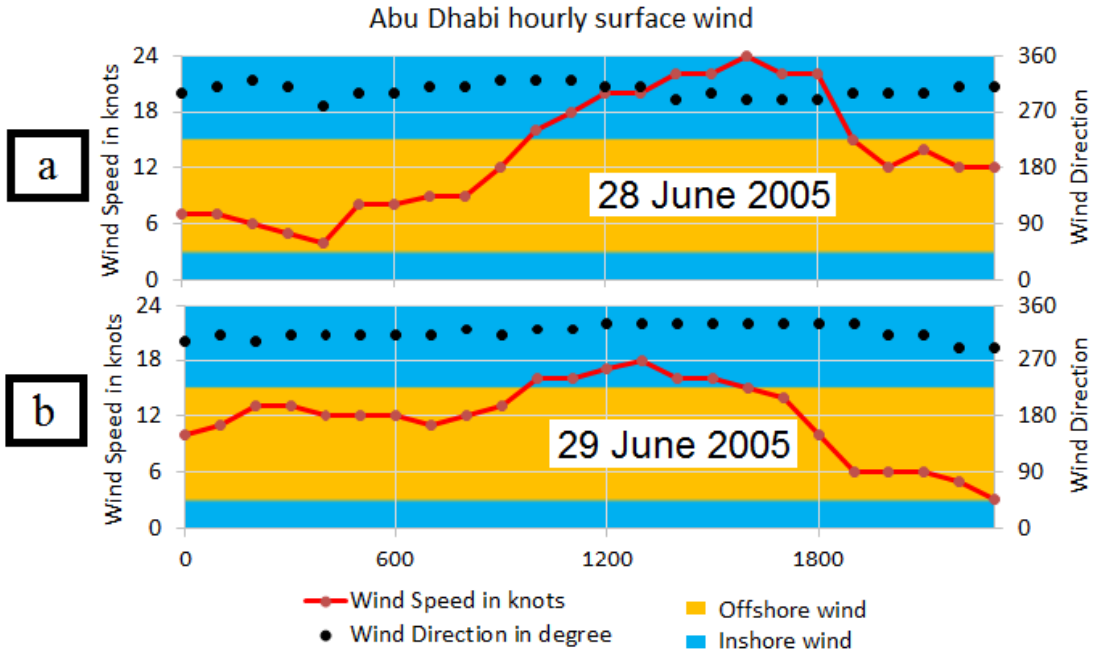

Figure 6.21. Abu Dhabi hourly surface wind chart for (a) 28 June 2005 (b) 29 June 2005. These charts represent the variation in the surface wind direction and strength during the summer Shamal day.

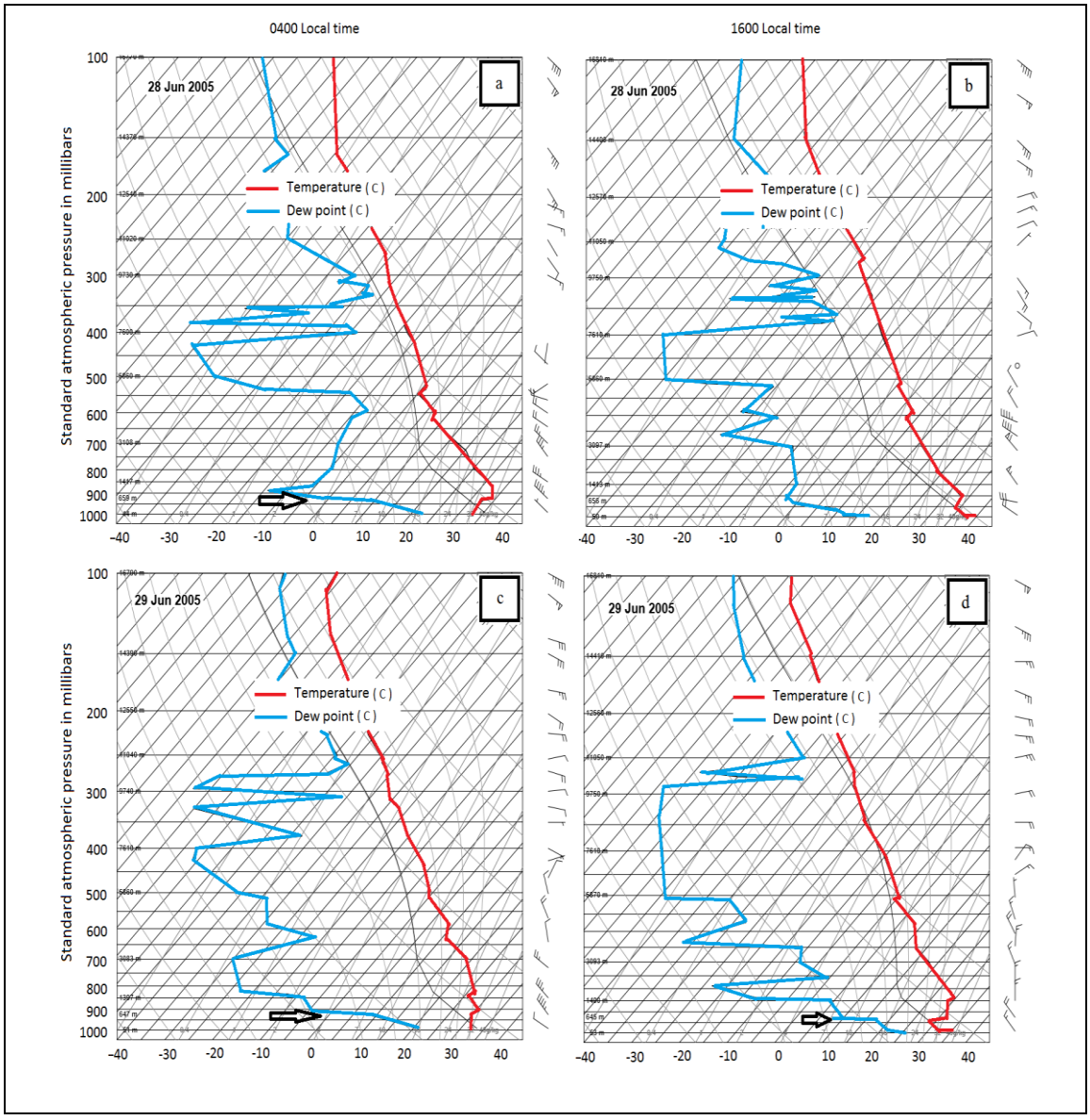

Figure 6.22. Summer Shamal radiosonde conditions during 28 (a-b) and 29 (c-d) June 2005 illustrating the variation of temperature and dew point with height at 0400 (a-c) and 1600 (b-d). Furthermore, black arrows point to the layer of potential atmospheric ducting.

On 28 June at 0400 (Figure 6.22a), there was a light north-westerly surface wind, which may have enhanced the amount of moisture at the surface, and a weak inversion developed. This meteorological condition could be the reason for an evaporation duct height of 38 meters and a surface based duct with a height of 604 meters. In the afternoon at 1600 local

time the surface-based duct was minimised to 4 meters; due to strong surface north-westerly winds which reached 24knots. The height of the evaporation duct was 40 meters at 1600. On 29 June at 0400, surface north-westerly winds decreased to 10 knots, which might have allowed the increase of the surface based duct to a height of 434 meters. The evaporation duct reduced to 35 meters which may have been due to the cooling effect of the strong north-westerly wind. At 1600 the evaporation duct height increased 33 meters and the height of the surface based duct decreased (353meters). Further details are contained within table 6.7. The simulation of the AEW radar propagation within the duct is illustrated in figure 6.23.

Table 6.7. The atmospheric ducting summary for the period 28-29 June 2005 and associated wind system. All heights in meters.

Date	Meteorological conditions	At 0400 local time			At 1600 local time		
		Evaporation Duct	Surface based duct	Elevated duct	Evaporation Duct	Surface based duct	Elevated duct
28	Gentle (7 knots) flow	28	604	-	38	42	-
29	Moderate (11 knots) Shamal day	34	4	506-794	36	51	1330-1497

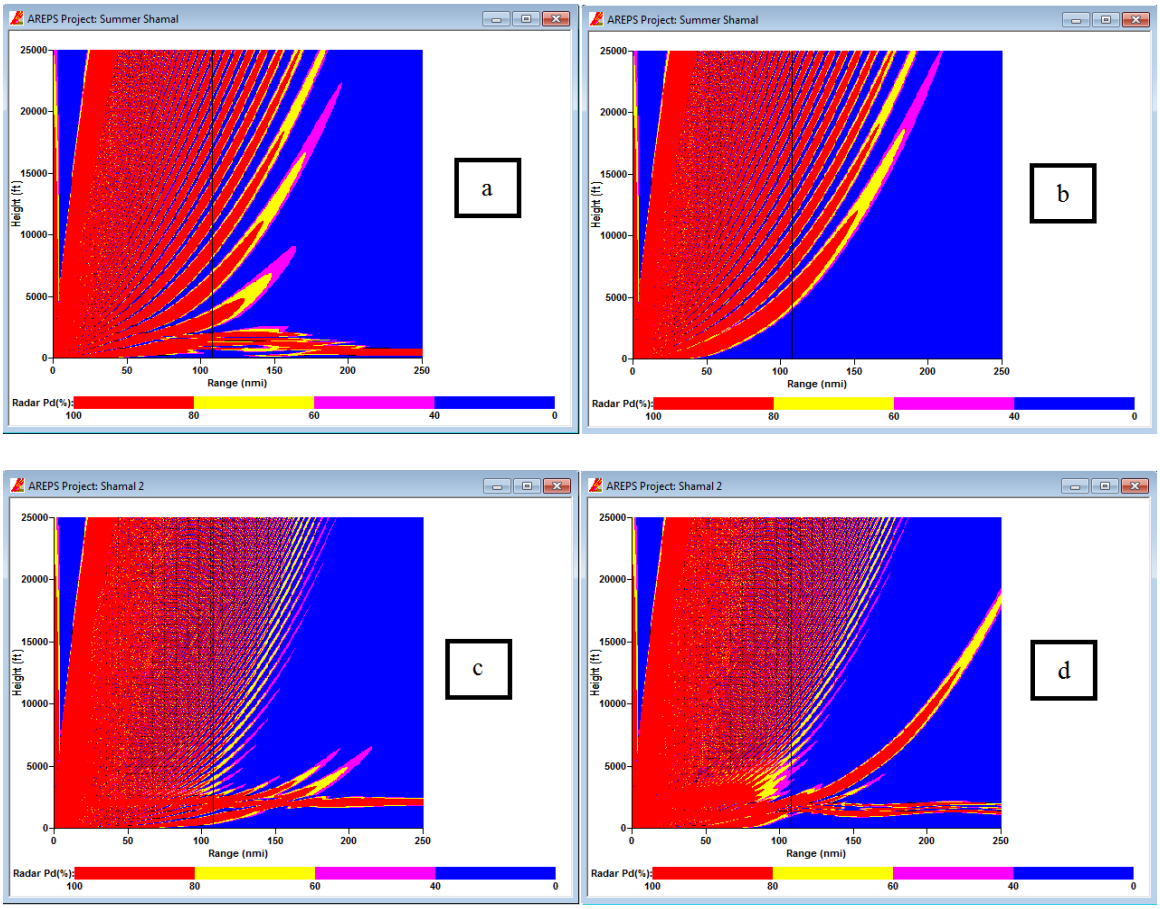

Figure 6.23. Radar propagation performance for each meteorological condition at 0400 (a-c) and 1600 (b-d) local time on the 28 (a-b) and 29 (c-d) June 2005. There is an elevated duct associated with the summer Shamal.

6.2.4 Summary of the duct conditions in summer air masses

The summer Shamal wind is associated with an elevated duct. By comparison, Suhaili is associated with standard atmospheric refractivity due to its characteristics. Land and sea breezes are usually associated with surface-based ducts causing good surface coverage for AEW radar. Evaporation duct height increased with strong wind but reached its maximum with a Suhaili dry wind and its height was minimised in the land and sea breeze. Summer air masses and associated major ducts are summarised in table 6.8.

Table 6.8. illustrating major ducts which can be expected during the summer season (May - October).

Air-masses	Expected duct
LSBC	Evaporation duct (10-20 meter), usually surface based duct ≈ 150-300 meter and sometimes elevated duct in layer between 1500-3500 meters.
Suhaili	Evaporation duct (35-40 meter) really thin layer (below 100meter) elevated duct.
Shamal	Evaporation duct (30-35 meter), elevated duct (≈ 250-300 meter) in the level of 500-2000metres

6.4 Conclusion

Atmospheric ducts are permanent phenomena over the area of study. It has been observed that there are three important ducts: evaporation duct, surface based duct and elevated duct. However, these occurred at different thicknesses and with a varying percentage of occurrences. The AREPS model was used to examine atmospheric refractivity under different meteorological conditions. Evaporation ducting occurred 100% of the time with an average height of 24 meters. The surface-based duct occurred 75% of the time with an average height of 117 meters. The elevated duct occurred 53% of the time with an average thickness of 260 meters.

Moderate and stronger (summer and winter) Suhaili and Al Nashi produced standard atmospheric refractivity. They drive dry air masses that weaken or destroy the sharp decrease in water vapour. In contrast, Shamals (both winter and summer) drive more water vapour from the sea enhancing moisture levels, which are then capped by sharp decreases

in moisture. Breeze circulations associated with significant surface-based ducts could be a result of night cooling.

In winter, contrary to summer, the weak sea breezes will not contribute to make any significant duct. The simulation of AEW radar illustrates that standard propagation conditions are associated with winter and summer Suhaili, Al Nashi, and weak sea breezes. In contrast during both moderate Shamal conditions, the elevated propagation duct was observed. The air mass refractivity condition is not limited to these results but they represent the general picture for these air masses. There may well be some occasions when the air masses will have different atmospheric refractivity conditions.

Chapter 7 - General Conclusions

Thirty years (1981-2010) of observations and NCEP/NCAR reanalysis data have been used to produce a better understanding of local meteorological conditions over the southern coast of the Arabian Gulf and how those conditions affect electromagnetic wave propagation in the region. The propagation of electromagnetic waves of frequencies above 100MHz can be seriously affected by atmospheric ducting, the trapping of EM propagation in a horizontal layer low in the atmosphere (Turton et al., 1988). This can occur due to an increase in temperature, and/or a decrease in air moisture with height (Katzin et al., 1960).

As a shallow body of water surrounded by desert landmass, the Arabian Gulf is often singled out for study (Brooks, Goroch and Rogers, 1999), though this is also at least partly due to the political and military focus of such a strategically important area. Because the topography of the area and its coastal configuration lead to high water temperatures and large amounts of evaporation (Atkinson and Zhu, 2005), the Arabian Gulf is an area with one of the highest probabilities of atmospheric ducting in the world (Willis, 2007).

Recent research (Atkinson & Zhu, 2005) has shown that ambient winds in the Arabian Gulf have a major impact on atmospheric ducting. The Shamal wind is the primary ambient wind in the region and persists most of the year over the study area (Govinda, Al-Sulaiti and Al-Mulla, 2001).

Observational data from three sites (Bahrain, Sharjah, and Abu Dhabi) were subjected to detailed statistical analyses, while NCEP/ANCAR reanalysis data was used to analyse the

main synoptic situations and reveal any correlations between different atmospheric systems (Chapters 4 and 5). Radiosonde data from Abu Dhabi were used to study the most important meteorological conditions and their impact on EM wave propagation (Chapter 4 and 6). The methodological approaches were mainly statistical analyses and the AREPS model was used to examine EM propagation in different air masses (Chapter 6). The AREPS model was developed by SPAWAR for the US Navy to predict electromagnetic wave propagation in different atmospheric conditions. It requires temperature, dew point and pressure with height as input, and it gives duct type, thickness and height. It also simulates electromagnetic propagation in different air masses. Furthermore, simulation of the evaporation duct requires sea surface temperature and wind speed as additional inputs.

NCEP/NCAR reanalysis data were validated against the observational data from the three sites (section 3.2). The validation process included calculation of statistical parameters (BIAS and RMSE) for wind speed and visual validation of wind directions in order to quantify the quality of the reanalysis data. The wind data validation of the NCEP/NCAR reanalysis shows that NCEP/NCAR agreed reasonably well with the observational data at Bahrain and Abu Dhabi (paragraph 3.2.3).

In the following sections, the main conclusions of this study are given in accordance to the specified objectives.

Objective 1: To introduce the local meteorology of the study area and specify the different air masses (warm/cold, moist/dry) that affect the area

Chapter 4 shows that there is a wide variation in topography over the area of study (section 4.1). Both topography and coastal configuration have a clear effect upon the wind direction and strength over the study area (paragraph 4.1.2.3). There were five synoptic winds affecting the area including winter and summer Shamal, winter and summer Suhaili and wintry Al-Nashi (paragraphs 4.2.1.2- 4.2.1.6).

As described, the Summer Shamal Days are associated with a subtropical high at 500mb, a surface westerly extension of a deep IMTL in the east and an easterly extension of the Azores High in the west. The Azores High is a semi-permanent system, while the IMTL starts to develop by the end of April/beginning of May and disappears during October. In contrast, Winter Shamal Days are associated with an upper air trough driven within the Rossby waves at 500mb. The upper air trough is associated with the passage of the surface westerly depression. The Winter Shamal persists after the passage of a westerly depression and the extension of the Siberian high pressure. The Siberian high pressure replaces the Indian Monsoon Thermal Low from November until April.

The position of the 5850m line at 500mb geopotential height is the separation between the Rossby wave and subtropical high (paragraph 4.3.1). The 5850m line is north of the study area from May until October which is considered to be the summer season, and lies to the south of the study area during the remaining period (November – April) which is considered to be the winter season (figure 4.11). Therefore, Shamal days are discussed in chapter 5 as two seasons: winter (November - April) and summer (May - October).

The second important synoptic wind is the Suhaili (south-easterly wind) which can occur any time of the year (winter or summer) but less infrequently than the Shamal. The winter Suhaili is associated with Rossby waves and the passage of westerly depressions. It starts as a westerly depression and moves from the eastern Mediterranean towards the study area and ends as it passes over the area of study. The Summer Suhaili is associated with the subtropical high and is the result of thermal heating west of the study area.

Al-Nashi (north-easterly) is a wintry cold and dry synoptic wind and is a rare occurrence compared to the others. It is associated with an upper air trough extension from central Asia and a strong Siberian high north of Iran (paragraph 4.2.1.6).

Land and sea breeze circulation is affected by the prevailing synoptic wind. Usually, there are weak land breezes and strong sea breezes due to the persistence of the Shamal wind. The onset time is also sensitive to the synoptic wind. The Shamal enhances an early start to sea breezes while the Suhaili delays its onset (paragraph 4.2.2.2). Katabatic wind effects are apparent over Sharjah, rather less over Abu Dhabi and cannot be observed at all over Bahrain due to the distance from the Hajar Mountains (paragraph 4.2.2.1).

The winter and Summer Shamal, winter and summer Suhaili, and Al-Nashi are the five synoptic winds that are considered in Chapter 6 to examine the refractivity and propagation of electromagnetic waves.

Objective 2: To identify the general regional features that characterize the region's meteorology.

Shamal is the main meteorological feature that characterizes the region (figure 4.3, 4.4). It persists throughout the year but with different characteristics, as has been illustrated in the previous objective (paragraph 4.2.1.2, 4.2.1.3). It enhances the strength of the sea breezes and decreases the southerly flow and land breezes. Due to its route, it could enhance the amount of moisture over the land of the southern coast. Furthermore, it has been observed that the vertical structure of the Shamal enhances the development of the elevated inversion at 850mb (which is potentially an atmospheric duct layer) (figure 4.5, 4.6). Therefore, a good understanding of the behaviour of the Shamal and its connection with the global circulation will enable its prediction and an understanding of its influence on local meteorology.

Objective 3: Examine the inter-annual variability of Shamal Days and its correlation with the global circulation pattern.

The variability of the Shamal wind and the connection between the Shamal and the global circulation are examined in chapter 5. Statistical analysis shows that there was a decline in wind strength over the period of study(paragraph 5.1.1.1). Bahrain trends data were used to represent the wind strength and the frequency of Shamal days in the area of study due to its location, coastal configuration and topography.

The decline in wind strength and frequency of Shamal days in Bahrain trends data was found to be statistically significant. It is likely, therefore, that the decline in the total wind strength over the period of study was the result of the decline in the frequency of Shamal days (section 5.1). Furthermore, during the period of study there was a significant reduction in the number of Winter Shamal days. The month of June showed the highest frequency in the number of Shamal days. However, a significant decline in the frequency of June Shamal days has been observed (paragraph 5.1.2.1).

During Summer Shamal Days (SSDs), there were two atmospheric fluctuations (over the Caspian Sea and Siberia) which interconnected with the SSD variability. The correlation between the frequency of the SSDs and the 500mb level geopotential height were examined by ANOVA-F test and found to be statistically significant (section 5.2).

During high frequency SSDs, above-average pressure occurs over the Caspian Sea which limits the westerly extension of the thermal low by the cooler northerly wind, resulting in below average SSDs. On the other hand, below-average pressure over the Caspian Sea enhances the westerly extension of the thermal low over the Zagros Mountains caused by a warm southerly winds.

During low frequency SSDs above-average pressure over Siberia feeds cold air into the easterly Mediterranean High, which concurrently is associated with an above average meridional wind at 500mb level west of the Caspian Sea. This subsequently extends to the

surface over the Zagros Mountains enhancing a deepening of the thermal low; this topographic feature consequently causes above average SSDs. The 500mb level Meridional wind south west of the Caspian Sea shows the best correlation (74%) with the frequency of the WSDs.

During Winter Shamal Days (WSDs) (section 5.3), there were two different atmospheric fluctuations (over the east of Greenland and west Europe) which interconnect with the frequency of WSDs variability. For the six-month period only atmospheric fluctuations over Greenland was significantly correlated with the WSD variation.

In contrast, during the period of increased frequency of WSDs (December, January, and February), atmospheric fluctuations over the west of Europe became more significant to the frequency of the WSD's variation. Both systems have no direct effect upon WSD variation, but they do affect the frequency of Mediterranean storms that cross the area and which may be considered as the ignition of WSDs. Therefore, it is suggested that the main reason for the reduction in the frequency of WSDs is the reduction in the number of westerly depressions crossing the area. Further research could use statistical analysis of 500mb geo-potential height to track troughs crossing the area, and correlate this with the frequency of WSDs. Finally, the NOA index and the AO index are statistically significantly correlated with the frequency of WSDs. These phenomena (NOA and AO) have correlation coefficients with the frequency of WSDs of 0.41 and 0.49 respectively.

Objective 4: Examine EM propagation variability under different meteorological conditions.

Chapter 6 illustrates the investigation of the EM propagation variability over the southern Arabian Gulf. EM propagation is affected by atmospheric refractivity. Ducting is one type of atmospheric refractivity with significant effects over the area of study (in agreement with Katzin et al., 1960). The AREPS model was used to examine atmospheric refractivity under different meteorological conditions. Atmospheric ducts are permanent phenomena over the area of study. It has been observed that there are three important ducts: evaporation ducts, surface-based ducts and elevated ducts. However, these occurred with different thicknesses and with varying percentages of occurrence as follows:

- Evaporation ducting (paragraph 6.1.1) occurred 100% of the time with an average height of 24 meters. Its height reach a maximum during dry, windy summer days. This meteorological condition is usually associated with the summer Suhaili. In contrast, it reaches the minimum during humid, calm winter days. This meteorological condition is usually associated with wintry light sea breezes.

- The surface-based duct (paragraph 6.1.2) occurred 75% of the time with an average height of 117 meters. Its height increased during calm, humid summer days, possibly due to night cooling. This meteorological condition is usually associated with land and sea breezes. Furthermore, surface-based duct height minimised or dissolve during dry, windy, wintry days, due to the vertical mixing of the air. Usually it minimises or disappears with synoptic winds such as Shamal, Suhaili and Al-Nashi.

- The elevated duct (paragraph 6.1.3) occurred 54% of the study time with an average thickness of 260 meters. It mostly occurred in altitudes approximately between 1000-

2000 meters during winter and 1500-3500 meters during summer. It was rarely (9% of the time) associated with an additional elevated duct at higher altitude (approximately between 3000-4000 meters). The elevated duct is more frequent during January, October, November and December. Its occurrence decreases in the remaining months and it reaches the minimum occurrence during May. Elevated ducts were observed on 81% of the Shamal days, 52% of the wind which is less than 11knots. They were rarely observed (7%) on Suhaili days and if present, were usually a thin layer (less than 100 meters).

Moderate and stronger (summer and winter) Suhaili and Al Nashi produced standard atmospheric refractivity (paragraphs 6.2.2 , 6.2.3). These winds drive dry air masses that weaken or destroy the sharp decrease in water vapour. In contrast, winter and summer Shamals drive more water vapour from the sea that enhances moisture levels, which are then capped by sharp decreases in moisture at higher elevations (paragraph 6.2.3, 6.3.3). Breeze circulations associated with significant surface-based ducts could be a result of night cooling.

In winter, contrary to summer, the weak sea breezes will not contribute to the formation of significant ducting (paragraphs 6.2.2, 6.3.1). The simulation of AEW radar illustrates that standard propagation conditions are associated with winter and summer Suhaili, Al Nashi, and weak sea breezes. In contrast, the elevated propagation duct was observed during both moderate Shamal conditions and strong summer sea breezes (section 6.2 and 6.3).

In summary, the main finding is that there was decline in the number of the Shamal days during period of the study (1981-2010). The 5850meter line at 500mb geopotential height level is the separation between Rossby waves and the Subtropical high. Both atmospheric systems influence the area of the study, but at different times of the year depending on the position of the 5850meter in regard to the study area. If the 5850meter line is at 500mb level north of the study area, then the area of the study will be affected by summer winds. The frequency of summer Shamal days is influenced by atmospheric fluctuations over Siberia and the Caspian Sea. While if the 5850metre line is at 500mb level south of the study area, then the area of the study will be effected by a wintry wind pattern. The number of winter Shamal Days is influenced by atmospheric fluctuations over Greenland and Western Europe. Furthermore, NAO and AO showed links with the number of Shamal days during December, January, and February. Also, it has been found that winter and summer Shamal usually (more than 80%) are associated with an elevated duct. Both Suhaili and Al-Nashi have standard atmospheric refraction due to their meteorological characteristics. Suhaili enhances the height of the evaporation duct which reaches maximum 40 meters from the sea surface. The height of the evaporation duct could be increased due to the strong wind; dry air; and high sea surface and air temperature. Finally, land and breeze circulation is usually associated with the surface-based duct and sometimes with the elevated duct.

References

Ahrens, C.D., (2009); Meteorology Today, Tenth Edition, Belmont: Brooks Cole.

Ali A., 1994; Wind regime of the Arabian Gulf. In The Gulf War and the Environment. El-Baz F, Maharita RM. (eds.) 31–48. Gordon and Breach: Lausanne, Switzerland.

Al Senafi, F. and Anis, A., (2015); Shamals and climate variability in the Northern Arabian Gulf from 1973 to 2012. International Journal of Climatology Vol. 35, Issue 15, December 2015, pp. 4509-28

Almandoos, A., (2005); Synoptic and Atmospheric Stability Classification for the UAE, [online] University of the Witwatersrand, Available at: < http://wiredspace.wits.ac.za/handle/10539/1774 > [Accessed 3 March 2011].

Anderson, K., (1995); Radar Detection of Low-Altitude Targets in a Maritime Environment, IEEE Transactions on Antennas and Propagation, Vol. 43, No. 6, June 1995, pp. 609-13

Arritt, R., (1989); Numerical Modelling of the offshore extent of sea breezes. Quarterly journal of the Royal Metrological Society, Vol 115, Issue 487, pp 547-570.

Atkinson, B., LI, J., and Plant, R. (2001); Numerical modeling of the propagation environment in the atmospheric boundary layer over the Persian Gulf, Journal of applied meteorology, Vol 40, pp 586 – 603.

Atkinson, B. and Zhu, M. (2004); Observed and modelled climatology of the land – sea breeze circulation over the Persian Gulf, International Journal of climatology, Vol 24, pp 883-905.

Atkinson, B. and Zhu, M. (2005); Radar duct and boundary layer characteristics over the area of the Gulf, Quarterly journal of the Royal Metrological Society, Vol 131, pp1923-1953.

Atkinson, B. and Zhu, M. (2006); Coastal effects on propagation in atmospheric ducting conditions, Meteorol. Appl., Vol13, pp 53-62.

Barlow, M., Cullen, H., and Lyon, B., (2002); Drought in Central and Southwest Asia: La Nin˜a, the Warm Pool, and Indian Ocean Precipitation, Journal of climate, Vol 15, No 7, pp 697-700.

Barrios, A., (2003); Considerations In the Development of the Advanced Propagation Model (APM) For US Navy Applications; In. SPAWARSYSCEN San Diego, 2003 IEEE International Radar conference, Hilton Hotel in Adelaide Australia, 3-5 sept 2003, USA, IEEE.

Bean, B., and Dutton, E, (1968); Radio Meteorology, Dover Publications, PP 435.

Branstator, G., (2002); Circumglobal Teleconnections, the Jet Stream Waveguide, and the North Atlantic Oscillation, Journal of Climate Vol. 15 (July 2002), pp. 1893-1910.

Brooks, I., Goroch, A., and Rogers, D., (1999); Observation of strong surface radar ducts over the Persian Gulf, Journal of applied meteorology, Vol 38, pp1293-1310.

Bruce W., (2006); Atmospheric refraction: how electromagnetic waves bend in the atmosphere and why it matters [online] Naval postgraduate school library, Available at: < http://webcache.googleusercontent.com/search?q=cache:nE0WSh3n3_oJ:www.met.nps.edu/~psguest/EMEO_online/module4/Atmospheric_Refraction_of_EM_Waves.doc+&cd=2&hl=en&ct=clnk&gl=uk > [Accessed 20 February 2011].

Chakraborty, A., Mujumdar, M., Behera, S., Ohba, R., and Yamagata, T., (2006); A cyclone over Saudi Arabia on 5 January 2002: A case study, Meteorology and Atmospheric Physics 93, 115–122.

Cheong, B., Palmer, R., Curtis, C., and Yu, T., (2005); Refractivity Measurements from Ground Clutter using the National Weather Radar Testbed Phased Array radar. [online] University of Oklahoma, Available at: < http://arrc.ou.edu/~boonleng/pdf/ext_abs_par_refr.pdf> [Accessed 23 February 2011].

Cheung, H., Zhou, W., Mok, H., Wu, M., (2012): Relationship between Ural-Siberian blocking and East Asian winter monsoon in relation to Arctic oscillation and El Niño/Southern Oscillation, Journal of Climate. Doi: 10.1175/JCLI-D-11-00225.1.

Chou Y, and Kiang J, (2014); Ducting and turbulence effects on radio-wave propagation in an atmospheric boundary layer, Progress In Electromagnetics Research B, Vol. 60, 301-315.

Craig, K.H., (2003); Clear- air characteristics of the troposphere. In: Barclay, L.W., ed. 2003. Propagation of Radiowaves (2nd Edition). London: IET. Ch.7

Derley, D., (2006); Remote sensing of the refractive environment above the marine stratocumulus topped boundary layer. [online] Naval postgraduate school, Available at: < http://library.nps.navy.mil/uhtbin/hyperion/06Sep%5FDerley.pdf > [Accessed 1st February 2011].

Eager, R., Raman, S., Almandoos, A., Westphal, D., Reid, J., (2008); A climatology study of the sea and land breezes in the Arabian Gulf region, journal of geophysical research, vol.113, d15106, pp12, doi:10.1029/2007jd009710.

El-Kadi, A., (2001); Variation of rainfall and drought conditions in GAZA- Palestine on a regional and global context, Journal of the Islamic University of Gaza, Vol. 9, No. 2, pp41 – p66 .

Emery, C. and Tai., E. (2001); Enhanced Meteorological Modeling and Performance Evaluation for Two Texas Ozone Episodes. Final Report Submitted to Texas Natural Resources Conservation Commission, prepared by ENVIRON, International Corp., Novato.

Engeln, A., Teixeira, J., (2004); A Ducting Climatology derived from ECMWF Global analysis fields, Journal Of Geophysical Research, Vol. 109, d18104, pp15, doi:10.1029/2003jd004380

Esfahany, M., Ahmadi-Givi, F., and Mohebalhojeh, A., (2011); An energetic view of the relation between the Mediterranean storm track and the North Atlantic Oscillation, Quarterly Journal of the Royal Meteorological Society, Vol 137, Issue 656, pages 749–756, April 2011 Part A

Federation of UAE chambers of Commerce & industry, (2010); Geographic location [online], Available at: <http://www.fcciuae.ae/en/geo-loc-en.php> [Accessed 01 March 2011].

Galvin, J.F.P., (2007a); The weather and climate of the tropics: Part 1 – Setting the scene, Weather (Royal Meteorological Society), September 2007, Vol. 62, No. 9, pp. 245-51

Galvin, J.F.P., (2007b); The weather and climate of the tropics: Part 2 – The subtropical jet streams, Weather (Royal Meteorological Society), November 2007, Vol. 62, No. 11, pp. 295-9

Galvin, J.F.P., (2008); The weather and climate of the tropics: Part 6 – Monsoons, Weather (Royal Meteorological Society), May 2008, Vol. 63, No. 5, pp. 129-137

Gao, J., Thoppil, P., Gomes, H., and Fasullo, J. (2005); Warming of the Eurasian Landmass Is Making the Arabian Sea More Productive, Science, Vol. 308, pp 545-547.

Gao, J., Brewster, K., and Xue, M., (2008); Variation of radio refractivity with respect to moisture and temperature and influence on radar ray path, Advance in atmospheric sciences, Vol 25, No.6 , 1098-1106.

Glennie K, and Singhvi A (2002); Event stratigraphy paleo-environment and chronology of SE Arabian deserts, Quaternary Science Reviews, Vol 21 (2002), 853 – 869.

Gopal Raj, N. (2004); El Nino and Indian Ocean Dipole, the Hindu, online edition of India's National Newspaper, [online], Available at: <

http://hindu.com/2004/05/04/stories/20040504 01861000.htm> [Accessed 24 May 2012].

Goswami, B.N., Sengupta, D., (2003); A note on the deficiency of NCEP/NCAR reanalysis surface winds over the equatorial Indian Ocean, Journal of Geophysical Research: Oceans, Vol. 108, Issue C4 (April 2003)

Govett M, (2014); chapter 3, ESRL Radiosonde Database, [online], Available at: < http://esrl.noaa.gov/raobs/General_Information.html> [Accessed 24 May 2015].

Govinda, R., Al-Sulaiti, M., Al-Mulla, A., (2001); Winter Shamals in Qatar, Arabian Gulf, Weather, Vol 56, No.12, PP 444-451.

Govinda R., Hatwar, H., Al-Sulaiti, M., Al-Mulla, A., (2003); Summer Shamal over the Arabian Gulf, Weather, Vol 58, No.12, PP 471-477.

Grabner M, Kvicera V, (2011): Atmospheric refraction and propagation in lower troposphere, Electromagnetic Waves 139–156.

Habib, A., (2011); Discussion about the South easterly wind over the Arabian gulf [phone], (personal communication, 25 April 2011).

Hasanean, H., (2003); Teleconnection between global climatic events, atmospheric circulation changes and stream flow over the River Nile. Journal of Meteorology, Vol. 28, No. 279, 161-177

Hasanean, H., (2010); Middle East meteorology, Tropical meteorology, Earth and atmospheric sciences, Encyclopaedia Of Life Support Systems (EOLSS). United Nation Educational Scientific and Cultural Organisation (UNESCO), [online],

Available at: < http://www.eolss.net/Sample-Chapters/C01/E6-158-19.pdf > [Accessed 24 May 2012].

Hodges, G., (2000); the new cold war: Stalking arctic climate change by submarine. National Geographic, March, 30-41.

Hurrell, J., Kuschnir, Y., and Visbeck, M., (2001); The North Atlantic oscillation, Science, Vol. 291, pp 603-605.

Hydrographic office (1994); The Effects of the Environment on Radio and Radar Wave Propagation, Naval Oceanography and Meteorology Memorandum No 1/94 NP 486A (21).

IPCC (Intergovernmental Panel on Climate Change), (2013); Fifth Assessment Report, Climate Change, The Scientific Basis, Chapter 2, [online]. Available at https://www.ipcc.ch/pdf/assessment-report/ar5/wg1/WG1AR5_Chapter02_FINAL.pdf [Accessed 13 November 2016]

Kalnay, Kanamitsu, Kistler, Collins, Deaven, Gandin, Iredell, Saha, White, Woollen, Zhu, Leetmaa, Reynolds (1996). The NCEP/NCAR 40-year reanalysis project. Bull. Amer. Meteor. Soc. 77: 437–471.

Katzin, M., Pezzner, H., Koo, B., Larson, J., Katzin, J., (1960); The Trade-Wind Inversion as a Transoceanic Duct, Journal of research of the National Bureau of Standards, Section D: Radio propagation, Vol.64D, No.3, pp 247-253

Kingsley, S. and Quegan, S., (1999) Understanding Radar Systems. Mendham: SciTech.

Kistler R, Kalnay E, Collins W, Saha S, White G, Woollen J, Chelliah M, Ebisuzaki W, Kanamitsu M, Kousky V, Den Dool H V, Jenne R, Fiorino M, (2001): The NCEP–NCAR 50–Year Reanalysis: Monthly Means CD–ROM and Documentation. Bull. Amer. Meteor. Soc., 82, 247–267.

Krichak, S., Alpert, P., and Krishnamurti, T., (1997); Red Sea Trough/Cyclone Development- Numerical Investigation, Meteorology and Atmospheric Physics, Vol 63, pp 159-169.

Laing, A., Evans, J., (2011); Introduction to the tropical meteorology, second edition, [online], MetEd website by UCAR Available at: <http://www.meted.ucar.edu/tropical/textbook_2nd_ edition/> [Accessed 3 May 2012].

Lionello, P. & Giorgi, F. (2007) Winter precipitation and cyclones in the Mediterranean region: future climate scenarios in a regional simulation. Adv. Geosci. 12, 153–158. (doi:10.5194/ adgeo-12-153-2007)

Malekifard, F., & Rezazadeh, P., (2009); North Atlantic Oscillation (NAO) and Its Effects On temperature and precipitation over North-West of Iran, [online], Available at: <http://balwois.com/balwois/administration/full_paper/ffp-465.pdf> [Accessed 15 March 2011].

Mariotti, A., Ballabrera, J., and Zeng, N., (2005); Tropical influence on Euro-Asian autumn rainfall. Climate Dynamics, Vol 24, No 5, pp 511-521.

Met office, (2015); Mountain weather [online] met office services, Available at: <http://www.metoffice.gov.uk/services/mountain/weather> [Accessed 20 February 2016].

Musa, A., Bashir, S.O., Abdalla, A.H., (2014); Review and Assessment of Electromagnetic Wave Propagation in Sand and Dust Storms at Microwave and Millimeter Wave Bands – Part II. Progress in Electromagnetics Research M, Vol. 40, 2014, pp. 101-110.

Nazemosadat, M., Samani, N., Barry, D., and Niko, M., (2006); ENSO forcing on climate change in Iran: Precipitation analysis, Iranian Journal of Science & Technology, Transaction B, Engineering, Vol. 30, No B4, p. 555-565.

NOAA (National Oceanic and Atmospheric Administration), (2003); NOAA's Climate summaries for the Middle East and Iraq, [online], Available at: <http://www.magazine.noaa.gov/stories/mag87.htm> [Accessed 14 March 2011].

NOAA, (n,d); El-Nino, [online], available at : < http://www.pmel.noaa.gov/tao/elnino/nino-home.html# >[Accessed 15 March 2011].

Panagiotopoulos, F., Shahgedanova, M., Hannachi, A. and Stephenson, D.B., (2004) Observed Trends and Teleconnections of the Siberian High: A Recently Declining Center of Action, Journal of Climate, Vol. 18, May 2005, pp. 1411-1422

Patterson, (1998); Technical document 3028 Advanced Refractive effects Prediction System (AREPS) Version 1.0 User's Manual, SPAce and naval WARfare Systems centre (SPAWAR) San Diego, CA 92152-5001.

Reid, J., Piketh, S., Walker, A., Burger, R., Ross, K., Westphal, D., Bruintjes, R., Holben, B., Hsu, C., Jensen, T., Kahn, R., Kuciauskas, A., Mandoos, A., Mangoosh, A., Miller, S., Porter, J., Reid, E., Tsay, S.,(2008); An overview of IAE flight operations: Observations of 30 summertime atmospheric thermodynamic ana aerosol profiles of the southern Arabian Gulf, Journal Of Geophysical Research, Vol. 113, D14213, pp14 , doi:10.1029/2007JD009435.

Saji NH, Goswami BN, Vinayachandran PN, Yamagata T (1999) A dipole mode in the tropical Indian Ocean. Nature 401: pp. 360-363.

Sarachik, E.S., and Cane, M.A. (2010); The El Niño-Southern Oscillation Phenomenon. Cambridge: Cambridge University Press

SPAWAR, (2006); Statement of functionality for AREPS system [online], Available at: < http://areps.spawar.navy.mil/2858/software/areps/arepsdownload/sofAREPS_36.pdf > [Accessed 23 February 2011].

Turton, J., Bennetts, D., and Farmer, S., (1988); An Introduction to radio ducting, Meteorological magazine. Val 117, PP 245-254.

United Arab Emirates (UAE) Climate. (1996). UAE Climate. 1st edition. Ministry of Communications. Cultural Foundation Publications: Abu Dhabi.

UAE ministry of energy (2006); Initial National Communication to the United Nations Framework Convention on Climate Change, pp 66.

UCAR (University Corporation for Atmospheric Research), (2010); The Indian Ocean Dipole (IOD), [online], Available at: <http://www2.ucar.edu/news/backgrounders /weather-maker-patterns-interactive-map#map> [Accessed 7 June 2011].

UKHO (United Kingdom Hydrographic Office), (2013); Admiralty Sailing Directions, Persian Gulf Pilot, NP63, Sixteenth Edition, pp. 15-35

Villiers, M., (2010); Predicting the development of weather phenomena that influence aviation at Abu Dhabi, Electronic Theses and Dissertations, University of Pretoria, [online], Available at: < http://upetd.up.ac.za/thesis/available/etd-02082010-193833/> [Accessed 15 May 2012].

Walters, K.R. Sr. (1990); The Persian Gulf Region a Climatological Study, Department of the Navy, U.S. Marine Corps, FMFRP 0-54 (Operational Handbook 0-54)

Wang, B., (2006); The Asian Monsoon, Published by Springer and Praxis Publishing,

Wang, J., Wu, B., IARC, Univ. of Alaska, Fairbanks, AK, (2001); Impacts of Winter Arctic Oscillation on the Siberian High, the East Asian Winter Monsoon, and Sea-Ice Extent; In. National Ice Center, Washington, 6th Conference on Polar Meteorology and Oceanography (Compact View), SAN DIEGO, 15 may 2001, UAS, American Meteorological Society.

Willis, M. (2007); Microwave propagation. [online] Available at: <http://www.mike-willis.com/Tutorial/PF6.htm> [Accessed 1st February 2011].

Wu, B., and Wang, J., (2002); Winter Arctic Oscillation, Siberian High and east Asian winter monsoon, Geophysical research letters, Vol. 29, pp1897-1901

Yakir, D., Lev-yadun, S., Zangvil, A., (1996); El Niño and tree growth near Jerusalem over the last 20 years, Global Change Biology, Issue 2, page 97-101

Wisniewski, M. (2009) *Quantitative Methods for Decision Makers (5th Ed.),* Pearson: Harlow

Yu, Y., Notaro, M., Liu, Z., Wang, F., Alkolibi, F., Fadda, E., Bakhrjy, F., (2015) Climate Controls on the interannual to decadal variability in Saudi Arabian dust activity: Toward the development of a seasonal dust prediction model, Journal of Geophysical Research: Atmospheres, Vol 120, Issue 5, 16 March 2015, pp. 1739-58

Yu, Y., Notaro, M., Kalashnikova, O.V., Garay, M.J., (2016) Climatology of summer Shamal wind in the Middle East, Journal of Geophysical Research: Atmospheres, Vol 121, Issue 1, 16 January 2016, pp. 289-305